Synthesis, structure and electrochemistry of organometallic compounds bearing C(_n)N ligands

Richard L. Cordiner

University of Durham

A thesis entitled:

"Synthesis, Structure and Electrochemistry of Organometallic Compounds Bearing C_nN Ligands"

By

Richard L. Cordiner
(Trevelyan College)

Chemistry Department,
South Road Laboratories,
South Road,
Durham,
DH1 3LE

A candidate for the degree of Doctor of Philosophy

August 2005

Abstract

In this thesis, the synthesis of the organic cyanoacetylenes $NCC{\equiv}CC_6H_5$ and $NCC{\equiv}CC_6H_4$-4-NMe_2 and the metal cyanoacetylides $Ru(C{\equiv}CC{\equiv}N)(PPh_3)_2Cp$, $Ru(C{\equiv}CC{\equiv}N)(dppe)Cp^*$ and $Fe(C{\equiv}CC{\equiv}N)(dppe)Cp$ is presented and their coordination chemistry is explored. The structure and electrochemical behaviour of these novel cyano-carbon complexes is investigated and spectro-electrochemical methods are used to investigate the electronic structure of the cyanoacetylide compounds. In addition, in order to gain a greater understanding of the metal/ligand bonding interaction in these systems, the synthesis, structure and electrochemical behaviour of a series of metal nitriles $[Ru(N{\equiv}CC_6H_4X)(PPh_3)_2Cp][PF_6]$ ($X = NO_2$, NMe_2, CN) and $[M(N{\equiv}CC_6H_4X)L_2Cp'][PF_6]$ ($M = Ru$, $L = PPh_3$, $Cp' = Cp$; $M = Ru$, $L_2 = dppe$, $Cp' = Cp^*$; $M = Fe$, $L_2 = dppe$, $Cp' = Cp$) were investigated, as were the complexes $[\{Ru(PPh_3)_2Cp\}_2\{\mu\text{-}M(CN)_4\}]$ ($M = Ni$, Pd, Pt) and $[\{Ru(dppe)Cp^*\}_2\{\mu\text{-}M(CN)_4\}]$ ($M = Ni$, Pd , Pt), which feature a group 10 tetracyanometallate as a bridging moiety.

Statement of Copyright

Declaration

The work described in this thesis was carried out at the University of Durham, Department of Chemistry between October 2001 and September 2004. All the work is my own unless stated otherwise and it has not been submitted previously for a degree at this or any other university.

Financial Support

The Engineering and Physical Science Research Council (EPSRC) is gratefully acknowledged for providing funding for the work described herein.

Acknowledgements

The list is too long and the space is too short to say an individual thanks to all those who've been of help during the production of this thesis. However especial thanks must be made to several people.

Firstly, thanks to all members, past and present, of "lab shack 100" whose help and support has been invaluable. Particular thanks to Rachel Roberts, fellow potential circus star.

Secondly, thanks to all the service staff in the Department of Chemistry for much advice and assistance.

In the "outside world", thanks must go to the staff at Trevelyan College for constant support, especially Carole Laverick and Maggie Prestwich. Furthermore, thanks must go to Lani Smales, Carl Barker and Chris Broadbent for soothing frazzled brummie nerves with cheer, patience, beer and films.

Finally, and most importantly, I'd like to thank Dr. Paul Low, whose advice and support has been invaluable and without whom, none of this would have been possible.

Contents

Abbreviations

(+)-DIOP	4,5 - bis(diphenylphosphinomethyl)-2,2-dimethyl-1,3-dioxolane
Abs	Absorption
bpy	2,2' - bipyridine
cm-1	Reciprocal centimetres
Cp	Cyclopentadienyl anion
Cp*	Pentamethylcyclopentadienyl anion
CV	Cyclic voltammetry
Cy	Cyclohexyl
DCA	Dicyanoacetylene
DCM	Dichloromethane
DFA	Diferrocenylacetylene
dippe	1,2 - bis(diisopropylphosphino)ethane
dmpe	1,2 - bis(dimethylphosphino)ethane
dppe	1,2 - bis(diphenylphosphino)ethane
dppf	1,1' - bis(diphenylphosphino)ferrocene
dppm	1,2 - bis(diphenylphosphino)methane
DPV	Differential pulse voltammetry
ε	Extinction coefficient
EPR	Electron paramagnetic resonance
ES(-)-MS	Negative-ion electrospray mass spectrometry
ES(+)-MS	Positive-ion electrospray mass spectrometry
Et	Ethyl
Fc	Ferrocenyl anion

FT-IR	Fourier transform infra-red
HOMO	Highest occupied molecular orbital
IR	Infra-red
IVCT	Intervalence charge transfer
M	Molar
Me	Methyl
MeOH	Methanol
mg	Milligrams
MLCT	Metal-ligand charge trancfer
mM	Millimolar
MMCT	Metal-metal charge transfer
mmoles	Millimoles
ν	Wavenumber (for infra-red spectra)
$\bar{\nu}$	Wavenumber (for electronic absorption spectra)
NIR	Near infra-red
NLO	Non-linear optics
nm	Nanometres
NMR	Nuclear magnetic resonance
ORTEP	Oak-Ridge thermal ellipsoid plot
OTTLE	Optically-transparent thin layer electrode
Phen	1,10 Phenanthroline
Pn	Propylene diamine
ppm	parts per million
PPN	Bis(triphenylphosphine)iminium

py	Pyridine
pyr	Pyrazine
SCE	Standard calomel electrode
SHG	Second harmonic generation
TBA	tetra-butyl ammonium
TCNE	Tetracyanoethylene
THF	Tetrahydrofuran
tol	Tolyl
tpy	1,2':6':2' -terpyridine
triphos	1,1,1 - tris(diphenylphosphinomethyl)ethane
UV-vis	Ultraviolet-visible
Vab	Coupling constant

Introduction

Understanding electron transfer processes is vital to understanding a wide variety of subjects such as biological photosynthetic pathways, catalytic reaction cycles and the design of light-emitting devices through to the nascent fields of molecular electronics and nanotechnology. The understanding of inter- and intra-molecular charge transfer between remote sites is fundamental to the design of materials for these applications.

Possibly the most historically important example of a complex that displays charge-transfer between two metal sites is the cyanide-bridged di-iron complex Prussian Blue ($KFe[Fe(CN)_6]$). Although known for some 300 years (its discovery is credited to a Berlin painter named Diesbach, in 1704) it is only relatively recently that the physical properties of this material have been studied with regards to its charge transfer behaviour.[1] The intense blue colour of Prussian Blue arises from the metal-metal charge transfer (MMCT) interaction between the two iron centres, one of which is formally Fe^{II}, the other being formally Fe^{III}. Being a material that contains two metal centres in differing oxidation states, Prussian Blue is also the first example of a "mixed valence" complex.

Mixed valence complexes can arise either from compounds where the two metal centres are in different oxidations states as a result of the synthetic method employed (as in the case of Prussian Blue), or can be generated from bimetallic precursors by electrochemical or chemical redox processes. The degree of interaction between the metal centres in mixed valence compounds can be classified using the system devised by Robin and Day.[2] Broadly speaking, those mixed-valence compounds for which

there is no interaction between the metal centres are referred to as Class 1 compounds. Where there is such a high degree of delocalisation across the complex that only an average valence can be determined for the metal centres the material comes under the Class 3 heading. All other complexes are referred to as Class 2 (or "valence trapped") species. Common features of mixed-valence complexes include the observation of distinct oxidation potentials for each redox site by cyclic voltammetry and the appearance of absorption bands in the near infra-red (NIR) region of the material's electronic absorption spectrum. The NIR bands correspond to optically-induced charge transfer from one metal centre to another and are referred to as "metal-metal charge transfer" (MMCT) or "inter-valence charge transfer" (IVCT) bands. In Class 3 complexes these IVCT bands tend to be narrower than those observed for Class 2 complexes (see Chapter 4 – Tetracyanometallate Complexes). There have been numerous reviews of inter-valence electron transfer discussing various theoretical aspects of these processes and further discussion will not be made here.[3-6]

Many mixed-valence materials of contemporary interest are derived from a common $[L_xM]$-B-$[ML_x]$ structure, in which two (redox-active) metal fragments ML_x, featuring a metal centre in oxidation state n, are linked by some bridging ligand, B. The mixed valence state is generated by *one-electron* oxidation (or reduction) of the assembly. One of the earliest, and most thoroughly studied examples of such a bimetallic bridged species is the ruthenium-based mixed valence complex $[\{(NH_3)_5Ru\}_2pyr]^{n+}$ (n = 5) (Figure 1.1), also known as the "Creutz-Taube Ion".[7]

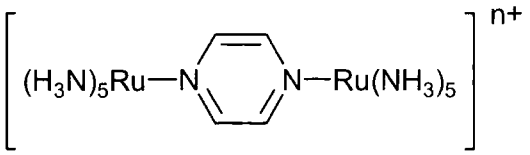

Figure 1.1. The Creutz-Taube ion

In the cases where n = 4 and 6, both the ruthenium centres are in the same oxidation states (Ru^{II} and Ru^{III} respectively). However, in the case where n = 5 the mixed valence (Ru^{II}/Ru^{III}) complex is formed. There has been much debate as to whether the mixed-valence form of the Creutz-Taube ion falls into the Class 2 or Class 3 grouping. The electronic absorption spectrum of the mixed-valence complex reveals a narrow, solvent-independent band in the NIR region and EPR data suggests that the odd-electron occupies an orbital that lies along this Ru-pyr-Ru axis, all of which is consistent with a Class 3 compound.[7-10] However, Mössbauer spectroscopy has been used to demonstrate that equal numbers of Ru^{II} and Ru^{III} centres occur in the mixed-valence species and the molecular structure obtained at 100 K for the tosylate salt has shown that slightly different geometries exist at either ruthenium centre which suggests Class 2 behaviour.[11,12] Whilst some recent theoretical work has concurred with the Class 2 designation of the mixed-valence complex, other results suggest Class 3.[13,14] The debate surrounding the Creutz-Taube ion has highlighted the somewhat "fuzzy" distinction between the Class 2/Class 3 divide and even led to the recent suggestion that such compounds should be given their own classification.[15]

The fascination with the Creutz-Taube ion has led to a host of studies of mixed-valence compounds featuring various combinations of metals, supporting ligands and bridging moieties. Of particular interest to this research group are those compounds

bearing polycarbon (C_n) and cyano/nitrile (C≡N) based bridging ligands. A general description of recent work in this area will follow for the remainder of this introduction whilst each following chapter will contain a specific discussion of elements related to the work therein.

Cyanide Bridges

The cyanide moiety $^-$[C≡N] has been used to bridge an extensive range of metal centres and the synthesis and electrochemistry of such compounds have been described in a large number of review articles,[17-21] although it is only relatively recently that similar investigations of yndiyl (C_2^{2-}) bridged complexes have been undertaken in detail.[22] Chapter 4 contains a discussion of the electrochemical and mixed-valence nature of cyanide-bridged compounds but some general features of cyanide bridges in comparison to acetylenic bridges should be made at this point.

The simple substitution of one atom for another between the cyano and alkynyl moieties is fundamental to the differences between the $[C{\equiv}N]^-$ and $[C{\equiv}C]^{2-}$ ligands. The presence of the nitrogen centre in cyanide generates a net dipole in the fragment and means that it is no longer a symmetrical ligand in contrast to the alkyne dianion $[C{\equiv}C]^{2-}$ (the point group of the cyano moiety is $C_{\infty v}$, whilst that of the acetylene fragment is $D_{\infty h}$). This inherent dipole moment, combined with the differing bonding characteristics of the carbon and nitrogen centres (see below) opens up the possibility of differing properties between bridging isomers of the same material.

The two ends of the ambidentate cyanide ion coordinate to metal centres in different manners. The carbon centre coordinates to a metal centre via a σ-interaction with a metal orbital of σ-symmetry as well as a π-type back-bonding interaction from the metal d-orbitals into the π* anti-bonding orbitals of the cyano moiety. In contrast, the interaction between the nitrogen atom and a metal centre is predominantly a σ-interaction between the σ* orbital of the cyano moiety (formally located at the lone pair on the nitrogen atom) and a σ-symmetry metal orbital.[23] This results in the carbon end of the cyanide bridge behaving as a strong-field ligand with an affinity for more electron-rich metal centres whilst the nitrogen end acts as a medium-field ligand with a preference for more electron-poor metal centres. Thus, for example, in the infinite network Prussian Blue structure, the carbon atom is always coordinated to the Fe^{II} centre whilst the nitrogen atom is coordinated to the Fe^{III} centre.[17,24]

Whilst the orientation of the CN moiety in Prussian Blue may be invariant (Fe^{II}-CN-Fe^{III}), the structures of some of its analogues are not. Shriver and co-workers used a combination of spectroscopic, magnetic and X-ray methods to demonstrate thermal CN isomerism in Fe/Cr, Fe/Mn, and Co/Cr Prussian Blue analogues whilst the first pair of *molecular* compounds showing cyanide isomerism was the $[\{Co(NH_3)_5\}(\mu\text{-}C\equiv N)\{Co(CN)_5\}]$ and $[\{Co(CN)_5\}(\mu\text{-}C\equiv N)\{Co(NH_3)_5\}]$ couple prepared by Haim and co-workers.[25-29] Spontaneous isomerism of the cyanide bridge has also been observed. For example, both the reaction of $[Ag(CN)_2]^-$ with $[ML_n]^+$ *and* the reaction of AgCN with ML_nCN (ML_n = $Ru(PPh_3)_2Cp$, Fe(dppe)Cp) results in the formation of $[\{ML_n\}(\mu\text{-}C\equiv N)Ag(CN)]$ (Figure 1.2). Reaction of the product with a second metal end cap results in the trimetallic system $[\{ML_n\}(\mu\text{-}C\equiv N)Ag(\mu\text{-}N\equiv C)\{ML_n\}]^+$.

Irrespective of the cyanide coordination in the starting materials, the products have been shown to always contain silver-isocyanide coordination.[30]

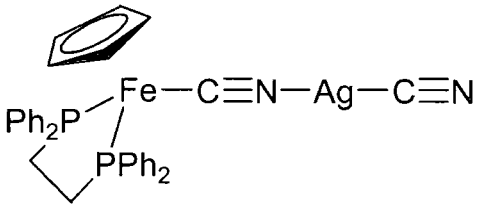

Figure 1.2. Isocyanide coordination to a silver centre.

Vahrenkamp has investigated a series of bridging isomers of general type $ML_n(\mu\text{-}C{\equiv}N)M'L_n$ and these compounds clearly demonstrate the effect of cyanide isomerism on the physical properties of these materials. For example, the Fe-P bond lengths in the compound [{Fe(dppe)Cp}(μ-C≡N){$Cr(CO)_5$}] (2.184(1) and 2.187(1) Å) are significantly shorter than those in the bridging isomer [{Fe(dppe)Cp}(μ-N≡C){$Cr(CO)_5$}] (2.200(1) and 2.204(1) Å). In addition, the ν(C≡N) stretching frequencies were shown to differ depending on the orientation of the cyano moiety (Table 1.1) as well as the oxidation potentials (Table 1.2).[31]

Table 1.1. IR stretching frequencies of cyano-bridged complexes and their bridging isomers

Metal Centre 1	Metal Centre 2	$\nu(C\equiv N)^a$ (cm^{-1})	$\nu(C\equiv N)^b$ (cm^{-1})
$Cr(CO)_5$	$Fe(CO)_2Cp$	2132	2157
$Cr(CO)_5$	Fe(dppe)Cp	2115	2103
$W(CO)_5$	$Fe(CO)_2Cp$	2134	1251
$Fe(CO)_2Cp$	$Mn(CO)_2Cp$	2147	2094
Fe(dppe)Cp	$Mn(CO)_2Cp$	2105	2087

[a]Denotes stretching frequency for complex with C-terminus bound to metal centre 1, [b]Denotes stretching frequency for complex with C-terminus bound to metal centre 2.[31]

Table 1.2. Oxidation potentials of cyano-bridged complexes and their bridging isomers[a]

Metal Centre 1	Metal Centre 2	E_{OX}^b (V)	E_{OX}^c (V)
$Cr(CO)_5$	$Fe(CO)_2Cp$	+0.80	+0.68
$Cr(CO)_5$	Fe(dppe)Cp	+0.28, +0.97	+0.46, +0.91
$Fe(CO)_2Cp$	$Mn(CO)_2Cp$	+0.02	+0.24
Fe(dppe)Cp	$Mn(CO)_2Cp$	+0.18, +0.70	+0.00, +0.61

[a]Measured in CH_2Cl_2 vs. Ag/AgCl, [b]Denotes oxidation potentials for complex with C-terminus bound to metal centre 1, [c]Denotes oxidation potentials for complex with C-terminus bound to metal centre 2.[31]

Transition Metal C_n-Bridged Species

There has been a great deal of interest in systems bridged by polyynyl ligands $(C{\equiv}C)_n$. A polyynyl ligand is perhaps one of the simplest forms of a "molecular wire", being a chain of unsaturated carbon atoms C_n. Compounds bearing polyynyl bridging ligands have been extensively reviewed of late.[22]

By far the most common systems are those bridged by the diyndiyl dianion $[C{\equiv}CC{\equiv}C]^{2-}$ (i.e. n =2), resulting in a range of bimetallic complexes bearing both identical (Table 1.3) and differing (Table 1.4) metal end-caps. Of particular interest to this research group are those systems bearing group 8 metal end-caps, and the electrochemistry of the group 8 diyndiyl-bridged systems is discussed in Chapter 7.

Table 1.3. Diydiyl bridged systems bearing identical metal end-caps

Metal end-cap	Reference
$Mo(CO)_3Cp$	32
$Mo(CO)_2Tp'$	33
$W(CO)_3Cp$	32
$W(CO)_2Tp'$	33
$W(CO)_3Cp^*$	34
$W(O)_2Cp^*$	34
$Mn(dmpe)_2I$	35
$Mn(C{\equiv}CH)(dmpe)_2$	36
$Re(NO)(PPh_3)Cp^*$	37
$Re(NO)(P(tol)_3)Cp^*$	38
$Re(NO)(P(C_6H_4\text{-}4\text{-}^tBu)_3)Cp^*$	38
$Re(CO)_3(bpy)$	39
$Fe(CO)_2Cp$	40
$Fe(dppe)Cp^*$	41
$Fe(dippe)Cp^*$	42
$Ru(PPh_3)_2Cp$	43
$Ru(PPh_3)(PMe_3)Cp$	44
$Ru(dppe)Cp$	45
$Ru(dppm)Cp^*$	46
$Ru(dppe)Cp^*$	46
cis-$RuCl(bpy)_2$	47
trans-$Rh(CO)(PiPr_3)_2$	48
trans-$RhH(=C=CHPh)(PiPr_3)_4$	48
trans-$RhH(C{\equiv}CPh)(PiPr_3)_3$	48
trans-$RhHCl(PiPr_3)_2$	49
trans-$RhHCl(py)(PiPr_3)_3$	49
trans-$IrCl(CO)(NCMe)(PPh_3)_2$	50
$Ni(CN)(NH_3)_3$	51
$Ni(PPh_3)Cp$	40
$PdCl(PnBu_3)_2$	52
$PtCl(PnBu_3)_2$	53
PtMe(cod)	54
$Pt(C_6F_5)(P(tol)_3)_2$	55
$Au(PCy_3)$	56

Table 1.4. Diyndiyl bridged systems bearing non-identical metal end-caps

Metal end-cap (1)	Metal end-cap (2)	Ref
$W(CO)_3Cp$	$Mo(CO)_3Cp$	57
$W(CO)_3Cp$	$Mn(CO)_5$	57
$W(CO)_3Cp$	$Ru(CO)_2Cp$	57
$W(CO)_3Cp$	$Ru(PPh_3)_2Cp$	57
$W(CO)_3Cp$	$Au(PPh_3)$	57
$W(CO)_3Cp$	$M(CO)(PPh_3)_2$; M = Rh, Ir	58
$Re(NO)(PPh_3)Cp^*$	trans-$Rh(CO)(PPh_3)_2$	59
$Re(NO)(PPh_3)Cp^*$	trans-$Pd(PEt_3)_2Cl$	59
$Fe(CO)(L)Cp$; L = CO, PPh_3	$M(CO)_3Cp$; M = W, Mo	60
$Fe(CO)_2Cp$	$Fe(CO)(PPh_3)Cp$	60
$Fe(dppe)Cp^*$	$Fe(CO)_2Cp^*$	61
$Fe(dppe)Cp^*$	$Fe(CO)_2(\eta^5\text{-}C_5Ph_5)$	61
$Fe(dippe)Cp^*$	$Fe(CO)_2Cp^*$	42
$Fe(dppe)Cp^*$	$Re(NO)(PPh_3)Cp^*$	62
$Fe(dppe)Cp^*$	$Ru(dppe)Cp^*$	63
$Fe(dppe)Cp^*$	$Ru(PPh_3)_2Cp$	63
Cu(triphos)	$Au(P(tol)_3)$	64

There are two general synthetic routes to the formation of these diyndiyl systems. Firstly the two metal centres may be added to a central diynyl "building block". This addition of two metal centres may be performed simultaneously (to form complexes bearing identical end-caps) or sequentially (for those complexes bearing differing metal end-caps). For example, due to the acidic nature of the acetylenic protons of butadiyne, the metal complex may be reacted with the diynyl dianion directly as shown below (Scheme 1.1).

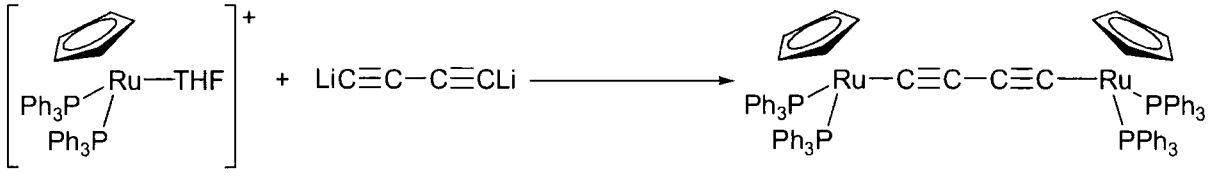

Scheme 1.1. Reaction of $[Ru(thf)(PPh_3)_2Cp][PF_6]$ with $LiC{\equiv}CC{\equiv}CLi$.[43]

In addition to the reaction with lithiated alkynes, metal complexes may be reacted with trialkyl-silyl reagents or with tetravalent tin butadiynes. For example, the di-ruthenium complex in Scheme 1 has been synthesized from reaction of $Me_3SiC{\equiv}CC{\equiv}CSiMe_3$ with potassium fluoride in methanolic solution[43] whilst Stille coupling of $Me_3SnC{\equiv}CC{\equiv}CSnMe_3$ with metal halides and using a Pd^0 catalyst has also been reported for complexes bearing iron (Scheme 1.2), molybdenum and tungsten centres.[65,66]

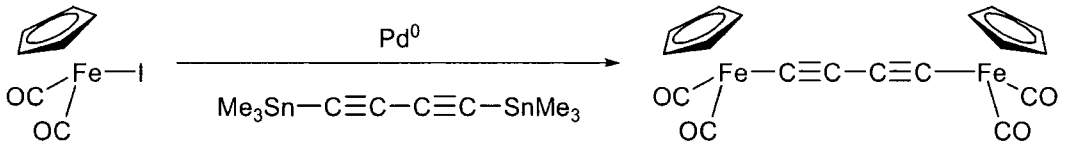

Scheme 1.2. Coupling of $FeI(CO)_2Cp$ with $Me_3SnC{\equiv}CC{\equiv}CSnMe_3$.[65]

Sequential addition of the metal termini may be achieved using the methods described above or by coupling of an "activated" butadiyne $HC{\equiv}CC{\equiv}CSiMe_3$ with a metal complex followed by a second reaction. Naturally enough this is the main method for the formation of complexes with non-identical end-groups.

The second general route for the formation of diyndiyl bridged bimetallic systems is by oxidative coupling of metal acetylides. Reaction of two equivalents of the metal acetylides $M(C{\equiv}CH)L_2Cp$ (M = Ni, L = PPh_3; M = Fe, L = CO) in the presence of copper chloride and oxygen (Hay conditions[67]) resulted in the formation of the bimetallic products shown in Scheme 1.3 whilst coupling of the C≡CH moieties in the

rhenium acetylide $Re(C{\equiv}CH)(PPh_3)(NO)$ using $Cu(OAc)_2$ in pyridine solution has also been demonstrated.[68]

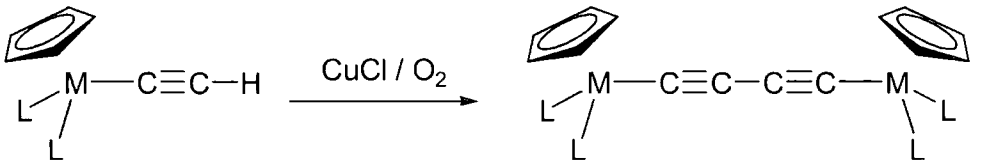

Scheme 1.3. Hay coupling of $M(C{\equiv}CH)L_2Cp$ (M = Ni, L = PPh3; M = Fe, L = CO).[40]

Lapinte and co-workers demonstrated an alternate method for the coupling of metal acetylide complexes in 1995 with the formation of the iron butadiynyl complex $[\{Fe(dppe)Cp^*\}_2(\mu\text{-}C{\equiv}CC{\equiv}C)]$ via a two-step *radical* coupling procedure.[41] The iron acetylide $Fe(C{\equiv}CH)(dppe)Cp^*$ was oxidised with ferrrocinium hexafluorophosphate to give the 17-electron species $[Fe(C{\equiv}CH)(dppe)Cp^*][PF_6]$. The steric crowding about the iron centre provided by the bulky supporting ligands prevents the metal centres from approaching close enough to allow the expected dimerisation.[69,70] Instead coupling occurs via the terminal carbon atoms of the acetylide ligand to give the *bis*-vinylidene complex $[\{Fe(dppe)Cp^*\}{=}C{=}CHCH{=}C{=}\{Fe(dppe)Cp^*\}][PF_6]_2$ (Scheme 1.4). Subsequent treatment with potassium *tert*-butoxide yields the butadienyl complex $[\{Fe(dppe)Cp^*\}_2(\mu\text{-}C{\equiv}CC{\equiv}C)]$.

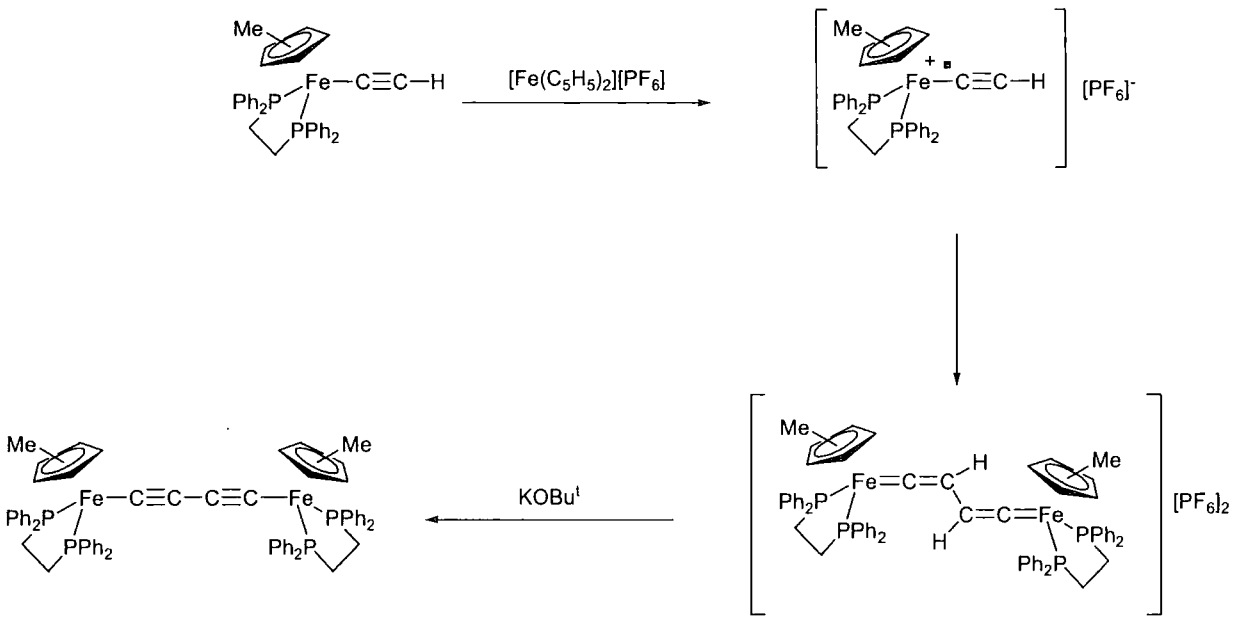

Scheme 1.4. Synthesis of [{Fe(dppe)Cp*}$_2$(μ-C≡CC≡C)]

Several systems have been isolated with chains longer than four carbon atoms, although these are much less common due to the difficulties presented in their synthesis. As with the diyndiyl compounds described above, copper catalysed coupling reactions have been used to couple M(C≡CC≡CH)L_nCp' materials to create materials with C_8 bridges bearing the metal end-caps [W(CO)$_3$Cp], [Fe(CO)$_2$Cp], [Re(NO)(PPh$_3$)] and [Fe(dppe)Cp*].[32,71-73]

Broadly speaking, the two successive oxidations in bimetallic bridged species can indicate electronic communication between the two metal centres and a greater separation between successive oxidations can be an indication of the strength of this interaction (see Chapter 4 for more detail). In investigations into the electrochemical behaviour of the compounds [{Re(NO)(PPh$_3$)}$_2$(μ-C_8)] and [{Fe(dppe)Cp*}$_2$(μ-C_8)] two, successive one-electron oxidations were observed.[72,73] In both cases the

difference in potential between the first and second oxidations of the C_8 complexes is lower than that found for the C_4 analogues. Whilst the redox behaviour of the C_8 systems suggests that there is poorer communication between the metal end-caps via the longer carbon chain, it must be noted that electrochemical measurements alone are not sufficient to elucidate details of electronic structure.

Gladysz *et al.* extended the study of C_n-bridged species to investigate longer carbon chains and managed to synthesise systems of type $[\{Re(NO)(PPh_3)\}_2(\mu\text{-}C_n)]$ with carbon bridges of up to 20 atoms in length.[74] As with the materials above, it was observed that increasing the length of the carbon chain reduced the gap between the first and second oxidation potentials. In the case of the 20 carbon atom chain only a single, apparently two-electron oxidation was observed and this indicates the length at which the electronic communication between the remote rhenium centres ceased.

Ferrocenyl Species C_n-Bridged Species

Ferrocene $[Fe(\eta^5\text{-}C_5H_5)_2$, FcH] behaves as a stable, one electron redox systems (and hence is often used as a reference in electrochemical measurements) and it is therefore unsurprising that it should be used as a metal end-cap in investigations of mixed-valence compounds.[75] The acetylide bridged species FcC≡CFc (diferrrocenylacetylene, DFA) was first synthesised in 1966 and the electrochemical behaviour was probed by Cowan and co-workers eight years later.[76,77] DFA was found to undergo two, reversible one-electron oxidations with a separation of 130 mV between the two oxidation events indicating a moderate degree of interaction between

the two metal centres. As with the systems discussed above, increasing the length of the carbon chain was found to reduce the separation of the oxidation events, becoming a single oxidation event in the tetrayne species $Fc(C{\equiv}C)_4Fc$.[78,79]

The electronic absorption spectra of the compounds $[Fc(C{\equiv}C)_nFc]^{m+}$ (n = 1, 2; m = 0, 1, 2) have also been obtained.[78] Low intensity absorption bands that were found in the NIR region of the spectra for the mono-oxidised species, but were absent in both the neutral and di-oxidised materials, were assigned to IVCT transitions. It is notable that the energy of the IVCT bands increases with chain length (n = 1, λ_{max} = 1560 nm; n= 2, λ_{max} = 1180 nm), reflecting the decrease in metal-metal communication with increasing chain length demonstrated by the electrochemical data.

In addition to the singly bridged species, the doubly bridged material has also been isolated and electrochemically characterised (Figure 1.3).[78]

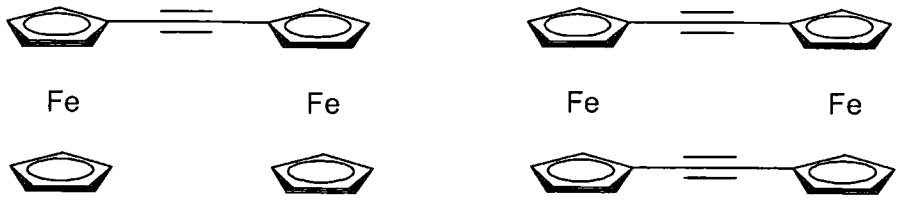

Figure 1.3. Singly and doubly acetylene-bridged ferrocenes.

The doubly bridged material shows a far greater separation of redox potentials than the singly bridged species (355 mV vs 130 mV respectively). In addition, the IVCT band associated with mono-oxidised version of the doubly bridged species was moved

to much lower energy (λ_{max} = 1760 nm). Thus the addition of a second acetylene bridge between the end-caps strengthens the metal-metal interaction.

Aromatic Spacer Groups

In the case of acetylide-bridged ferrocene systems such as those described above, the introduction of an aromatic moiety into the acetylene chain to create a diethynyl aromatic bridge results in a large decrease in the separation of oxidation potentials.[80-85] The cyclic voltammograms of the diethynyl aromatic bridged ferrocenes display oxidation waves that arise either from single, two-electron processes or (in the case of voltammograms with large peak-peak separations) oxidation events that are very poorly separated. Interestingly, the 2,5-diethynlpyridine bridged ferrocene system (Figure 1.4) undergoes a single oxidation event unless the nitrogen centre of the pyridine moiety is methylated, in which case two oxidation events with a separation of 160 mV are observed.[86]

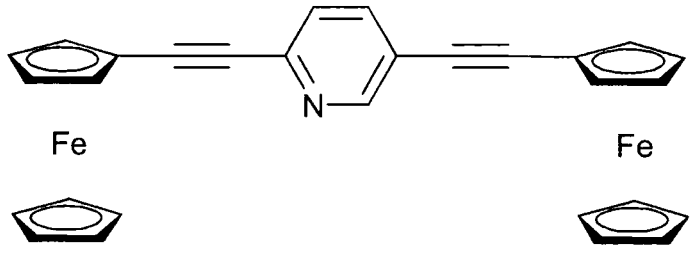

Figure 1.4. 2,5-*bis*(ferrocenethynyl)pyridine

Whilst addition of an aromatic moiety into the ethynyl bridge in these ferrocene-capped compounds reduces the degree of interaction between the redox-active centres,

different behaviour is observed when those centres are incorporated directly into the π-system of the bridging ligand. Whilst there have been many preparations reported of diethynyl aromatic-bridged metal complexes of general type ML_n-C≡C-Ar-C≡C-ML_n, surprisingly few have been subjected to electrochemical study. There have been several studies of compounds bearing pseudo-octahedral metal end-caps and it has been shown that the degree of interaction between the metal centres in such systems is sensitive to the nature of the end-caps.[87-91] Thus the electron-rich di-iron complex [*trans*-{FeCl(dmpe)$_2$}$_2$(μ-1,4-C≡CC_6H_4C≡C)] undergoes two, one electron oxidation processes separated by 200 mV, whilst the *bis*-bimetallic complex [{Ru_2(ap)$_4$}$_2$(μ-1,4-C≡CC_6H_4C≡C)] (ap = 2-anilinopyridinate) undergoes a single, two-electron oxidation event.[87,92]

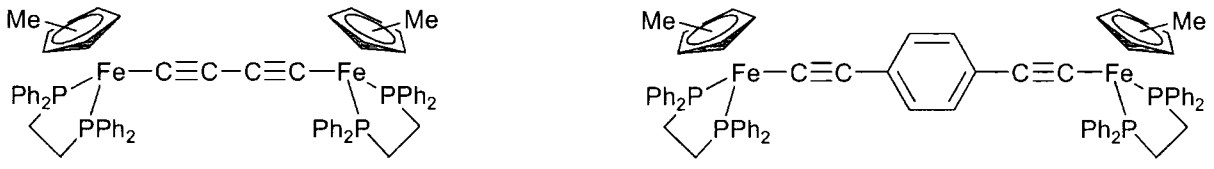

Figure 1.5. The di-iron complexes [{Fe(dppe)Cp*}$_2$(μ-C≡CC_2≡C)] and [{Fe(dppe)Cp*}$_2$(μ-1,4-C≡CC_6H_4C≡C)]

The di-iron complex [{Fe(dppe)Cp*}$_2$(μ-1,4-C≡CC_6H_4C≡C)] bears an obvious resemblance to the diyndiyl bridged system [{Fe(dppe)Cp*}$_2$(μ-C≡CC_2≡C)] (Figure 1.5) The diyndiyl complex undergoes two, reversible one-electron oxidation processes separated by 700 mV whilst the incorporation of the phenyl group into the bridging ligand reduces the separation of the oxidation events to 260 mV. Whilst the addition of the phenyl spacer has reduced the interaction between the two metal centres it is clear that the ligand is still capable of mediating a degree of electronic communication

between the two over a distance of 12 Å.[41,90] The use of a thiophene moiety as the aromatic spacer resulted in a potential separation of 340 mV, larger than that observed for the phenyl spacer but still less than in the diyndiyl system.[93]

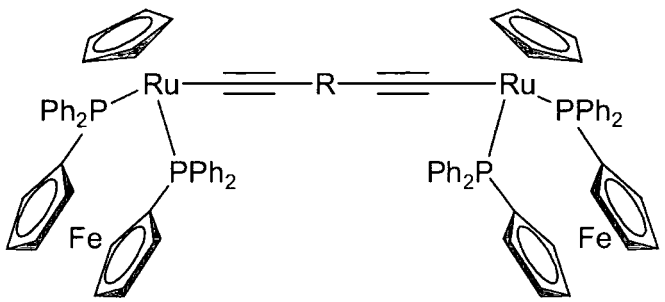

Figure 1.6. diethynyl aromatic bridge between [Ru(dppf)Cp] centres (R = 0, 1,4-benzenediyl, 1,4- naphthalenediyl, 9,10-anthracenediyl)

Chen and co-workers have investigated a series of compounds of type [{Ru(dppf)Cp}(μ-C≡C-R-C≡C)] (dppf = 1,1'-bis(dphenylphosphino)ferrocene, R = 0, 1,4-benzenediyl, 1,4- naphthalenediyl, 9,10-anthracenediyl) (Figure 1.6), synthesised by reaction of the metal chloride RuCl(dppf)Cp with the appropriate $Me_3SiC{\equiv}C\text{-}R\text{-}C{\equiv}CSiMe_3$ ligand and KF. For each of these compounds, two one-electron oxidation processes corresponding to the stepwise oxidation of the ruthenium centres was observed. The separation of these oxidation events was greatest for the diynyl system (650 mV) whilst each of the compounds with the aromatic spacer in the bridging ligand showed smaller separations (260-290 mV). Each of the complexes [{Ru(dppf)Cp}(μ-C≡C-R-C≡C)], with the exception of that where R = 1,4-benzenediyl, were chemically oxidised to the mono-cations and isolated as the $[PF_6]^-$ salts. The electronic absorption spectra of each mono-cation showed an IVCT transition in the NIR region of the spectrum. In the case of the diyndiyl-bridged

complex this transition was observed as a sharp absorption band at 906 nm and was assigned as arising from a Class 3 mixed-valence complex on the basis of the band's sharpness and the coupling constant derived from Hush-analysis. In the napthyl and anthryl complexes, IVCT bands were also observed, although the slight solvent dependence of these bands and the reduced coupling constant derived from them suggested that those materials with an aromatic spacer in the bridging ligand were Class 2 compounds. Thus the electronic absorption spectra are in agreement with the electrochemical data for these compounds and suggest that the diethynyl aromatic bridges are capable of mediating electronic communication between the metal end-caps, albeit with a reduced effectiveness compared to the diethynyl bridged species.[94]

Considering the similarities the cyanoacetylene (RC≡CC≡N) and cyanoacetylide ([C≡CC≡N]) ligands bear to both the cyanide and diyndiyl moieties it is somewhat surprising that these system remain relatively unexplored. Those materials that have been isolated and characterised are discussed in later chapters (see Chapters 5 and 6). Few deliberate syntheses of η^1-coordinated cyanoacetylides have been reported and, prior to the work contained herein, no cyanoacetylide-bridged materials have been studied.

In this study, a novel synthesis of the metal cyanoacetylides has been developed. Their coordination chemistry has been explored along with the physical and electrochemical behaviour of both the cyanoacetylide "metallo-ligand" and its coordination products. Prior to this, however, a systematic study of the coordination of: 1) a series of para-substituted benzonitrile ligands and 2) the cyanoacetylene ligands $NCC{\equiv}CC_6H_5$ and $NCC{\equiv}CC_6H_4$-4-NMe_2 to metal centres was undertaken in

order to better understand the nature of the interaction between the C≡N moiety and a metal centre. In addition, the use of group 10 tetracyanometallates as bridging ligands between two metal centres was studied in order to gain some understanding of role the individual metal centres and supporting ligands might play on any electronic interactions which might occur through the tetracyanometallate bridge.

References

1 A. Ludi, *J. Chem. Educ.*, 1981, **58**, 1013.

2 M. B. Robin, P. Day, *Advan. Inorg. Chem. Radiochem.*, 1967, **10**, 247.

3 C. Creutz, *Prog. Inorg. Chem.*, 1983, **30**, 1.

4 B. S. Brunschwig, C. Creutz, N. Sutin, *Coord. Chem. Rev.*, 1998, **177**, 61.

5 J.-P. Launay, *Chem. Soc. Rev.*, 2001, **30**, 386.

6 B. S. Brunschwig, C. Creutz, N. Sutin, *Chem. Soc. Rev.*, 2002, **31**, 168.

7 C. Creutz, H. Taube, *J. Am. Chem. Soc.*, 1969, **91**, 3988.

8 C. Creutz, H. Taube, *J. Am. Chem. Soc.*, 1973, **95**, 1086.

9 C. Creutz, M. H. Chou, *Inorg. Chem.*, 1987, **26**, 2995.

10 A. Stebler, J. H. Ammeter, U. Fürholtz, A. Ludi, *Inorg. Chem.*, 1984, **23**, 2764.

11 C. Creutz, M. L. Good, S. Chandra, *Inorg. Nucl. Chem. Lett.*, 1973, **9**, 171.

12 U. Fürholtz, S. Joss, H. A. Bürgi, A. Ludi, *Inorg. Chem.*, 1985, **24**, 9143.

13 A. Broo, P. Lincoln, *Inorg. Chem.*, 1997, **36**, 2544.

14 A. Bencini, I. Ciofini, C. A. Daul, A. Ferretti, *J. Am. Chem. Soc.*, 1999, **121**, 11418.

15 K. D. Demadis, C. M. Hartshorn, T. J. Meyer, *Chem. Rev.*, 2001, **101**, 2655.

16 A. Vogler, A. H. Osman, H. Kunkely, *Coord. Chem. Rev.*, 1985, **64**, 159.

17 F. Scandola, R. Argazzi, C. A. Bignozzi, C. Chiorboli, M. T. Indelli, M. A. Rampi, *Coord. Chem. Rev.*, 1993, **125**, 283.

18 W. P. Fehlhammer, M. Fritz, *Chem. Rev.*, 1993, **93**, 1243.

19 K. Kalyanasundaram, Md. K. Nazeeruddin, *Inorg. Chim. Acta*, 1994, **226**, 213.

20 K. R. Dunbar, R. A. Heintz, *Prog. Inorg. Chem.*, 1997, **45**, 283

21 H. Vahrenkamp, A. Geiβ, G. N. Richardson, *J. Chem. Soc., Dalton Trans.*, 1997, 3643.

22 M. I. Bruce, P. J. Low, *Adv. Organomet. Chem.*, 2004, **50**, 179.

23 D. F. Shriver, *Struct. Bonding*, 1966, **1**, 32.

24 H. J. Buser, D. Schwarzenbach, W. Petter, A. Ludi, *Inorg. Chem.*, 1977, **16**, 2704.

25 D. F. Shriver, S. A. Shriver, S. E. Anderson, *Inorg. Chem.*, 1965, **4**, 725.

26 D. B. Brown, D. F. Shriver, L. H. Schwartz, *Inorg. Chem.*, 1968, **7**, 77.

27 D. B. Brown, D. F. Shriver, *Inorg. Chem.*, 1969, **8**, 42.

28 R. A. de Castello, C. P. McColl, N. B. Egen, A. Haim, *Inorg. Chem.*, 1969, **8**, 699.

29 R. A. Castello, C. P. McColl, A. Haim, *Inorg. Chem.*, 1971, **10**, 23

30 V. Comte, Z.-N. Chen, M.-L. Flay, H. Vahrenkamp, *J. Organomet. Chem.*, 2000, **614-615**, 131.

31 N. Zhu, H. Vahrenkamp, *Chem. Ber./Recueil*, 1997, **130**, 1241.

32 M. I. Bruce, M. Ke, P. J. Low, *J. Chem. Soc., Chem. Commun.*, 1996, 2405.

33 B. E. Woodworth, P. S. White, J. L. Templeton, *J. Am. Chem. Soc.*, 1997, **119**, 828.

34 R. L. Roberts, H. Puschmann, J. A. K. Howard, J. H. Yamammoto, A. J. Carty, P. J. Low, *J. Chem. Soc., Dalton Trans.*, 2003, 1099.

35 S. Kheradmandan, K. Heinze, H. W. Schmalle, H. Berke, *Angew. Chem. Int. Ed. Engl.*, 1999, **38**, 2270.

36 F. J. Fernandez, L. Blacque, M. Alfonso, H. Berke, *Chem. Commun.*, 2001, 1266.

37 Y. Zhou, J. W. Sweyler, W. Weng, A. M. Arif, J. A. Gladysz, *J. Am. Chem. Soc.*, 1993, **115**, 8509.

38 W. E. Meyer, A. J. Amoroso, C. R. Horn, M. Jaeger, J. A. Gladysz,

Organometallics, 2001, **20**, 1115.

39 V. W.-W. Yam, V. C.-Y. Lau, K.-K Cheiung, *Organometallics*, 1996, **15**, 1740.

40 J. Kim, H. Masai, K. Sonogoshira, N. Hagihara, *Inorg. Nucl. Chem. Lett.*, 1970, **6**, 181

41 N. Le Narvor, L. Toupet, C. Lapinte, *J. Am. Chem. Soc.*, 1995, **117**, 7129.

42 M. Guillemot, L. Toupet, C. Lapinte, *Organometallics*, 1998, **17**, 1928.

43 M. I. Bruce, P. Hinterding, B. W. Skelton, E. R. T. Tiekink, A. H. White, *J. Organomet. Chem.*, 1993, **450**, 209.

44 M. I. Bruce, L. I. Denisovich, P. J. Low, S. M. Peregudova, A. N. Ustynyuk, *Mendeleev Commun.*, 1996, 200.

45 M. I. Bruce, B. G. Ellis, M. Gaudio, C. Lapinte, G. Melino, F. Paul, B. W. Skelton, M. E. Smith, L. Toupet, A. H. White, *Dalton Trans.*, 2004, 1601.

46 M. I. Bruce, B. G. Ellis, P. J. Low, B. W. Skelton, A. H. White, *Organometallics*, 2003, **22**, 3184.

47 E. Stein, S. Oki, E. J. S. Vichi, *J. Braz. Chem. Soc.*, 2000, **11**, 252.

48 O. Gevert, J. Wolf, H. Werner, *Organometallics*, 1996, **15**, 2806.

49 T. Rappert, O. Nurnberg, H. Werner, *Organometallics*, 1993, **12**, 1359.

50 P. J. Stang, R. Tykwinski, *J. Am. Chm. Soc.*, 1992, **114**, 4411.

51 R. Nast, F. Z. Urban, *Anorg. Allg. Chem.*, 1957, **289**, 244.

52 K. Sonogoshira, S. Kataoka, S. Takahashi, N. Hagihara, *J. Organomet. Chem.*, 1978, **160**, 319.

53 S. Takahashi, E. Murata, S. Sonogashira, N. Hagihara, *J. Poly. Sci. Polym. Chem. Ed.*, 1980, **18**, 661.

54 A. Klein, K.-W. Klinkhammer, T. Scheiring, *J. Organomet. Chem.*, 1999, **592**,

128.

55 G. R. Owen, F. Hampel, J. A. Gladysz, *Organometallics*, 2004, **23**, 5893.

56 C.-M. Che, H.-Y. Chao, V. M. Miskowski, Y. Li, K.-K. Cheung, *J. Am. Chem. Soc.*, 2001, **123**, 4985.

57 M. I. Bruce, P. J. Low, M. Ke, B. D. Kelly, B. W. Skelton, M. E. Smith, A. H. White, N. B. Witton, *Aust. J. Chem.*, 2001, **54**, 453.

58 M. I. Bruce, B. G. Ellis, B. W. Skelton, A. H. White, *J. Organomet. Chem.*, 2000, **607**, 137.

59 W. Weng, T. Bartik, M. Brady, B. Bartik, J. A. Ramsden, A. M. Arif, J. A. Gladysz, *J. Am. Chem. Soc.*, 1995, **117**, 11922.

60 A. Wong, P. C. W. Kang, C. D. Tagge, D. R. Leon, *Organometallics*, 1990, **9**, 1992.

61 F. Coat, M.-A., Guillevic, L. Toupet, F. Paul, C. Lapinte, *Organometallics*, 1997, **16**, 5988.

62 F. Paul, W. E. Meyer, L. Toupet, H. Jiao, J. A. Gladysz, C. Lapinte, *J. Am. Chem. Soc.*, 2000, **122**, 9405.

63 M. I. Bruce, K. Costuas, T. Davin, B. G. Ellis, J.-F. Halet, C. Lapinte, P. J. Low, M. E. Smith, B. W. Skelton, L. Toupet, A. H. White, *Organometallics*, submitted.

64 M. I. Bruce, M. E. Smith, N. N. Zaitseva, B. W. Skelton, A. H. White, *J. Organomet. Chem.*, 2003, **670**, 170.

65 R. Crescenzi, C. Lo Sterzo, *Organometallics*, 1992, **11**, 4301

66 E. Viola, C. Lo Sterzo, R. Crescenzi, G. Frachey, *J. Organomet. Chem.*, 1995, **493**, 55.

67 A. S. Hay, *J. Org. Chem.*, 1962, **27**, 3320.

68 M. Brady, W. Weng, Y. Zhou, J. W. Seyler, A. J. Amoroso, A. M. Arif, M. Bohme, G. Frenking, J. A. Gladysz, *J. Am. Chem. Soc.*, 1997, **119**, 775.

69 D. Astruc, *Chem. Rev.*, 1988, **88**, 1189.

70 M. C. Baird, *Chem. Rev.*, 1988, **88**, 1217.

71 M. Akita, M.-C. Chung, A. Sakurai, S. Sugimoto, M. Terada, M. Tanaka, Y. Moro-oka, *Organometallics*, 1997, **16**, 4882.

72 M. Brady, W. Weng, J. A. Gladysz, *J. Chem. Soc., Chem. Commun.*, 1994, 2655.

73 F. Coat, C. Lapinte, *Organometallics*, 1996, **15**, 477.

74 R. Dembinski, T. Bartik, B. Bartik, M. Jaeger, J. A. Gladysz, *J. Am. Chem. Soc.*, 2000, **122**, 810.

75 N.G. Connelly and W.E. Geiger, *Chem. Rev.*, 1996, **96**, 877.

76 M. Rosenblum, N. Braun, J. Papenmeier, M. Applebaum, *J. Organomet. Chem.*, 1966, **6**, 173.

77 C. LeVanda, D. O. Cowan, C. Leitch, K. Bechgaard, *J. Am. Chem., Soc.*, 1974, **96**, 6788.

78 C. LeVanda, K. Bechgaard, D. O. Cowan., *J. Org. Chem.*, 1976, **41**, 2700.

79 C. J. McAdam, J. J. Brunton, B. H. Robinson, J. Simpson, *J. Chem. Soc., Dalton Trans.*, 1999, 2487.

80 P. Jutzi, B. Kleinebekel, *J. Organomet. Chem.*, 1997, **545-546**, 573.

81 K. R. J. Thomas, J. T. Lin, Y. S. Wen, *Organometallics*, 2000, **19**, 1008.

82 Y. Zhu, M. O. Wolf, *J. Am. Chem. Soc.*, 2000, **122**, 10121.

83 W. Y. Wong, G. L. Lu, K. F. Ng, C. K. Wong, K. H. Choi, *J. Organomet. Chem.*, 2001, **637-639**, 159.

84 W. Y. Wong, K. Y. Ho, K. H. Choi, *J. Organomet. Chem.*, 2003, **670**, 17.

85 N. Chawdhury, N. J. Long, M. F. Mahon, L. Ooi, P. R. Raithby, S. Rooke, A. J. P. White, D. J. Williams, M. Younas, *J. Organomet. Chem.*, 2004, **689**, 840.

86 C. Engtrakul, L. R. Sita, *Nano. Lett.*, 2001, **1**, 541.

87 L. D. Field, A. V. George, F. Laschi, E. Y. Malouf, P. Zanello, *J. Organomet. Chem.*, 1992, **435**, 347.

88 D. Beljonne, M. C. B. Colbert, P. R. Raithby, R. H. Friend, J. L. Bredas, *Synth. Met.*, 1996, **81**, 179.

89 O. Lavastre, J. Plass, P. Bachmann, S. Gusemi, C. Moinet, P. H. Dixneuf, *Organometallics*, 1997, **16**, 184.

90 N. Le Narvor, C. Lapinte, *Organometallics*, 1995, **14**, 634.

91 S. K. Hurst, M. P. Cifuentes, A. M. McDonagh, M. G. Humphrey, M. Samoc, B. Luther-Davies, I. Asselberghs, A. Persoons, *J. Organomet. Chem.*, 2002, **642**, 259.

92 S. K. Hurst, T. Ren, *J. Organomet. Chem.*, 2002, **660**, 1.

93 S. Le Stang, F. Paul, C. Lapinte, *Organometallics*, 2000, **19**, 1035.

94 L.-B. Gao, L.-Y. Zhang, L.-X. Shi, Z.-N. Chen, *Organometallics*, 2005, **24**, 1678

Experimental Methods

General Methods

Mass Spectra were recorded on a Micromass LCT instrument running in positive-ion electrospray mode. NMR spectra were recorded on a Varian Unity-300 (^{1}H and ^{31}P) or an INOVA 500 MHz instrument ($^{13}C\{^{1}H\}$). Unless otherwise stated, all spectra were recorded in $CDCl_3$ at ambient temperature and all chemical shifts are reported in δ (ppm). ^{1}H NMR spectra were referenced to residual protio impurity in the solvent ($CHCl_3$, 7.26 ppm). ^{13}C spectra were referenced against the solvent resonance ($CDCl_3$, 77.0 ppm). The following abbreviations are used to describe multiplicities: s (singlet). d (doublet), t (triplet), m (multiplet), br (broad). Infra-red spectra (with the exception of the spectro-electrochemical studies described below) were recorded using a Nicolet Avatar 360 FT-IR controlled by a PC running OMNIC 5.1b. Spectra were recorded either as a Nujol mull between NaCl plates or in a solution cell bearing CaF_2 windows. Elemental analysis was performed by the microanalytical service within the Department of Chemistry at the University of Durham.

Crystallographic data collection and refinement were undertaken by Drs. Puschmann, Batsanov, Yufit, and Albesa-Jové of the Durham Crystallographic service. Their efforts and those of the group leader Prof. J. A. K. Howard are gratefully acknowledged. The description of the crystallographic methods provided by the crystallographers is as follows: X-ray diffraction data were collected on Bruker 3-circle diffractometers equipped with CCD area detectors SMART APEX, SMART 6K or SMART 1K, using graphite-monochromated Mo-K_α radiation from a 60W

microfocus Bede Microsource® with glass polycapillary optics or a sealed tube. The crystals were cooled to 120 K using Cryostream (Oxford cryosystem) open flow N_2 cryostats.

Reflection intensities were integrated using *SAINT* software[1] and corrected for absorption by numerical integration based on crystal face indexing or by semi-empirical method[2] based on Laue equivalents. The structures were solved by direct methods and refined by full matrix least-squares against F^2 of all data using *SHELXTL* software.[3] All non-hydrogen atoms where refined in anisotropic approximation (except minor positions of the disordered atoms) with hydrogen atoms treated in riding model (methyl groups as rigid bodies).

Cyclic Voltammetry

Cyclic voltammetry (CV) is a potential sweep method for studying electrode processes. A cyclic voltammogram is obtained by recording the current intensity observed at a *working electrode* as a function of the applied potential. The applied potential is scanned linearly as a function of time from a potential at which no electrode reaction occurs up to an arbitrary maximum beyond the potential of the electrode reaction. At this point the direction of the potential is reversed and swept linearly back to its original value. The initial sweep (to positive potential) records a cathodic reaction (positive current) by which *heterogeneous electron transfer* occurs at the interface between the solution (in which the species under study is dissolved) and the electrode surface. The reverse sweep records an anodic reaction of the

material back to the original state. A plot of potential vs. current for this process results in a cyclic voltammogram like the one shown below (Figure 2.1).

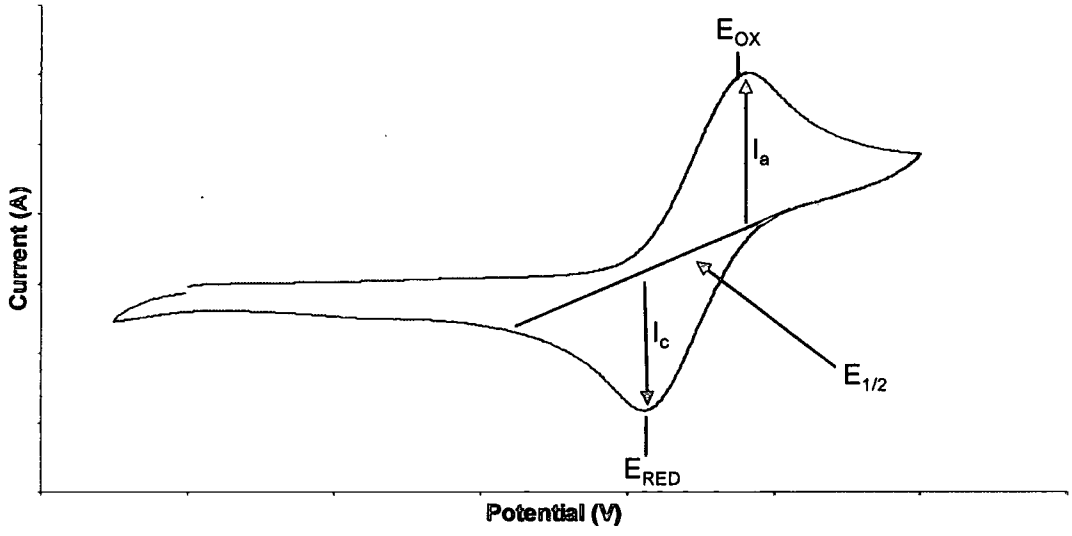

Figure 2.1. A cyclic voltammogram for a single oxidation

In the case shown above, an oxidation occurs as the potential is increased, resulting in an oxidative or anodic wave with a peak current of I_a occurring at a potential E_{OX}. On reversal of the potential sweep, a corresponding reductive or cathodic wave is observed with a peak current of I_c and a potential E_{RED}. The standard redox potential ($E_{1/2}$) of a reversible redox process is defined as the potential midway between E_{OX} and E_{RED}. The ratio of the peak currents for an electrochemically reversible event should be 1. These potentials are measured relative to a standard reference potential (see below).

The sample under study is dissolved in solution using dry solvents which have been purged with dry nitrogen to remove oxygen (which would be apparent in the cyclic voltammogram). As electron transfer can only occur at the electrode/solution

interface, a zone of reacted material builds up around the electrode which is different from the bulk solution and increases as the reaction proceeds. Unreacted material must pass through this zone by diffusion in order to react at the electrode surface and hence this zone of reacted material is referred to as the diffusion layer. In order to ensure that current migrates through the diffusion layer and the bulk solution a supporting, redox-inactive electrolyte is added to the solution. This is added in large excess to ensure that the charge is transferred by the electrolyte and not by the species under study. In this thesis, the electrolytes used were tetra-n-butylammonium tetrafluoroborate ($TBABF_4$) and hexafluorophosphate ($TBAPF_6$). Both of these electrolytes are redox-inactive over a broad potential range.

In order to complete the electrical circuit and allow current to pass requires a second electrode, called the *counter electrode*. A redox reaction also occurs at this electrode and is of an opposite nature to that at the working electrode. In an electrochemical experiment, only differences in potentials can be measured and in order to achieve this a third, independent electrode is required called the *reference electrode*. A reference electrode performs a known electrochemical process at a certain potential which is insensitive to small variations of temperature or the passage of a small current within the solution. Examples include the Saturated Calomel Electrode (SCE) in which the redox reaction occurs between Hg and $HgCl_2$ or the Ag/AgCl electrode.

An alternative to the standard reference electrode, and one used in this thesis, is to use an internal reference instead. In this case the reference electrode is replaced by a pseudo-reference (platinum wire in this case) and a reference species is added to the solution being studied. This reference species is one for which the standard redox

potential of that species under specific conditions (and relative to a known reference potential) is known.

In this study cyclic voltammograms were recorded using an Eco Chemie PGStat 30 controlled by a PC running GPES v4.9 for Windows. The electrochemical cell used was an EG & G PARC micro-cell fitted with a nitrogen feed for the bubbler and purge inlets (Figure 2.2). The working electrodes were EG & G PARC millielectrodes with a 2 mm diameter electrode surface. Counter and pseudo-reference electrodes were platinum wires. Solvents used were deoxygenated by bubbling through with nitrogen prior to taking the measurements and blanketed with nitrogen during the scans.

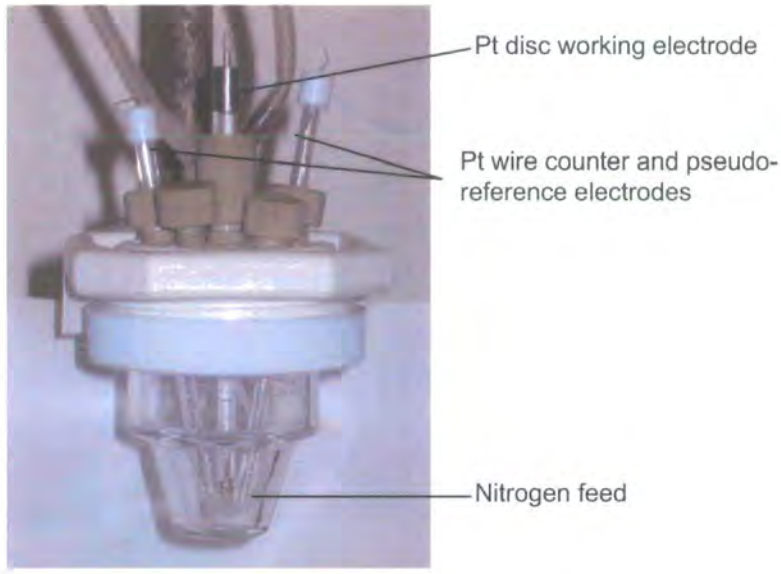

Figure 2.2. Electrochemical cell

Spectro-electrochemistry

Within this thesis, spectro-electrochemical methods are used in order to obtain infra-red (IR) and electronic absorption spectra of oxidised species and thus study some of

the effects of oxidation upon the materials under investigation. By these methods oxidised species are generated in-situ and their spectra acquired. This technique requires that the probe light passes through a solution of the material under study whilst it is in close proximity to the working electrode. In order to achieve this, a metal minigrid is used as the working electrode. These minigrids consist of a fine mesh of a selected metal (platinum in the cases used herein although silver and gold are often used as well) which is inserted into a short pathlength cell along with accompanying reference and counter electrodes. This produces an optically transparent thin layer electrode (OTTLE) cell.[4,5]

The use of a small volume allows bulk electrolysis to be performed in a short space of time. Therefore, the spectrum of the species under study, X, is recorded at a potential where X is stable. The potential applied to the solution of X is then increased step-wise and a new spectrum is acquired at each step after the current has dropped to zero (and thus the system is at electrochemical equilibrium). This provides sequential spectra of the oxidation of X to X^+. In some cases electro-generated species, whilst electrochemically stable in a cyclic voltammogram are insufficiently stable over the longer time-period required for bulk electrolysis. In these circumstances, variable-temperature apparatuses are required in order to reduce the temperature of the solution and hence stabilise the redox product.

Inra-red spectra for spectro-electrochemical studies were collected at the Universiteit van Amsterdam (UvA) using a BioRad FTS-7 spectrometer. Oxidised species were generated using a platinum minigrid working electrode (32 wires/cm) with a platinum wire counter electrode and a silver wire pseudo-reference electrode. These were melt-

sealed into a smooth polyethylene space sandwiched between two CaF_2 windows within a thermostated Cu block to form the OTTLE cell. The working electrode surroundings were masked to avoid spectral interference from the non-electrolysed solution. The OTTLE cell itself fitted into double-walled nitrogen bath cryostat permitting the acquisition of spectra over a temperature range of 295-173 K (Figure 2.3).[6] The potential during these measurements was controlled by a PA4 (EKOM, Czech Republic) potentiostat. Details of the sample concentrations and supporting electrolyte are given in the text.

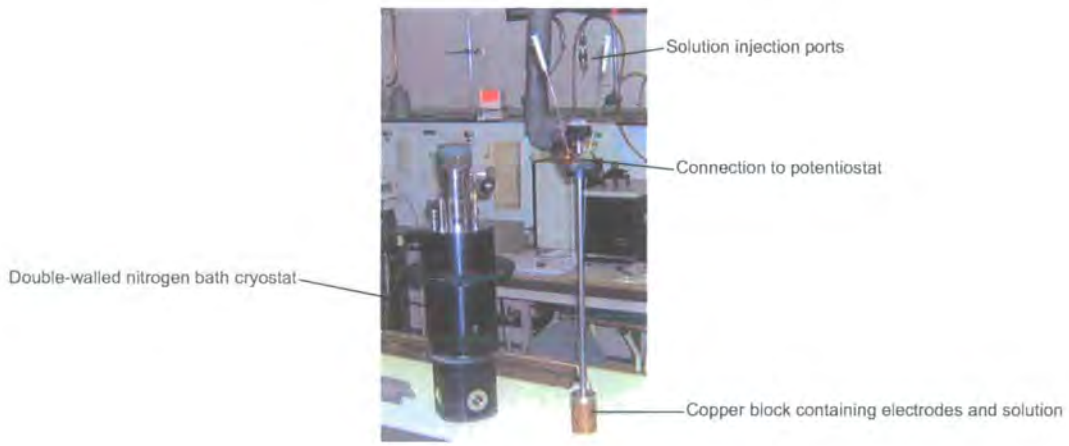

Figure 2.3. Spectro-electrochemical apparatus for infra-red measurements

UV-vis-NIR spectra for spectro-electrochemical studies were acquired using a Varian Cary-5 spectrophotometer. Oxidised species were generated using a platinum minigrid working electrode and platinum wire counter and pseudo-reference electrodes. The three-electrode system was contained within a 30 x 10 x 1 mm quartz cuvette (Figure 2.4). This in turn was held within a teflon mount which permitted cooling of the solution to sub-ambient temperatures (Figure 2.5). Cooling of the sample was achieved by the passing of dry nitrogen gas through a copper coil immersed in liquid nitrogen and the rate of flow of gas was used to control the

temperature. In order to prevent condensation on the cell windows, both the cell mount and sample compartment were purged with dry nitrogen prior to and during the acquisition of spectra. Details of the sample concentrations and supporting electrolyte are given in the text.

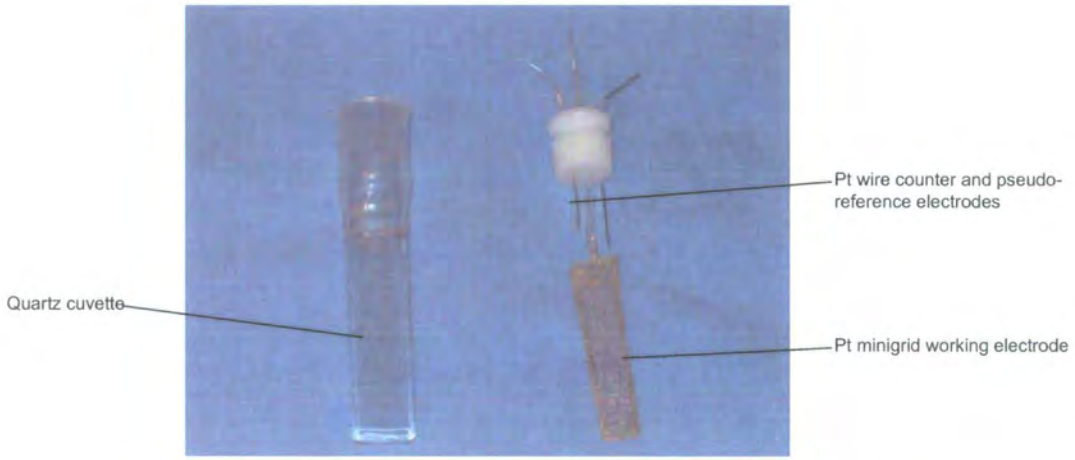

Figure 2.4. Electrochemical Cell for UV-vis-IR spectro-electrochemical measurements

Figure 2.5. Spectro-electrochemical apparatus for UV-vis-NIR measurements

References

1 SAINT, version 6.45, Bruker-Nonius AXS, Madison, Wisconsin, USA (2003)

2 SADABS, version 2.10, Bruker-Nonius AXS, Madison, Wisconsin, USA (2003)

3 SHELXTL, version 6.12, Bruker AXS, Madison, Wisconsin, USA (2001)

4 C. M. Duff, G. A. Heath, *Inorg. Chem.*, 1991, **30**, 2528.

5 A. Neudeck, L. Kress, *J. Electroanal. Chem.*, 1997, **437**, 141.

6 F. Hartl, H. Luyten, H. A. Nieuwenhaus, G. C. Shoemaker, *Applied Spectroscopy*, 1994, **48(12)**, 1522.

Introduction

Nitrile ligands, RC≡N, offer a combination of N localised σ-orbitals and C≡N π and π* orbitals for bonding to metal centres and as such have been the subject of much study for their reaction and coordination chemistry, physical properties and biological roles.[1-4] Early examples of nitrile complexes to ruthenium and iron centres include the cationic iron complexes $[Fe(NCMe)(CO)_2Cp]^+$ and $[Fe(NCMe)(CO)(PPh_3)Cp]^+$ and the cationic ruthenium complex $[Ru(NCMe)(PPh_3)_2Cp]^+$ (with a variety of counter-ions).[5,6] This was followed by the formation of the neutral boro-nitrile complex $Ru(NCBX_3)L_2Cp$ (L = CO, PPh_3; X = H, C_6H_5) which readily re-arranged to form the isonitrile material (Figure 3.1) and a series of nitrile complexes of type $[Ru(NCR)(PPh_3)_2Cp]^+$.[7,8]

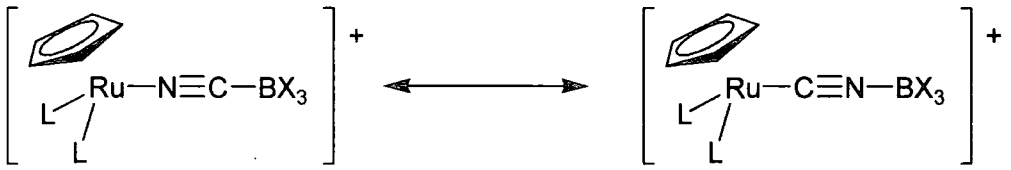

Figure 3.1. Nitrile/isonitrile isomerism in $Ru(NCBX_3)L_2Cp$ (L = CO, PPh_3; X = H, C_6H_5).

In addition to these materials the iron-nitrile complex $[Fe(NCMe)(dppe)Cp][BPh_4]$ and a series of osmium-nitrile complexes were also isolated at about the same time.[8,9] More recently, a rise in interest in materials with high second-order hyperpolarisabilities for non-linear-optics (NLO), together with the observation of

appreciable NLO behaviour in ferrocene derivatives, led to an increase in the study of numerous metal complexes featuring π-conjugated ligands, including nitriles.[10-15]

In benzonitrile complexes there is a σ-interaction between the σ*-orbitals on the R-C≡N moiety and an empty orbital of appropriate symmetry on the metal centre. Furthermore, the π/π* systems of the nitrile ligand are of the correct symmetries to interact with d-orbitals of the metal centre. Thus there is the possibility for a degree of charge-delocalisation across the metal-nitrile complex to a pendant donor/acceptor group. However, there has been some debate in the literature as to the exact nature of the interaction between a metal centre and a coordinated nitrile ligand. Early work suggested that there was a degree of π back bonding from the metal d-orbitals into the π* orbitals of the N≡C moiety. For example, Dias and co-workers carried out a study of para-substituted benzonitrile complexes of type $[Fe(N{\equiv}C\text{-}C_6H_4\text{-}R)\{(+)\text{-DIOP}\}Cp]^+$ (R = Me, OMe, NH_2, NMe_2, Ph, F, NO_2, $C_6H_4\text{-}NO_2$) (Figure 3.2) in order to determine their NLO responses.[12]

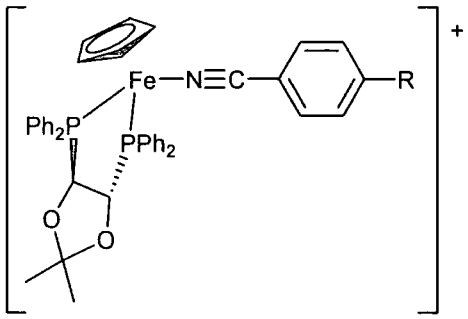

Figure 3.2. $[Fe(N{\equiv}C\text{-}C_6H_4\text{-}R)\{(+)\text{-DIOP}\}Cp]^+$ (R = Me, OMe, NH_2, NMe_2, Ph, F, NO_2, $C_6H_4\text{-}NO_2$).

The Dias group found that the electronic properties of the nitrile substituents resulted in several changes in the spectroscopic signatures of their complexes. In the NMR spectra they found that the ^{1}H and ^{13}C resonances of the Cp moiety were shifted to higher frequency upon moving from the electron-donating NMe_2 substituent to the electron-withdrawing NO_2 moiety. Further, whilst in most cases the $\nu(C\equiv N)$ band in the IR spectrum of these complexes remained relatively unchanged from that of the free ligand [i.e. $\Delta\nu(C\equiv N) = \nu(C\equiv N)_{free\ ligand} - \nu(C\equiv N)_{complex} \approx 0$], in the case of R = NO_2 the $\nu(C\equiv N)$ band was found to move to lower wavenumbers [$\Delta\nu(C\equiv N) = -35$ cm^{-1}]. At the time, these observations were attributed to stabilisation of the ligand π^* orbitals by the more electron-withdrawing group, leading to a greater degree of metal-($d\pi$) to $N\equiv C$ (π^*) back bonding. Therefore, as the electron-withdrawing nature of the nitrile substituent increased more electron density was removed from the metal centre by back-bonding to the nitrile. In turn this would lead to greater donation from the Cp moiety to the metal centre, resulting in a de-shielding effect and the observed NMR response.

Later work on the analogous ruthenium complexes $[Ru(N\equiv CC_6H_4\text{-}4\text{-}NO_2)\{(+)\text{-DIOP}\}Cp][X]$ ($X = Cl^-, NO_3^-, BF_4^-, p\text{-}CH_3C_6H_3SO_3^-, PF_6^-, ClO_4^-, CF_3SO_3^-$) found no change in the $\nu(C\equiv N)$ band in the IR spectrum, relative to the free ligand. This was attributed to the fact that the ruthenium centre was a poorer π-donor than Fe and hence there was a balance between the donation from the nitrile σ^* orbital and back-donation into the π^* orbital which resulted in no net change in the $\nu(C\equiv N)$ frequency.[13]

This metal to ligand π back-bonding picture also provided an explanation for the variation in the degree of NLO behaviour in coordinated benzonitrile complexes. Some of the compounds of type $[M(N{\equiv}C\text{-}C_6H_4\text{-}R)L_2Cp']^+$ described above displayed large values for second harmonic generation (SHG). One of the criteria for NLO behaviour is that a material should consist of polarisable, dipolar molecules which offer a large difference in their ground and excited state dipoles. Hence, coordination of a benzonitrile ligand $N{\equiv}C\text{-}C_6H_4\text{-}R$ (where R is an electron-withdrawing group) to a metal centre should lead to a donor-acceptor system in which the metal centre is the donor and the electron-withdrawing R group is the acceptor. The $[Fe(N{\equiv}CC_6H_4\text{-}NO_2)\{(+)\text{-DIOP}\}Cp]^+$ system showed an SHG signal that was 38 times that of urea (i.e. a relative SHG value of 38). and this was attributed to the $[Fe\{(+)\text{-DIOP}\}Cp]^+$ fragment acting as a π-donor via d-π*(NC) orbitals towards the NO_2 group.[12] The analogous ruthenium complex $[Ru(N{\equiv}CC_6H_4\text{-}NO_2)\{(+)\text{-DIOP}\}Cp]^+$ displayed a much smaller relative SHG value of 2.7. This decrease was attributed to the poorer donating power of the $[Ru\{(+)\text{-DIOP}\}Cp]^+$ fragment relative to the Fe analogue.[13] Low-level extended Hückel calculations seemed to support the possibility of a limited degree of metal nitrile back-bonding.[14,15]

However, more recent work has suggested another explanation of these effects. More detailed calculations have shown that, whilst there is a contribution from the π orbitals, the bonding interaction is, in fact, predominantly σ in character between the metal dz^2 orbital and the σ* orbital on the nitrile moiety. The nitrile π* levels are too far removed in energy to take part in back-bonding interactions of great significance with the filled $M_{d\pi}$ levels.[16-18] This is comparable with the leading model proposed for metal complexes featuring the isolobal and isoelectronic acetylide ligands. In the

case of metal acetylide complexes it has been shown that the primary bonding interaction between $^{-}$[C≡C-R] and a metal centre occurs primarily though the σ-orbitals of the acetylide and the metal dz^2 orbital. Although there is an interaction between the metal d-orbitals of π-symmetry and the acetylide π-system (Figure 3.3), in the case of low valent late metals of particular interest here, the bonding and anti-bonding combinations are both fully occupied and so there is no *net* π-bonding.[19,20] The very high energy of the acetylide π* system means that the degree of π back-bonding between the metal and the acetylide fragment is negligible compared to the dominant influence of the σ-bonding interactions.[21]

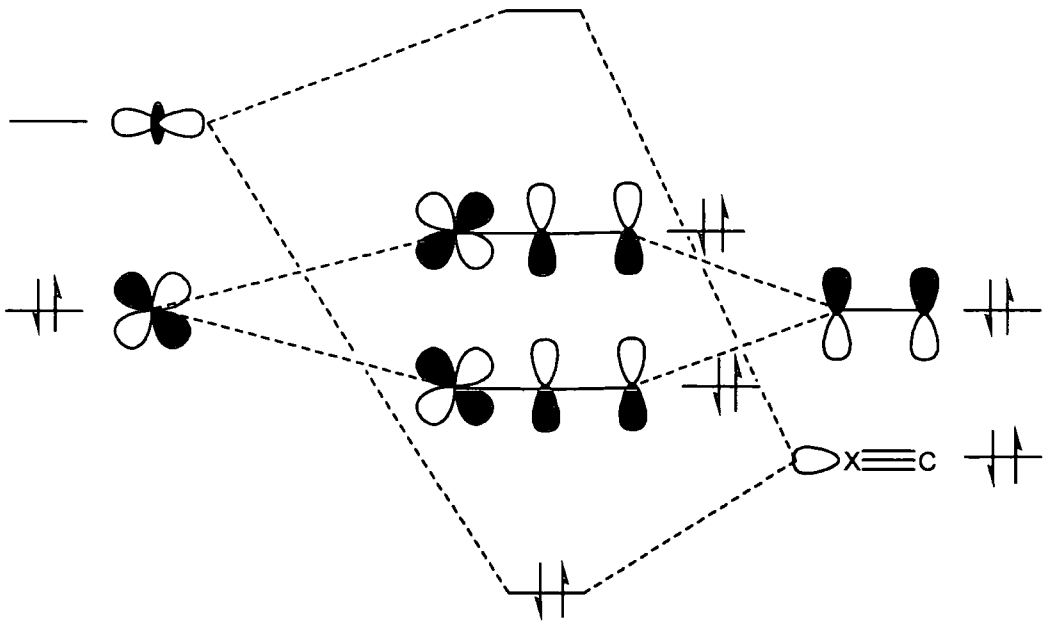

Figure 3.3. Orbital Overlap Diagram for Metal/Ligand Interaction (X = N, C)

In order to better understand the nature of the bonding interaction in metal complexes featuring cyanoacetylenes (R-C≡C-C≡N) (Chapter 5) or metal cyanoacetylides ($L_2Cp'M$-C≡C-C≡N) (Chapter 6) as ligands, we undertook a systematic study of

complexes of type $[M(N{\equiv}C\ R)L_2Cp']^+$ featuring *para*-substituted benzonitrile ligands and examined the effects of variation of both the metal and the nature of the para-substituent in the structural, electrochemical and spectroscopic properties of complexes of these systems. Since counter ion effects have previously been noted to influence these properties in solid state samples[13] we chose to examine a consistent series of $[PF_6]^-$ salts.

Results

Syntheses

In methanolic solution, the M-Cl bond in compounds of type $MClL_xCp'$ (where L = phosphine ligand, Cp' = Cp or Cp*) is partially ionised, and can be readily replaced by a range of donor ligands.[6-8] The additional presence of a halide abstracting agent such as NH_4PF_6 assists this process by precipitating NH_4Cl and driving the equilibrium forwards (Scheme 3.1).

$$MClL_xCp' + D: \rightleftharpoons [MDL_xCp']^+ + Cl^-$$

Scheme 3.1.

In this study, metal complexes of type $MClL_2Cp'$ (M = Ru, L = PPh_3, Cp' = Cp; M = Ru, L_2 = dppe, Cp' = Cp*; M = Fe, L_2 = dppe, Cp' = Cp) were allowed to react with benzonitrile (NCC_6H_5) in refluxing methanol in the presence of NH_4PF_6. Subsequent work-up resulted in the isolation of the complex salts $[Ru(N{\equiv}CC_6H_5)(PPh_3)_2Cp][PF_6]$ (**1**),[8] $[Ru(N{\equiv}CC_6H_5)(dppe)Cp^*][PF_6]$ (**2**), and $[Fe(N{\equiv}CC_6H_5)(dppe)Cp][PF_6]$ (**3**). Similarly, reaction of $RuCl(PPh_3)_2Cp$ with the *para*-substituted benzonitriles $N{\equiv}CC_6H_4X$ resulted in the formation of the substituted ruthenium complexes $[Ru(N{\equiv}CC_6H_4X)(PPh_3)_2Cp][PF_6]$ [X = NO_2 (**4**), NMe_2 (**5**), CN (**6**)] (Scheme 3.2).

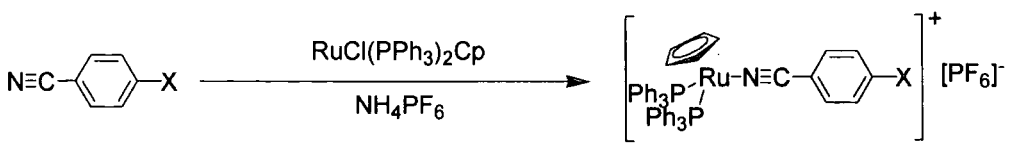

Scheme 3.2.

In addition to these mono-metallic compounds, nitrile ligands were used to obtain multi-metallic complexes. Reaction of $N{\equiv}CC_6H_4C{\equiv}N$-4 with NH_4PF_6 and two equivalents of $RuCl(PPh_3)_2Cp$ in refluxing methanol resulted in the formation of the bi-metallic complex $[\{Ru(PPh_3)_2Cp\}_2(\mu\text{-}1,4\text{-}N{\equiv}CC_6H_4C{\equiv}N)][PF_6]_2$ (**7**). It was found that **7** could also be obtained from solutions of compound **6** after approximately 24 hours. This observation is discussed in more detail later in this section. Reaction of $RuCl(PPh_3)_2Cp$ with one equivalent of the cluster-substituted nitrile $Co_2(\mu, \eta^2\text{-}HC_2C_6H_4C{\equiv}N\text{-}4)(CO)_4(dppm)$[22] under analogous conditions to those described above resulted in the formation of the heterometallic complex $[Co_2(\mu, \eta^2\text{-}HC_2C_6H_4C{\equiv}N\text{-}4)\{Ru(PPh_3)_2Cp\}(CO)_4(dppm)](PF_6)$ (**8**).

Spectroscopic Characterisation

The benzonitrile complex $[Ru(NCC_6H_5)(PPh_3)_2Cp]PF_6$ (**1**) was readily characterised from the associated spectroscopic data. In the ^1H NMR spectrum the PPh_3 ligands gave the usual resonances in the region 7.09-7.57 ppm, which were overlapped with the signals from the phenyl protons of the benzonitrile moiety. The Cp protons gave rise to a singlet at 4.55 ppm, which is in good agreement with that previously reported (4.58 ppm).[8] In the $^{13}C\{^1H\}$ NMR spectrum, the Cp ligand was characterised by a sharp, single resonance at 84.38 ppm while the carbon atoms of the aromatic rings were found within the usual range (136.02-128.67 ppm). The ^{31}P NMR spectrum confirmed the presence of both the PPh_3 ligand (42.89 ppm) and the PF_6^- counter ion (-142.97 ppm, J_{PF} = 713 Hz). In the IR spectrum, the $\nu(C{\equiv}N)$ band was observed at

2233 cm^{-1}. The positive ion mass spectrum (ES(+)-MS) contained an isotopic envelope for the intact cation of the complex salt (*m/z* = 794) and for the fragment ion arising from the loss of the benzonitrile ligand (*m/z* = 691).

The bright yellow complex salt [Ru(N≡CC_6H_5)(dppe)Cp*][PF_6] (**2**) was characterised in a similar fashion. The presence of the Cp* ligand was clearly visible in both the ^1H and $^{13}C\{^1H\}$ NMR spectra with resonances at 1.51 ppm (^1H NMR) and 93.18 (C_5Me_5) and 9.68 ppm (C_5Me_5) ($^{13}C\{^1H\}$ NMR). Two broad signals in the ^1H NMR at 2.46 and 2.50 ppm revealed the presence of the dppe protons and the ligand was detected in the $^{13}C\{^1H\}$ NMR spectrum as a multiplet in the range 28.41-28.77 ppm . Furthermore, it was possible to distinguish the ortho-protons of the benzonitrile ligand as a pseudo-doublet at 6.56 ppm with an apparent J_{HH} = 8.40 Hz. The dppe and PF_6 moieties gave the expected resonances in the ^{31}P NMR spectrum (a sharp singlet at 76.15 and a heptet at -143.42 ppm, J_{PF} = 710 Hz) and the ν(C≡N) band was observed at 2227 cm^{-1} in the IR spectrum. ES(+)-MS results showed the presence of the complex cation (m/z = 794) as well as a fragment resulting from the loss of the benzonitrile ligand (m/z = 635). Despite numerous attempts, the micro-analytical result for this compound returned consistently low in carbon which could not be accounted for by the presence of solvent molecules.

The analogous iron-based complex [Fe(N≡CC_6H_5)(dppe)Cp][PF_6] (**3**) was characterised by resonances in the ^1H and $^{13}C\{^1H\}$ NMR spectra corresponding to the Cp moiety [singlets at 4.45 ppm (^1H NMR) and 79.90 ppm (^{13}C NMR)] and the dppe ligand (two unresolved multiplets at 2.45 and 2.63 ppm in the ^1H spectrum and a multiplet at 28.13 ppm in the $^{13}C\{^1H\}$ spectrum). As with compound **2**, it was

possible to distinguish a signal arising from the two ortho-protons of the benzonitrile ligand which in this case were observed as a broad singlet at 6.46 ppm. The ^{31}P NMR showed the expected sharp singlet resonance for the dppe ligand at 98.32 ppm and a heptet corresponding to the $[PF_6]^-$ counter ion at -143.13 (J_{PF} = 713 Hz). The ν(C≡N) band in the IR spectrum was observed at 2217 cm^{-1} and ES(+)-MS showed the cation of the complex salt (*m/z* = 622) and a fragment ion resulting from loss of the benzonitrile ligand (*m/z* = 519).

In comparison with **1**, the presence of the electron-withdrawing NO_2 group in $[Ru(N{\equiv}CC_6H_4NO_2\text{-}4)(PPh_3)_2Cp]PF_6$ (**4**) results in a shift of the Cp resonances in the NMR spectra to higher chemical shifts (^1H = 4.64 ppm, ^{13}C = 84.98 ppm) relative to those in **1**. In addition, the nitrile carbon and the associated *ipso*-carbon of the $C_6H_4NO_2$ aromatic ring could be identified in the $^{13}C\{^1H\}$ NMR spectrum (127.91 ppm and 117.46 ppm respectively), as could the carbon adjacent to the NO_2 group (150.04 ppm) by comparison with the spectrum of **5** (see below) and data reported previously from similar complexes.[23-26] The PPh_3 ligands and the $[PF_6]^-$ counter-ion gave the expected resonances (a sharp singlet at 42.97 and a heptet at -142.93 ppm, J_{PF} = 713 Hz respectively), whilst the ν (C≡N) band was observed at 2228 cm^{-1} in the IR spectrum. Isotopic envelopes consistent with $[Ru(N{\equiv}CC_6H_4NO_2\text{-}4)(PPh_3)_2Cp]^+$ (*m/z* = 839) and $[Ru(PPh_3)_2Cp]$ (*m/z* = 691) were observed by ES(+)-MS.

The spectroscopic properties of the yellow complex salt $[Ru(NCC_6H_4NMe_2\text{-}4)(PPh_3)Cp]PF_6$ (**5**) shows the effect of the electron-donating NMe_2 group on more remote parts of the metal fragment. The Cp resonances in the NMR spectra (^1H = 4.42 ppm, $^{13}C\{^1H\}$ = 83.81 ppm) are moved to lower frequency relative to those in

compound **1**. The methyl protons on the NMe_2 moiety gave rise to a singlet resonance at 2.97 ppm. In the $^{13}C\{^1H\}$ NMR spectrum, the corresponding methyl carbons gave a sharp resonance at 40.17 ppm. The ipso carbon of the benzonitrile phenyl ring was also identified in the $^{13}C\{^1H\}$ NMR spectrum (95.61 ppm) as was the carbon adjacent to the NMe_2 group (153.23 ppm). The PPh_3 ligands and the PF_6^- counter-ion gave the expected resonances (a sharp singlet at 42.82 and a heptet at -143.04 ppm, J_{PF} = 713 Hz). The ν(C≡N) band was observed at 2221 cm^{-1} in the IR spectrum. The ES(+)-MS results contained an isotopic envelope consistent with the cationic portion of the compound (*m/z* = 837) and the fragment ion arising from the loss of the $NCC_6H_4NMe_2$-4 ligand (*m/z* = 691).

The solid isolated from the 1:1 reaction of $RuCl(PPh_3)_2Cp$ with terephtalonitrile (1,4 –dicyanobenzene) was a mixture of two compounds, as evidenced by the observation of two chemically distinct Cp moieties in the ^1H NMR spectrum at 4.57 and 4.62 ppm. Neither of these species correspond to the starting material $[RuCl(PPh_3)_2Cp]$ for which the Cp signal appears at 4.03 ppm. Further experimentation using a 2:1 molar ratio of the ruthenium reagent:terephthalonitrile gave a single complex, identified as the di-ruthenium complex $[\{Ru(PPh_3)Cp\}_2(\mu\text{-}NCC_6H_4CN\text{-}4)](PF_6)_2$ (**7**) [$\delta_{Cp}(^1H)$: 4.57ppm]. A similar reaction with a ten-fold excess of the ligand afforded the monometallic complex $[Ru(NCC_6H_4CN\text{-}4)(PPh_3)Cp](PF_6)$ (**6**) [$\delta_{Cp}(^1H)$: 4.62ppm] . In DCM solution, **6** disproportionates to **7** and free ligand over a 24 hour period. Hence the di-ruthenium complex **7** would appear to be the thermodynamic sink for the reaction.

In addition to the ^{1}H NMR resonances discussed above, ^{31}P NMR resonances for **6** were observed arising from the PPh_3 (singlet at 42.58 ppm) ligand and the $[PF_6]^-$ counter-ion (heptet at -142.93 ppm, J_{PF} = 713 Hz). A $^{13}C\{^{1}H\}$ NMR spectrum of **6** could not be obtained due to the disproportionation problem described above. ES(+)-MS results showed isotopic envelopes corresponding to $[Ru(NCC_6H_4CN)(PPh_3)_2Cp]^+$ (*m/z* = 819) and $[Ru(PPh_3)Cp]^+$ (*m/z* = 691). There was only one ν(C≡N) band observed in the IR spectrum (2221 cm^{-1}).

The PPh_3 and $[PF_6]^-$ ligands in **7** gave rise to singlet and heptet resonances in the ^{31}P spectrum at 42.58 ppm and -142.84 ppm (J_{PF} = 713 Hz) respectively. The ν(C≡N) band was observed at 2226 cm^{-1} in the IR spectrum and ES(+)-MS results show the complex cation $[\{Ru_2(NCC_6H_4CN)(PPh_3)_4Cp_2\}[PF_6]]^+$ (*m/z* = 1655) as well as isotopic envelopes arising from $[Ru(NCC_6H_4CN)(PPh_3)_2Cp]^+$ (*m/z* = 819) and $[Ru(PPh_3)Cp]^+$ (*m/z* = 691).

The Cp resonances in the red-coloured complex salt $[Co_2(\mu, \eta^2\text{-}HC_2C_6H_4C{\equiv}N\text{-}4)\{Ru(PPh_3)_2Cp\}(CO)_4(dppm)](PF_6)$ (**8**) were shifted to lower chemical shift relative to compound **1** (^{1}H = 4.47 ppm, $^{13}C\{^{1}H\}$ = 83.95 ppm). Resonances from the dppm protons were observed as doublets of triplets centred at 3.06 ppm (J_{HP} = 13 Hz, J_{HH} = 10 Hz) and 3.60 ppm (J_{HP} = 13 Hz, J_{HH} = 10 Hz). The IR spectrum showed the ν(CO) bands at 2021, 1993, 1973 and 1955 cm^{-1} but the ν (C≡N) band was not observed. The ES(+)-MS contained isotopic envelopes arising from the molecular ion for the cationic portion of the compound (*m/z* = 1432) and the fragment ion arising from $[Ru(PPh_3)_2Cp]^+$ (*m/z* = 690).

Electronic Spectra

With the exception of **6** (due to the disproportionation problems described above) and **2** (which proved to be insoluble in THF) the electronic absorption spectra of compounds each compound were recorded as 0.1 mM solutions in both DCM and THF (Table 3.1). Each compound exhibited an absorption band with a λ_{max} in the range 240-260 nm which displayed no solvatochromic behaviour and was assigned to the localised π/π^* transitions of the phosphine ligands. Similar assignments have been made previously for a series of closely related compounds.[27] In addition, each compound gave rise to a broad absorption envelope between 300-450 nm. This envelope contained two absorption bands, the relative positions and intensities of which varied between complexes. These were tentatively assigned as MLCT $Ru_{d\pi}$-Cp for the higher energy transition and MLCT $Ru_{d\pi}$-NC_{π^*} for the lower (see Discussion section). The marked solvatochromic effect seen for compound **4** (which bears the strongly electron-withdrawing NO_2 group) supports this assignment. However, in the case of compounds **1**, **4** and **5** these bands overlapped to such an extent that it was impossible to establish the positions of the two separate band maxima and the only distinguishable band maximum is reported here.

Table 3.1. Electronic Absorption data for complexes **1-8**

Complex	λ_{max}/nm (ε / M^{-1} cm^{-1}) (CH_2Cl_2)	λ_{max}/nm (ε / M^{-1} cm^{-1}) (THF)
1	238 (52900), 307 (13600)	230 (70400), 307 (13500)
2	249 (26900), 310 (8400), 346 (6600)	n/a
3	258 (17800), 328 (5600), 391 (2500)	260 (17100), 331 (5900), 391 (3200)
4	237 (43200), 384 (6900)	229 (51000), 329 (6900)
5	230 (62700), 332 (55000)	234 (45400), 332 (45000)
7	247 (85400), 363 (20900), 420 (17100)	225 (55600), 363 (10300), 420 (8300)
8	270 (30800), 360 (15200), 550 (2400)	270 (55400), 360 (29500), 550 (1800)

Molecular Structures

While attempts to obtain single crystals of $[Ru(NCC_6H_4CN\text{-}4)(PPh_3)_2Cp][PF_6]$ (**6**) were complicated by disproportionation to $[\{Ru(PPh_3)_2Cp\}_2(\mu\text{-}1,4\text{-}NCC_6H_4CN)][PF_6]_2$ (**7**) and the free ligand commented upon earlier, it did prove possible to obtain single crystals of the other complexes **1-5**, **7** and **8**. The molecular structures for the complexes bearing the benzonitrile ligand (**1-3**) are shown in Figure 3.4, with crystallographic details summarised in Table 3.2 and selected bond lengths and angles in Table 3.3. Compounds of type $[Ru(N{\equiv}CC_6H_4X)(PPh_3)_2Cp][PF_6]$ [X = NO_2 (**4**), NMe_2 (**5**)] as well as the di-ruthenium complex $[\{Ru(PPh_3)Cp\}_2(\mu\text{-}NCC_6H_4CN\text{-}4)][PF_6]_2$ (**7**) and the mixed-metal complex $[Co_2(\mu, \eta^2\text{-}HC_2C_6H_4C{\equiv}N\text{-}4)\{Ru(PPh_3)_2Cp\}(CO)_4(dppm)][PF_6]$ (**8**) are shown in Figure 3.5, with crystallographic details summarised in Table 3.4 and selected bond lengths and angles in Table 3.5.

In the case of compounds **4**, **7**, and **8** molecules of solvent (CH_2Cl_2) were found in the molecular structure. The solvent molecules are also accounted for in the micro-analyses of these compounds (see Experimental section). Given the sensitivity of the details of the molecular structures to variations in electronic properties of the metal and the supporting ligands (e.g. phosphines and Cp') as well as those associated with the nitrile ligand of particular interest here, it is only illustrative to consider subtle variations within the series of most structurally comparable metal fragments.

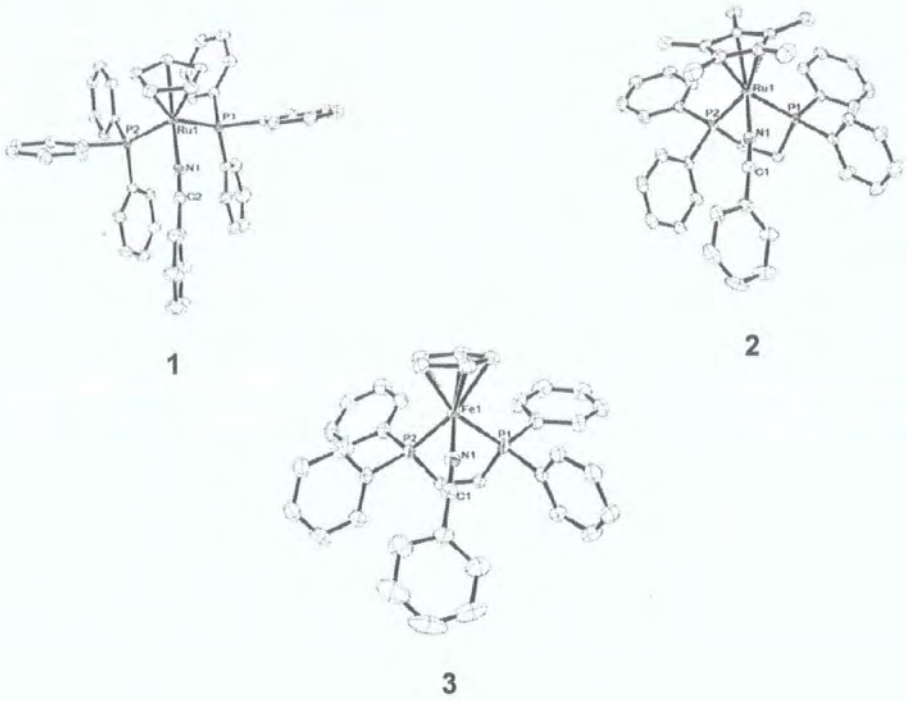

Figure 3.4. ORTEP plots of benzonitrile compounds **1-3** showing numbering scheme (in this and all subsequent figures, hydrogen atoms have been omitted for clarity).

Table 3.2. Crystallographic data for complexes **1-3**

Compound	**1**	**2**	**3**
Formula	$C_{48}H_{40}F_6NP_3Ru$	$C_{43}H_{44}F_6NP_3Ru$	$C_{38}H_{34}F_6NP_3Fe$
M	938.79	882.77	767.42
***a* (Å)**	15.6383(4)	11.8209(6)	10.5129(5)
***b* (Å)**	13.9146(3)	17.8172(9)	16.4328(8)
***c* (Å)**	20.1345(5)	19.7578(10)	20.0776(10)
α (°)	90	90	90
β (°)	108.921(1)	92.623(2)	90
γ (°)	90	90	90
V (Å^3)	4144.5(2)	4156.9(4)	3468.5(3)
ρ (Mg/m^3)	1.505	1.411	1.470
T (K)	120(2)	120(2)	120(2)
Crystal system	Monoclinic	Monoclinic	Orthorhombic
Space Group	$P2_1/n$	$P2_1/n$	$P\,2_1\,2_1\,2_1$
Z	4	4	4
μ (mm^{-1})	0.557	0.550	0.635
Reflections collected	44123	38442	32697
Independent reflections (R_{int})	10287 [R(int) = 0.0171]	12677 [R(int) = 0.0452]	10550 [R(int) = 0.0375]
Final R indices (all data)	$R_1 = 0.0260$, $wR_2 = 0.0602$	$R_1 = 0.1184$, $wR_2 = 0.3299$	$R_1 = 0.0512$, $wR_2 = 0.1037$

Table 3.3. Selected bond lengths and angles for compounds **1-3**.

Compound	M-N(1) (Å)	N(1)-C(1) (Å)	C(1)-C(ipso) (Å)	M-P(1) (Å)	M-(P2) (Å)	M-N(1)-C(1) (°)	N(1)-C(1)-C(ipso) (°)	P(1)-M-(P(2) (°)
1	2.037(1)	1.145(2)	1.440(2)	2.334(1)	2.335(1)	171.70(12)	177.84(16)	97.46(1)
2	2.027(5)	1.146(7)	1.438(7)	2.315(1)	2.315(1)	173.6(4)	174.9(6)	83.50(5)
3	1.892(2)	1.141(3)	1.444(3)	2.207(1)	2.206(1)	172.16(18)	174.5(2)	84.37(6)
$[Fe(N{\equiv}CC_6H_4NO_2)(dppe)(Cp^*)][PF_6]$	1.874(11)	1.129(14)	1.420(2)	2.210(4)	2.209(3)	176.6(11)	177.4(15)	87.70(12)

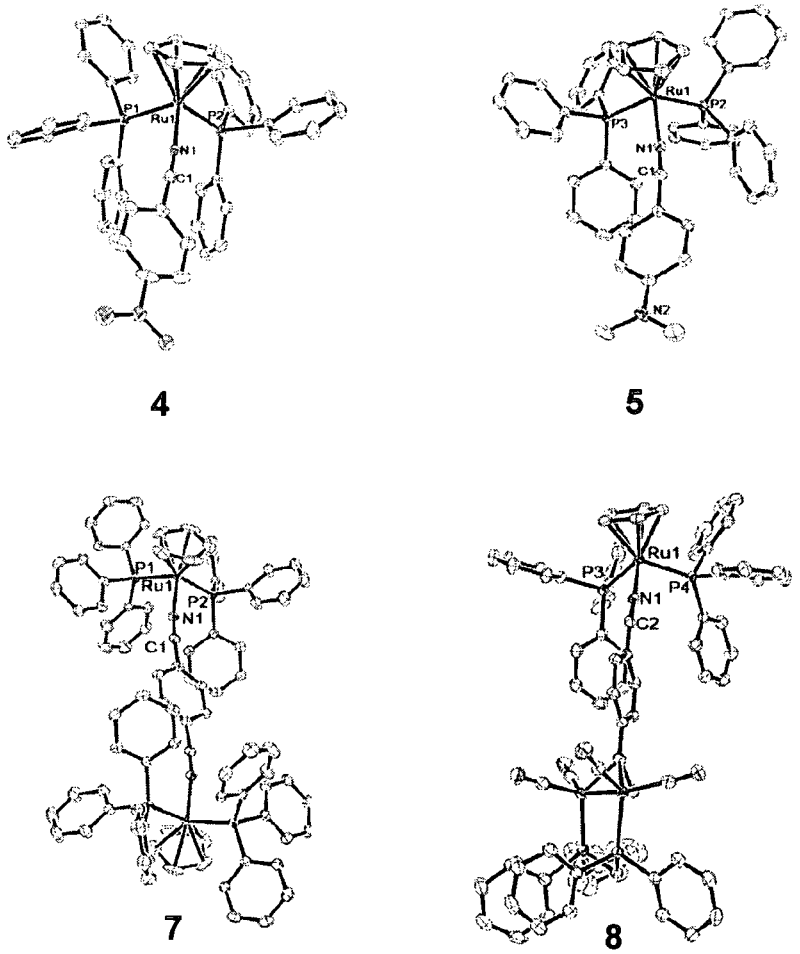

Figure 3.5. ORTEP plots of substituted benzonitrile compounds **4**, **5**, **7**, and **8** showing numbering scheme.

Table 3.4. Crystallographic data for complexes **4, 5, 7,** and **8**

Compound	**4**	**5**	**7**	**8**
Formula	$C_{48}H_{39}F_6N_2P_3O_2Ru.CH_2Cl_2$	$C_{50}H_{45}F_6N_2P_3Ru$	$C_{90}H_{70}F_{12}N_2P_6Ru_2.2(CH_2Cl_2)$	$C_{79}H_{62}Co_2RuO_4P_5NF_6.CH_2Cl_2$
M	1068.72	981.86	1969.32	
***a* (Å)**	13.4710(11)	11.4435(5)	17.9679(7)	13.6667(18)
***b* (Å)**	18.9603(13)	13.8495(7)	16.5775(7)	16.392(2)
***c* (Å)**	18.1940(14)	15.2404(7)	28.5453(12)	16.958(2)
***α* (°)**	90	87.187(2)	90	98.113(4)
***β* (°)**	95.816(4)	72.213(2)	90	105.243(4)
***γ* (°)**	90	73.038(2)	90	97.515(4)
V (Å^3)	4623.1(6)	2197.76(18)	8502.6(6)	3572.1(8)
ρ (Mg/m^3)	1.535	1.484	1.538	1.519
T (K)	120(2)	120(2)	120(2)	120(2)
Crystal system	Monoclinic	Triclinic	Orthorhombic	Triclinic
Space Group	P2(1)/n	P -1	Pbca	P -1
Z	4	2	4	2
μ (mm^{-1})	0.625	0.530	0.669	0.893
Reflections collected	37877	31076	81098	42947
Independent reflections (R_{int})	11417 [R(int) = 0.0299]	13334 [R(int) = 0.0203]	9288 [R(int) = 0.0683]	17982 [R(int) = 0.0324]
Final R indices (all data)	R_1 = 0.0396, wR_2 = 0.0741	R_1 = 0.0395, wR_2 = 0.0863	R_1 = 0.0551, wR_2 = 0.0971	R_1 = 0.0589, wR_2 = 0.1147

Table 3.5. Selected bond lengths and angles for compounds **4, 5, 7,** and **8**

Compound	**M-N(1) (Å)**	**N(1)-C(1) (Å)**	**C(1)-C(ipso) (Å)**	**M-P(1) (Å)**	**M-(P2) (Å)**	**M-N(1)-C(1) (°)**	**N(1)-C(1)-C(ipso) (°)**	**P(1)-M-(P(2) (°)**
4	2.023(2)	1.146(2)	1.442(3)	2.329(1)	2.330(1)	171.24(15)	177.8(2)	100.30(2)
5	2.031(1)	1.149(2)	1.424(2)	2.325(1)	2.321(1)	173.52(14)	175.15(18)	104.24(2)
[Ru(N≡CC$_6$H$_4$OEt)(PPh$_3$)$_2$Cp][PF$_6$]	2.041(5)	1.152	1.405	2.352	2.337	175.6	175.1	100.6
7	2.018(2)	1.146(3)	1.442(4)	2.348(1)	2.344(1)	166.9(2)	176.6(3)	102.89(2)
8	2.0383	1.138	1.443(3)	2.3498	2.3445	176.6	170.46(11)	102.6

The geometries around the metal centres in the Ru(PPh$_3$)$_2$Cp family of nitrile complexes **1**, **4**, **5**, **7**, **8** and the related complex [Ru(N≡CC$_6$H$_4$OEt)(PPh$_3$)$_2$Cp][PF$_6$][28] are similar. The Ru-P distances are essentially invariant, spanning a narrow range of values from 2.321(1)-2.350(1) Å with a mean value of 2.337 Å. The N-C bond lengths are similarly unperturbed by the nature of the *para*-substituent of the benzonitrile ligand. The range of values found for N-C [1.142(4)-1.149(2) Å] are

experimentally identical and fall within the range of values found for the free ligands (1.14-1.16 Å)[29,30], although relative imprecision of the ligand structures makes the worth of such direct comparisons questionable.

Of more interest are the C(1)-C(ipso) bonds which display a trend towards shorter lengths in the case of the complexes $[Ru(NCC_6H_4NMe_2)(PPh_3)_2Cp][PF_6]$ (**5**) and $[Ru(N{\equiv}CC_6H_4OEt)(PPh_3)_2Cp][PF_6]$ which bear inductively electron-donating substituents [1.424(2) Å and 1.405 Å respectively vs. 1.440(2) Å for compound **1**]. In contrast, the shortest Ru-N bond length is associated with the substituted nitrile complexes $[Ru(NCC_6H_4NO_2)(PPh_3)_2Cp][PF_6]$ (**4**) and **7**, although it must be noted that the difference in this parameter between **4** and **5** is on the borderline of statistical significance.

The introduction of more electron-donating supporting ligands has a greater effect on these structural parameters. Therefore $[Ru(NCC_6H_5)(dppe)Cp^*][PF_6]$ (**2**) exhibits significantly shorter Ru-P bond lengths [2.315(1) Å] than the analogous compounds $[Ru(NCC_6H_5)(PPh_3)_2Cp][PF_6]$ (**1**) [2.334(1) and 2.335(1) Å] and **4** [2.329(1) and 2.330(1) Å], likely a consequence of the synergic σ-donating/π-back-bonding nature of the metal-phosphorus bond.[31] The N-C and M-N bond lengths in these Ru complexes are, however, remarkably insensitive to the nature of the supporting ligand, albeit in the limited range of data available (see Table 3).

Unsurprisingly, the smaller iron centre in $[Fe(NCC_6H_5)(dppe)(Cp)][PF_6]$ (**3**) and the NO_2-substituted analogue $[Fe(N{\equiv}CC_6H_4NO_2)(dppe)(Cp^*)][PF_6]$[15] gives rise to shorter M-L contacts than those in the ruthenium complexes described above. It is, however,

interesting to note that whilst the Fe-P, C(1)-C(ipso), and N-C bond distances in **3** and $[Fe(N{\equiv}CC_6H_4NO_2)(dppe)(Cp^*)][PF_6]$ are experimentally indistinguishable, there is a significant contraction of the Fe-N bond length (from 2.027 Å in **3** to 1.874(11) Å) brought about by the introduction of the electron-withdrawing NO_2 group. This observation is consistent with the trends noted above for the ruthenium species.

Electrochemistry

The electrochemical response of each of the compounds **1-8** was investigated by cyclic voltammetry (CV). These studies were performed using a platinum disc working electrode and platinum wire counter and pseudo-reference electrodes. Measurements were carried out in a 0.1M $[N(C_4H_9)_4][BF_4]$ solution in DCM. Internal decamethylferrocene [Fc^*/Fc^{*+} = -0.02 V vs. SCE] or ferrocene [Fc/Fc^+ = +0.46 V vs. SCE] standards were used to give electrode potentials relative to SCE.[32]

The electrochemical response of **1** at a platinum electrode was characterised by a single oxidation event at +1.30 V vs. SCE, the reversibility of which was improved at sub-ambient temperatures (-30 °C). Compounds **2** and **3** displayed oxidation waves (at +1.10 and +0.83 V respectively) which were reversible at room temperature. Compounds **4-8** displayed an irreversible, poorly defined oxidation event, the reversibility which could not be improved even at sub-ambient temperatures and faster scan rates (< 5 V/s).

Discussion

The qualitative molecular orbital description of the metal-nitrile interaction described in the introduction to this chapter is consistent with the spectroscopic behaviour of the benzonitrile complexes in this study. The IR data for the compounds **1-8** (Table 3.6) show the effect coordination of the nitrile ligand to a metal centre has on the ν(C≡N) band. The ν(C≡N) of the ligands are 2229 cm^{-1} (N≡C-C_6H_5), 2240 cm^{-1} (N≡C-C_6H_4-4-NO_2), 2210 cm^{-1} (N≡C-C_6H_4-4-NMe_2) and 2230 cm^{-1} (N≡C-C_6H_4-4-CN). The complexes bearing *para*-substituted benzonitrile ligands all have values of ν(C≡N) within a narrow range and most of these are within ca. 10 cm^{-1} of the free ligand value.

Table 3.6. IR data for compounds **1-8** and free ligands

Compound	ν(C≡N) cm^{-1}
N≡CC_6H_5	2229
N≡C$C_6H_4NO_2$	2240
N≡C$C_6H_4NMe_2$	2210
1	2233
2	2227
3	2217
4	2228
5	2221
6	2221
7	2226
8	Not observed

A variation of the metal fragment produces a more systematic variation in the ν(C≡N) frequencies [$\Delta\nu(C{\equiv}N) = \nu(C{\equiv}N)_{(complex)}-\nu(C{\equiv}N)_{(ligand)}$] for the compounds **1** ($\Delta\nu(C{\equiv}N)$

= +4 cm^{-1}), **2** ($\Delta\nu(C\equiv N)$ = -2 cm^{-1}) and **3** ($\Delta\nu(C\equiv N)$ = -12 cm^{-1}). Whilst the $\Delta\nu(C\equiv N)$ values for **2** and **3** are quite small, and must be taken as within the limits of precision for the experiment, that of -12 cm^{-1} for the iron complex **3** is significant. In terms of a metal-ligand π interaction this could be explained on the basis of the enhanced back-bonding from the better π- donating Fe centre towards the nitrile moiety. However, orbital polarisation as a result of the smaller iron centre could also account for this effect.

The position of Cp resonances in ^1H and $^{13}C\{^1H\}$ NMR spectra of complexes of type MXL_2Cp is known to be sensitive to the electron density at the metal centre. In neutral complexes these ^1H NMR Cp resonances tend to appear near 4.1 ppm (cf. $RuCl(PPh_3)_2Cp$ at 4.10 ppm[33] and $RuH(PPh_3)_2Cp$ at 4.09 ppm[34]) whilst for cationic derivatives of the $Ru(PPh_3)_2Cp$ fragment these usually appear in the range 4.5-5.0 ppm. The Cp resonance in the ^1H NMR spectrum of the nitrile complex $[Ru(NCMe)(PPh_3)_2Cp][BPh_4]$, for example, is found at 4.46 ppm.

The NMR spectra of the compounds in this study show that the Cp resonances show sensitivity to the nature of the benzonitrile substituent. The Cp resonances of **1** occur at 4.55 ppm and 84.38 ppm in the ^1H and ^{13}C spectra respectively. However when the *para*-substituent is changed from the H atom to the NO_2 moiety in **4** these resonances are moved to 4.64 ppm (^1H) and 84.98 ppm ($^{13}C\{^1H\}$). The presence of the electron-withdrawing NO_2 group results in a reduction of electron density at the nitrile moiety and hence the donating power of the $NCC_6H_4NO_2$ ligand is reduced with respect to that of the parent benzonitrile. More electron density is therefore drawn from Cp moiety which de-shields the Cp ligand and produces a shift in Cp resonances.

Compound **6**, which similarly has an electron-withdrawing para-substituent, displays a Cp resonance in the ^{1}H NMR spectrum at 4.62 ppm. Unfortunately the problems of disproportionation of **6** in solution described previously (see Results) prevented the acquisition of $^{13}C\{^{1}H\}$ NMR data for comparison.

Conversely, for compound **5**, which bears the electron-donating NMe_2 substituent, the reverse effect is seen. This substituent increases the electron density at the N≡C moiety and hence improves the donor strength of the ligand. This in turn donates more electron density to the metal fragment resulting in greater shielding of the Cp moiety and a shift of the Cp resonances to 4.42 ppm (^{1}H) and 83.81 ppm ($^{13}C\{^{1}H\}$).

The crystal structures of these compounds show how the same donor strength variations affect the M-N bond lengths. This distance is 2.037(1) Å for compound **1** but is reduced to 2.023(2) Å upon the addition of the electron-withdrawing NO_2 moiety. This may be due to a degree of π-back-bonding from the metal into the π* orbital of the CN moiety. Whilst there is no concomitant lengthening of the C≡N bond observed in the molecular structure, X-ray diffraction may be insufficiently sensitive to observe this. When the para-substituent is the electron-donating NMe_2 group in compound **5**, the donor strength of the ligand is increased. However the M-N bond length [2.031(1) Å] is virtually identical to that in **1**.

Whilst these variations in the M-N bond length could be explained in terms of π back-bonding from the ruthenium centre to the nitrile π* orbitals this would not be consistent with the rest of the crystallographic data. The π back-bonding model would suggest that complex **4**, bearing the NO_2 group would exhibit a greater degree

of back-bonding and hence shorten the Ru-N bond length and concomitantly lengthen the N-C bond whilst the reverse effect would be seen for the NMe_2-bearing complex **5**. However there is no evidence for this in the crystallographic results. All of the C-N bond lengths for all the compounds **1-8** are identical within the limits of precision of the experiment. This argues against the possibility of a back-bonding influence in these compounds and suggests that the bonding occurs predominantly via the σ interaction. It is possible, however, that these structural parameters are an insufficiently sensitive probe of the subtle variations in electron density across the C≡N moiety.

A further effect of the electron-donating properties of the N≡C-C_6H_4-4-NMe_2 ligand is seen in the Ru-P bond lengths of compound **5**. These bond lengths are 2.334(1) and 2.335(1) Å in compound **1** (and similar in **4**) but decrease to 2.325(1) and 2.321(1) Å in compound **5.** The electron-donating NMe_2 group increases the electron-density of the benzonitrile ligand and that this is transmitted via the σ-bonding interaction to the metal centre. This increases the electron-density at the metal centre allowing greater π back-bonding between the metal and the phosphine ligands and hence the bond length is decreased. This use of the Ru-P bond lengths as a sensitive probe of electron density at a metal centre can be seen for the molecular structures of compounds **1-3** where there is a shortening of these bonds as the donor strength of the metal fragment increased. This effect is, of course, exaggerated in the case of compound **3** where the smaller iron atom allows a closer approach of the phosphine ligand.

An increase in electron density at the metal centre results in the metal fragment becoming a poorer acceptor of electron density from the benzonitrile ligand. This is

evident in the ^{1}H NMR spectrum as variations in the positions of resonances arising from the ortho-protons of the benzonitrile ligand. In the case of **1**, these resonances are indistinguishable from those arising from the other phenyl protons. However, in the case of compound **2** the poorer acceptor qualities of the metal centre mean that less electron density is drawn from the ligand and so the ortho-protons are shielded to a greater degree than they are in **1** and are visible as a pseudo-doublet centred at about 6.55 ppm. In compound **3**, in which these protons are further shielded, these resonances are found as a broad singlet at 6.46 ppm.

The electronic spectra of the compounds **1-8** not only confirm the increase in electron density at the metal centre for compounds **1-3** but also provide further evidence that the bonding interaction between the metal and the nitrile moiety is primarily σ in character. The electronic spectra of these compounds all have the same general features. They all have a transition with a λ_{max} of about 240 nm (due to the π/π^* interaction in the phosphine ligands) and a set of lower energy absorption bands in the range 300-450 nm.

A study of similar compounds was carried out by Agarwala et al in 1990.[35] The reaction of 4-cyanopyridine, 1,4-dicyanobenzene and 1,4 dicyanobutene with both [$RuClL_2Cp$] (L = $(PPh_3)_2$, $(AsPh_3)_2$, dppe, dppm) and [$RuHCl(CO)(EPh_3)_3$] (E = P, As) afforded the corresponding mono- and di-metallic species. Some of these exhibited bands in the UV spectrum at 350 nm and 420 nm which were attributed to two MLCT transitions. The band at 350 nm was assigned to MLCT between the Ru centre and the Cp anti-bonding orbitals and the band at 420 nm was assigned to

MLCT between the Ru centre and the π^* orbitals of the nitrile ligands. Furthermore they also observed a solvatochromic effect to support this assignment.

The same arguments can be applied to the absorption spectra of the benzonitrile complexes in this study. Each compound exhibits two overlapping bands in the 300-450 nm region comparable with those found by Agarawala and co-workers. In DCM solution the energy of these charge-transfer bands in compound **2** (310 and 346 nm) are of lower energy than those in **1** (λ_{max} = 310 and 346 nm for **2** vs 307 nm for **1**) and they move to even lower energy for compound **3** (328 and 391 nm). As the nature of the co-ordinating nitrile is invariant between these complexes, this effect is therefore due to an increase of electron density at the metal fragment in the order **3** > **2** > **1**. This increase in electron density raises the energy of the metal d-orbitals such that the energy gap between those orbitals and the acceptors on the Cp and nitrile moieties is decreased and hence the transitions move to lower energy.

The electronic spectra of the para-substituted benzonitriles displayed absorption bands similar to those seen for compounds **1-3**, demonstrating further that the bonding interaction between the ligand and the metal fragment contains no contribution from the nitrile π-system. Complexes **7** and **8** displayed two distinct bands in the 300-550 nm region (**7** 365, 410 nm; **8**: 360, 550 nm). In the case of **4** and **5** these two bands overlapped to such an extent that only one maximum was clearly discernable. For compound **4** there is a strong solvatochromic effect on the position of this series of curves. The λ_{max} for these bands moves from 329 nm to 386 nm indicating that the excited state is of higher energy in DCM solution. It may be possible, however, to move these two absorptions apart from each other and distinguish them more clearly

by changing the metal fragment in the manner demonstrated in compounds **1**, **2** and **3** and this is an area for further study.

Whilst this work was in progress, other work in this laboratory resulted in the formation of $[\{Ru(PPh_3)_2Cp\}_2(\mu\text{-}C{\equiv}CC_6H_4CN\text{-}4)][PF_6]$ (**7a**) (Figure 3.6) which bears obvious comparisons to the terephthalonitrile complex $[\{Ru(PPh_3)_2Cp\}_2(\mu\text{-}N{\equiv}CC_6H_4CN\text{-}4)][PF_6]_2$ (**7**).

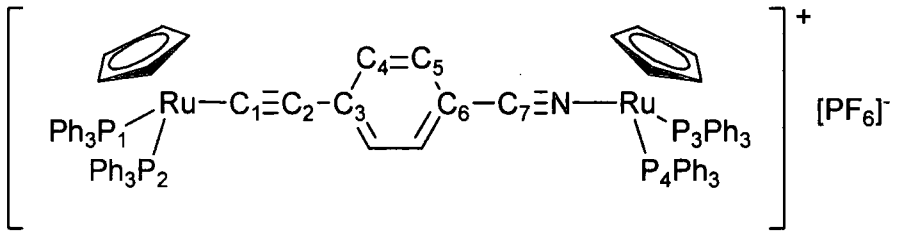

Figure 3.6. $[\{Ru(PPh_3)_2Cp\}_2(\mu\text{-}C{\equiv}CC_6H_4CN\text{-}4)][PF_6]$ (**7a**) showing numbering scheme.

The structure of the dicationic complex **7** has an inversion centre located at the mid-point of the phenyl ring of the bridging ligand. The Ru-N and Ru-P bond lengths are shorter and longer respectively than those of the related monometallic complex **1**. Recent calculations involving Re and Pt systems have shown a degree of polarisation in the M-N bond with a large portion of the electron density residing on the N atom.[16-18] This leads to a strong electrostatic interaction between the ruthenium centre and the nitrile ligand, shortening the Ru-N bond in **7** relative to **1**. The N-C and C-C(ipso) bonds in **7** are identical to those of **1**, suggesting that there is no communication between the metal centres via the π-system. Compound **7a** combines both metal-acetylide and metal-nitrile bonding motifs in the bridging ligand. The N≡C and C≡C

bond lengths as well as the metal-bridging ligand contacts are essentially unchanged from the model complexes **1** and $Ru(C{\equiv}C\text{-}C_6H_5)(PPh_3)_2Cp$[36,37] but there is an apparent degree of quinoidal character in the ring system of the bridging ligand as evidenced by the short C(2)-C(3) (1.419(7) Å) and C(6)-C(9) (1.415(7) Å) bond lengths in **7a**. A comparison of the Ru(1)-P(1, 2) bond lengths (2.290(1) and 2.305(1) Å) of **7a** with the Ru-P bond lengths of $Ru(C{\equiv}C\text{-}C_6H_5)(PPh_3)_2Cp$ (2.229(3) and 2.228(3) Å), and of Ru(2)-P(3, 4) (2.310(1) and 2.322(1) Å) with those of **1** (2.334(1) and 2.335(1) Å) reveals Ru(1)-P(1, 2) to be significantly longer than the corresponding bond lengths in the monometallic nitrile or acetylide complexes. Furthermore, the Ru(2)-P(3,4) bonds on the nitrile-coordinated metal centre are amongst the shortest Ru-P bond lengths reported for this class of complex. When taken as a whole, these structural parameters provide clear evidence for the donation of electron density from Ru(1) to Ru(2) via the polarised σ-bond framework of the ethynylbenzonitrile bridge.

In summary the experimental evidence presented in this chapter is in good agreement with recent DFT calculations which suggest limited M-N≡C back-bonding in metal-nitrile complexes. Furthermore, the ν(C≡N) frequencies have proven to be an insensitive probe as to the metal-nitrile bonding interaction and the M-P bond lengths of the compounds are much closer tracks of the electronic nature of the metal-ligand interaction.

Experimental

The following numbering scheme is used in the assignment of ^{13}C NMR resonances in the phenyl ring of the benzonitrile ligands:

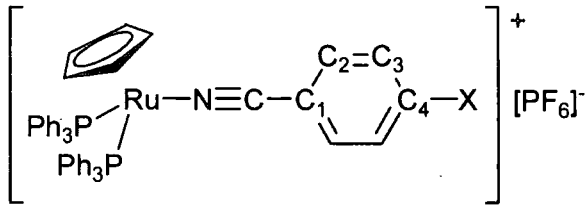

[Ru(NCC$_6$H$_5$)(PPh$_3$)$_2$Cp][PF$_6$] (1)

An oven-dried, two-necked Schlenk flask was fitted with a stirrer bar and cooled under nitrogen. The flask was charged with RuCl(PPh$_3$)$_2$Cp (250 mg, 0.345 mmol), C$_6$H$_5$CN (0.1 ml, 0.97 mmol), and NH$_4$PF$_6$ (200 mg, 1.22 mmol). The solids were suspended in MeOH (20 ml) and the mixture heated to reflux under a nitrogen atmosphere. After 30 minutes the yellow solution that had formed was allowed to cool to room temperature and was then further cooled using an ice/water bath. The resulting yellow precipitate was collected by filtration and washed with cold methanol to give **1** as a yellow solid (146 mg, 0.156 mmol, 45 %). Crystals suitable for X-ray diffraction studies were obtained by slow diffusion of MeOH into a DCM solution of **1**. Found: C, 61.29; H, 4.30; N, 1.52. C$_{48}$H$_{40}$P$_3$F$_6$NRu requires: C, 61.41; H, 4.29; N, 1.49. ^1H NMR (CDCl$_3$): δ 4.55 (s, 5H, Cp); 7.09-7.57 (m, 35H, Ph). $^{13}C\{^1H\}$ NMR (CDCl$_3$): δ 135.9 (m, J_{CP} = 23.13 Hz, C_{ipso} PPh$_3$); 133.82 (s, C4); 133.49 (t, J_{CP} = 5.28 Hz, C_{ortho} PPh$_3$); 132.73 (s, C2); 130.37 (s, C_{para}); 129.49 (s, C3); 128.70 (t, J_{CP} = 4.78

Hz, C_{meta} PPh_3); 111.50 (s, C1); 84.38 (s, Cp). $^{31}P\{^1H\}$ NMR ($CDCl_3$): δ 42.89 (s, PPh_3); -142.97 (ht, J_{PF} = 713 Hz PF_6). ES(+)-MS (*m/z*): 794 $[Ru(NCC_6H_5)(PPh_3)_2Cp]^+$; 691 $[Ru(PPh_3)_2Cp]^+$. IR (nujol mull): ν(C≡N) 2233 cm^{-1}.

[Ru(NCC$_6$H$_5$)(dppe)Cp*][PF$_6$] (2)

In a manner similar to that described for the preparation of **1**, a suspension of RuCl(dppe)Cp* (200 mg, 0.299 mmol), C_6H_5CN (0.1 ml, 0.97 mmol), and NH_4PF_6 (195 mg, 1.20 mmol) in refluxing MeOH (10 ml) was allowed to react for 1 hr. The resulting yellow solution was cooled to room temperature and solvent removed. The yellow residue was dissolved in the minimum quantity of DCM, filtered and the product crystallised by slow diffusion of hexane into a DCM solution, affording yellow crystals of **2** (207 mg, 0.235 mmol, 78 %). Found: C, 57.18; H, 4.91; N, 1.49. $C_{43}H_{44}P_3NF_6Ru$ requires: C, 58.50; H, 5.02; N, 1.59. ^1H NMR (CD_2Cl_2): δ 1.51 (s, 15H, Cp*); 2.46, 2.50 (2 x br, 4H, dppe); 6.54, 6.57 (pseudo-d, $2H_{ortho}$, PhCN); 7.26-7.62 (m, 23H, Ph). $^{13}C\{^1H\}$ NMR (CD_2Cl_2): δ 134.63-126.20 (m, Ph); 133.78 (s, C_4); 126.20 (s, C≡N) 111.26 (s, C_1); 93.18 (s, C_5Me_5); 28.77-28.41 (m, dppe); 9.68 (s, C_5Me_5). $^{31}P\{^1H\}$ NMR (CD_2Cl_2): δ 76.15 (s, dppe); -143.42 (ht, J_{PF} = 710 Hz PF_6). ES(+)-MS (*m/z*): 794 $[Ru(NCC_6H_5)(dppe)Cp^*]^+$; 635 $[Ru(dppe)Cp^*]^+$. IR (nujol mull): ν(C≡N) 2227 cm^{-1}.

[Fe(NCC$_6$H$_5$)(dppe)(Cp)][PF$_6$] (3)

An analogous procedure using FeCl(dppe)(Cp) (200 mg, 0.361 mmol), C_6H_5CN (0.1 ml, 0.97 mmol) and NH_4PF_6 (235 mg, 1.44 mmol) followed by recrystallisation by diffusion of MeOH into a DCM solution of **3** resulted in the formation of red crystals of **3** (163 mg, 0.213 mmol, 59 %). Found: C, 59.17; H, 4.43; N, 1.88. $C_{38}H_{34}P_3NF_6Fe$ requires: C, 59.47; H, 4.47; N, 1.83. ^{1}H NMR ($CDCl_3$): δ 4.45 (s, 5H, Cp); 2.45, 2.63 (2 x br, 4H, dppe); 6.46 (s, 2H$_{ortho}$, PhCN); 7.16 -7.86 (m, 23H, Ph). ^{13}C{^{1}H} NMR (CD_2Cl_2): δ 136.74 (m, 2 x C$_{ipso}$); 134.33 (s, C4), 133.36 (s, C2); 133.00 (br, C$_{ortho}$); 132.04 (s, C3); 131.45 (br, C$_{ortho}$); 131.32 (s, C$_{para}$); 130.93 (s, C$_{para}$); 129.69 (br, C$_{meta}$); 129.53 (br, C$_{meta}$); 129.13 (s, CN); 111.41 (s, C1), 79.90 (s, Cp), 28.13 (m, dppe). ^{31}P{^{1}H} NMR ($CDCl_3$): δ 98.32 (s, dppe); -143.13 (ht, J_{PF} = 713 Hz PF_6). ES(+)-MS (*m/z*): 622 [Fe(NCC$_6$H$_5$)(dppe)Cp]$^+$; 519 [Fe(dppe)Cp]$^+$. IR (nujol mull): ν (C≡N) 2217 cm^{-1}.

[Ru(NCC$_6$H$_4$NO$_2$)(PPh$_3$)$_2$Cp][PF$_6$] (4)

The reaction between RuCl(PPh$_3$)$_2$Cp (100 mg, 0.138 mmol), $NCC_6H_4NO_2$ (20.4 mg, 0.138 mmol), and NH_4PF_6 (80 mg, 0.49 mmol) in refluxing MeOH (20 ml) afforded an orange solution after 30 minutes which was cooled (ice/water) to afford **4** as an orange precipitate (90 mg, 0.092 mmol, 66 %). Crystals suitable for X-ray diffraction studies were obtained from slow diffusion of MeOH into a solution of **4** in DCM. Found: C, 54.57; H, 3.84; N, 2.66. $C_{48}H_{39}N_2P_3F_6O_2Ru.CH_2Cl_2$ requires: C, 55.07; H, 3.87; N, 2.62. ^{1}H NMR ($CDCl_3$): δ 4.64 (s, 5H, Cp); 7.11-7.39 (m, 40H,

Ph). $^{13}C\{^1H\}$ NMR ($CDCl_3$): δ 150.04 (s, C4) 135.64 (m, J_{CP} = 22.50 Hz, C_{ipso} PPh_3); 134.21 (s, C_3) 133.50 (t, J_{CP} = 4.78 Hz, C_{ortho} PPh_3); 130.50 (s, C_{para}); 128.80 (t, J_{CP} = 4.77 Hz, C_{meta} PPh_3); 127.91 (s, CN); 124.31 (s, C_2); 117.46 (s, C_1); 84.98 (s, Cp). $^{31}P\{^1H\}$ NMR ($CDCl_3$): δ 42.97 (s, PPh_3); -142.93 (ht, J_{PF} = 713 Hz PF_6). ES(+)-MS (*m/z*): 839 $[Ru(NCC_6H_4NO_2)(PPh_3)_2Cp]^+$; 691 $[Ru(PPh_3)Cp]^+$. IR (nujol mull): ν(C≡N) 2228 cm^{-1}.

$[Ru(NCC_6H_4NMe_2)(PPh_3)_2Cp][PF_6]$ (5)

A procedure analogous to that described for **4** using $RuCl(PPh_3)_2Cp$ (100 mg, 0.138 mmol), $NCC_6H_4NMe_2$ (20 mg, 0.138 mmol), and NH_4PF_6 (80 mg, 0.49 mmol) yielded **5** as a yellow solid (65 mg, 0.066 mmol, 48 %). Crystals suitable for X-Ray diffraction were obtained from slow diffusion of hexane into a solution of **5** in $CHCl_3$. Found: C, 60.69; H, 4.61; N, 2.84. $RuC_{50}H_{45}N_2P_3F_6$ requires: C, 61.16; H, 4.62; N, 2.85. ^1H NMR ($CDCl_3$): δ 4.42 (s, 5H, Cp); 7.00-7.30 (m, 37H, Ph); 2.97 (s, 6H, $N(CH_3)_2$. $^{13}C\{^1H\}$ NMR ($CDCl_3$): δ 153.23 (s, C4) 136.07 (m, J_{CP} = 22.63 Hz, C_{ipso} PPh_3); 133.84 (s, C2) 133.48 (t, J_{CP} = 5.15 Hz, C_{ortho} PPh_3); 130.31 (s, C_{para}); 128.63 (t, J_{CP} = 4.90 Hz, C_{meta} PPh_3); 111.77 (s, C3); 95.61 (s, C1); 83.81 (s, Cp); 40.17 (s, Me). $^{31}P\{^1H\}$ NMR ($CDCl_3$): δ 42.82 (s, PPh_3); -143.04 (ht, J_{PF} = 713 Hz PF_6). ES(+)-MS (*m/z*): 837 $[Ru(NCC_6H_4NMe_2)(PPh_3)_2Cp]^+$; 691 $[Ru(PPh_3)Cp]^+$. IR (nujol mull): ν (C≡N) 2221 cm^{-1}.

[Ru(NCC$_6$H$_4$CN-4)(PPh$_3$)$_2$Cp][PF$_6$] (6)

A two-necked, nitrogen cooled, 50 ml Schlenk flask was charged with RuCl(PPh$_3$)$_2$Cp (100 mg, 0.138 mmol), NCC$_6$H$_4$CN (173 mg, 1.38 mmol), and NH$_4$PF$_6$ (80 mg, 0.49 mmol). MeOH (20 ml) was added and the suspension was heated to reflux under a nitrogen atmosphere. After 30 minutes the yellow solution was cooled and the solvent removed. The yellow residue was dissolved in the minimum quantity of DCM, filtered and precipitated into Et$_2$O. The precipitate formed was collected and dried to obtain **6** as a pale yellow powder (100 mg, 0.104 mmol, 75 %). Found: C, 59.99; H, 3.98; N, 2.82. RuC$_{49}$H$_{39}$N$_2$P$_3$F$_6$ requires: C, 61.06; H, 4.08; N, 2.91. ^{1}H NMR (CDCl$_3$): δ 4.62 (s, 5H, Cp); 6.98-7.37 (m, 74H, Ph). ^{31}P{^{1}H} NMR (CDCl$_3$): δ 42.58 (s, PPh$_3$); -142.93 (ht, J_{PF} = 713 Hz, PF$_6$). ES(+)-MS (*m/z*): 819 [Ru(NCC$_6$H$_4$CN)(PPh$_3$)$_2$Cp]$^+$; 691 [Ru(PPh$_3$)Cp]$^+$. IR (nujol mull): ν(C≡N) 2221 cm^{-1}.

[{Ru(PPh$_3$)$_2$Cp}$_2$(μ-1,4-NCC$_6$H$_4$CN)][PF$_6$]$_2$ (7)

The reaction of RuCl(PPh$_3$)$_2$Cp (200 mg, 0.276 mmol), NCC$_6$H$_4$CN (18 mg, 0.136 mmol), and NH$_4$PF$_6$ (160 mg, 0.98 mmol) in the usual manner yielded 7 as a yellow solid (140mg, 0.078mmol, 57 %). Recrystallisation by slow diffusion of methanol into a solution of 7 in DCM afforded bright yellow crystals suitable for x-ray. Found: C, 56.03; H, 3.79; N, 1.40. Ru$_2$C$_{90}$H$_{70}$N$_2$P$_6$F$_{12}$.2(CH$_2$Cl$_2$) requires: C, 56.11; H, 3.99; N, 1.42. ^{1}H NMR (CDCl$_3$): δ 4.57 (s, 10H, Cp); 6.98-7.37 (m, 74H, Ph). ^{31}P{^{1}H} NMR (CDCl$_3$): δ 42.58 (s, PPh$_3$); -142.84 (ht, J_{PF} = 713 Hz PF$_6$). ES(+)-MS (*m/z*):

1655 $[Ru_2(NCC_6H_4CN)(PPh_3)_4Cp_2]PF_6^+$; 819 $[Ru(NCC_6H_4CN)(PPh_3)_2Cp]^+$; 691 $[Ru(PPh_3)Cp]^+$. IR (nujol mull): ν(C≡N) 2226 cm^{-1}.

$[Co_2(\mu, \eta^2\text{-}HC_2C_6H_4CN\text{-}4)\{Ru(PPh_3)_2Cp\}(CO)_4(dppm)](PF_6)$ (8)

In a procedure analogous to that described for **4**, $RuCl(PPh_3)_2Cp$ (97.9 mg, 0.135 mmol), $Co_2(\mu, \eta^2\text{-}HC_2C_6H_4CN\text{-}4)(CO)_4(dppm)$ (100 mg, 0.135 mmol), and NH_4PF_6 (80 mg, 0.49 mmol), were allowed to react in refluxing MeOH (15 ml) and THF (5 ml) for 2.5 hours after which the solvent was removed and the residue recrystallised by slow diffusion of MeOH into a DCM solution to afford **8** as dark red crystals (141 mg, 0.089 mmol, 66 %). Found: C, 57.75; H, 3.77; N, 0.86. $C_{79}H_{662}Co_2RuO_4P_5NF_6.CH_2Cl_2$ requires: C, 57.81; H, 3.88; N, 0.84. ^1H NMR ($CDCl_3$): δ 3.06 (dt, 1H, J_{HP} = 13 Hz, J_{HH} = 9Hz, C*H*P_2); 3.60 (dt, 1H, J_{HP} = 13 Hz, J_{HH} = 10Hz, C*H*P_2); 4.47 (s, 5H, Cp); 5.80 (s, 1H, J_{HP} = 7 Hz, Co_2C_2H); 7.05-7.50 (m, 54H, Ph). $^{13}C\{^1H\}$ NMR ($CDCl_3$): δ 83.95 (s, Cp); 128.45-133.20 (m, Ph). $^{31}P\{^1H\}$ NMR ($CDCl_3$): δ 42.76 (s, dppm); 43.84 (br, PPh_3). ES(+)-MS (*m/z*): 1432 $[Co_2(\mu, \eta^2\text{-}HC_2C_6H_4CN\text{-}4)\{Ru(PPh_3)_2Cp\}(CO)_4(dppm)]^+$; 691 $[Ru(PPh3)2Cp]^+$. IR (nujol mull): ν(CO) 2021, 1993, 1973 1955 cm^{-1}.

References

1 D. Astruc, J. C. Blais, E. Clontet, L. Djakovitch, S. Rigaut, J. Ruiz, V. Sartor, C. Valeria, *Top. Curr. Chem.*, 2000, **210**, 229.

2 V. Y. Kukushkin, A. J. L. Pombiero, *Chem. Rev.*, 2002, **102**, 1771.

3 P. K. Mascharak, *Coord. Chem. Rev.*, 2002, **225**, 201.

4 L. Martinkova, V. Mylerova, *Curr. Org. Chem.*, 2003, **7**, 1279.

5 P. M. Treichel, R. L. Shubkin, K. W. Barnett, D. Reichard, *Inorg. Chem.*, 1966, **5**, 1177.

6 T. Blackmore, M. I. Bruce, F. G. A. Stone, *J. Chem. Soc.(A)*, 1971, 2376.

7 R. J. Haines, A. L. du Preez, *J. Organomet. Chem.*, 1975, **84**, 357.

8 G. S. Ashby, M. I. Bruce, I. B. Tomkins, R. C. Wallis, *Aust. J. Chem.*, 1979, **32**, 1003.

9 P. E. Riley, C. E. Capshaw, P. Pettit, R. E. Davies, *Inorg. Chem.*, 1978, **17**, 408.

10 J. C. Calabrese, L. T. Cheng, J. C. Green, S. R. Marder, W. Tam, *J. Am. Chem. Soc.*, 1991, **113**, 7227.

11 S. Barlow, H. E. Bunting, C. Righam, J. C. Green, G. U. Bublitz, S. G. Boxer, J. W. Perry, S. R. Marder, *J. Am. Chem. Soc.*, 1999, **121**, 3715.

12 A. R. Dias, M. H. Garcia, M. P. Robalo, M. L. H. Green, K. K. Lai, A. J. Pulham, S. M. Klueber, G. Balvoine, *J. Organomet. Chem.*, 1993, **453**, 241.

13 A. R. Dias, M. H. Garcia, J. C. Rodrigues, M. L. H. Green and S. M. Kuebler, *J. Organomet. Chem.*, 1994, **475**, 241.

14 A. R. Dias, M. H. Garcia, P. Mendes, M. F. M. Piedade, M. T. Duarte, M. J. Calhorda, C. Mealli, W. Wenseleers, A. W. Gerbrandij, E. Goovaerts, *J.*

Organomet. Chem., 1998, **553**, 115.

15 M. H. Garcia, M. P. Robalo, A. R. Dias, M. F. M. Piedade, A. Galvão, W. Wenseleers, E. Goovaerts, *J. Organomet. Chem.*, 2001, **619**, 252.

16 M.L. Kuznetsov and A.J.L. Pombiero, *Dalton Trans*, 2003, 738.

17 M. L. Kuznetsov, *J. Mol. Struct. (Theochem)*, 2004, **671**, 229.

18 M. L. Kuznetsov, *J. Mol. Struct. (Theochem)*, 2004, **674**, 33.

19 I. R. Whittall, M. G. Humphrey, D. C. R. Hockless, B. W. Skelton, A. H. White, *Organometallics*, 1995, **14**, 3970.

20 O. F. Koentjoro, R. Rousseau, P.J. Low, *Organometallics*, 20001, **20**, 4502.

21 J. E. McGrady, T. Lovell, R. Stranger, M. G. Humphrey, *Organometallics*, 1997, **16**, 4004.

22 T. J. Snaith, P. J. Low, R. Rousseau, H. Puschmann, J. A. K. Howard, *J. Chem. Soc., Dalton, Trans*, 2001, 292.

23 W. Winseleers, A. W. Gerbrandij, E. Goovaerts, M. H. Garcia, M. P. Robalo, P. J. Mendes, J. C. Rodrigues, A. R. Dias, *J. Mater. Chem.*, 1998, **8**, 925.

24 M. H. Garcia, J. C. Rodrigues, A. R. Dias, M. F. M. Piedade, M. T. Duarte, M. P. Robalo, N. Lopes, *J. Organomet. Chem.*, 2001, **632**, 133.

25 M. H. Garcia, M. P. Robalo, A. P. S, Teixeira, A. R. Dias, M. F. M. Piedade, M. T. Duarte, *J. Organomet. Chem.*, 2001, **632**, 145.

26 M. H. Garcia, M. P. Robalo, A. R. Dias, M. T. Duarte, W. Winseleers, G. Aerts, E. Goovaerts, M. P. Cifuentes, S. Hurst, M. G. Humphrey, M. Samoc, B. Luther-Davies, *Organometallics*, 2002, **21**, 2107.

27 H.C. Aspinall, A.J. Deeming, S. Donovan-Mtzuni, *J. Chem. Soc. Dalton Trans.*, 1983, 2669.

28 J.F. Costello, S.G. Davies, R.M. Highcock, M.E.C. Polywka, M.W. Poulter, T.

Richardson, G.G. Roberts, *J. Chem. Soc., Dalton Trans.*, 1997, 105.

29 T. Higashi and K. Osaki, *Acta Crystallogr., Sect. B Struct. Crystallogr. Cryst. Chem.*, 1977, **33**, 2337.

30 G. Fauvet, M. Massauz and R. Chevalier, *Acta Crystallogr., Sect. B Struct. Crystallogr. Cryst. Chem.*, 1978, **34**, 1376.

31 C. Elschenbroich, A. Salzer, "Organometallics: A Concise Introduction", Wienheim: VCH Verlagsgesellschaft, 1992.

32 N.G. Connelly and W.E. Geiger, *Chem. Rev.*, 1996, **96**, 877.

33 M. I. Bruce, C. Hameister, A. G. Swincer, R. C. Wallis, *Inorg. Synth.*, 1982, **21**, 78.

34 T. Wilczewski, M Bocheńska, J. F. Biernat, *J. Organomet. Chem.*, 1981, **215**, 87.

35 D.S. Pandey, R.L. Mishra, A. Mishra, U.L Agarwala, *Polyhedron*, 1990, **9**, 2153.

36 J. M. Wisner, T. J. Bartczak, J. A. Ibers, *Inorg. Chim. Acta*, 1985, **100**, 115.

37 M.I. Bruce, M.G. Humphrey, M.R. Snow, E.R.T. Tiekink, *J. Organomet. Chem.*, 1986, **314**, 213

Compounds List - Nitriles

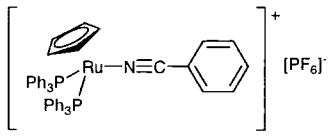

1

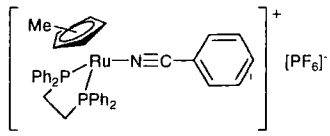

2

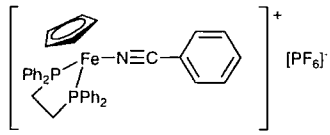

3

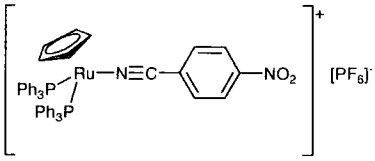

4

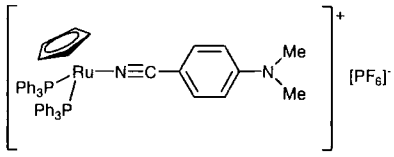

5

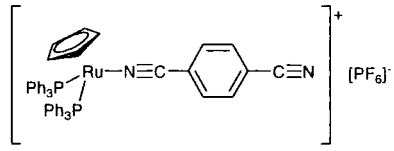

6

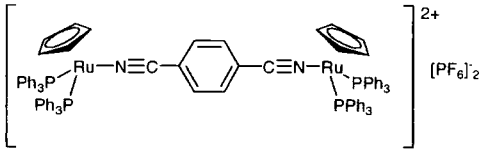

7

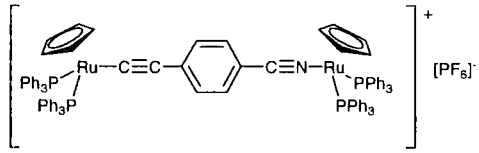

7a

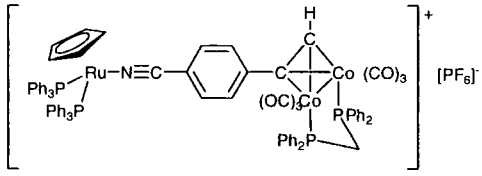

8

Introduction

The bidentate, but non-chelating, nature of the cyanide anion ($^{-}C\equiv N$), together with its orthogonal π-systems, makes it a suitable ligand for bridging and promoting interactions between two metal centres. The anion can coordinate via the carbon atom in an $\eta^1(C)$ fashion as a combination of σ-donation from the carbon ligand (from the lone pair of electrons resultant from the negative charge, located in the cyanide σ* anti-bonding orbital) as well as a degree of π back-bonding from the metal centre into the π* anti-bonding orbital of the C≡N moiety. The coordinated CN moiety can also coordinate in an $\eta^1(N)$ fashion by donation of electron density from an orbital of σ-symmetry essentially localised on the N-atom (which may be formally regarded as the lone pair on the nitrogen atom of the N≡C moiety) giving rise to a μ-$\eta^1(C)$, $\eta^1(N)$ mode. Whilst there may be a degree of π back-donation from the metal centre to the C≡N moiety via the N-atom this is much weaker than at the carbon end. As a result of the coordinative flexibility of the $[CN]^-$ unit, a host of cyanide bridged metal species are known, and many have been studied in exquisite detail.[1-8]

Of particular historical importance is Prussian Blue, a mixed-valence $Fe^{II/III}$ complex $KFe[Fe(CN)_6]$ with an infinite network structure.[9] The interest in such CN bridged systems are the same as those highlighted earlier (see main introduction) for bridged bimetallic complexes in general, namely: molecular structure and thermal and photo-induced electron transfer.

In the late 1990's Vahrenkamp and co-workers carried out an extensive study of a range of dinuclear cyanide-bridged organometallic complexes.[10] The redox chemistry

and mixed-valence behaviour of a series of iron based complexes of type [{ML_n}(μ-CN)[Fe(dppe)Cp}]$^{n+}$ (ML_n = $Cr(CO)_5$, $Mo(CO)_5$, $W(CO)_5$, $Fe(CO)_2Cp$, Fe(CO)(CN)Cp, $Ru(PPh_3)_2Cp$), was of particular interest and each of these complexes were studied in at least two of the chemically accessible oxidation states.

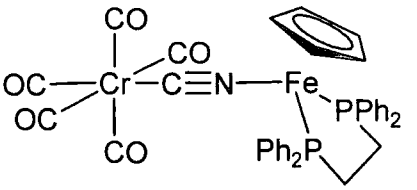

Figure 4.1. The cyanide-bridged bimetallic complex [{$Cr(CO)_5$}(μ-CN)[Fe(dppe)Cp}]

Comparison of the molecular structures of the neutral and oxidised forms of the iron/chromium complex [{$Cr(CO)_5$}(μ-CN)[Fe(dppe)Cp}] (Figure 4.1) showed elongation of the Fe-P and Fe-Cp bonds and contraction of the Fe-N bond upon oxidation, but little change (a decrease of 0.02 Å) in C-N bond length. This suggested that the oxidation was largely iron-centred and that the loss of electron density resulted in a reduction of back-bonding to the phosphine and Cp ligand. The Fe-N bond is contracted, however, and this is not consistent with back-bonding from the iron to the C≡N moiety. Instead, oxidation at the iron centre increases the coulombic interaction between the positively-charged iron centre and the electron pair at the N-atom and reduces the distance between them.

However, despite the relatively small change in CN bond length observed upon oxidation of [{$Cr(CO)_5$}(μ-CN)[Fe(dppe)Cp}], each of the materials described above showed a decrease in the ν(C≡N) stretching frequency upon oxidation. Oxidation of

the iron centre creates a net flow of electron density from the C-bound metal centre towards the N-terminus, corresponding to increased back donation for the C-bound metal into the π^* anti-bonding orbitals of the CN moiety. This results in a weakening of the CN bond and hence a decrease in the $\nu(C\equiv N)$ stretching frequency. The degree to which the $\nu(C\equiv N)$ stretching frequency decreases upon oxidation is dependant on the donor-strength of the C-bound unit. Hence a greater decrease in $\nu(C\equiv N)$ was found following oxidation of the ruthenium/iron complex [{$Ru(PPh_3)_2Cp$}(μ-CN)[Fe(dppe)Cp}] (-73 cm^{-1}) than for the di-iron complex [{$Fe(CO)_2Cp$}(μ-CN)[Fe(dppe)Cp}] (-25 cm^{-1}). These observations suggest that the CN bond length is a poor probe of the bonding interaction between the CN moiety and a metal centre.

In addition to the IR data, electronic absorption spectra of the oxidised (35-electron) bimetallic complexes showed bands in the near-infra-red (NIR) region of the spectrum. These bands are indicative of charge-transfer between metal centres in bridged complexes and analysis of the band-shape suggested that the compounds belonged in the "valence-trapped" (Class 2) grouping (see following results and discussion section for a more detailed description of these "metal to metal" charge-transfer bands). The coupling constants derived for the compounds (an indication of the degree of interaction between the two metal centres) showed stronger coupling for the compounds where the C-bound metal was a stronger donor, mirroring the IR data.

Trimetallic cyanide-bridged complexes have been under study since Siebert's use of the cobalt cyanide complex $[Co(NH_3)_5CN]^{2+}$ to coordinate to silver and mercury centres.[11] Since then, the majority of trimetallic complexes have contained central $Ru(bpy)_2$ units (or analogues thereof) in the interests of investigating photon-induced

electron-transfer.[6] Until the late 1990's there had been few studies of bridging or cis/trans isomerism in trimetallic species, the majority of work focussing on spectroscopic trends and redox properties.[12-15] In addition, there were very few examples of unsymmetrical trinuclear complexes that had been isolated and fully characterised.[16-19]

A series of compounds of type $[\{ML_n\}(\mu\text{-NC})\{Fe(CO)Cp\}(\mu\text{-CN})\{ML_n\}]^+$ (ML_n = $Fe(CO)_2Cp$, Fe(dppe)Cp, $Ru(PPh_3)_2$) featuring a bent geometry about the central iron atom were obtained by Vahrenkamp and co-workers (Figure 4.2) from reactions of $K[Fe(CN)_2(CO)Cp]$ with $[Fe(THF)(CO)_2Cp][BF_4]$, FeBr(dppe)Cp and $RuCl(PPh_3)_2Cp$ in methanol.[20]

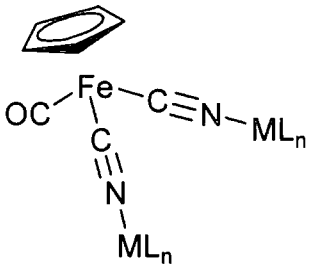

Figure 4.2. The bent geometry of $[\{ML_n\}(\mu\text{-NC})\{Fe(CO)Cp\}(\mu\text{-CN})\{ML_n\}]^+$ (ML_n = $Fe(CO)_2Cp$, Fe(dppe)Cp, $Ru(PPh_3)_2$)

In each case, coordination of the CN moieties via the N-atom to another metal centre caused an increase in the $\nu(C\equiv N)$ stretching frequencies in the same manner as found for the bimetallic complexes. This increase in $\nu(C\equiv N)$ values can be attributed partly to a kinematic effect as well as to the loss of electron density from the CN σ^* orbital upon coordination. Interestingly, a greater increase in the $\nu(C\equiv N)$ stretching frequency was observed in the case where the metal end-cap was the more electron-

withdrawing $Fe(CO)_2Cp$ centre. Curiously, cyclic voltammetry for the compound $[\{Ru(PPh_3)_2\}(\mu\text{-}NC)\{Fe(CO)Cp\}(\mu\text{-}CN)\{Ru(PPh_3)_2\}][PF_6]$ suggested some degree of electronic communication between the remote ruthenium centres and evidence for this was also seen in the electronic absorption spectra of the oxidised complex. This is unusual as electronic communication between remote termini had previously been shown to be inhibited by a *cis*-configuration.[21]

In an extension of the work of Siebert, Connelly and co-workers have shown that the metal-cyanide complexes are good N-donor ligands to M^+ and MCl_2 centres.[12,22,23] This led to an investigation of the physical properties of the compounds $[\{Fe(dppe)Cp\}(\mu\text{-}CN)MCl_2(\mu\text{-}NC)\{Fe(dppe)Cp\}]$ (M = Ni, Cu, Zn)[24] which allowed for comparisons of tetrahedral (Ni, Zn) and square planar (Cu) geometries as well as the effect of redox-active (Ni, Cu) and non-redox active (Zn) central metals on the interactions through the assembly. However, the only complex which showed any evidence of electronic communication between the remote iron centres was the zinc complex $[\{Fe(dppe)Cp\}(\mu\text{-}CN)ZnCl_2(\mu\text{-}NC)\{Fe(dppe)Cp\}]$ (Figure 4.3) for which cyclic voltammetry showed separate oxidation waves for the two iron centres.

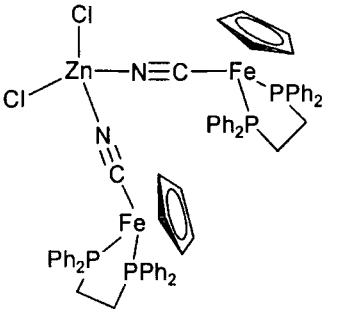

Figure 4.3. $[\{Fe(dppe)Cp\}(\mu\text{-}CN)ZnCl_2(\mu\text{-}NC)\{Fe(dppe)Cp\}]$

Vahrenkamp and co-workers have studied a series of trimetallic complexes bearing central platinum units coordinated to the metal fragments $[Ru(PPh_3)_2]$ and [Fe(dppe)Cp] via cyanide bridges.[25] This resulted in a series of compounds where the remote metal centres were arranged in *cis* and *trans* geometries and with bridging isomers apparent as well. Electrochemistry showed that each of the cis-compounds *cis*-$[\{Fe(\mu\text{-}CN)(dppe)Cp\}_2Pt(bpy)][SbF_6]_2$, *cis*-$[\{Fe(\mu\text{-}CN)(dppe)Cp\}_2Pt(phen)][SbF_6]_2$ and *cis*-$[\{Fe(\mu\text{-}NC)(dppe)Cp\}_2Pt(bpy)][SbF_6]_2$ (Figure 4.4) underwent single two electron oxidation events The complexes with a *trans* geometry about the platinum centre, however underwent two, one-electron oxidation events which suggests that a *trans*-geometry is essential for metal-metal communication irrespective of the orientation of the cyanide bridge. Furthermore, it indicates that the remote metal-metal interaction is a through bond interaction via the π-system of the trimetallic species.

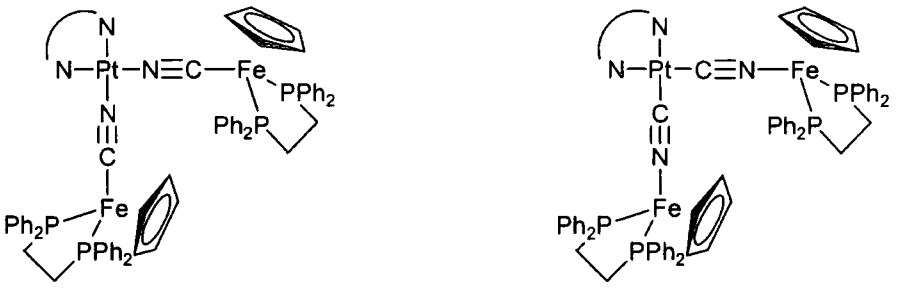

a **b**

Figure 4.4. Square planar platinum *cis*-complexes (**a**: N-N = bpy, phen; **b**: N-N = bpy)

The electrochemical response of the trimetallic, *trans*-configured tetracyanoplatinate complexes $[\{Fe(dppe)Cp\}_2\{\mu\text{-}Pt(CN)_4\}]$ and $[\{Fe(dppe)Cp\}\{\mu\text{-}Pt(CN)_4\}\{Ru(PPh_3)_2Cp\}]$ (Figure 4.5) revealed two, one-electron oxidations, the

separation of which indicated thermodynamic stability of the mono-oxidised form with respect to disproportionation. Chemical oxidation of the trimetallic complexes with ferrocinium hexafluorophosphate duly gave the mono-oxidised materials, isolated as $[PF_6]^-$ salts.[25]

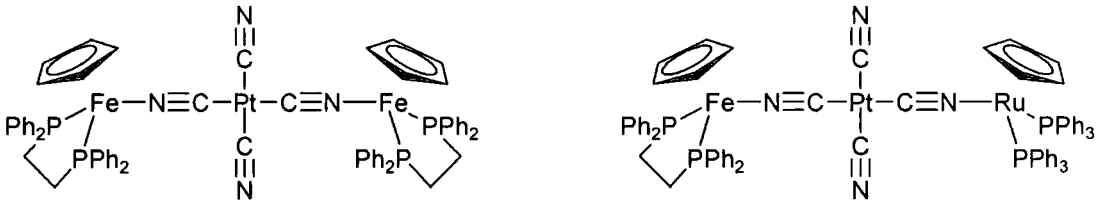

Figure 4.5. Trimetallic tetracyanoplatinate complexes

Infra-red spectroscopy revealed an increase in the ν(C≡N) stretching frequencies of the coordinated CN moieties upon oxidation. The oxidation of one of metal terminus results in a flow of electron density across the complex from the remote metal terminus to the oxidised centre. This in turn leads to two competing effects: increased N→M σ-donation which strengthens the CN bond and increased Pt→C back-bonding, which would weaken the CN bond. It is apparent from the resultant increase in ν(C≡N) upon oxidation that the effect of increased σ-donation is more pronounced. The electronic absorption spectra of the oxidised materials showed IVCT bands in the NIR region of the spectrum corresponding to $M^{II} \rightarrow M^{III}$ charge transfer. In the case of the di-iron complex $[\{Fe(dppe)Cp\}_2\{\mu\text{-}Pt(CN)_4\}]^+$ the IVCT band was observed at 6410 cm^{-1} but this was moved to higher energy in the mixed-metal complex $[\{Fe(dppe)Cp\}\{\mu\text{-}Pt(CN)_4\}\{Ru(PPh_3)_2Cp\}]^+$ (13300 cm^{-1}). Assuming that the oxidation occurred at the iron centre then this shift of IVCT energy to higher energy is

consistent with the poorer electron-donor ability of the $[Ru(PPh_3)_2Cp]$ end-cap relative to [Fe(dppe)Cp].

Coordination of a third metal centre to one of the pendant CN moieties of the di-iron complex resulted in the formation of the tetrametallic complexes shown below (Figure 4.6).[26]

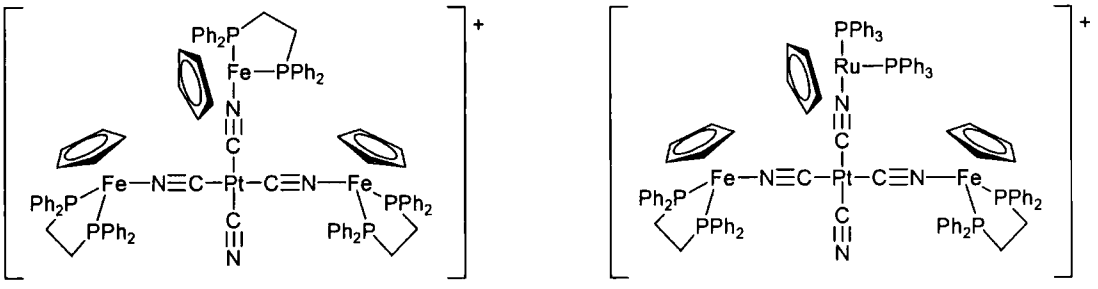

Figure 4.6. Tetrametallic tetracyanoplatinate complexes

Cyclic voltammetry of the tri-iron complex revealed a one-electron oxidation event followed by a two-electron oxidation process. The iron-ruthenium complex, however, underwent three one-electron oxidations, the first two of which corresponded with those observed for $[\{Fe(dppe)Cp\}_2\{\mu\text{-}Pt(CN)_4\}]$ whilst the third, which was well separated from the first two (E_2-E_1 = 0.11 V, E_3-E_2 = 0.55 V) was characteristic of oxidation of a $[Ru(PPh_3)_2Cp]^+$ centre. The electronic absorption spectrum of the iron/ruthenium complex after oxidation was found to be very similar to that of the di-iron complex $[\{Fe(dppe)Cp\}_2\{\mu\text{-}Pt(CN)_4\}]$. Thus it seems that there is little communication between the *cis* termini and that the *trans* interaction between the remote iron centres is relatively unaffected by coordination of a third metal centre.

The work of Vahrenkamp and co-workers has shown that the square planar tetracyanometallate dianions of Group 10 metals, $[M(CN)_4]^{2-}$, are rather useful, if relatively unexplored, cyanometallate ligands capable of bridging, in principle, up to four metal centres.[25,26] Greater interest in these complexes has been driven the by the discovery of complexes such as Krogmann salts ($K_2[Pt(CN)_4]$), which form chain-like, or pseudo one-dimensional, arrays of platinum centres.[27-29] The various coordination modes which might be envisioned arising from the $[M(CN)_4]^{2-}$ fragment, and those of the corresponding tetra(cyanoacetylide) dianions $[M(C{\equiv}CC{\equiv}N)_4]^{2-}$ prepared by Miller,[30] prompted us to consider a systematic investigation of complexes of the general form $[M'L_2Cp']_2\{\mu\text{-}M(CN)_4\}$ and the role the nature of the individual metal centres and supporting ligands might play on the electronic interactions which might occur through the $M(CN)_4$ bidentate metallo-ligand.

Results and Discussion

Syntheses and Physical Properties

The compounds **9-14** were prepared by reaction of the half-sandwich metal chlorides $RuCl(PPh_3)_2Cp$ or RuCl(dppe)Cp* with one half-equivalent of the appropriate potassium tetracyanometallate (Scheme 4.1). The KCl by-product was removed by extraction and filtration and the pure trimetallic compounds were obtained as yellow crystalline solids in moderate to good yield after crystallisation.

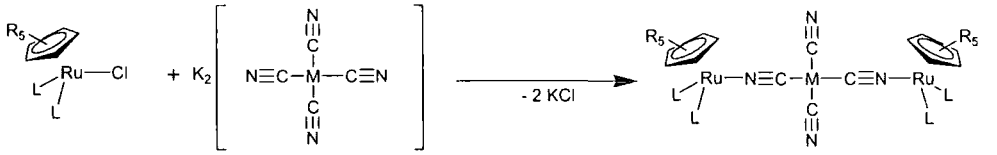

Scheme 4.1. Synthesis of $[\{Ru(PPh_3)_2Cp\}_2\{\mu\text{-}M(CN)_4\}]$ {M = Ni (**9**), Pd (**10**), Pt (**11**)} and $[\{Ru(dppe)Cp^*\}_2\{\mu\text{-}M(CN)_4\}]$ {M = Ni (**12**), Pd (**13**), Pt (**14**)}

In each case the IR spectrum clearly revealed two ν(C≡N) bands which were assigned to bridging (2136-2157 cm^{-1}) and non-bridging (2118-2130 cm^{-1}) CN moieties, the assignment being made by comparison with the spectra of the precursor $K_2[M(CN)_4]$ species. These data are discussed in more detail below.

The Cp' ligands gave rise to the expected resonances in the ^{1}H NMR spectra in the narrow ranges 4.29-4.30 ppm (Cp, **9-11**) and 1.45-1.48 ppm (Cp*, **12-14**). Further, for compounds **12-14**, resonances arising from the ethyl protons of the dppe ligand backbone were observed as multiplets in the range 2.00-2.64 ppm. Similarly, Cp' resonances were also observed in the $^{13}C\{^{1}H\}$ NMR spectra with Cp resonances falling in the narrow range 82.16-83.43 ppm (**9-11**) and Cp* resonances occurring in the narrow ranges 91.68-91.70 ppm (C_5Me_5, **12-14**) and 10.08-10.13 ppm (C_5Me_5, **12-14**). The ^{31}P NMR spectra were also unremarkable, and simply served to confirm the presence of the phosphine ligands with singlet resonances occurring in the ranges 43.12-43.40 ppm (PPh_3, **9-11**) and 71.71-75.79 ppm (dppe, **12-14**). No Pt coupling was observed in the case of **11** or **14**. With the exception of compound **10**, positive-ion electrospray mass spectrometry (ES(+)-MS) of each compound displayed isotopic envelopes arising from the $[M+H]^+$ (**9**, **11**) or $[M+Na]^+$ ions (**12-14**) as well as fragment ions corresponding to the $[Ru(PPh_3)_2Cp]^+$ and $[Ru(dppe)Cp^*]^+$ fragments at *m/z* values of 691 and 635 respectively. Attempts to acquire a mass spectrum for **10** were unsuccessful, with no identifiable fragment of **10** being observed.

The bimetallic complex anion $[Ru(dppe)Cp^*\{Pt(CN)_4\}]^-$ was obtained as its potassium salt (**15**) which was isolated as a pure powder from a 1.5:1 reaction of $K_2[Pt(CN)_4]$ with RuCl(dppe)Cp* in refluxing methanol and subsequent work-up. The complex salt was characterised by the usual spectroscopic techniques, with ^{1}H NMR spectroscopy revealing the presence of the Cp* ligand at 1.47 ppm. The dppe ligand gave two broad resonances at 2.08 and 2.64 ppm (C_2H_4) as well as multiple resonances in the range 7.20-7.68 ppm corresponding to the phenyl protons. The dppe ligand was also apparent in the ^{31}P NMR spectrum as a sharp singlet occurring at

75.67 ppm. Negative-ion electrospray mass spectrometry (ES(-)-MS) displayed isotopic envelopes at *m/z* = 932 ($[Ru(dppe)Cp^*\{Pt(CN)_4\}]^-$) and 273 ($[Pt(CN)_3]^-$) whilst the fragment ion $[Ru(dppe)Cp^*]^+$ was visible in the ES(+)-MS as an intense isotopic envelope at *m/z* = 635. Infra-red spectroscopy revealed a single ν(C≡N) band at 2130 cm^{-1}, corresponding to the non-bridging CN moieties by analogy with the complexes described above. The ν(C≡N) band of the bridging moiety was not observed.

With a range of ruthenium complexes in hand, analogous species featuring the more electron-rich/ π-donating $[Fe(dppe)Cp]^+$ fragment were also sought. Reaction of the iron complex FeCl(dppe)Cp with $K_2[Pt(CN)_4]$ in refluxing methanol resulted in the formation of a red solution. After purification by column chromatography, and subsequent recrystallisation, $[\{Fe(dppe)Cp\}_2\{\mu\text{-}Pt(CN)_4\}]$ (**16**) was obtained as a red crystalline solid in 43 % isolated yield. The ^1H NMR spectrum revealed a Cp resonance at 4.19 ppm as well as two broad resonances corresponding to the methylene protons of the dppe ligand at 2.08 and 2.63 ppm. Infra-red spectroscopy revealed ν(C≡N) bands at 2128 cm^{-1} (non-bridging CN) and 2149 cm^{-1} (bridging CN). This synthesis represents a modification of that described previously by the Vahrenkamp group, which involved the reaction of $PPN_2[Pt(CN)_4]$ with FeCl(dppe)Cp in DCM for 3 days to afford **16** in 72% yield.[25] The yield of the reaction used herein is lower, however this is counterbalanced by the greatly reduced reaction time and the commercial availability of the potassium tetracyanoplatinate starting material.

Curiously, attempts to form complexes [{Fe(dppe)Cp}$_2${μ-M(CN)$_4$}] (M = Pd, Ni) using similar conditions were not successful. Reaction of FeCl(dppe)Cp with $K_2[Ni(CN)_4]$ in refluxing methanol resulted in a red/orange solution from which orange crystals were obtained upon work-up. Spectroscopic analysis of this material revealed a single ν(C≡N) band in the IR spectrum at 2063 cm^{-1} as well as ^{1}H NMR resonances at 4.31 ppm (Cp) and broad signals at 2.62 and 2.37 ppm (dppm). Comparison of these data with literature values,[31] together with a single-crystal structure study, revealed this compound to be Fe(CN)(dppe)Cp, formed by cyanide ligand abstraction from the nickel precursor, and isolated in 48 % yield.

Reaction of FeCl(dppe)Cp with $K_2[Pd(CN)_4]$ in refluxing methanol resulted in a red/orange powder. Analysis of the powder by IR spectroscopy revealed ν(C≡N) bands consistent with [{Fe(dppe)Cp}$_2${μ-Pd(CN)$_4$}] at 2134 and 2127 cm^{-1} as well as a band arising from Fe(CN)(dppe)Cp at 2063 cm^{-1}. Attempts to separate this mixture have, as yet, been unsuccessful.

Table 4.1. Selected spectroscopic data for compounds **9-16**

Compound	(CN) bridging (cm^{-1})	(CN) non-bridging (cm^{-1})	^{1}H δ(Cp/Cp*)	^{13}C{^{1}H} δ(Cp/Cp*)
$K_2[Ni(CN)_4]$		2124[a]		
$K_2[Pd(CN)_4]$		2136[a]		
$K_2[Pt(CN)_4]$		2133[a]		
9	2143	2119	4.29	83.43
10	2157	2130	4.30	82.16
11	2157	2129	4.30	83.43
12	2136	2118	1.45	91.68/10.08
13	2146	2129	1.48	91.68/10.13
14	2150	2128	1.48	91.70/10.07
15	not observed	2130	1.47	90.40/8.79
16	2149	2128	4.19	not obtained

[a] Literature value, recorded in aqueous solution as species insoluble in DCM[32].

In the case of $[M(CN)_4]^{2-}$ anions, vibrational spectroscopy has been used to probe the M-C and C≡N force constants and the nature of the M-C bond. The relative energies of the ν(CN) bands in the series $K_2[M(CN)_4]$ suggested that, whilst the σ-acceptor strength of the metal increased in the order Ni < Pd < Pt , the π back-bonding ability increased in the order Pd < Ni < Pt.[32,33] To the best of our knowledge, the orbital interactions between the group 10 metal and the cyano moiety in these group 10 tetracyanometallates have not yet been the subject of computational modelling studies.

The differing σ-acceptor/π-donor abilities of the group 10 metal can be seen in the ν(C≡N) values of the $K_2[M(CN)_4]$ (M = Ni, Pd, Pt) starting materials (Table 4.1). The increase of 12 cm^{-1} upon exchanging Pd for Ni is explained as follows: as Pd is the stronger σ-acceptor it draws more electron density from the σ* orbital of the CN moiety and so the C≡N bond strength is increased relative to the Ni complex. Platinum, whilst being the strongest σ-acceptor of the three metals is also the strongest π-donor. The net result of these two competing effects is that the C≡N bond strength, and hence the ν(C≡N) value, falls between those determined for the Ni and Pd complexes.

The IR data for the compounds **9-14** (Table 4.1) are of great use in beginning to understand the bonding interactions between the central $[M(CN)_4]^{2-}$ units and the ruthenium end-caps. In the case of $\mu,\eta^1(C),\eta^1(N)$ coordination of cyanide, interaction of the CN moiety to a second metal via the lone pair of the N atom removes electron density from the anti-bonding σ* orbital, thereby increasing the bond strength and

hence the ν(CN) frequency. With each of the trimetallic compounds **9-14**, there is an increase in ν(C≡N) upon coordination of the CN moiety to the ruthenium or iron centres. Unsurprisingly, this increase is greatest for those compounds where the CN moiety is coordinated to the $[Ru(PPh_3)_2Cp]^+$ fragment (**9-11**) and less significant in the case of complexes **12-14**, in which the ruthenium centre bears the more electron-donating Cp*/dppe moieties. It is even less so in the case of the $[Fe(dppe)Cp]^+$ complex **16** which features the most electron-rich Group 8 metal end-cap.

Within the two groups of complexes **9-11** and **12-14,** in which the only variation is the nature of the central metal atom, some small variations in ν(C≡N) as a function of the central metal atom can be observed when, for example, the nickel complexes **9** and **12** are used as a point for comparison. Upon substituting Pd for Ni there is an increase of about 10-15 cm^{-1} in ν(C≡N) of the bridging CN moiety (i.e. $\Delta\nu(C\equiv N) = +10\text{-}15\ cm^{-1}$). Palladium, being described as the better σ-acceptor on the basis of the vibrational studies mentioned above, draws more electron density from the CN σ* orbital than Ni and so the CN bond strength is increased. Upon substituting Pt for the central metal, however, there is little or no increase in ν(C≡N) ($\Delta\nu(C\equiv N)$ for **10**→**11** = 0 cm^{-1}; $\Delta\nu(C\equiv N)$ for **13**→**14** = 4 cm^{-1}). Again, this may be due to the presence of the markedly more π-donating Pt centre resulting in a degree of population of the CN π* anti-bonding orbital and counteracting the increased σ-accepting nature of the metal. It must be stressed, however, that these variations in ν(C≡N) are small, and while the vibrational data can be related to the underlying electronic structure of these materials by a simple fragment approach, simple interpretations of the $\nu(\eta^1\text{-CN})$ and $\nu(\mu,\eta^1,\eta^1\text{-CN})$ can be complicated by kinematic effects, and more extensive orbital mixing.

Interestingly, coordination of the half-sandwich metal fragments to the tetracyanometallate anions seems to have an effect on the non-bridging CN groups as well, reflecting the overall variation in electron density at the central atom. In each case there is a decrease of about 4-6 cm^{-1} in the ν(C≡N) associated with the uncoordinated cyano group relative to the ν(CN) frequency in the appropriate $K_2[M(CN)_4]$ starting material. While small, these deviations are within the limits of precision of the experiment (the Avatar IR spectrometer used in the study has a resolution of 2 cm^{-1}) and presumably arise from a small increase in the group 10 metal-CN back-bonding interaction.

Molecular Structures

The molecular structure of the di-iron complex **16** has been reported by the Vahrenkamp group and will be discussed in comparison with the structures of the ruthenium complexes.[25] Each of the ruthenium complexes **9-14** were subjected to X-ray diffraction studies to confirm the *trans* geometry about the cyanometallate bridge and to investigate the series for systematic differences, which might be useful structural probes of the underlying electronic structure. The crystallographic data is summarised in Tables 4.2 (**9-11**) and 4.3 (**12-14**), whilst selected bond lengths, and bond angles are summarised in Tables 4.4 and 4.5 whilst Figures 4.7 and 4.8 show representative molecular structures for compounds bearing $[Ru(PPh_3)_2Cp]$ and [Ru(dppe)Cp*] end-caps respectively.

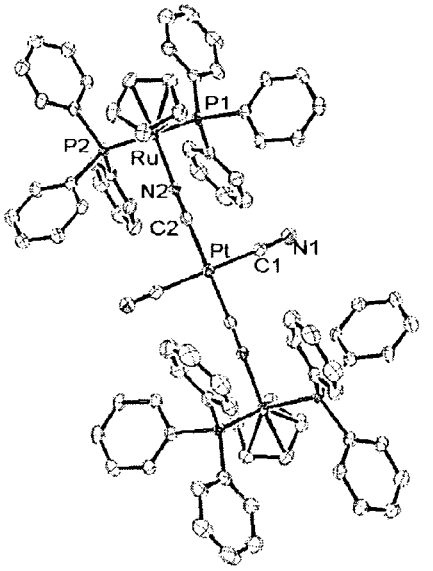

Figure 4.7. ORTEP Plot of $[\{Ru(PPh_3)_2Cp\}_2\{\mu\text{-}Pt(CN)_4\}]$ (**11**).

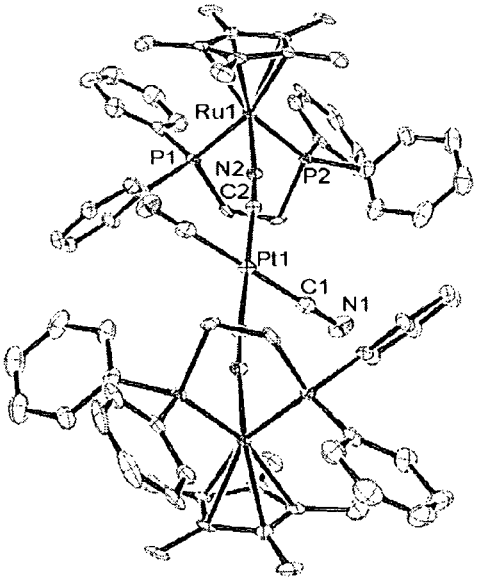

Figure 4.8. ORTEP Plot of $[\{Ru(dppe)Cp\}_2\{\mu\text{-}Pt(CN)_4\}]$ (**14**).

Table 4.2 Crystallographic details for compounds **9-11**.

Compound	9	10	11
Formula	$C_{86}H_{70}N_4P_4Ru_2Ni.2CH_2Cl_2$	$C_{86}H_{70}N_4P_4Ru_2Pd.2(CH_2Cl_2)+2(MeOH)$	$C_{86}H_{70}N_4P_4Ru_2Pt.2(CH_2Cl_2)+2(MeOH)$
M	1714.04	1825.82	1914.51
a (Å)	9.8590(3)	10.5596(10)	10.5697(5)
b (Å)	23.3226(7)	22.500(2)	22.5080(9)
c (Å)	17.7015(5)	17.1648(13)	17.1733(7)
α (°)	90	90	90
β (°)	92.1780(10)	99.559(6)	99.628(2)
γ (°)	90	90	90
V (Å^3)	4067.3(2)	4021.6(6)	4028.0(3)
D (Mg/m^3)	1.400	1.508	1.578
T (K)	120(2)	120(2)	120(2)
Crystal system	Monoclinic	Monoclinic	Monoclinic
Space Group	$P2_1/n$	$P2_1/n$	$P2_1/n$
Z	2	2	2
μ (mm^{-1})	0.853	0.856	2.366
Reflections collected	29274	45343	43801
Independent reflections (R_{int})	10051 [$R_{(int)}$ = 0.0582]	10830 [$R_{(int)}$ = 0.0987]	12290 [$R_{(int)}$ = 0.0559]
Final R indices (all data)	R_1 = 0.1523, wR_2 = 0.3129	R_1 = 0.1167, wR_2 = 0.1281	R_1 = 0.0643, wR_2 = 0.1132

Table 4.3 Crystallographic details for compounds **12-14**.

Compound	**12**	**13**	**14**
Formula	$C_{76}H_{78}N_4P_4Ru_2Ni.2(CHCl_3)$	$C_{76}H_{78}N_4P_4Ru_2Pd.2(C_2H_5OH)$	$C_{76}H_{78}N_4P_4Ru_2Pt.2(C_2H_5OH)$
M	1551.5	1572	1661
***a* (Å)**	11.3214(10)	8.5279(8)	8.5326(12)
***b* (Å)**	12.3886(11)	24.917(2)	25.012(3)
***c* (Å)**	14.3895(11)	19.1022(16)	20.777(3)
***α* (°)**	71.639(3)	90	90
***β* (°)**	75.692(4)	90.971(4)	113.577(5)
***γ* (°)**	78.916(4)	90	90
V (Å^3)	1841.6(3)	4058.5(6)	4064.0(10)
D (Mg/m^3)	1.507	1.286	1.357
T (K)	120(2)	120(2)	120(2)
Crystal system	Triclinic	Monoclinic	Monoclinic
Space Group	$P\bar{1}$	$P2_1/n$	$P2_1/c$
Z	1	2	2
μ (mm^{-1})	1.009	0.710	2.207
Reflections collected	22020	50442	28553
Independent reflections (R_{int})	10996 [$R_{(int)}$ = 0.0276]	12325 [$R_{(int)}$ = 0.0281]	11443 [$R_{(int)}$ = 0.1025]
Final R indices (all data)	R_1 = 0.0669, wR_2 = 0.1511	R_1 = 0.0371, wR_2 = 0.0800	R_1 = 0.0669, wR_2 = 0.1513

Table 4.4. Selected bond lengths (Å) for the complexes **9-14** and **16**

Compound	M-N(2)	N(2)-C(2)	C(2)-M'	C(2)-M' (Normalised)	M'-C(1)	M'-C(1) (Normalised)	C(1)-N(1)	M-P(1)	M-P(2)
9	2.060(8)	1.144(13)	1.877(10)	1.387(10)	1.891(12)	1.401(12)	1.127(15)	2.317(3)	2.333(3)
10	2.069(3)	1.141(5)	2.002(4)	1.362(4)	2.010(5)	1.370(5)	1.133(6)	2.3160(12)	2.3221(11)
11	2.065(3)	1.150(5)	1.994(4)	1.394(4)	1.991(4)	1.391(4)	1.149(5)	2.3183(9)	2.3231(9)
12	2.037(3)	1.148(5)	1.854(4)	1.364(4)	1.876(4)	1.386(4)	1.148(5)	2.2921(9)	2.3126(9)
13	2.048(2)	1.149(2)	1.990(2)	1.350(2)	2.004(2)	1.364(2)	1.148(3)	2.2927(5)	2.2783(5)
14	2.049(6)	1.139(9)	1.992(7)	1.392(7)	2.004(9)	1.404(9)	1.170(10)	2.293(2)	2.275(2)
16[a]	1.914(5)	1.131(8)	1.993(6)	1.393(6)	1.990(8)	1.390(8)	1.153(10)	Average = 2.207(4)	

[a]Literature values.[25]

Table 4.5. Selected bond angles (°) for the complexes **9-14** and **16**

Compound	M-N(2)-C(2)	N(2)-C(2)-M'	C(2)-M'-C(1)	M'-C(1)-N(1)	P(1)-M-P(2)
9	169.4(8)	176.7(9)	92.7(4)	178.3(11)	101.11(10)
10	171.3(4)	178.4(4)	88.49(17)	177.2(5)	100.74(4)
11	171.0(3)	178.2(3)	88.65(14)	177.6(4)	100.68(3)
12	169.2(3)	172.4(3)	87.96(15)	177.2(36)	82.65(3)
13	175.83(14)	174.60(16)	91.55(7)	177.8(2)	82.87(2)
14	174.7(6)	175.9(7)	91.3(3)	177.1(7)	82.82(7)
16[a]	168.5(5)	176.0(6)		178.8(7)	

[a]Literature values.[25]

For each compound, the Group 10 metal centre was found residing on a centre of inversion in the molecule, and as such for any given complex the parameters at each Group 8 metal centre are identical. All but one were found to be monoclinic crystals of space group $P2_1/n$, the exception being compound **12,** for which a triclinic crystal system of space group $P\bar{1}$ was found. The geometry about the ruthenium centres is not unusual, and is probably best described as a distorted octahedron with the Cp ligand occupying three of the coordination sites. The geometry about the central metal M (M = Ni, Pd, Pt) is essentially square planar with C(1)-M-C(2) angles falling in the range 87.96 (15) (**12**) to 92.74(4)° (**9**). In each case, the sum of these angles about the group 10 metal is essentially 360°, confirming the square planar geometry of this site.

It is difficult to compare the M-C (M = Ni, Pd, Pt) bond lengths directly as the experimentally determined bond length is usually defined as the distance from the centre of one atom to the centre of another. Thus, while in the case of atoms of similar size direct comparisons are appropriate, in the case of the compounds studied herein the marked difference in the effective ionic radii of the group 10 metals complicates this simple analysis. The effective ionic radii of square planar Ni^{2+}, Pd^{2+}

and Pt^{2+} are said to be 0.49 Å, 0.64 Å and 0.60 Å respectively.[34] Subtraction of these values from the experimentally determined M-C(1) and M-C(2) bond lengths results in their "normalisation" (Table 4.4), and in doing so it is apparent that there is no statistically significant variation in these normalised M-C bond lengths.

The Ru-N(2) bond lengths for compounds **9-11** fall in the narrow range 2.060(8)-2.069(3) Å whilst for compounds **12-14** this range is 2.037(3)-2.049(2), revealing an apparent shortening of this bond upon increasing the electron density at the ruthenium centre. This is probably a consequence of increasing electrostatic factors. In the case of the bridging cyano moieties C(2)-N(2), the bond length is essentially the same across the series of compounds **9-14**, with an average value of 1.146 Å. Compounds **9** and **10**, which feature $[Ru(PPh_3)_2Cp]^+$ end-caps with Ni and Pd metal centres respectively, have C(1)-N(1) bond lengths of 1.127(14) and 1.133(6) Å respectively, whilst this value is 1.149 (5) Å for the platinum compound **11**. Similarly, **12** and **13** have C(1)-N(1) bond lengths of 1.148(5) and 1.148(3) Å respectively whilst that for **14** is 1.170 (10) Å. Whilst at first glance the pendant C(1)-N(1) bond lengths appear longer in the case of the platinum complexes (**11** and **14**) than either the nickel (**9** and **12**) or palladium (**10** and **13**) examples, and the pendant C(1)-N(1) bond lengths appear elongated in the more electron-rich series based upon Ru(dppe)Cp* when compared with the $Ru(PPh_3)_2Cp$ analogues, these distances are, again, experimentally indistinguishable and must be treated as such.

The crystal structure of the iron/platinum complex **16** has been reported previously.[25] As with the ruthenium complexes this structure was found to be centrosymmetric about the $[M(CN)_4]$ moiety. The bond lengths of the bridging and non-bridging CN

CN units were 1.131(8) and 1.153(10) Å respectively which is consistent with those in the ruthenium complexes **9-14**, as are the corresponding Pt-C distances of 1.993(6) Å [Pt-C(2)] and 1.990(8) Å [Pt-C(1)]. The only notable differences in the structure of **16** compared to its ruthenium analogues arise from the smaller size of the iron centre, which results in shortening of the Fe-N and Fe-P distances relative to the Ru-N and Ru-P distances in **11**. For **16** these are 1.914(5) Å and an average of 2.207(4) respectively which compare with those of **11** (Ru-N = 2.065(3) Å, $Ru\text{-}P_{average}$ = 2.3207(9)) and **14** (Ru-N = 2.042(7) Å, $Ru\text{-}P_{average}$ = 2.2845(2)).

In summary, the molecular structures of the compounds **9-14** and **16** are almost identical and hence show little evidence for the possible variation in σ/π-bonding effects. There is no variation in the C(2)-N(2) bond lengths as might be expected if there were varying degrees of back-bonding into the π* anti-bonding orbital, nor is there any change in the C(2)-M' bond lengths with variation of M' (M' = Ni, Pd, Pt). There is, however, an apparent increase in the C(1)-N(1) bond length brought about exchanging Pd for Pt. This is a very small change and approaches the limits of precision of the measurements. It is possible that this may be induced by back bonding from the Pt centre to the π* orbital of the terminal CN moiety. However, this would be expected to be accompanied by a concomitant shortening of the Pt-C(1) bond which is not observed here. It has been stated above that the observed patterns in ν(C≡N) are very small and it may be that the possible factors affecting their variations simply do not appear in the structural data. Similar observations have been made for bimetallic cyanide-bridged species.[10]

Electrochemistry

The great interest in the properties of compounds in which redox active moieties are separated by some bridging moiety prompted an examination of the cyanometallate bridged complexes **9-16** by cyclic and differential pulse voltammetry (CV and DPV respectively). These electrochemical measurements were made using a platinum disc working electrode and platinum wire counter and pseudo-reference electrodes. Measurements were carried out in a 0.1M $[N(C_4H_9)_4][BF_4]$ solution in DCM solution for all complexes and also in THF solution for compounds **9-14**. Internal decamethylferrocene [Fc^*/Fc^{*+} = -0.02 V vs. SCE (DCM) or 0.13 V vs. SCE (THF)] or ferrocene [Fc/Fc^+ = +0.46 V vs. SCE (DCM) or +0.56 V vs. SCE (THF)] standards were used to give electrode potentials relative to SCE (Table 4.6).[35]

Table 4.6. Electrochemical data

Compound/solvent	$E_{ox}(1)$ (V)	$E_{ox}(2)$ (V)	ΔE_{ox} (V)	Kc[c]
9[a]	0.95	1.06	0.11	190
9[b]	1.11	1.20	0.09	75
10[a]	1.00	1.08	0.08	45
10[b]	1.14	1.20	0.06	20
11[a]	0.97	1.08	0.11	190
11[b]	1.08	1.20	0.12	310
12[a]	0.69	0.82	0.13	155
12[b]	0.81	0.90	0.09	35
13[a]	0.72	0.84	0.12	105
13[b]	0.82	0.90	0.08	20
14[a]	0.71	0.85	0.14	230
14[b]	0.82	0.92	0.10	50
15[a]	0.74	n/a	n/a	n/a
16[a]	0.34	0.45	0.11	70

[a]DCM, [b]THF, [c]$Kc = \exp\{\Delta E_{ox}F/RT\}$ where $F/RT = 47.76\ V^{-1}$ at 243K (**9-11**) and $38.92\ V^{-1}$ at 298 K (**12-14**)

For compounds **9-14** and **16**, two oxidation events were observed at a platinum electrode. Whilst these events were fully chemically and electrochemically reversible at room temperature for compounds **12-14** and **16**, sub-ambient temperatures (-30 °C) were required to improve the reversibility of the oxidations of compounds **9-11**. The small difference between the half-wave potentials, ΔE, necessitated that in some cases differential pulse voltammetry be used to determine accurately the oxidation potentials. The electrochemical response of the bimetallic anion **15** was characterised by a single reversible oxidation occurring at 0.74 V.

For the compounds of type $[\{Ru(PPh_3)_2Cp\}_2\{\mu\text{-}M(CN)_4\}]$ (M=Ni, Pd, Pt) (**9-11**) the oxidation potentials fall in the range 0.95-1.2 V. A variety of solvation factors and ion-paring phenomena can influence oxidation potentials, and this point has recently been highlighted by Keene as a potential complication in the determination of "electronic coupling" on the basis of electrochemical measurements alone.[36] The electrochemical responses of these systems were recorded in two different solvents in an effort to distinguish through-bond from through-space effects. The difference between the two oxidation potentials ($\Delta E_{1/2}$) is somewhat smaller in THF than DCM for **9** (from 0.11 to 0.09 V) and **10** (from 0.08 to 0.06 V), with the decreased separation of the oxidation potentials arising from the greater relative shift of the first oxidation event to higher potentials. The value of $\Delta E_{1/2}$ for compound **11** remains constant at 0.12 V upon changing solvent. Thus it would appear that there is some contribution to the thermodynamic stability of the one-electron oxidation products arising from solvation factors, with an underlying contribution from through-bond interactions.

Oxidation potentials of the compounds [{Ru(dppe)Cp*}$_2${μ-M(CN)$_4$}] (M=Ni, Pd, Pt) (**12-14**) fall in the range 0.69-0.92 V and in each case changing the solvent from DCM to THF resulted in a shift of the oxidation potentials to higher potential with a corresponding decrease in the values of $\Delta E_{1/2}$. As with the Ru(PPh$_3$)$_2$Cp derived complexes [**9**]$^+$-[**11**]$^+$, the thermodynamic stability of the one-electron oxidised species [**12**]$^+$, [**13**]$^+$, and [**14**]$^+$ with respect to disproportionation was decreased in THF relative to DCM as evidenced by the smaller separation of the electrochemical events and consequently giving rise to lower values of the comproportionation constant, K_c. The redox behaviour of compound **16** has already been described by Vahrenkamp,[25] with two successive oxidations at +0.34 V and +0.45 V vs. SCE being observed.

The lower oxidation potentials of the compounds **12-14** relative to **9-11** can be attributed to the variations in the supporting ligands: the Cp* and dppe ligands in **12-14** are more strongly electron donating than their PPh$_3$ and Cp analogues in **9-11**. Unsurprisingly, the very electron-rich iron end-caps in **16** further lower the oxidation potentials relative to the ruthenium based series. However, it is the occurrence of two oxidation waves for each trimetallic compound, and the fact that the first oxidation potential of [{Ru(dppe)Cp*}$_2${Pt(CN)$_4$}] (**14**) is lower than the oxidation potential of the mono-ruthenium analogue K[Ru(dppe)Cp*{Pt(CN)$_4$}] (**15**) (+0.71 V and +0.74 V respectively), that indicate metal/metal interactions throughout the assembly. Before attempting to quantify these interactions it is useful to introduce some of the elementary relationships used in the data analysis.

Consider a sequence of redox reactions:

$$X \underset{+e^-}{\overset{-e^-}{\rightleftharpoons}} X^+ \underset{+e^-}{\overset{-e^-}{\rightleftharpoons}} X^{2+} \qquad (1)$$

Which can also be expressed in terms of the half-equations:

$$X \underset{E_1}{\rightleftharpoons} X^+ + e^- \qquad (2)$$

$$X^+ \underset{E_2}{\rightleftharpoons} X^{2+} + e^- \qquad (3)$$

Where E_1 and E_2 are the oxidation potentials associated with each process. The stability of the first oxidation product can be gauged by the equilibrium constant for the comproportionation reaction, K_c.

$$X + X^{2+} \overset{K_c}{\rightleftharpoons} 2X^+ \quad (4)$$

Electrochemical methods can be used to determine K_c via the Nernst equation (5) shown below.

$$E = E^0 - \left[\frac{RT}{nF}\right] \ln Q \qquad (5)$$

n = no. of electrons, Q = reaction quotient, T = temperature in K, F = Faraday constant, R = Gas constant

At equilibrium E = 0 and the reaction quotient (Q) becomes the constant of the equilibrium (K_c). Thus the Nernst equation becomes:

$$E^0 = \left[\frac{RT}{nF}\right] \ln K_c \qquad \mathbf{(6)}$$

which can be re-arranged to:

$$\ln K_c = \left[\frac{nE^0F}{RT}\right] \quad (7)$$

As equation (4) can also be written:

$$[X^+ + e^-] + [X^+ - e^-] \overset{K_c}{\rightleftharpoons} 2X^+ \quad (8)$$

and since $E^0 = E_2 - E_1$ (from 2, 3, and 6) then 7 becomes:

$$K_c = \exp\left[\frac{(\Delta E)F}{RT}\right] \quad (9)$$

The comproportionation constant, and hence a measure of the thermodynamic stability of the first oxidation product, can therefore be determined from measurement of the half-wave potentials of the sequential oxidation reactions shown in equations 1-3.

Whilst it is often true that metal-metal interactions across a bridged system lead to very stable odd-electron species (i.e. X^+ in equation 4), and hence large values of K_c, it is important to stress that metal-metal interactions are not necessarily the sole factor involved in affecting the magnitude of ΔE. Various solvent and salt effects can also influence the stability of the first oxidation product, and hence K_c. In the case of the cyanometallates in this study, there is a definite solvent effect on the stabilisation of the first oxidation product. In each case the separation between the two oxidation potentials of any one species (ΔE) is decreased upon reducing the polarity of the solvent. As with previously described trends within the groups **9-11** and **12-14**, there seems to be a dependence of the stability of the first oxidation product of these materials upon the nature of the central metal. There is an apparent *reduction* in the value of ΔE_{OX} upon substituting Pd for Ni followed by an *increase* upon substituting Pt for Pd. The comproportionation constants (K_c), calculated from the values of ΔE_{OX} naturally follow the same trend. This enhanced stability may be brought about by a greater degree of delocalisation in the case of the Ni and Pt complexes relative to the

Pd materials. However, this effect cannot be substantiated on the basis of this electrochemical data alone and the crystallographic data argues against differences in the degree of delocalisation in these complexes.

Keene has recently reminded the community that the anion of the electrolyte used in potential measurements can have a drastic effect on the potentials, hence altering ΔE and K_c for a material.[36] Therefore it is important to remember that, whilst a large K_c value can often be an indication of metal-metal communication, it is not, by itself, a definitive "litmus test" and it is important that other techniques such as vibrational and/or electronic spectroscopy be used in addition to potential measurements before claims of "electronic communication" in a bridged bimetallic assembly be made.

Mixed-Valence Complexes

When the electro-generated species X^+ described above is derived from a bimetallic complex, that complex becomes a mixed-valence species. The notion of metal-metal communication in such systems has been thoroughly studied (with many electron-transfer parameters being available from spectral data) and such species may be classified according to the Robin-Day classification system described previously (see Introduction).[37] For compounds that fall into the valence-trapped Class 2 grouping, the transfer of the odd-electron from one metal centre to the other can be induced either by thermal or optical methods. Noel Hush, in 1967, predicted the occurrence of an inter-valence charge transfer (IVCT) band in the electronic spectra of these Class 2 complexes, occurring in the near infra-red (NIR) region of the spectrum.

Furthermore, a rationale was developed by which the physical properties of these mixed-valence complexes could be determined by careful analysis of the shape of this IVCT band.[38] According to the treatment developed by Hush, the width of the IVCT band at half its maximum height ($\Delta\bar{\nu}_{1/2}$) should be related to the energy of the band maximum ($\bar{\nu}_{max}$) by the relationship:

$$\Delta\bar{\nu}_{1/2} = \sqrt{2310(\bar{\nu}_{max})} \qquad \textbf{(10)}$$

Whilst vibrational effects may result in a broadening of this band, it is generally found that Class 2 mixed valence systems give rise to IVCT bands with shapes in agreement with (**10**). Generally speaking, those complexes for which $\Delta\bar{\nu}_{1/2(obs)}$ is significantly narrower than $\Delta\bar{\nu}_{1/2(calc)}$ are considered to be Class 3.

The strength of the interaction between the two metal centres in a mixed valence compound is determined by the coupling constant V_{ab} (also termed H_{ab} in some treatments). For Class 2 complexes this parameter is given by:

$$V_{ab} = \frac{0.0205\sqrt{\bar{\nu}_{max}\Delta\bar{\nu}_{1/2}\varepsilon_{max}}}{r} \qquad \textbf{(11)}$$

where ε is the extinction coefficient of the IVCT band and r is is the electron-transfer distance (in Angstroms). In the case of Class 3 compounds V_{ab} is given by:

$$V_{ab} = \frac{\bar{\nu}_{max}}{2} \qquad (12)$$

For a full description of the background theory underpinning these expression see the excellent reviews by Cruetz, Meyer and Launay.[39-41]

Based on the brief description above, the electronic spectra of the oxidised versions of the complexes in this study would be expected to show IVCT bands in those cases where metal-metal communication is suspected. Furthermore band shape analysis would be expected to reveal the extent of the communication between the metal centres and any trends that occur as a function of the central metal would become apparent. Rather than prepare each oxidised species chemically, spectra were obtained using spectro-electrochemical methods (see Experimental Methods chapter).

The UV-Vis-NIR spectra were collected from DCM solutions approximately 0.1 mmolar in analyte and containing 0.1M $TBABF_4$ as a supporting electrolyte. Whilst on the CV timescales (< 10 seconds) the oxidations of compounds **9-16** were fully reversible, the first oxidation states of **9** and **10** were insufficiently reversible on the longer timeframe required for bulk electrolysis in the OTTLE cell (1-5 hours) for acquisition of meaningful spectra. Therefore, in the interests of obtaining a complete data set, only the Ru(dppe)Cp* derived complexes **12-16** were studied. However, even in these cases, only the first oxidation product could be obtained with complete reversibility and then only at sub-ambient temperatures. The experiments were performed at -30 °C in a 0.1 cm quartz cuvette using an optically transparent thin-layer electrode (OTTLE) similar to that described by Duff and Heath.[42] This

consisted of a platinum mesh as the working electrode as well as platinum wire counter and pseudo-reference electrodes.

The neutral compounds **12-15** displayed two absorption bands in the UV (35,000-20,000 cm^{-1}) region of the spectrum, the lower energy band appearing as a shoulder in the case of compounds **12-15**. For example, in the case of **12** these two bands were observed at 32,680 and 25,900 cm^{-1}. Compound **16** displays an absorption band at 29,850 cm^{-1} as well as a broader absorption envelope with apparent band maxima at 21,740 and 19,690 cm^{-1} (Table 4.7).

Table 4.7. Uv-vis data for compounds **12-16**

Compound	$\bar{\nu}_{max}$/cm^{-1} and (ε/$mol^{-1}dm^3cm^{-1}$)
12	32,680 (12,280); 25,900 (3,900)
13	31,250 (3,860); 27,250 (2,480)
14	31,060 (14,540); 26,390 (3,920)
15	31,150 (2,680); 26,460 (1,370)
16	29,850 (8,673); 21,740 (1,360); 19,690 (1,120)

In the oxidised samples the bands described above each moved to slightly lower energy with the exception of compound **16** for which the reverse behaviour was seen. The bimetallic compound $[\mathbf{15}]^+$ displayed no features beyond 20,000 cm^{-1}, however oxidation of **15** to $[\mathbf{15}]^+$ did result in the growth of a new absorption band at 20,330 cm^{-1}.

In addition to the bands already described, new features were seen in the UV-Vis-NIR spectra of the oxidised trimetallic compounds $[\mathbf{12}]^+$, $[\mathbf{13}]^+$ and $[\mathbf{14}]^+$. In each case, a new band of moderate intensity was formed in the 20,000 – 21,000 cm^{-1} region of the spectrum as well as an absorption band in the NIR region of the spectrum, the high

energy side of which was overlapped by the tails of bands from the higher energy end of the spectrum. An example spectrum below shows the oxidation of $[\{Ru(dppe)Cp^*\}_2\{Ni(CN)_4\}]$ (**12**) in the range 25,000-4,000 cm^{-1} (Figure 4.9). Critically, the NIR region of $[\mathbf{15}]^+$ remained transparent during oxidation and therefore the NIR absorption observed in $[\mathbf{12}]^+$, $[\mathbf{13}]^+$ and $[\mathbf{14}]^+$ can be confidently assigned to a genuine Ru^{II}/Ru^{III} IVCT transition.

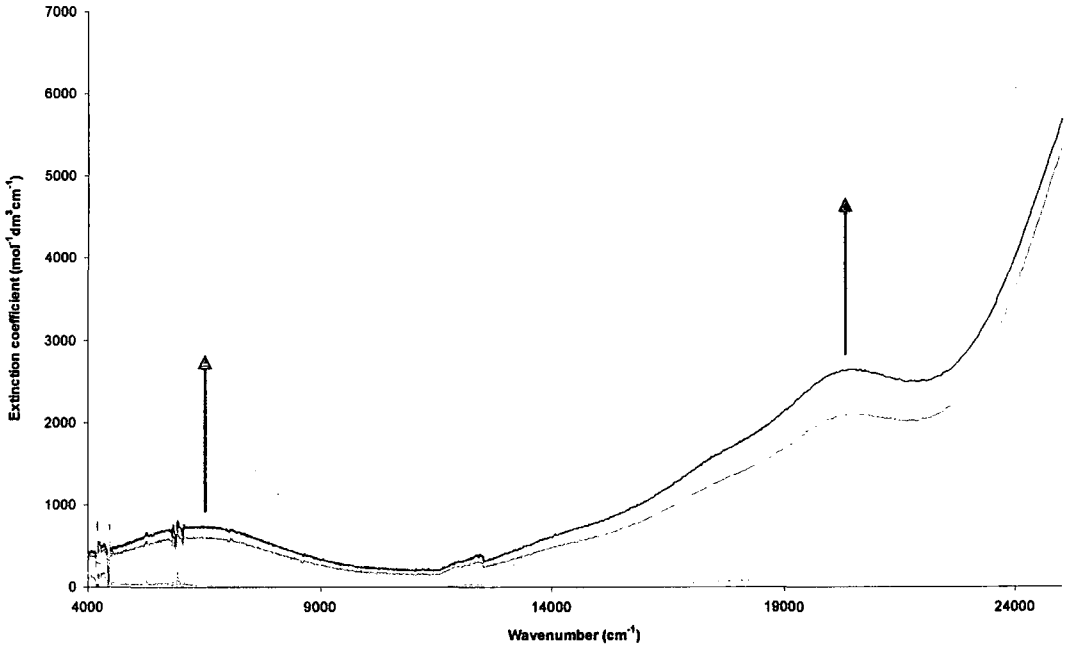

Figure 4.9. Oxidation of **12** to $[\mathbf{12}]^+$.

An important point must be made at this stage. The magnitude of the comproportionation constant (K_c) indicates that at equilibrium the solutions will contain neutral, mono-oxidised and di-oxidised species. Therefore, a correction must be made to the concentration of the solution to accurately assess the molar extinction coefficient of the mono-oxidised species. The proportion (P) of the mono-oxidised

complex in solution can be determined from the comproportionation constant K_c using equation 13.[41]

$$P = \frac{\sqrt{Kc}}{2 + \sqrt{Kc}} \qquad \textbf{(13)}$$

All of the extinction coefficients determined for the oxidised species in this chapter have been corrected to allow for this comproportionation equilibrium.

The high energy side of the NIR band in $[\mathbf{12}]^+$, $[\mathbf{13}]^+$ and $[\mathbf{14}]^+$ was partially obscured by overlap with one of the higher energy transitions. Therefore, in order to better estimate $\bar{\nu}_{1/2}$, it was necessary to subject the spectra to spectral deconvolution, with the experimental spectrum described as the sum of several Gaussian-shaped curves. An example of such a process for complex $[\mathbf{13}]^+$ is shown below (Figure 4.10).

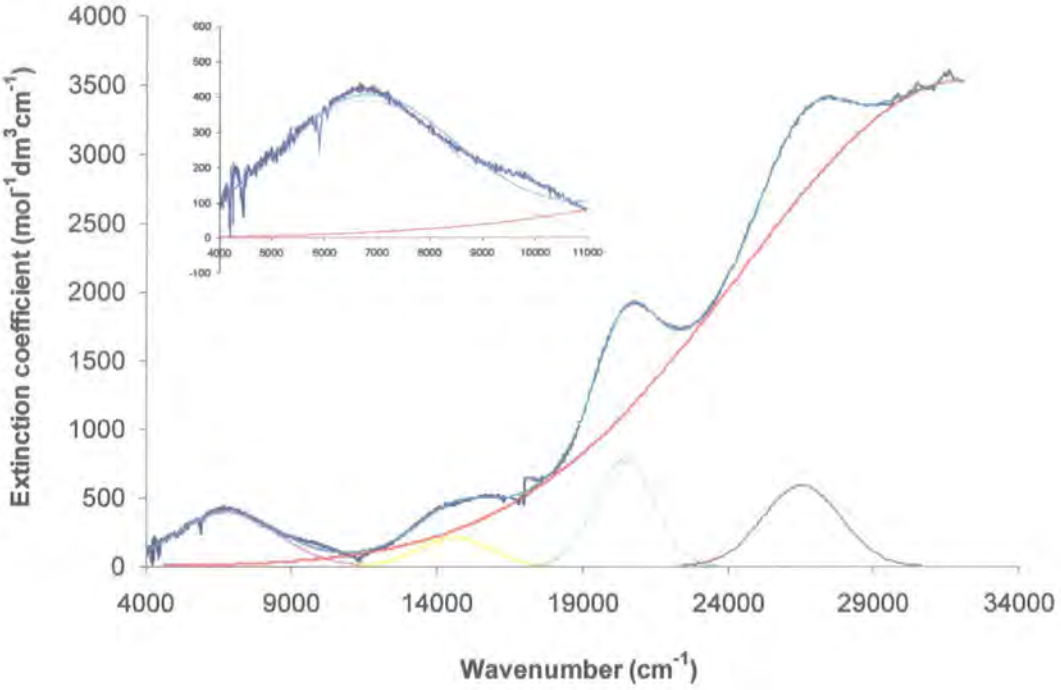

Figure 4.10. Gaussian curve fitting for UV-vis-NIR spectrum of $[\mathbf{13}]^+$ with NIR band inset.

In the case of the compounds $[\mathbf{12}]^+$, $[\mathbf{13}]^+$, and $[\mathbf{14}]^+$ the NIR band observed for these weakly coupled systems is well approximated by a single Gaussian band (inset in Figure 4.10 above). In each case the value of $\Delta\bar{\nu}_{1/2}$ calculated from (**10**) is narrower than that found by experiment. This suggests that each of the compounds falls into the Class 2 grouping. It should be noted, however, that this is not a definite basis for assignment and that investigations into solvent effects have yet to be made in order to confirm this. The band parameters, r distances (taken as the crystallographically determined Ru-Ru distance) and coupling constants are shown in Table 4.8 below.

Table 4.8. NIR data for $[\mathbf{12}]^+$, $[\mathbf{13}]^+$, and $[\mathbf{14}]^+$

Compound	$\bar{\nu}_{max}$ (cm^{-1})	$\Delta\bar{\nu}_{1/2\,(calc)}$ (cm^{-1})	$\Delta\bar{\nu}_{1/2\,(found)}$ (cm^{-1})	ε ($mol^{-1}dm^3cm^{-1}$)	r (Å)[a]	V_{ab}
$[\mathbf{12}]^+$	6380	3800	4800	730	10.38	300
$[\mathbf{13}]^+$	6780	4000	4000	500	10.38	230
$[\mathbf{14}]^+$	5680	3600	5100	535	10.38	250

[a]This distance is taken as the point-to-point distance between ruthenium centres and is *not* the sum of the bond lengths.

In each case there is very little difference between the compounds, with the NIR band-shape analysis consistent with assignment as a Class 2 system in each case. The absorption data, therefore, confirms the picture described by the spectroscopic properties and molecular structures of the neutral compounds as well as the electrochemistry. There is a very slight decrease in coupling constant upon changing the central metal from Ni to Pd as the Pd is a poorer π-donor and so the degree of delocalisation across the system is reduced. When the central metal is Pt, however, there is a very slight rise in the coupling constant again, consistent with the increased π-donor ability of Pt relative to Pd. This pattern matches with that observed for the K_c values of these materials.

In summary, the electronic structure of these materials seems to show little sensitivity to the nature of the central metal. When the results from the series of complexes $[\{RuP_2Cp'\}_2(\{\mu\text{-}M(CN)_4\}]$ (M = Ni, Pd, Pt) are taken together with Vahrenkamp's work with $[\{MP_2Cp'\}_2(\{\mu\text{-}Pt(CN)_4\}]$[25] it is clear that by far the greatest effects on the metal-metal coupling or "communication" in these systems are brought about by the nature of the metal end-caps rather than the central bridging moiety.

Experimental

General Procedure – Preparation of [{RuL$_2$Cp'}$_2${μ-M(CN$_4$)}] (L = PPh$_3$, Cp' = Cp; L$_2$ = dppe, Cp' = Cp*; M = Ni, Pd, Pt)

A 50 ml, two-necked Schlenk flask was cooled under nitrogen and charged with $K_2[M(CN)_4]$ (0.208 mmol) and $RuClL_2Cp'$ (0.415 mmol). The mixture was suspended in MeOH (30 ml) and heated at reflux for one hour. After this time a bright yellow suspension had formed. The solution was allowed to cool and the precipitate was collected and washed with cold methanol to afford **[{RuL$_2$Cp'}$_2${μ-M(CN$_4$)}]** as a bright yellow solid. Crystals of compounds **9-11** suitable for X-ray diffraction studies were obtained by slow diffusion of MeOH into a DCM solution of **[{Ru(PPh$_3$)$_2$Cp}$_2${μ-M(CN$_4$)}]**. Crystals of compounds **12** and **14** suitable for X-ray diffraction studies were obtained by slow diffusion of EtOH into a $CHCl_3$ solution of **[{Ru(dppe)Cp*}$_2${μ-M(CN$_4$)}]**. Crystals of compound 13 were obtained by slow diffusion of EtOH into a DCM solution of **[{Ru(dppe)Cp*}$_2${μ-Pd(CN$_4$)}]**.

[{Ru(PPh$_3$)$_2$Cp}$_2${Ni(CN)$_4$}] (9) (0.149 mmol, 72 %). Found: C, 65.78; H, 4.52; N, 3.59. $C_{86}H_{70}P_4N_4Ru_2Ni$ $0.5(CH_2Cl_2)$ requires: C, 65.48; H, 4.51; N, 3.53. ^{1}H NMR ($CDCl_3$): δ 4.29 (s, 10H, Cp); 7.30-7.25 (m, 72 H, PPh_3). ^{13}C {^{1}H} NMR ($CDCl_3$): δ 137.41 (m, J_{CP} = 22 Hz, C_{ipso}); 133.76 (t, J_{CP} = 5.28 Hz, C_{ortho}); 129.30 (s, C_{para}); 128.28 (t, J_{CP} = 4.78 Hz, C_{meta}); 83.43 (s, Cp). ^{31}P {^{1}H} NMR ($CDCl_3$): δ 43.40 (s, PPh_3). ES(+)-MS (*m/z*): 1568 $[M+Na]^+$, 691 $[Ru(PPh_3)_2Cp]^+$. IR (CH_2Cl_2): ν(C≡N) 2143, 2119 cm^{-1}.

[{Ru(PPh$_3$)$_2$Cp}$_2${Pd(CN)$_4$}] (10) (0.100 mmol, 48 %). Found: C, 63.38; H, 4.39; N, 3.57. $C_{86}H_{70}P_4N_4Ru_2Pd.0.5CH_2Cl_2$ requires: C, 63.56; H, 4.38; N,3.43. ^{1}H NMR ($CDCl_3$): δ 4.30 (s, 10H, Cp); 7.33-7.10 (m, 72 H, PPh_3). ^{13}C {^{1}H} NMR ($CDCl_3$): δ 136.02 (m, J_{CP} = 20 Hz, C_{ipso}); 132.46 (t, J_{CP} = 5.28 Hz, C_{ortho}); 128.08 (s, C_{para}); 127.01 (t, J_{CP} = 4.78 Hz, C_{meta}); 82.16 (s, Cp). ^{31}P {^{1}H} NMR ($CDCl_3$): δ 43.21 (s, PPh_3). IR (CH_2Cl_2): ν(C≡N) 2157, 2130 cm^{-1}.

[{Ru(PPh$_3$)$_2$Cp}$_2${Pt(CN)$_4$}] (11) (0.095 mmol, 46 %). Found C, 60.64; H, 4.12; N, 3.37. $C_{86}H_{70}P_4N_4Ru_2Pt$ 0.5(CH_2Cl_2) requires: C, 60.30; H, 4.15; N,3.25. ^{1}H NMR ($CDCl_3$): δ 4.30 (s, 10H, Cp); 7.30-7.26 (m, 72 H, PPh_3). ^{13}C {^{1}H} NMR ($CDCl_3$): δ 137.30 (m, J_{CP} = 22 Hz, C_{ipso}); 133.73 (t, J_{CP} = 5.28 Hz, C_{ortho}); 129.35 (s, C_{para}); 128.28 (t, J_{CP} = 4.27 Hz, C_{meta}); 83.43 (s, Cp). ^{31}P {^{1}H} NMR ($CDCl_3$): δ 43.12 (s, PPh_3). ES(+)-MS (*m/z*): 1705 [M+Na]$^+$; 691 [Ru(PPh$_3$)$_2$Cp]$^+$. IR (CH_2Cl_2): ν(C≡N) 2157, 2129 cm^{-1}.

[{Ru(dppe)Cp*}$_2${Ni(CN)$_4$}] (12) (0.129 mmol, 68 %). Found: C, 63.37; H, 5.45; N, 3.97. $C_{76}H_{78}P_4N_4Ru_2Ni$ requires: C, 63.74; H, 5.49; N,3.91. ^{1}H NMR ($CDCl_3$): δ 1.45 (s, 15H, Cp*); 2.06, 2.62 (m, 4H, dppe); 7.15-7.70 (m, 20H, Ph). ^{13}C {^{1}H} NMR ($CDCl_3$): δ 142.95 (s, CN); 136.88 (m, J_{CP} = 18 Hz, C_{ipso}); 134.22 (m, J_{CP} = 18 Hz, C_{ipso}); 133.64 (m, 2 x C_{ortho}); 130.04 (s, CN); 129.87 (s, C_{para}); 129.73 (s, C_{para}); 128.58 (t, J_{CP} = 4.78 Hz, C_{meta}); 127.97 (t, J_{CP} = 4.78 Hz, C_{meta}); 91.70 (s, C_5Me_5);

28.79-28.44 (m, dppe); 10.07 (s, C_5Me_5). ^{31}P NMR ($CDCl_3$): δ 71.71 (s, dppe). ES(+)-MS (*m/z*): 1433 $[M + H]^+$; 635 $[Ru(dppe)Cp^*]^+$. IR (CH_2Cl_2): ν(C≡N) 2118, 2136 cm^{-1}.

[{Ru(dppe)Cp*}$_2${Pd(CN)$_4$}] (13) (0.068 mmol, 37%). Found: C, 60.81; H, 5.25; N, 3.70. $C_{76}H_{78}P_4N_4Ru_2Pd.2(C_2H_5OH)$ requires: C, 61.21; H, 5.77; N,3.56. ^1H NMR ($CDCl_3$): δ 1.48 (s, 15H, Cp*); 2.00, 2.57 (m, 4H, dppe); 7.10-7.70 (m, 20H, Ph). ^{13}C $\{^1H\}$ NMR ($CDCl_3$): δ 140.85 (s, CN); 136.72 (m, J_{CP} = 20 Hz, C_{ipso}); 134.01 (m, J_{CP} = 20 Hz, C_{ipso}); 133.64 (t, J_{CP} = 5.28 Hz, C_{ortho}); 133.53 (t, J_{CP} = 5.28 Hz, C_{ortho}); 129.95 (s, C_{para}); 129.78 (s, C_{para}); 128.66 (t, J_{CP} = 4.90 Hz, C_{meta}); 128.02 (t, J_{CP} = 4.78 Hz, C_{meta}); 127.22 (s, CN); 91.68 (s, C_5Me_5); 28.77-28.43 (m, dppe); 10.13 (s, C_5Me_5). ^{31}P NMR ($CDCl_3$): δ 75.79 (s, dppe). ES(+)-MS (*m/z*): 1481 $[M + H]^+$; 635 $[Ru(dppe)Cp^*]^+$. IR (CH_2Cl_2): ν(C≡N) 2129, 2146 cm^{-1}.

[{Ru(dppe)Cp*}$_2${Pt(CN)$_4$}] (14) (1.08 mmol, 57 %). Found: C, 58.16; H, 4.98; N, 3.54. $C_{76}H_{78}P_4N_4Ru_2Pt$ requires: C, 58.19; H, 5.01; N, 3.57. ^1H NMR ($CDCl_3$): δ 1.48 (s, 15H, Cp*); 2.08, 2.63 (m, 4H, dppe), 7.15-7.75 (m, 20H, Ph). ^{13}C $\{^1H\}$ NMR ($CDCl_3$): δ 136.67 (m, J_{CP} = 19 Hz, C_{ipso}); 134.00 (m, J_{CP} = 20 Hz, C_{ipso}); 133.66 (t, J_{CP} = 5.28 Hz, C_{ortho}); 133.56 (s, CN); 133.47 (t, J_{CP} = 5.28 Hz, C_{ortho}); 129.95 (s, C_{para}); 129.80 (s, C_{para}); 128.73 (t, J_{CP} = 4.90 Hz, C_{meta}); 128.02 (t, J_{CP} = 4.27 Hz, C_{meta}); 121.62 (s, CN); 91.68 (s, C_5Me_5); 28.80-28.45 (m, dppe); 10.08 (s,

C_5Me_5). ^{31}P NMR ($CDCl_3$): δ 75.73 (s, dppe). ES(+)-MS (*m/z*): 1569 $[M + H]^+$; 635 $[Ru(dppe)Cp^*]^+$. IR (CH_2Cl_2): ν(C≡N) 2128, 2150 cm^{-1}.

K[Ru(dppe)Cp*{Pt(CN)$_4$}] (15)

A 50ml, two-necked schlenk flask was cooled under nitrogen and charged with $K_2[Pt(CN)_4]$ (127 mg, 0.337 mmol) and RuCl(dppe)Cp* (150 mg, 0.224 mmol). The mixture was suspended in MeOH (10 ml) and heated at reflux for 1.5 hrs after which time the solution was cooled and the solvent removed. The yellow residue was dissolved in the minimum quantity of DCM and filtered. Removal of solvent afforded **15** as a yellow powder (168mg. 0.172 mmol, 77 %). Found: C, 48.85; H, 4.07; N, 5.28. $C_{40}H_{39}P_2N_4RuPtK$ requires: C, 49.38; H, 4.04; N, 5.76. ^1H NMR ($CDCl_3$): δ 1.47 (s, 15H, Cp*); 2.08, 2.64 (m, 4H, dppe); 7.20-7.68 (m, 20H, Ph). ^{31}P NMR ($CDCl_3$): δ 75.67 (s, dppe). ES(+)-MS (*m/z*): 635 $[Ru(dppe)Cp^*]^+$. ES(-)-MS (*m/z*): 932 $[Ru(dppe)Cp^*\{Pt(CN)_4\}]^-$; 273 $[Pt(CN)_3]^-$. IR (CH_2Cl_2): ν(C≡N) 2130 cm^{-1}.

[{Fe(dppe)Cp}$_2${Pt(CN)$_4$}] (16)

A 50ml, two-necked schlenk flask was cooled under nitrogen and charged with $K_2[Pt(CN)_4]$ (102 mg, 0.27 mmol) and FeCl(dppe)Cp (300 mg, 0.54 mmol). The mixture was suspended in MeOH (30 ml) and heated at reflux for 90 minutes after which time reaction was cooled and the solvent removed. The residue was then dissolved in a minimum volume of DCM, filtered, loaded onto a silica column and

eluted with 60:40 acetone:hexane solution. The resultant red band was collected and the solvent removed. Subsequent crystallisation from slow diffusion of MeOH into a DCM solution resulted in the formation of **16** as red crystals (156 mg, 0.12 mmol, 43 %). ^{1}H NMR ($CDCl_3$): δ 2.08, 2.63 (2 x br, 4H, dppe); 4.19 (s, 5H, Cp); 7.20-7.79 (m, 20H, Ph). ^{31}P NMR ($CDCl_3$): δ 100.34 (s, dppe). IR (CH_2Cl_2): ν(C≡N) 2128, 2149 cm^{-1}.

References

1 A. Vogler, A. H. Osman, H. Kunkely, Coord. *Chem. Rev.*, 1985, **64**, 159.

2 F. Scandola, R. Argazzi, C. A. Bignozzi, C. Chiorboli, M. T. Indelli, M. A. Rampi, *Coord. Chem. Rev.*, 1993, **125**, 283.

3 W. P. Fehlhammer, M. Fritz, *Chem. Rev.*, 1993, **93**, 1243.

4 K. Kalyanasundaram, Md. K. Nazeeruddin, *Inorg. Chim. Acta*, 1994, **226**, 213.

5 K. R. Dunbar, R. A. Heintz, *Prog. Inorg. Chem.*, 1997, **45**, 283.

6 H. Vahrenkamp, A. Geiβ, G. N. Richardson, *J. Chem. Soc., Dalton Trans.*, 1997, 3643.

7 L. Toma, R. Lescouëzec, J. Vaissermann, F. S. Delgado, C. Ruiz-Pérez, R. Carrasco, J. Cano, F. Lloret, M. Julve, *Chem. Eur. J.*, 2004, **10**, 6130.

8 S. Ahmad, *Coord. Chem. Rev.*, 2004, **248**, 231.

9 A. Ludi, *J. Chem. Educ.*, 1981, **58**, 1013.

10 N. Zhu, H. Vahrenkamp, *Chem. Ber/ Recueil*, 1997, **130**, 1241.

11 H. Siebert, *Z. Anorg. Allg. Chem.*, 1964, **327**, 63.

12 N. C. Brown, G. B. Carpenter, N. G. Connelly, J. G. Crossley, A. Martin, A. G. Orpen, A. L. Rieger, P. H. Rieger, G. H. Worth, *J. Chem. Soc., Dalton Trans.*, 1996, 3977.

13 W. M. Laidlaw, R. G. Denning, *Inorg. Chim. Acta*, 1996, **248**, 51.

14 P. Braunstein, D. Cauzzi, D. Kelly, M. Lanfranchi, A. Tripicchio, *Inorg. Chem.*, 1993, **32**, 337.

15 F. L. Atkinson, A. Christofides, N. G. Connelly, H. J. Lawson, A. G. Orpen, G. M. Rosair, G. H. Worth, *J. Chem. Soc., Dalton Trans.*, 1993, 1441.

16 C. A. Bignozzi, C. Paradisi, S. Roffia, F. Scandola, *Inorg. Chem.*, 1988, **27**, 408.

17 R. Argazzi, C. A. Bignozzi, C. G. Garcia, T. J. Meyer, F. Scandola, J. R. Schoonover, *J. Am. Chem. Soc.*, 1992, **114**, 8727.

18 H. Kunkely, A. Vogler, *Inorg. Chim. Acta*, 1993, **209**, 93.

19 H. Kunkely, V. Pawlowski, A. Vogler, *Inorg. Chim. Acta*, 1994, **225**, 327.

20 N. Zhu, H. Vahrenkamp, *J. Organomet. Chem.*, 1999, **573**, 67.

21 F. L. Atkinson, A. Christophides, N. G. Connelly, H. J. Lawson, A. C. Loyns, A. G. Orpen, G. M. Rosair, G. H. Worth, *J. Chem. Soc., Dalton Trans.*, 1993, 1441.

22 N. G. Connelly, D. M. Hicks, G. R. Lewis, A. G. Orpen, A. J. Wood, *J. Chem. Soc., Chem. Commun.*, 1998, 517.

23 N. G. Connelly, G. R. Lewis, M. T. Moreno, A. G. Orpen, *J. Chem. Soc., Dalton Trans.*, 1998, 1905.

24 G. N. Richardson, H. Vahrenkamp, *J. Organomet. Chem.*, 2000, **593**, 44.

25 G. N. Richardson, U. Brand, H. Vahrenkamp, *Inorg. Chem.*, 1999, **38**, 3070.

26 G. N. Richardson, H. Vahrenkamp, *J. Organomet. Chem.*, 2000, **597**, 38.

27 A. N. Bloch, R. B. Weisman, *Adv. Chem. Ser.*, 1974, **5**, 356.

28 S. W. Peterson, *Ferroelectrics*, 1977, **16**, 145.

29 D. W. Bullett, *Solid State Commun.*, 1978, **27**, 467.

30 Y. Zhou, A.M. Arif, J. S. Miller, *Chem. Commun.*, 1996, 1881.

31 G. J. Baird, S. G. Davies, *J. Organomet. Chem.*, 1984, **262**, 215.

32 G. J. Kubas, L. H. Jones, *Inorg. Chem.*, 1974, **13**, 2816

33 M.N. Memering, L. H. Jones, J. C. Blair, *Inorg. Chem.*, 1973, **12**, 2793.

34 R. D. Shannon, *Acta Cryst.*, 1976, **A32**, 751.

35 N.G. Connelly and W.E. Geiger, *Chem. Rev.*, 1996, **96**, 877.

36 D.M. D' Alessandro, F. R. Keene, *Dalton Trans.*, 2004, 3950.

37 M.B. Robin, P. Day, *Adv. Inorg. Chem. Radiochem.*, 1967, **10**, 247.

38 N.S. Hush, *Prog. Inorg. Chem.*, 1967, **8**, 391.

39 B. S. Braunshwig, C. Creutz, N. Sutin, *Chem. Soc. Rev.*, 2002, **31**, 168.

40 K. D. Demadis, C. M. Hartshom, T. J. Meyer, *Chem. Rev.*, 2001, **101**, 2655.

41 J-P Launay, *Chem. Soc. Rev.*, 2001, **30**, 386.

42 C. M. Duff, G. A. Heath, *Inorg. Chem.*, 1991, **30**, 2528.

Compounds List - Tetracyanometallates

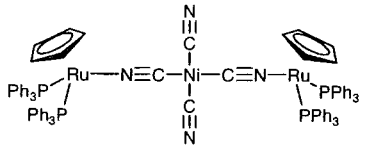

9

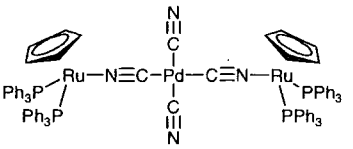

10

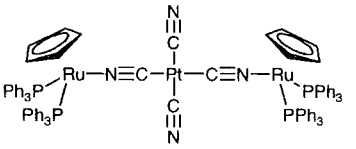

11

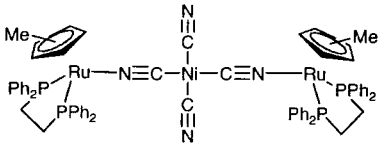

12

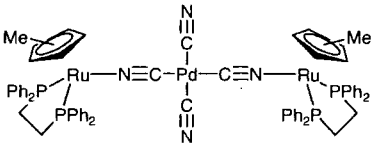

13

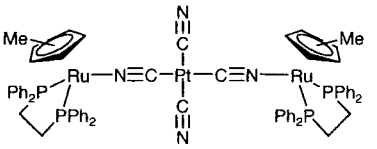

14

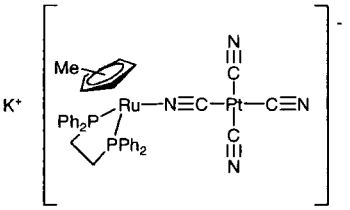

15

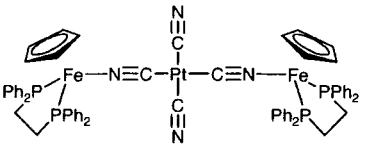

16

Introduction

The cyanoacetylene moiety possesses a lone pair of electrons at the N-atom which can bond to metal centres in an η^1(N) fashion. In addition to this it has an alkyne π-system which is conjugated with the C≡N moiety (allowing for delocalisation of electron density) and can also bond to metal centres itself. In addition to this, the extended π-system offered by the cyanoacetylene ligand should make it more polarisable than simple nitriles, which may be of particular utility in the design of complexes with significant non-linear optical responses.[1,2]

Early work on the coordination chemistry of cyanoacetylenes focussed on the co-ordination of the alkyne moiety to metal centres in an η^2 fashion. In 1968, Dickson and Yawney showed the possibility of incorporating the dicyanoacetylene moiety into metal complexes through coordination of the alkyne π-system in reaction with $Co_2(CO)_8$.[3] Infra-red data obtained from the reaction showed that ν(C≡C), the alkyne stretching frequency, disappeared upon formation of the product (from 2119 cm^{-1} in DCA), consistent with the formation of a four-atom Co_2C_2 cluster (Figure 5.1).

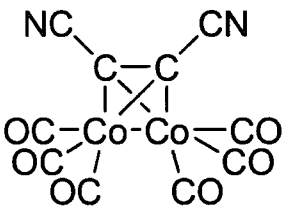

Figure 5.1. Proposed product from the reaction of DCA with $Co_2(CO)_8$.[3]

Furthermore there was a marked decrease $\nu(C\equiv N)$ upon complexation from 2290 cm^{-1} in DCA to 2198 cm^{-1} in the cobalt/carbon cluster. This results from a loss of electron density from the CN moieties upon forming the cluster and is also observed in the reaction of DCA with nickelocene to form the analogous nickel/carbon cluster ($\nu(C\equiv N)$ = 2205 cm^{-1}).[4]

Further η^2 complexes of DCA were synthesised by McClure and Baddley with iridium, rhodium and palladium centres.[5] DCA was reacted with the iridium complexes $[IrX(CO)(EPh_3)_2]$ (E = As, X = Cl; E = P, X = Cl, Br, I, NCS), to give stable products of type $[IrX(CO)(C_4N_2)(EPh_3)_2]$ for which the structure shown in Figure 5.2 was proposed.

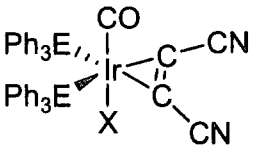

Figure 5.2. Suggested structure of $[IrX(CO)(C_4N_2)(EPh_3)_2]$

The $\nu(CO)$ stretching frequencies of the material $[IrCl(CO)(C_4N_2)(PPh_3)_2]$ were compared with those of a series of compounds of type $[IrCl(CO)(Ligand)(PPh_3)_2]$ as it has been suggested that the value of the $\nu(CO)$ frequency correlates with the degree to which the ligand has removed electron density from the iridium centre on complexation.[6] The study of McClure and Baddley put the electron withdrawing strength of the DCA ligand equal with that of O_2 and SO_2 and much less than that of the strongly electrophilic tetracyanoethylene (TCNE) ligand.[5] Interestingly, reaction of the dicarbonyl iridium hydride $[IrH(CO)_2(PPh_3)_2]$ with DCA resulted in the

formation of Ir{C(CN)CCN}η^2-$NCC_2CN(CO)(PPh_3)_2$ derived from coordination of one DCA ligand in η^2 fashion and insertion of DCA into the Ir-H bond to give the dicyanovinyl ligand (Figure 5.3). The *trans* nature of the dicyanovinyl ligand was later established by crystallographic methods.[7]

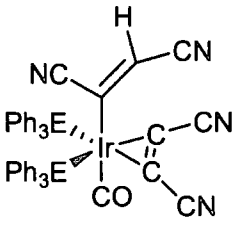

Figure 5.3. Product of the two-fold addition of DCA to $[IrH(CO)_2(PPh_3)_2]$

Reaction of DCA with rhodium complexes $RhCl(PPh_3)_3$, $[RhCl(PPh_3)_2]_2$, $RhCl(CO)(PPh_3)_2$, $RhCl(CO)_2(PPh_3)$ and $[RhCl(CO)_2]_2$ gave only intractable tars rather than isolable, well-characterised metal-complexes. This was attributed to a combination of the high reactivity of the DCA ligand and the catalytic nature of the Rh^I centre.[7] Reaction of DCA with $Pt(PPh_3)_4$ resulted in the η^2 coordinated complex Pt(η^2-$NCC_2CN)(PPh_3)_2$ which is discussed further in Chapter 6.

Complexes exhibiting similar η^2-alkyne ligands have also been isolated following coordination of cyanoacetylene (HC≡CC≡N) to a tungsten centre.[8] This reaction was shown to proceed both in warm toluene (60 °C over a period of 8 hours) and by photolysis (Scheme 5.1).

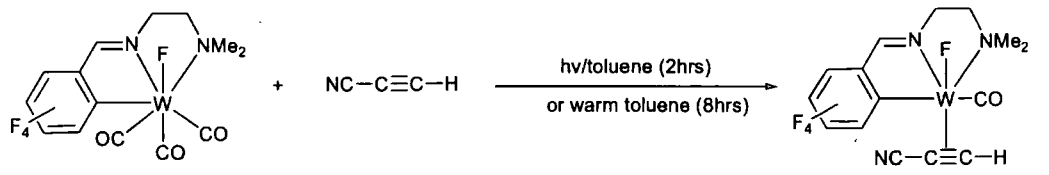

Scheme 5.1. η^2 co-ordination of cyanoacetylene to a tungsten centre.

However such simple coordination reactions of cyanoacetylene are rare, with the metal chemistry of cyanoacetylene being instead dominated by the formation of σ-vinyl complexes. In the early 1980's Scordia *et al.* studied the insertion of mono- and di-cyanoacetylene into the M-H bonds of $[(C_5H_5)_2MH_2]$ (M = Mo, W) to give $[(Cp)_2MH(\sigma\text{-trans-}C(CN)=CHCN)]$ and $[(Cp)_2MH(\sigma\text{-}C(CN)=CH_2)]$.[9] This was followed by the investigation of insertion reactions of both cyanoacetylene and DCA into the M-H bond of $[MH(CO)_3Cp]$ (M = Mo, W) to give the complexes $[M(\sigma\text{-}CR=CHCN)(CO)_3Cp]$ (M = Mo, W; R = H, CN) (Figure 5.4).[10]

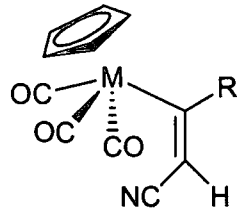

Figure 5.4. Cyanoacetylene insertions into the M-H bond of $MH(CO)_3Cp$ complexes (M = Mo, R = CN; M = W, R = H, CN).

In each case the reaction resulted in the *trans*-product shown above, and in no cases were any η^2 coordination products formed unlike those for acetylenes bearing other electron-withdrawing groups such as $F_3CC{\equiv}CCF_3$.[11,12] This was taken as an indication that the cyanoacetylene ligands behave as stronger electrophiles than other

activated alkynes and that the electron densities at the Mo and W centres above were not sufficiently electron-rich to stabilise the π-coordination product.

Examples of similar insertions into M-H bonds by cyanoacetylenes followed for similar compounds, including the iron species $[FeH(CO)Cp]_2(\mu\text{-dppm})$[13] and the species Cp_2MH (M=Re, Ta).[14,15] Furthermore, insertion reactions of mono- and di-cyanoacetylenes into M-S bonds have been studied, showing that, for example, reaction of $[W(SMe)(CO)_3Cp]$ with HC≡CCN will produce $[W(CH{=}C(CN)SMe)(CO)_3Cp]$.[16]

Examples of η^1-(N) bonded cyanoacetylenes are scarce, with only the complexes $[Ru(NC{\equiv}CC{\equiv}R)(tpy)(bpy)](PF_6)_2$ (tpy = 1,2':6':2'-terpyridine, bpy = 2,2'-bipyridine, R = H, Ph), which were characterised solely on the basis of electronic spectroscopy and elemental analysis, reported prior to the work in this thesis.[17]

The cyanoacetylene ligands HCC≡CCN and NCC≡CCN are both highly reactive and prone to polymerisation. However, Murray and Zweifel have described the synthesis of substituted cyanoacetylides from the parent acetylides RC≡CH by removal of the acetylenic proton to form $RC{\equiv}C^-$ followed by reaction with phenyl cyanate (PhOCN) to form RC≡CCN.[18] This simple procedure allows ready access to cyanoacetylene compounds which display increased stability due to the presence of bulky R-groups such as a phenyl moiety. In this chapter the coordination chemistry of $N{\equiv}CC{\equiv}CC_6H_5$ and the *para*-substituted derivative $N{\equiv}CC{\equiv}CC_6H_4\text{-}4\text{-}NMe_2$ is described.

Results

Synthesis

The organic cyanoacetylenes $NCC{\equiv}CC_6H_5$[18] and $NCC{\equiv}CC_6H_4$-4-NMe_2 were prepared from the parent acetylenes by reaction with butyl lithium (BuLi) and phenyl cyanate (PhOCN) according to the general method described by Murray and Zweifel (Scheme 5.2).[18]

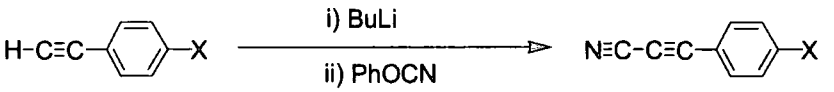

Scheme 5.2. Formation of cyanoacetylene ligand (X = H, NMe_2)

Treatment of a methanolic solution of $RuCl(PPh_3)_2Cp$ with $NCC{\equiv}CC_6H_5$ in the presence of NH_4PF_6 led to the formation of a bright yellow suspension from which the complex salt $[Ru(NCC{\equiv}CC_6H_5)(PPh_3)_2Cp][PF_6]$ (17) could be isolated in good yield and crystallised to afford bright yellow crystals (Scheme 5.3). This compound was characterised by the usual spectroscopic techniques. The Cp ligand gave rise to singlet resonances in the NMR spectra at 4.52 ppm (^1H) and 84.90 ppm ($^{13}C\{^1H\}$). Furthermore, resonances arising from the acetylenic carbon atoms of the cyanoacetylene ligand were apparent as singlets in the $^{13}C\{^1H\}$ spectrum at 116.63 and 115.88 ppm. Resonances arising from the phenyl rings of the phosphine and cyanoacetylene ligands were found in the range 6.98-7.57 ppm (^1H) and 135.20-128.43 ppm ($^{13}C\{^1H\}$). The ^{31}P NMR spectrum showed the expected resonances arising from the PPh_3 and $[PF_6]^-$ moieties as a singlet at 41.86 ppm and a heptet at -

143.02 ppm (J_{PF} = 713 Hz), respectively. In the IR spectrum, a single absorption band was observed at 2141 cm^{-1} which compares with the free ligand vibration at 2145 cm^{-1}. No absorption band in the region commonly associated with coordinated nitriles (ca. 2200 cm^{-1}, see Chapter 3) was observed. The ES(+)-MS displayed an intense isotopic envelope arising from the complex cation $[Ru(NCC{\equiv}CC_6H_5)(PPh_3)_2Cp]^+$ at *m/z* = 818, and a fragment corresponding to $[Ru(PPh_3)_2Cp]^+$ was apparent at *m/z* = 691.

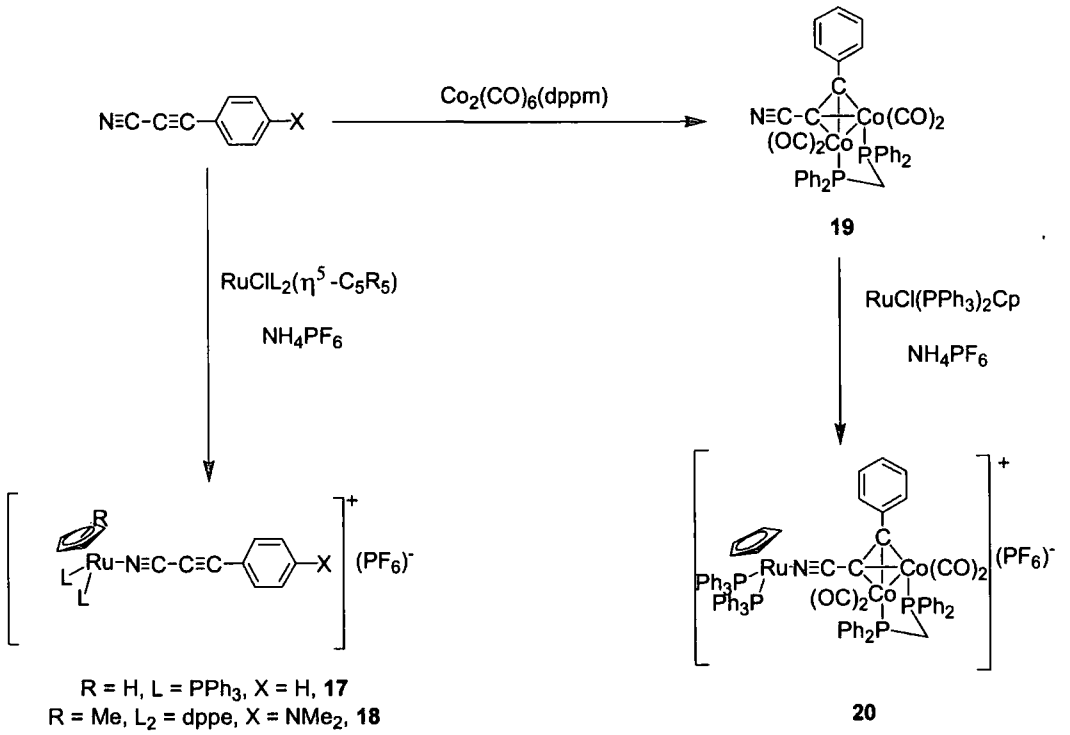

Scheme 5.3. Synthesis of cyanoacetylene compounds **17- 20**.

A similar reaction using RuCl(dppe)Cp* and $NCC{\equiv}CC_6H_4$-4-NMe_2 resulted in the isolation of yellow, needle-like crystals of $[Ru(NCC{\equiv}CC_6H_4$-4-$NMe_2)(dppe)_2Cp^*][PF_6]$ (**18**) which had an almost metallic lustre. The Cp* ligand

was observed as a singlet resonance at 1.47 ppm in the ^{1}H NMR spectrum, while a singlet at 3.05 ppm corresponding to the methyl protons of the NMe_2 substituent was also observed. The resonances arising from the alkyl protons of the dppe ligand were evident as an unresolved multiplet in the range 2.31-2.56 ppm. Whilst most of the phenyl protons were apparent as multiple resonances in the 7.23-7.54 ppm region of the spectrum, it was possible to distinguish a pseudo-doublet at 6.58 ppm (J_{HH} = 9 Hz) arising from the ortho phenyl protons of the cyanoacetylene ligand. The presence of the Cp* ligand was confirmed in the $^{13}C\{^1H\}$ NMR spectrum with singlet resonances at 93.75 and 9.83 ppm arising from the ring and methyl carbon atoms respectively. Furthermore, the C_2H_4 carbon atoms of the dppe ligand were apparent as multiplets in the range 28.90-28.55 ppm, although J_{CP} was not resolved, and the NMe_2 substituent of the cyanoacetylene ligand resulted in a singlet resonance at 40.20 ppm. A sharp singlet resonance at 75.10 ppm in the ^{31}P NMR spectrum was assigned to the dppe ligand whilst a heptet at -143.21 ppm (J_{PF} = 713 Hz) corresponding to the $[PF_6]^-$ counter-ion was also observed. Absorption bands resulting from the C≡N and C≡C portions of the ligand were visible in the IR spectrum at 2216 and 2123 cm^{-1} respectively, which compare with the free ligand bands at 2273 and 2145 cm^{-1}. Finally, ES(+)-MS showed the complex cation $[Ru(NCC{\equiv}CC_6H_4NMe_2)(dppe)Cp^*]^+$ at m/z = 804, as well as the fragment ion $[Ru(dppe)Cp^*]^+$ at m/z = 635.

Reaction of the cyanoacetylene ligand $NCC{\equiv}CC_6H_5$ with the known alkyne sequestering agent $Co_2(CO)_6(dppm)$ in refluxing benzene followed by removal of solvent and recrystallisation resulted in the formation of dark red crystals of $[Co_2(\mu,\eta^2\text{-}C_6H_5C_2CN)(CO)_4(\mu\text{-dppm})]$ (**19**) (Scheme 5.3). The expected doublet of triplet resonances corresponding to the CH_2 group of the dppm ligand in the ^{1}H NMR

spectrum were observed at 3.15 and 3.49 ppm. The same moiety was also evident in the $^{13}C\{^1H\}$ NMR spectrum as a triplet at 36.58 ppm (J_{CP} = 21 Hz). Two broad resonances at 205.89 and 199.21 ppm were assigned to the CO ligands and the carbon atoms of the Co_2C_2 cluster core were apparent as triplets occurring at 123.55 ppm (J_{CP} = 3 Hz) and 97.96 ppm (J_{CP} = 18 Hz). A sharp resonance arising from the dppm ligand was found in the ^{31}P NMR spectrum at 39.92 ppm. The IR spectrum showed the CO stretches in the 1970-2037 cm^{-1} region with the C≡N stretch apparent as a weaker band at 2167cm^{-1}. The ES(+)-MS spectrum displayed isotopic envelopes at *m/z* = 1504 ($[2M+Na]^+$) and 764 ($[M+Na]^+$).

Having synthesised examples of the co-ordination of the cyanoacetylene ligand in both η^1(N) and η^2(alkyne) bonding modes, attempts were made to form a multi-metallic compound through the simultaneous use of both bonding modes. Reaction of $[Ru(NCC{\equiv}CC_6H_5)(PPh_3)_2Cp][PF_6]$ (**17**) with $Co_2(CO)_6$(dppm) in refluxing benzene resulted in a dark red solution from which only $[Co_2(\mu,\eta^2\text{-}C_6H_5C_2CN)(CO)_4(\mu\text{-}dppm)]$ (**19**) could be isolated. However, reaction of **19** with $RuCl(PPh_3)_2Cp$ in the presence of NH_4PF_6 produced a bright red solution from which $[\{Co_2(\mu,\eta^2\text{-}C_6H_5C_2CN\{Ru(PPh_3)_2Cp\})(CO)_4(\mu\text{-}dppm)\}][PF_6]$ (**20**) could be isolated as a brick-red powder (Scheme 5.3). Careful crystallisation at low temperatures produced red, cubic crystals of **20**. Spectroscopic characterisation confirmed the formation of the heterometallic species. The presence of the Cp ligand was established by NMR resonances at 4.30 (^1H) and 100.01 ppm ($^{13}C\{^1H\}$) while the dppm ligand resulted in unresolved resonances at 3.28 (^1H), and 35.84 ppm ($^{13}C\{^1H\}$). The carbon atoms of the Co_2C_2 cluster core appeared as triplets at 123.56 ppm (J_{CP} = 3 Hz) and 97.96 ppm (J_{CP} = 19 Hz). The ^{31}P NMR spectrum showed two singlets at 42.00 and 37.67 ppm

corresponding to the PPh_3 and dppm ligands respectively. The $[PF_6]^-$ counter-ion gave the expected heptet at -142.96 ppm (J_{PF} = 711 Hz). ES(+)-MS agreed with the suspected composition with the complex cation $[\{Co_2(\mu,\eta^2\text{-}C_6H_5C_2CN\{Ru(PPh_3)_2Cp\})(CO)_4(\mu\text{-dppm})\}]^+$ giving rise to an isotopic envelope at *m/z* = 1431. The fragment $[Ru(PPh_3)_2Cp]^+$ was also observed at *m/z* = 691.

Reactivity of [Ru(NCC≡CC$_6$H$_5$)(PPh$_3$)$_2$Cp][PF$_6$]

In order to gain qualitative measure of the stability of the bond between the cyanoacetylene ligand and the metal centre, a sample of **17** in $CDCl_3$ was treated with one equivalent of MeCN and the reaction was monitored by ^1H NMR spectroscopy. Over a period of 24 hours, the Cp resonance at 4.52 ppm arising from **17** slowly diminshed and a new resonance grew in at 4.44 ppm. This was assigned to the species $[Ru(NCMe)(PPh_3)_2Cp]^+$ by comparison with an authentic sample (4.46 ppm).

The reaction of **17** with tetracyanoethylene (TCNE) was also investigated. The organic species TCNE has been shown to react readily with metal acetylide, diynyl and polyyndiyl complexes under mild conditions to afford products derived from [2+2] cyclisation reactions. The initial cyclobutene products often ring-open to afford highly conjugated cyanocarbon ligands.[19-22] The TCNE ligand has also been used as a η^1(N) bonding ligand, and has been shown to react with oxidisable metal centres to give products derived from charge transfer processes with the ligand best formulated as a TCNE radical or dianion.[23-31] Reaction of **17** at room temperature in dry, distilled THF with one equivalent of TCNE resulted in the rapid formation of a dark

green/blue solution. Removal of solvent and subsequent work-up resulted in the formation of $[\{Ru(PPh_3)_2Cp\}_2(\mu\text{-TCNE})][PF_6]_2$ (**21**) as a blue/grey solid. The Cp resonance showed a shift in the ^1H NMR with respect to **17** (4.58 ppm vs. 4.52 ppm respectively). Infra-red spectroscopy revealed absorption bands at 2139 cm^{-1} with a shoulder at 2164 cm^{-1}. Mass spectrometry [ES(+)-MS] showed an isotopic envelope arising from the cation $[\{Ru(PPh_3)_2Cp\}_2(\mu\text{-TCNE})]^+$ at $m/z = 818$ as well as the cationic fragment $[Ru(PPh_3)_2Cp]^+$ at $m/z = 691$. These data are inconclusive with regards to the formulation of **21** as either the mononuclear compound $[Ru(TCNE)(PPh_3)_2Cp][PF_6]$ or the binuclear species, which can be obtained, at least in principle, as either *cis* or *trans* forms. Recrystallisation of **21** from $CHCl_3$ resulted in the formation of sapphire-blue crystals suitable for X-ray diffraction studies which conclusively identified the bimetallic nature and the connectivity of the compound (see below).

Molecular Structures

The molecular structures of **17** and **19-20** were determined. Crystallographic details are summarised in Table 5.1 with selected bond lengths and angles in Tables 5.2 (**17**, **19** and **20**) and 5.3 (**21**, see below).

Table 5.1. Crystallographic Details.

Compound	17	19	20	21
Formula	$C_{50}H_{40}F_6NP_3Ru.0.7CH_2Cl_2$	$C_{38}H_{27}Co_2NO_4P_2$	$C_{79}H_{62}NO_4P_5F_6Co_2Ru.2CH_2Cl_2$	$C_{88}H_{70}N_2P_4Ru_2$
FW	1022.26	741.41	1746.93	1019.09
a (Å)	10.3647(5)	16.95859(8)	11.7464(7)	10.0332(4)
b (Å)	35.1128(16)	10.8413(5)	17.3929(10)	20.3162(9)
c (Å)	12.9836(6)	18.4223(9)	21.8925(13)	20.6003(9)
α (°)	90	90	71.121(3)	90
β (°)	104.145(2)	95.558(1)	76.244(2)	101.21(2)
γ (°)	90	90	73.405(2)	90
V(Å^3)	4581.9(4)	3297.0(3)	4003.4(4)	4118.9(3)
T(K)	120(2)	110(2)	120(2)	120(2)
Crystal System	Monoclinic	Monoclinic	Triclinic	Monoclinic
Space group	$P2_1/n$	$P2_1/n$	$P\bar{1}$	$P2_1/c$
Z	4	4	2	4
μ (mm^{-1})	0.59	1.146	0.892	0.757
Reflections collected	24223	25776	46232	35233
Independent reflections	918 1[$R_{(int)}$ = 0.0465]	9562 [$R_{(int)}$ = 0.0373]	19669 [$R_{(int)}$ = 0.0386]	10935 [$R_{(int)}$ = 0.0709]
Final R indices (all data)	R_1 = 0.0898, wR_2 = 0.13995	R_1 = 0.0706, wR_2 = 0.1486	R_1 = 0.0449, wR_2 = 0.0815	R_1 = 0.1195, wR_2 = 0.2672

Table 5.2. Selected bond lengths and angles for compounds **17**, **19**, and **20**.

Compound	17	19	20
Ru-N (Å)	2.002(4)	n/a	2.036(3)
N-C(2) (Å)	1.162(7)	1.153(2)	1.162(4)
C(2)-C(3) (Å)	1.365(8)	1.412(2)	1.393(5)
C(3)-C(4) (Å)	1.208(8)	1.370(2)	1.382(5)
C(4)-C(ipso) (Å)	1.430(8)	1.465(2)	1.460(5)
Co-Co (Å)	n/a	2.4651(3)	2.4846(7)
Ru-P(1) (Å)	2.355(2)	n/a	2.3420(9)
Ru-P(2) (Å)	2.352(2)	n/a	2.3343(9)
P(1)-Ru-P(2) (°)	101.25(5)	n/a	101.61(3)
Ru-N-C(2) (°)	177.4(4)	n/a	166.8(3)
N-C(2)-C(3) (°)	177.6(6)	175.0(4)	175.0(4)
C(2)-C(3)-C(4) (°)	175.9(7)	137.4(3)	137.4(3)
C(3)-C(4)-C(ipso) (°)	176.5(6)	140.4(3)	140.4(3)

The structure of **17** (Figure 5.5) is very similar to that of the benzonitrile complex $[Ru(N{\equiv}CC_6H_5)(PPh_3)_2Cp][PF_6]$ (**1**) (see Chapter 3). The Ru-P distances in **17** (2.352(1) and 2.355(1) Å) are slightly longer than those in **1** (2.334(1) and 2.335(1) Å in **1**) and the P(1)-Ru-P(2) angle is slightly larger (101.25(5)° in **17** and 97.46(1)° in

1). The Ru-N bond length in **17** is significantly shorter than that in **1** (2.002(4) Å in **17** vs. 2.037(1) Å in **1**). The N-C(1) bond length in **1** (1.145(2) Å) appears shorter than the equivalent N-C(2) length in **17** (1.162(7) Å) but these differences are within the limits of precision of the experiment. The C(2)-C(3), C(3)-C(4) and C(4)-C(ipso) bond lengths (1.365(8), 1.208(8) and 1.430(8) Å) are much as would be expected and agree with the representation of the structure of the ligand as alternating single and triple bonds. The Ru-N(1)-C(2) and C(3)-C(4)-C(ipso) fragment in **17** is essentially linear (177.4(4)°).

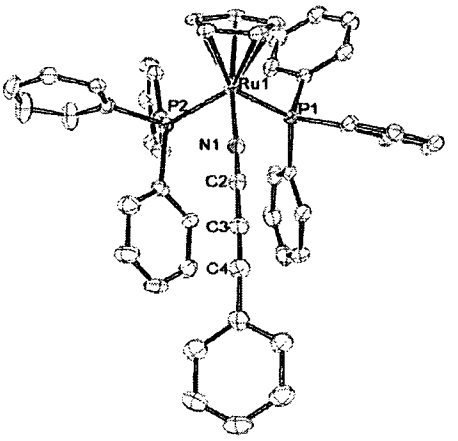

Figure 5.5. ORTEP Plot of $[Ru(NCC{\equiv}CC_6H_5)(PPh_3)_2Cp][PF_6]$ (**17**).

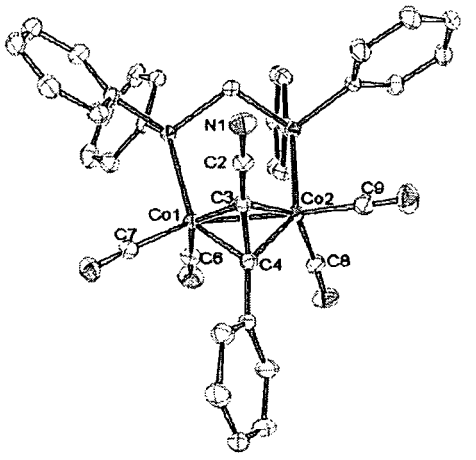

Figure 5.6. ORTEP Plot of $[Co_2(\mu,\eta^2\text{-}C_6H_5C_2CN)(CO)_4(\mu\text{-dppm})]$ (**19**).

The structure of **19** (Figure 5.6) clearly indicates the co-ordination of the alkyne moiety of the cyanoacetylene ligand to the dicobalt fragment in μ,η^2 fashion. The N-C(2) bond length seems unaffected by the mode of co-ordination (1.153(2) Å vs 1.162(7) Å in **17**), as is the C(4)-C(ipso) distance (1.465(2) Å vs. 1.430(8) Å in **17**). There is a marked lengthening of the C(3)-C(4) bond on co-ordination (from 1.208(8) Å in **17** to 1.370(2) Å in **19**) which is consistent with the loss of triple bond character upon formation of the Co_2C_2 cluster core. Also of note are the Co(1)-Co(2) and C(3)-C(4) bond lengths (2.4651(3) Å and 1.370(2) Å respectively) which are at the shorter and longer ends of the range of bond lengths normally associated with $[Co_2(\mu,\eta^2\text{-alkyne})(CO)_4(dppm)]$ complexes respectively.[32] Furthermore, the torsion angles C(6)-Co(1)-Co(2)-C(8) (-17.86(7)°), C(7)-Co(1)-Co(2)-C(9) (–36.1(1)°) and P(3)-Co(1)-Co(2)-P(4) (-11.13(2)°) are unusually large when compared against a series of closely related structures $[Co_2(\mu,\eta^2\text{-}RC_2C_6H_4X\text{-}4)(CO)_4(dppm)]$ (X = H, NO_2, CN, NMe_2).[32]

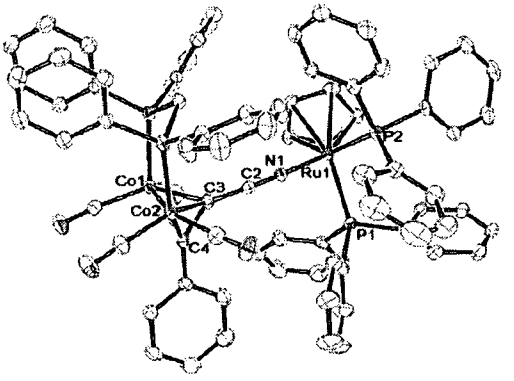

Figure 5.7. ORTEP Plot of [{$Co_2(\mu,\eta^2\text{-}C_6H_5C_2CN\{Ru(PPh_3)_2Cp\})(CO)_4(\mu$-dppm)}][$PF_6$] (**20**)

The molecular structure of **20** (Figure 5.7) clearly indicates the ability of the cyanoacetylene ligand to display both η^1-(N) and η^2-(alkyne) co-ordination modes simultaneously. The structure is similar to the combined structures of **17** and **19**. There is no statistically significant change in the bond lengths associated with the cyanoacetylene ligand upon co-ordination of the [$Ru(PPh_3)_2Cp$] fragment to the NC moiety with respect to **19**, although the Ru-N distance (2.036(1) Å) is longer than in **17** (2.002(4) Å). There is also some reduction in the distortion about the cobalt centres (C(7)-Co(1)-Co(2)-C(8) 5.0(2)°; C(6)-Co(1)-Co(2)-C(9) 25.6(3)°; P(3)-Co(1)-Co(2)-P(4) 8.85(4)°).

The molecular structure of the TCNE-bridged complex **21** shows contains a crystallographic centre of inversion at the mid-point of the TCNE C(2)=C(2A) double bond (Figure 5.8). Although one N-C bond length in the structure of **21** appears longer than the other (N(1)-C(1) = 1.151(7) Å, N(2)-C(3) = 1.135(8) Å), with the

longer of the two being that coordinated to the ruthenium centre, these are both the same within the limits of precision of the measurement. The C(1)-C(2)-C(3) angle is 119.3(5)° and the C(1)-C(2)-C(2A) angle is 121.3(6)°).

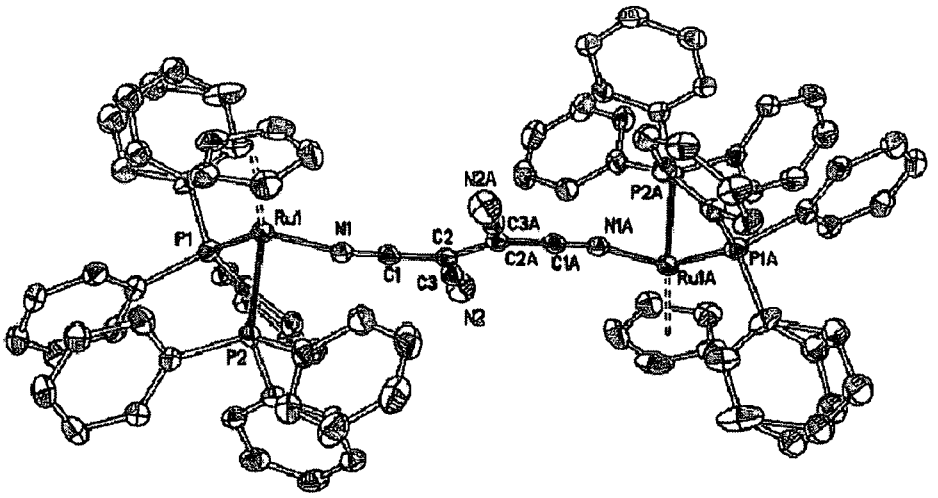

Figure 5.8. ORTEP Plot of $[\{Ru(PPh_3)_2Cp\}_2(\mu\text{-TCNE})][PF_6]_2$ (**21**) (Hydrogen atoms have been omitted for clarity)

Table 5.3. Selected bond lengths and angles for compound **21**.

Compound	**21**
Ru-N(1) (Å)	1.976(5)
N(1)-C(1) (Å)	1.151(7)
C(1)-C(2) (Å)	1.411(7)
C(2)-C(2a) (Å)	1.393(11)
C(2)-C(3) (Å)	1.432(8)
C(3)-N(2) (Å)	1.135(8)
Ru-P(1) (Å)	2.3424(17)
Ru-P(2) (Å)	2.3597(15)
P(1)-Ru-P(2) (°)	95.56(6)
Ru-N(1)-C(1) (°)	169.7(4)
N(1)-C(1)-C(2) (°)	177.3(6)
C(1)-C(2)-C(3) (°)	119.3(5)
C(1)-C(2)-C(2a) (°)	121.3(6)

Electrochemistry

Measurements were carried out in a 0.1M $[N(C_4H_9)_4][BF_4]$ solution in DCM. Internal decamethylferrocene [Fc^*/Fc^{*+} = -0.02 V vs. SCE] or ferrocene [Fc/Fc^+ = +0.46 V vs. SCE] standards were used to give electrode potentials relative to SCE.[33]

The electrochemical response of **17** at a platinum electrode was characterised by a single, irreversible oxidation (E_{pa} = +1.47 V) which contrasts with the reversible oxidation seen at lower potential for the analogous benzonitrile compound **1** (E° = +1.30 V). In contrast to this, **18** displayed a single oxidation event at +1.04 V, the reversibility of which was improved at sub-ambient temperatures (-30 °C).

The electrochemical response at a glassy-carbon electrode of the cobalt-carbon cluster compound **19** was characterised by both a single reduction and an oxidation wave. These were poorly reversible at room temperature but their reversibility improved upon cooling to -30°C (E_{red}° = -1.40 V, E_{ox}° = 0.98 V). These potentials may be compared with those of the closely related species $[Co_2(\mu\text{-}HC_2Ph)(CO)_4(dppm)]$ (E°_{red} = –1.73 V;E°_{ox} = +0.79 V).

Coordination of the ruthenium fragment to the NC moiety to form compound **20** resulted in a shift in the cobalt-carbon cluster based reduction potential to –1.23 V and the chemical reversibility of the reduction product was increased. However, the

oxidation of **20** became almost totally chemically irreversible (E_{pa} = +1.06 V). The TCNE-bridged bimetallic dication **21** underwent a single irreversible oxidation (E_{pa} +1.42 V). Evidently, there is little electronic interaction between the formally Ru(II) centres through the TCNE bridge.

Discussion

The cyanoacetylene ligand N≡CC≡CR is isolobal and isoelectronic with the diynyl anion $[RC{\equiv}CC{\equiv}C]^-$ and bears an obvious structural relationship with benzonitrile and related nitrile ligands. It follows that the spectroscopic and structural parameters of the cyanoacetylene complex $[Ru(NCC{\equiv}CC_6H_5)(PPh_3)_2Cp][PF_6]$ (**17**), which has been prepared in a similar fashion to the simple benzonitrile complex $[Ru(N{\equiv}CC_6H_5)(PPh_3)_2Cp][PF_6]$ (**1**) (see Chapter 3), may be compared to both **1** and the analogous diynyl complex $Ru(C{\equiv}CC{\equiv}CC_6H_5)(PPh_3)_2Cp$.[34]

Spectroscopically, there are marked differences between **17** and the analogous diynyl compounds. Resonances arising from the Cp moiety in the NMR spectra of **17** were found at 4.52 ppm (^1H) and 84.90 ppm ($^{13}C\{^1H\}$) whilst in the diynyl complex these appear at 4.35 ppm (^1H) and 85.71 ppm ($^{13}C\{^1H\}$). These NMR resonances are consistent with the more cationic ruthenium centre present in **17** and compare closely with those found for the Cp moiety of the benzonitrile complex **1** (4.55 ppm and 84.38 ppm for ^1H and ^{13}C respectively). Further, there are two clearly distinguishable $\nu(C{\equiv}C)$ bands in the IR spectrum of the diynyl complex (2162 and 2025 cm^{-1}) whereas in **17** only the acetylenic moiety is visible (2141 cm^{-1}). In contrast to the simple nitrile complexes described earlier in this thesis (see Chapter 3) the co-ordinated C≡N moiety is not observed in the IR spectrum of **17**.

Reaction of **17** under mild conditions with one equivalent of MeCN led to the substitution of the cyanoacetylene ligand by MeCN over a period of 24 hours. This was not observed in the case of $[Ru(NCC{\equiv}CC_6H_4\text{-}4\text{-}NMe_2)(dppe)_2Cp^*][PF_6]$ (**18**) and

is in good agreement with the electrochemical data. Complex **17** displays an irreversible oxidation at +1.47 V. This indicates a much more electron-poor metal centre than in the case of $[Ru(N{\equiv}CC_6H_5)(PPh_3)_2Cp][PF_6]$ (**1**) in which a reversible oxidation at +1.30 V is seen. Although the electrochemical response of **18** at room temperature was not chemically reversible, the reversibility of the oxidation was markedly improved at sub-ambient temperatures. At -30 °C a reversible oxidation at a platinum electrode with an oxidation potential of +1.04 V vs SCE was observed. Assuming that the relative oxidation potentials of the complexes reflect the net donor properties of the RCN ligands it may be concluded that there is a relative order of donor strength $N{\equiv}CC{\equiv}CC_6H_5 < NCPh < N{\equiv}CC{\equiv}CC_6H_4\text{-}4\text{-}NMe_2$.

The molecular structure of **17** may be compared to both the corresponding diynyl complex $Ru(C{\equiv}CC{\equiv}CC_6H_5)(PPh_3)_2Cp$ and the analogous benzonitrile compound $[Ru(N{\equiv}CC_6H_5)(PPh_3)_2Cp][PF_6]$ (**1**).[34] The Ru-X bond (where X = N or C) varies considerably between the three compounds, ranging from 1.994(4) Å in $Ru(C{\equiv}CC{\equiv}CC_6H_5)(PPh_3)_2Cp$ to 2.037(1) Å in **1**. The Ru-N bond length in compound **17** (2.002(4) Å) is therefore identical (within the limits of precision of the measurement) to that of the diynyl equivalent and significantly shorter than that in the benzonitrile complex **1**. The N-C bond of **17** is 1.162(7) Å which is similar to the benzonitrile analogue (1.145(2) Å) but shorter than that of the diynyl complex (1.206(5) Å). The bond lengths of the rest of the carbon chain in the cyanoacetylene ligand (C(1)-C(2) = 1.365(8) Å, C(2)-C(3) = 1.208(8) Å, C(3)-C(ispo) = 1.430(8) Å) are comparable to those in the diynyl complex (C(1)-C(2) = 1.389(6) Å, C(2)-C(3) = 1.200(6) Å, C(3)-C(ispo) = 1.416(6) Å). Although there is some degree of π back-bonding between the ligand and the metal centre in the diynyl complexes this is very

small and by far the strongest interaction is a σ-bonding interaction between the lone pair of the diynyl anion and the d_z^2 orbital of the metal fragment. An examination of the charge distribution in the diynyl complex $Ru[(C{\equiv}C)_nR](PPh_3)_2Cp$ shows a substantial amount of negative charge on the alkyne moiety adjacent to the metal centre, the degree of which increases with *n*.[35] This leads to a coulombic attraction between the negative alkyne moiety and the positive metal centre which also increases with *n*. By analogy, the cyanoacetylene would be expected to have a greater degree of electron density at the N≡C moiety than the benzonitrile ligand. Hence there is a greater coulombic attraction between the N atom and the metal centre in **17** than in **1** and this results in **17** having a shorter Ru-N distance whilst the N-C bond length is unaffected. The bond angles at the phenyl end of the $Ru\text{-}XC_3Ph$ chain are almost linear in **17** and the diynyl analogue.

It is worth noting that the orientation of the phenyl ring of the cyanoacetylene is approximately orthogonal to that in the benzonitrile complex. A similar phenomenon is seen in the behaviour of the phenyl acetylene and diynyl analogues $Ru(C{\equiv}CC_6H_5)(PPh_3)_2Cp$ and $Ru(C{\equiv}CC{\equiv}CC_6H_5)(PPh_3)Cp$.[34,36,37] The C≡C and C≡N moieties posses two orthogonal sets of π orbitals which can interact with the d-orbitals of the metal centre. There are then two possible, orthogonal orientations that the aromatic ring system can adopt and maintain conjugation with the C≡C, or C≡N, moiety. In the cases where there are only two atoms between the phenyl group of the ligand (C≡N or C≡C) and the metal centre, steric interactions between the phenyl ring and the phosphine moieties force the ligand to adopt a geometry with the aromatic ring sitting in the plane of the $Ru\text{-}Cp_{(centroid)}$ vector. In the case of the cyanoacetylene and diynyl ligands, the additional C≡C spacer increases the distance of the phenyl ring

from the phosphine moieties such that the ring can now adopt a position with its plane perpendicular to the Ru-$Cp_{(centroid)}$ vector.

The cyanoacetylene ligand can also co-ordinate in an η^2 fashion by reaction with the known alkyne sequestering agent $Co_2(CO)_6$(dppm) to give [$Co_2(\mu,\eta^2$-$C_6H_5C_2CN)(CO)_4(\mu$-dppm)] (**19**). A large number of similar complexes are known and the ν(CO) frequencies have been shown to be sensitive to the electronic properties of the aryl substituent.[32] The ν(CO) bands in the unsubstituted complex [$Co_2(\mu,\eta^2$-$HC_2C_6H_5)(CO)_4$(dppm)] occur in the range 2027-1956 cm^{-1} whilst for compound **19** these are found in the range 2037-1970 cm^{-1}. Hence the electron-withdrawing CN moiety of the coordinated cyanoacetylene ligand draws electron density away from the cluster core resulting in less back-bonding with the π* orbitals of the CO ligands and higher stretching frequencies. By comparison, the ν(CO) bands of the complex [$Co_2(\mu,\eta^2$-$HC_2C_6H_4$-4-CN)$(CO)_4$(dppm)] (an isomer of **19**) are found in the range 2030-1961 cm^{-1}. The fact that these ν(CO) bands fall in between those found for **19** and the unsubstitued complex shows that the electron-withdrawing effect of the CN moiety is diminished when separated from the cluster core by the phenyl spacer.

The effect of the electron-withdrawing CN ligand is also seen the electrochemical response of **19**. The withdrawal of electron-density from the cluster core relative to [$Co_2(\mu,\eta^2$-$HC_2C_6H_5)(CO)_4$(dppm)] facilitates the reduction of **19** and hence it has a lower reduction potential (-1.41 V vs. SCE) than the unsubstituted complex (-1.83 V vs. SCE). The same inductive electron-withdrawing makes the oxidation of **19** less

thermodynamically favourable than for the unsubstituted complex (+0.98 V vs SCE for **19** vs. +0.69 V vs SCE for $[Co_2(\mu,\eta^2\text{-}HC_2C_6H_5)(CO)_4(dppm)]$).

As has been stated earlier (see Results) there is very little change in either the N-C(1) or the C(3)-C(ipso) bond lengths of **19** (relative to **17**) upon coordination to form the cobalt-carbon cluster. Furthermore, the increase in the carbon-carbon bond length associated with the alkyne portion of the ligand can be accounted for by the change in hybridisation of the carbon atoms C(2) and C(3) from sp hybridisation in **17** to sp^3 in **19**. The C(2)-C(3) bond length in **19** is slightly "long" (1.370(2) Å) when compared to the analagous compounds $[Co_2(\mu,\eta^2\text{-}HC_2C_6H_4X\text{-}4)(CO)_4(dppm)]$ (X = H, NMe_2, NO_2, CN) in which the C(2)-C(3) bond length averages 1.348(2) Å. Also, the Co-Co bond in compound **19** (2.4651(3) Å) is at the short end of the range found in the acetylenes which fall in the range 2.4657(4) Å to 2.4950(4) Å.

An important point to note about the geometry of complex **19** is the torsion angles C(6)-Co(1)-Co(2)-C(8) (-17.86(7)°) and C(7)-Co(1)-Co(2)-C(9) (-36.1(1)°). These are large when compared to the analogous compounds mentioned above. Thorn and Hoffman have described the main bonding interactions in $[M_2(CO)_6(\mu\text{-}RC_2R)]$ (M = Fe, Co), a similar scheme being used for both complexes.[38] In their description the HOMO orbital for the Co complex (a_2) arises from an anti-bonding (π^*) M-M/C-C interaction (Figure 5.9).

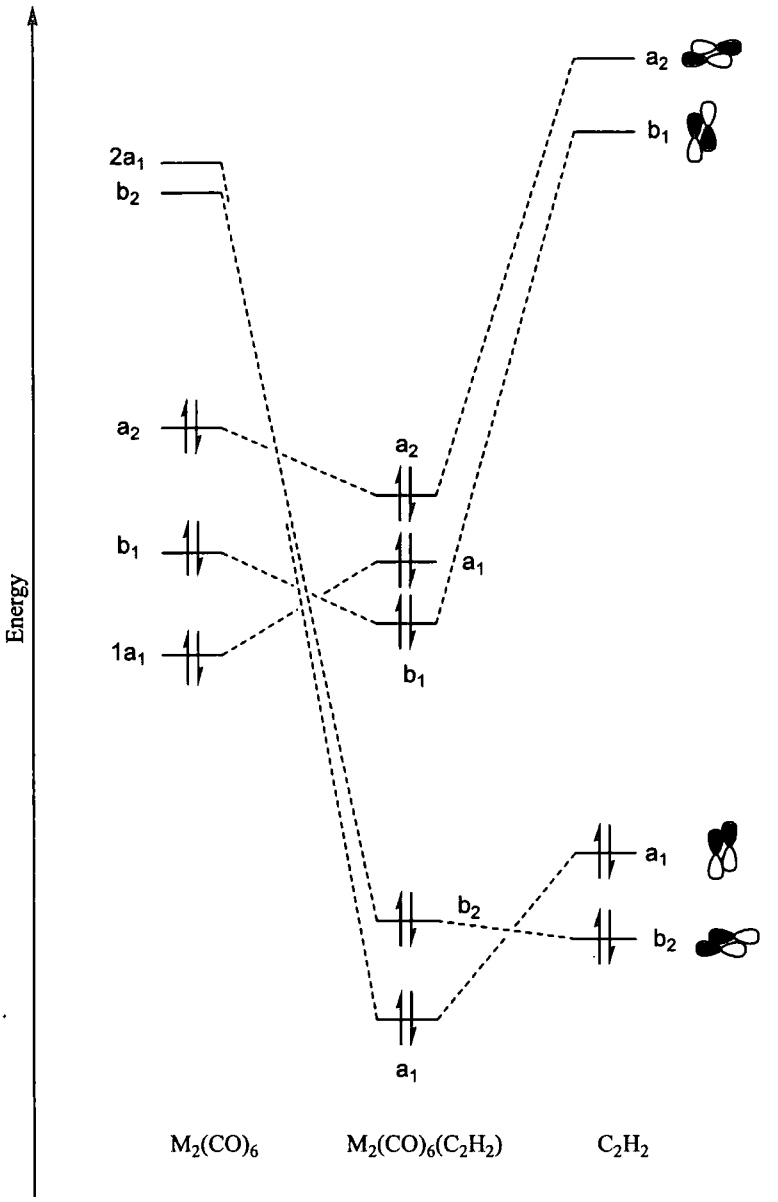

Figure 5.9. Frontier orbitals formed upon interaction of C_2H_2 with $M_2(CO)_6$ to form M_2/C_2 cluster core. Orbital occupancy for M = Co illustrated.[38]

Oxidation of the Co_2 complex depopulates the a_2 orbital and increases the bonding nature of the M-M/C-C interaction, decreasing the M-M distance. This leaves a low-lying empty orbital, which leads to a second-order Jahn-Teller distortion of the structure in order to raise the energy of that orbital (Figure 5.10)

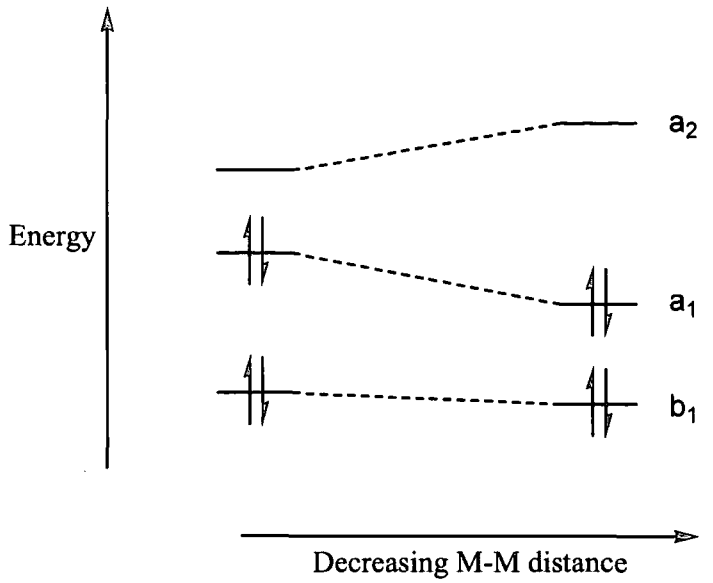

Figure 5.10. Jahn-Teller distortion of frontier orbital in $M_2(CO)_6(C_2H_2)$.[38]

Structural distortion can occur in one of two ways. Firstly, there can be a rotation on the C-C axis relative to the M-M bond. This twisting has been observed by Connelly et al in the solid state structures of $[Co_2(CO)_2(\mu\text{-}RC_2R)(\mu\text{-}dppm)_2]^{x+}$ (R = Me, Ph, CO_2Me).[39] It was shown that in the neutral species the M-M/C-C vectors were essentially perpendicular. Oxidation of these compounds by reaction with $[Fc]PF_6$ depopulated the a_2 orbital and the resultant Jahn-Teller distortion led to a twisting of the C-C vector, relative to the M-M axis (Figure 5.11).

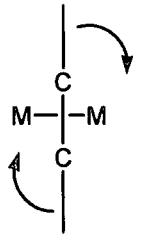

Figure 5.11. Twisting of C-C vector relative to M-M axis

A second way to achieve this Jahn-Teller distortion is for there to be a twisting about the M-M axis itself, rotating one $M(CO)_3$ fragment relative to the other to adopt a staggered conformation. This has been observed for the compound $Fe_2(CO)_6(\mu\text{-}^tBuC_2{}^tBu)$ (OC-Fe-Fe-CO torsion angle = ± 45°).[40] Each iron centre has one less electron than the comparable cobalt centre and thus electronic structure of the di-iron complex is the same as that of the di-oxidised di-cobalt analogue.

In compound **19** the alkyne and Co-Co axes are essentially perpendicular to one another (91.3°) but there is significant rotation about the Co-Co bond, as evidenced by the C(6)-Co(1)-Co(2)-C(8) and C(7)-Co(1)-Co(2)-C(9) torsion angles. The dppm ligand would, however, prevent the material from adopting a perfectly staggered conformation. This rotation would seem to indicate, therefore, that there is some de-population of the a_2 orbital in this compound. This may be due to the presence of the CN moiety which provides π-type orbitals that can conjugate with the HOMO of the Co_2C_2 cluster and hence allows for delocalisation of electron density across the structure. This is consistent with the effect of the CN ligand on the ν(CO) bands and the electrochemical response of **19** as described above.

Coordination of the electron-deficient $[Ru(PPh_3)_2Cp]^+$ fragment to the nitrile moiety of **19** results in the formation of the heterometallic complex **20**. Attempts to make this compound by reaction of the cobalt complex $Co_2(CO)_6$(dppm) with **17** resulted only in the formation of **19**. This is a further indication of the lability of the η^1(N) coordinated cyanoacetylene ligand and its poor σ-donor strength.

The addition of the ruthenium fragment has a perceptible effect on the electrochemical response of the material. The reduction of the cluster compound is further facilitated as the electron-deficient metal end-cap draws more electron density from the cluster core, making the addition of an electron easier. Hence **20** has a reduction potential of -1.23 V vs SCE compared to that of -1.40 V vs SCE for **19**. This reduction event is also far more stable in the case of **20**, being reversible at room temperature. Furthermore, the oxidation potential of **20** (+1.06 V vs SCE) is raised relative to that of **19** (+0.98 V vs SCE) and is now totally irreversible. This effect consistent with the further removal of electron density from the Co, however it must be noted that the complex **20** is a cation and hence there will be a coulombic effect here as well.

The crystallographically determined structure of **20** can be thought of as a superposition of the structures of **17** and **19** with a few notable distinctions. Firstly, the Ru-N bond length in **20** (2.036 Å) is longer than that in **17** (2.002(4) Å) and more of the order of those in the benzonitrile complexes **1**, **4**, **5**, **7** and **8**. A possible reason for this is that coordination of the cobalt complex to the acetylenic moiety of the cyanoacetylene ligand effectively destroys the cyanoacetylene character of the bonding orbitals. Hence a picture of a cluster-bound nitrile coordinating to the ruthenium fragment is more appropriate than one of a cyanoacetylene ligand. As discussed in Chapter 3, nitrile ligands are poor π-acceptors and so there is no back bonding from the ruthenium centre to the NC moiety in **20** and the bond is lengthened relative to **17**. The NC bond length in compounds **17** and **20** is identical and the curvature across the NC_3 linkage is the same in **19** and **20**. There is some distortion of **20** about the Co centres (C(7)-Co(1)-Co(2)-C(8) = 5.0(2)° and C(6)-Co(1)-Co(2)-C(9)

= 25.6(3)°). This rotation is not as great as in compound **19** but there is still some deviation from the norm.

The TCNE-bridged complex [{$Ru(PPh_3)_2Cp$}$_2$(μ-TCNE)] (**21**) displays a single irreversible oxidation wave at +1.42 V vs SCE. This is an indicator little or no electronic communication between the two metal centres. This lack of communication would seem to be borne out by the molecular structure of **21**. In a 1992 study, Bock and Ruppert established crystallographic parameters for TCNE as the neutral organic molecule, as the radical anion and as the dianion.[41] They showed that the bond lengths and angle were different in each case. In the neutral organic molecule, the C(2)-C(2a) bond length is 1.35 Å which lengthens with successive reductions to 1.43 Å in the radical anion and 1.47 Å in the dianion. Whilst most of the other bond lengths and angles remain relatively unaffected (although there is a small contraction of the C(1)-C(2) bond length with successive oxidations this only spans a 1.43-1.39 Å range), the dihedral angle C(1)-C(2)-C(2A)-C(3A) changes remarkably. In the neutral molecule this angle is 0° and the molecule is essentially planar. However this angle varies in the range 0-20° for the radical anion and is about 90° for the dianion. Examples of each type are to be found in the literature, with the neutral molecule coordinating via two or more N≡C moieties to form polymers[23] or extended sheets[30] in which the dihedral angle is 0° and the C(2)-C(2a) bond length averages about 1.33 Å. However in the case of two $Ir(PPh_3)_2CO$ centres bridged by the TCNE dianion,[24] for example, the C(2)-C2(a) bond length is found to be longer (1.478(8) Å) and the there is a much greater degree of twisting about the central axis (the dihedral angle C(1)-C(2)-C(2A)-C(3A) is 67.2°). There is no evident twisting of the two halves of the TCNE fragment in **21** (C(1)-C(2)-C(2A)-C(3A) 1.6°).

Compared to the parent organic molecule, there is a lengthening of the C=C bond upon co-ordination (from about 1.35 Å to 1.393(11) Å in **21**). There also appears to be a slight lengthening of the co-ordinated N-C(1) bond in comparison to the uncoordinated bond but this is within the limits of precision of the experiment (1.151(7) Å vs. 1.135(8) Å). Hence, the geometry of the TCNE ligand is little changed from the neutral organic molecule suggesting a neutral bridge rather than a radical anion or dianionic ligand*.

* Recent communication from Prof. J. S. Miller (Utah) suggests an alternative description of **21** in terms of a RuII/RuIII(μ - $TCNE^{\cdot-}$) mixed-valence species. Miller's query arises from the elongation of the C(2)-C(2a) bond length which falls between neutral and radical anion forms of TCNE. A sample of **21** has been supplied to the Utah group for variable temperature magnetic measurements to probe this alternate interpretation.

Experimental

[Ru(NCC≡CC$_6$H$_5$)(PPh$_3$)$_2$Cp][PF$_6$] (17)

A 50 ml, two-necked Schlenk flask was cooled under nitrogen and charged with RuCl(PPh$_3$)$_2$Cp (247 mg, 0.345 mmol), C$_6$H$_5$C≡CCN (122 mg, 0.961 mmol), and NH$_4$PF$_6$ (212 mg, 1.30 mmol). The mixture was then suspended in MeOH (20 ml) and heated to reflux under a nitrogen atmosphere. After 30 minutes at reflux a yellow solution formed and the reaction was cooled (ice/water). The yellow precipitate formed was collected and washed with cold methanol to afford **17** as a yellow powder (211 mg, 0.219 mmol, 64 %). Crystals suitable for x-ray diffraction studies were obtained by slow diffusion of MeOH into a DCM solution of **17**. Found: C, 61.90; H, 4.13; N, 1.50. RuC$_{50}$H$_{40}$P$_3$F$_6$N requires: C, 62.37; H, 4.19; N, 1.45. ^{1}H NMR (CDCl$_3$): δ 4.52 (s, 5H, Cp); 6.98-7.57 (m, 40H, Ph). ^{13}C{^{1}H} NMR (CDCl$_3$): δ 135.20-128.43 (m, Ph); 116.63, 115.88 (2 × s, C≡C); 84.90 (s, Cp). ^{31}P{^{1}H} NMR (CDCl$_3$): δ 41.86 (s, PPh$_3$); -143.02 (ht, J_{PF} = 713 Hz, [PF$_6$]$^-$). ES(+)-MS (*m/z*): 818 [Ru (NCC≡CC$_6$H$_5$)(PPh$_3$)$_2$Cp]$^+$; 691 [Ru(PPh$_3$)Cp]$^+$. IR (nujol mull): ν(C≡C) 2141 cm^{-1}.

[Ru(NCC≡CC$_6$H$_4$-4-NMe$_2$)(dppe)Cp*][PF$_6$] (18)

A 50 ml, two-necked Schlenk flask was cooled under nitrogen and charged with RuCl(dppe)Cp* (197 mg, 0.294 mmol), NCC≡CC$_6$H$_4$-4-NMe$_2$ (50 mg, 0.294 mmol), and NH$_4$PF$_6$ (192 mg, 1.18 mmol). The mixture was then suspended in MeOH (15

ml) and heated to reflux under a nitrogen atmosphere. After 1hr a brown/yellow solution formed. The reaction was allowed to cool to room temperature and the solvent was removed. The yellow/brown residue produced was dissolved in DCM and filtered. Slow diffusion of hexane into the DCM solution resulted in the formation of **18** as yellow, needle-like crystals (190 mg, 0.2mmol, 68 %). ^{1}H NMR ($CDCl_3$): δ 1.47 (s, 15H, Cp*); 2.31-2.56 (m, 4H, dppe); 3.05 (s, 6H, NMe_2); 6.58 (pseudo-d, J_{HH} = 9 Hz, $2H_{ortho}$, $NCC{\equiv}CC_6H_4$-4-NMe_2) 7.23-7.54 (m, 22H, Ph). $^{13}C\{^{1}H\}$ NMR ($CDCl_3$): δ 152.54 (s, C-C_3N); 135.86-129.00 (m, Ph); 93.75 (s, C_5Me_5); 40.20 (s, NMe_2); 28.90-28.55 (m, dppe); 9.83 (s, $C_5\mathit{Me}_5$). $^{31}P\{^{1}H\}$ NMR ($CDCl_3$): δ 75.10 (s, dppe); -143.21 (ht, J_{PF} = 713 Hz, $[PF_6]^-$). ES(+)-MS (*m/z*): 804 $[Ru(NCC{\equiv}CC_6H_4NMe_2)(dppe)Cp^*]^+$; 635 $[Ru(dppe)Cp^*]^+$. IR (CH_2Cl_2): ν(C≡N) 2216 cm^{-1}; ν (C≡C) 2123 cm^{-1}.

$[Co_2(\mu,\eta^2$-$C_6H_5C_2CN)(CO)_4(\mu$-dppm)] (19)

A 50 ml, two-necked Schlenk flask was cooled under nitrogen and charged with $Co_2(CO)_6$(dppm) (100 mg, 0.150mmol) and $C_6H_5C{\equiv}CCN$ (18.9 mg, 0.147 mmol). The solids were dissolved in benzene (10 ml) and heated at reflux under a nitrogen atmosphere. After 2 hours the dark red solution that formed was allowed to cool to room temperature. The solvent was removed to give a dark red solid which was recrystallised by slow diffusion of MeOH into a DCM solution to afford **19** as dark red/black crystals (50 mg, 0.032 mmol, 22 %). Found: C, 60.17; H, 3.75; N, 2.08. $C_{39}H_{31}Co_2O_5P_2N$ requires: C, 60.56; H, 3.67; N,1.89. ^{1}H NMR ($CDCl_3$): δ 3.15 (dt, 1H, C*H*P_2); 3.49 (dt, 1H, C*H*P_2); 7.06-7.70 (m, 24H, Ph). $^{13}C\{^{1}H\}$ NMR ($CDCl_3$): δ

205.89, 199.21 (2 x br, CO); 141.32-127.36 (m, Ph); 123.55 (t, J_{CP} = 3Hz, Co_2C_2); 97.96 (t, J_{CP} = 18 Hz, Co_2C_2); 36.58 (t, J_{CP} = 21 Hz, PCH_2P). $^{31}P\{^1H\}$ NMR ($CDCl_3$): δ 39.92 (s, dppm). ES(+)-MS (*m/z*): 1504 $[2M+Na]^+$; 764 $[M+Na]^+$. IR (nujol mull): ν(C≡N) 2167cm^{-1}, ν(CO) 2037s, 2011s, 1982vs, 1970sh cm^{-1}.

[{$Co_2(\mu,\eta^2$-$C_6H_5C_2CN${$Ru(PPh_3)_2Cp$})$(CO)_4$(μ-dppm)}][PF_6] (20)

A 50 ml, two-necked Schlenk flask was cooled under nitrogen and charged with $Co_2(\mu,\eta^2$-$C_6H_5C{\equiv}CCN)(CO)_4$(μ-dppm) (100 mg, 0.135 mmol), $RuCl(PPh_3)_2Cp$ (97 mg, 0.135 mmol), and NH_4PF_6 (22 mg, 0.135 mmol). The solids were dissolved in MeOH (20 ml) and heated at reflux under a nitrogen atmosphere. After 2 hours the resultant red solution was allowed to cool and the solvent was removed. The red/brown residue was dissolved in the minimum amount of DCM and precipitated into hexane to give **20** as a red/brown solid (160 mg, 75 %). Crystals suitable for x-ray diffraction studies were obtained by slow diffusion of MeOH into a DCM solution of **20**. Found: C, 60.13; H, 4.07; N, 0.99. $C_{79}H_{62}P_5F_6O_4Co_2NRu$ requires: C, 60.16; H, 3.96; N, 0.89. ^1H NMR ($CDCl_3$): δ 3.28 (m, 2H, PCH_2P); 4.30 (s, 5H, Cp); 7.12-7.25 (m, 62H, Ph). ^{13}C NMR ($CDCl_3$): δ 205.89, 199.21 (2 × br, 2 × CO); 141.31-128.36 (m, Ph); 123.56 (t, J_{CP} = 3Hz, Co_2C_2); 100.01 (s, Cp); 97.96 (t, J_{CP} = 19 Hz, Co_2C_2); 36.58 (t, J_{CP} = 21 Hz, PCH_2P). ^{31}P NMR ($CDCl_3$): δ 42.00 (s, PPh_3); 35.84 (s, dppm); -142.96 (heptet, J_{PF} = 711 Hz, $[PF_6]^-$). ES(+)-MS (*m/z*): 1431 $[Co_2(\mu,\eta^2$-$C_6H_5C_2CN){Ru(PPh_3)_2Cp}(CO)_4$(dppm)$]^+$; 691 $[Ru(PPh_3)_2Cp]^+$. IR (cyclohexane): ν(CO) 2040s, 2017s, 1990sh cm^{-1}. IR (nujol): ν(CO) 2037m, 2011s, 1985s, 1967sh.

[{Ru(PPh$_3$)$_2$Cp}$_2$(μ-TCNE)] (21)

A 2-necked, 50 ml, Schlenk flask was cooled under nitrogen and charged with [Ru(NCC≡CC$_6$H$_5$)(PPh$_3$)$_2$Cp](PF$_6$) (150 mg, 0.156 mmol) in distilled THF (10 ml). To this stirred solution was added tetracyanoethylene (TCNE) (20 mg, 0.156 mmol). A dark green solution rapidly formed after 15 minutes stirring and the solvent was removed. The green residue produced was dissolved in the minimum of DCM and precipitated into Et$_2$O to afford **21** as a blue/grey solid which was recrystallised from CHCl$_3$ to give the product as sapphire-blue crystals (90 mg, 0.05 mmol, 64%). Found: C, 58.09; H, 3.86; N, 2.92. C$_{88}$H$_{70}$N$_4$P$_6$F$_{12}$Ru$_2$ requires: C, 58.74; H, 3.92; N,3.11. ^{1}H NMR (CDCl$_3$): δ 6.87-7.19 (m, 60H, Ph); 4.58 (s, 10H, Cp). ^{31}P{^{1}H} NMR (CDCl$_3$): δ 41.87 (PPh$_3$); -142.95 (ht, J_{PF} = 713 Hz, PF$_6$). ES(+)-MS (*m/z*): 818 [Ru({C$_2$(CN)$_4$})(PPh$_3$)$_2$Cp]$^+$; 691 [Ru(PPh$_3$)$_2$Cp]$^+$. IR (nujol mull): ν(C≡N) 2164(sh); 2139 cm^{-1}.

References

1 I. R. Whittall, A. M. McDonagh, M. G. Humphrey, M. Samoc, *Adv. Organomet. Chem.*, 1998, **42**, 291.

2 I. R. Whittall, A. M. McDonagh, M. G. Humphrey, M. Samoc, *Adv. Organomet. Chem.*, 1998, **43**, 349.

3 R. S. Dickson, D. B. W. Yawney, *Aust. J. Chem.*, 1968, **21**, 1077.

4 M. I. Bruce, M. Z. Iqbal, *J. Organomet. Chem.*, 1969, **17**, 469.

5 G. L. McLure, W. H. Baddley, *J. Organomet. Chem.*, 1971, **27**, 155.

6 L. Vaska, *Accounts Chem. Res.*, 1968, **1**, 335.

7 R. M. Kirchner, J. A. Ibers, *J. Am. Chem. Soc.*, 1973, **95**, 1095.

8 J. L. Kiplinger, A. M. Arif, T. G. Richmond, *Inorg. Chem.*, 1995, **34**, 399.

9 H. Scordia, R. Kergoat, M. M. Kubicki, J. E. Gerchais, *J. Organomet. Chem.*, 1983, **249**, 371.

10 H. Scordia, R. Kergoat, M. M. Kubicki, J. E. Guerchais, P. L' Haridon, *Organometallics*, 1983, **2**, 1681.

11 J. L. Davidson, M. Green, F. G. A. Stone, A. J. Welch, *J. Chem. Soc., Dalton Trans*, 1976, 2044.

12 F. Y. Petillon, F. Le Floch Perennou, J. E. Guerchais, D. W. A. Sharp, Lj, Manojlovic-Muir, K. W. Muir, *J. Organomet. Chem.*, 1980, **202**, 23.

13 M. Cariou, M. Etienne, J. E. Guerchais, R. Kergoat, M. M. Kubicki, *J. Organomet. Chem.*, 1987, **327**, 393.

14 G. E. Herberich, W. Barlage, *J. Organomet. Chem.*, 1987, **331**, 63.

15 G. E. Herberich, U. Englert, M. Hoeveler, I. Savvopoulos, *J. Organomet. Chem.*, 1987, **367**, 143.

16 R. Kergoat, M. M. Kubicki, L. C. Goames de Lima, H. Scordia, J. E. Guerchais, P. L'Haridon, *J. Organomet. Chem.*, 1988, **340**, 41.

17 S. C. Rasmussen, *Inorg. Chem.*, 1995, **34**, 821.

18 R.E. Murray and G. Zweifel, *Synthesis*, 1980, 150.

19 A. Davison and J.P. Solar, *J. Organomet. Chem.*, 1979, **166**, C13.

20 M.I. Bruce, P.J. Low, B.W. Skelton and A.H. White, *New J. Chem.*, 1998, 419.

21 M.I. Bruce, B.D. Kelly, B.W. Skelton and A.H. White, *J. Organomet. Chem.*, 2000, **604**, 150.

22 M.I. Bruce, M. Ke, P.J. Low, B.W. Skelton and A.H. White, *Organometallics*, 1998, **17**, 3539.

23 A.G. Bunn, P.J. Carroll and B.B. Wayland, *Inorg. Chem.*, 1992, **31**, 1297.

24 G.T. Yee, J.C. Calabrese, C. Vazquez and J.S. Miller, *Inorg. Chem.*, 1993, **32**, 377.

25 S. Mikami, K. Sugiura, T. Maruta, Y. Maeda, M. Ohba, N. Usuki, H. Okawa, T. Akutagawa, S. Nishihara, T. Nakamura, K. Iwasaki, N. Miyazaki, S. Hino, E. Asato, J.S. Miller and Y. Sakata, *J. Chem. Soc., Dalton Trans.*, 2001, 448.

26 E.J. Brandon, A.M. Arif, B.M. Burkhart and J.S. Miller, *Inorg. Chem.*, 1998, **37**, 2792.

27 D.K. Rittenberg, A.M. Arif and J.S. Miller, *J. Chem. Soc., Dalton Trans.*, 2000, 3939.

28 W. Hibbs, D.K. Rittenberg, K. Sugiura, B.M. Burkhart, B.G. Morin, A.M. Arif, L. Liable-Sands, A.L. Rheingold, M. Sundaralingham, A.J. Epstein and J.S. Miller, *Inorg. Chem.*, 2001, **40**, 1915.

29 M.M. Olmstead, G. Speier and L. Szabó, *J. Chem. Soc., Chem. Commun.*,

1994, 541.

30 F.A. Cotton, Y. Kim, *J. Am. Chem. Soc.*, 1993, **115**, 8511.

31 F.A. Cotton, Y. Kim and J. Lu, *Inorg. Chim. Acta*, 1994, **221**, 1.

32 T.J. Snaith, P.J. Low, R. Rousseau, H. Puschmann, J.A.K. Howard, *J. Chem. Soc., Dalton Trans.*, 2001, 292.

33 N.G. Connelly and W.E. Geiger, *Chem. Rev.*, 1996, **96**, 877.

34 M.I. Bruce, B.C. Hall, B. D. Kelly, P.J. Low, B. W. Skelton, A. H. White; *J. Chem. Soc., Dalton Trans.*, 1999, 3719.

35 O. F. Koentjoro, R. Rousseau, P. J. Low, *Organometallics*, 2001, **20**, 4502.

36 J. M. Wisner, T. J. Bartczak, J. A. Ibers, *Inorg. Chim. Acta*, 1985, **100**, 115.

37 M.I. Bruce, M.G. Humphrey, M.R. Snow, E.R.T. Tiekink, *J. Organomet. Chem.*, 1986, **314**, 213.

38 D. L. Thorn, R. Hoffmann, *Inorg. Chem.*, 1978, **17(1)**, 126.

39 R.P. Aggarwal, N.G. Connelly, M.C. Crespo, B.J. Dunne, P.M. Hopkins, A.G. Orpen; *J. Chem. Soc, Dalton Trans.*; 1992, 655.

40 F.A. Cotton, J.D. Jameson, B.R. Stulls, *J. Am. Chem. Soc.*, 1976, **98**, 1774.

41 H. Bock and K. Ruppert, *Inorg. Chem.*, 1992, **31**, 5094.

Compounds List - Cyanoacetylenes

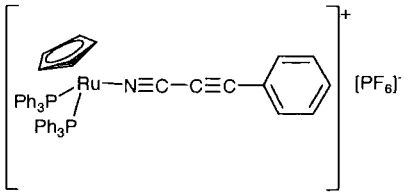

17

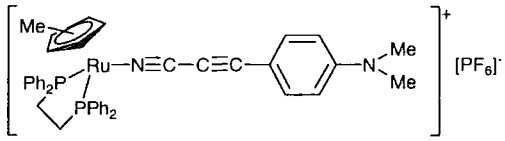

18

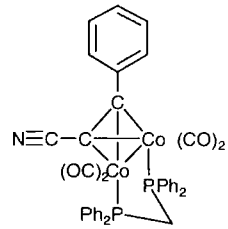

19

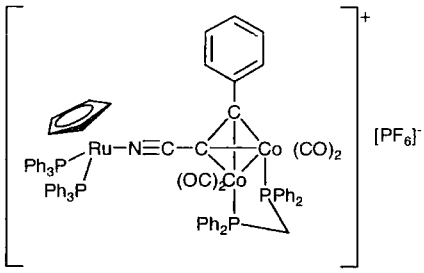

20

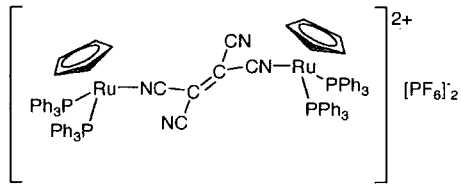

21

Introduction

There are few examples of η^1(C)-bonded cyanoacetylide ligands in the literature. The earliest example of an η^1(C)-bonded cyanoacetylide was reported by Baddley in the early 1970's where a platinum dicyanoacetylene complex was found to isomerise upon exposure to UV radiation to form $Pt(CN)(C{\equiv}CC{\equiv}N)(PPh_3)_2$ (Scheme 6.1).[1]

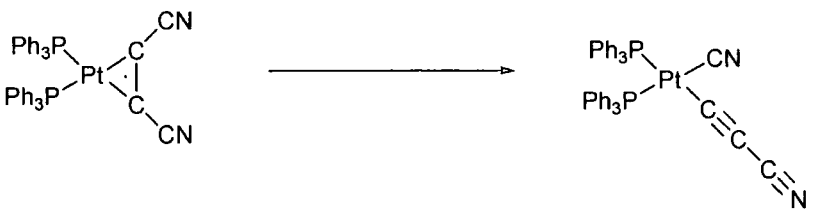

Scheme 6.1. UV-catalysed isomerisation of $Pt(PPh_3)_2(NC{-}C{\equiv}C{-}CN)$

The infra-red spectrum of the cyanoacetylide complex contained three absorption bands at 2070, 2140 and 2235 cm^{-1} corresponding to $\nu(C{\equiv}C)$, $\nu(C{\equiv}N)$(cyanoacetylide) and $\nu(C{\equiv}N)$(cyanide) respectively. X-ray crystallography showed that the C≡C and CC-CN bonds were respectively longer (1.24(5) Å) and shorter (1.31(5) Å) than would be expected for "triple" and "single" bonds. Furthermore, a lengthening of the Pt-P bonds relative to those in the comparable $Pt(PPh_3)_2(O_2)$ and $Pt(PPh_3)_2(NCCH{=}CHCN)$ complexes was also observed. At the time of the original report it was suggested that this indicated a degree of cumulenic character in the cyanoacetylide ligand, arising from the π-accepting capacity of the cyanocarbon fragment and resulting in the canonical forms shown below (Figure 6.1).

Figure 6.1. Canonical Forms of $Pt(CN)(C{\equiv}CC{\equiv}N)(PPh_3)_2$

The iron cyanoacetylide complex $Fe(C{\equiv}CC{\equiv}N)(CO)_2Cp$ was prepared by Kergoat following reaction of cyanoacetylene with a THF solution of $Fe(CO)_2(SCH_3)Cp$. The iron cyanoacetylide was one of four different products obtained from the reaction, but was isolated and crystallographically characterised (Scheme 6.2).[2] Infra-red spectroscopy showed that this iron complex contained both a $\nu(C{\equiv}N)$ band, at 2200 cm^{-1}, and a $\nu(C{\equiv}C)$ band at 2080 cm^{-1}. This stretching frequency was considered remarkably low for an alkyne system at the time, but it should be noted that this value is comparable with the absorption band at 2070 cm^{-1} found for $Pt(CN)(C{\equiv}CC{\equiv}N)(PPh_3)_2$. These authors also suggested that this low value could be accounted for either by the electron-withdrawing effect of the CN moiety and a π/π or π/π^* interaction with the metal centre.

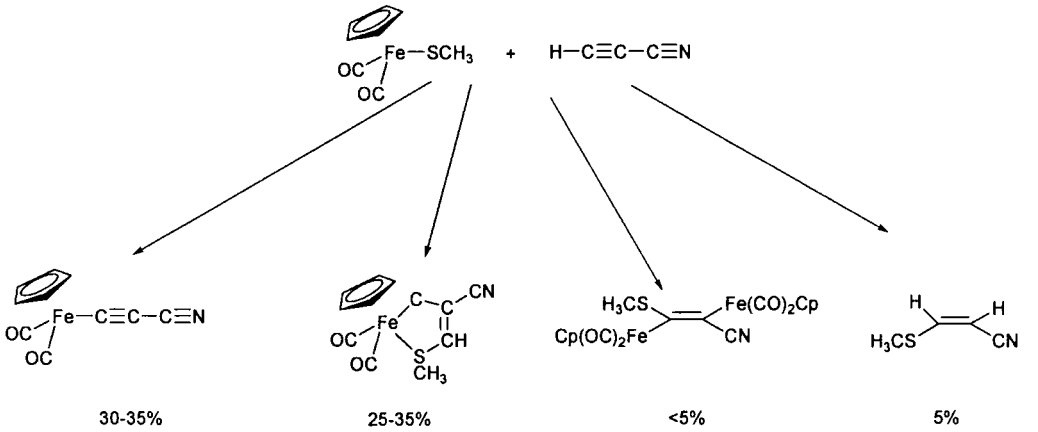

Scheme 6.2. Reaction products from $Fe(CO)_2(SCH_3)Cp$ reaction with cyanoacetylene

Condensation of HC≡CC≡N into a toluene solution of $Co(PPh_3)_2Cp$ frozen in liquid nitrogen, allowing the temperature to rise over a period of 30 minutes and subsequent purification resulted in the formation of the cobalt cyanoacetylide complex $Co(C{\equiv}CC{\equiv}N)(CH{=}CHCN)(PPh_3)Cp$ (65 %) and the di-cyanoacetylide cobalt complex $Co(C{\equiv}CC{\equiv}N)_2(PPh_3)Cp$ (20 %) (Scheme 3).[3] When a longer reaction period was used (3 hours) two isomeric forms of the mono-cyanoacetylide complex were isolated and were proposed to be those shown in Scheme 6.3.

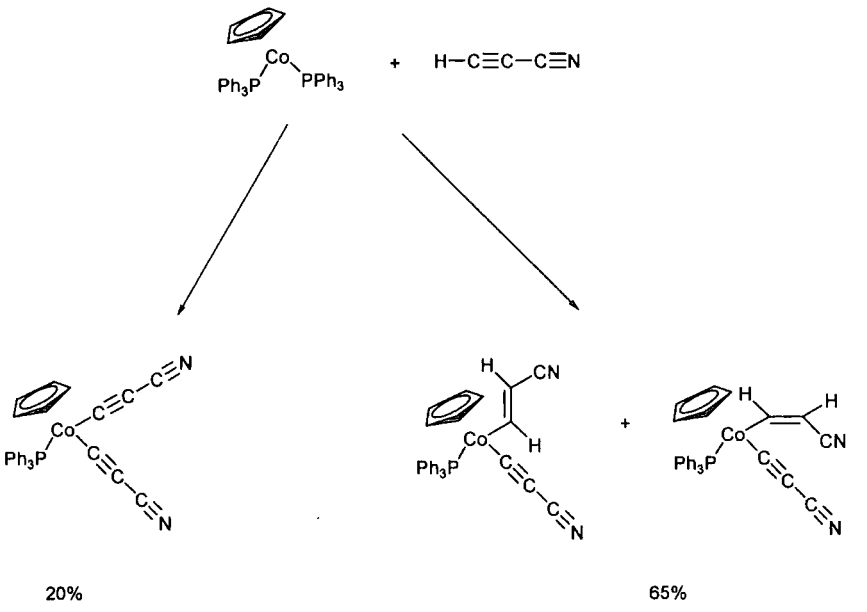

Scheme 6.3. Reaction products from $Co(PPh_3)_2Cp$ reaction with cyanoacetylene

Two ν(C≡N) stretches were observed for the *trans*-vinyl mono-cyanoacetylide complex (2230 and 2200 cm^{-1}) with the ν(C≡C) and ν(C=C) absorptions observed at 2145 cm^{-1} and 1570 cm^{-1} respectively. In the case of the di-cyanoacetylide complex, the ν(C≡N) and ν(C≡C) stretches were observed at 2200 cm^{-1} and 2040 cm^{-1}

respectively. Crystallographic characterisation of the di-cyanoacetylide $Co(C{\equiv}CC{\equiv}N)_2(PPh_3)Cp$ revealed a pseudo-octahedral geometry about the Co centre with Co-C bond lengths of 1.857(12) and 1.877(7) Å and C≡C bond lengths of 1.192(14) and 1.198(10) Å.

The tetracyanoacetylide complexes $[NEt_4]_2[M(C{\equiv}CC{\equiv}N)_4]$ (M = Ni, Pd, and Pt) have been synthesised and the crystal structure of $[NEt_4]_2[Ni(C{\equiv}CC{\equiv}N)_4]$ has been determined.[4] The products were synthesised by reaction of the appropriate metal tetrachloride $[NEt_4]_2[MCl_4]$ (M = Ni, Pd, Pt) with $Me_3SnC{\equiv}CC{\equiv}N$ in *N,N*-dimethylformamide over a period of 12 hours (Scheme 6.4). In the case of the platinum tetracyanoacetylide complex, an additional $PdCl_2(NCMe)_2$ catalyst was required in the reaction as without it the reaction took several days. In each case the ν(C≡C) stretch was observed in the 2040-2050 cm^{-1} region and the Ni complex demonstrated a C≡C bond length of 1.20 Å, which indicated some degree of lengthening of the C≡C bond brought about by π/π interactions between the metal centre and the cyanoacetylide ligand. The tetracyanoacetylide complexes $[NEt_4]_2[M(C{\equiv}CC{\equiv}N)_4]$ (M = Ni, Pd, and Pt) displayed two (Ni, Pd) or one (Pt) ν(C≡N) bands in the range 2170-2217 cm^{-1}. These ν(C≡N) values are moved to higher frequency than those in the analogous tetracyanometallates (ν(C≡N) = 2124-2136 cm^{-1}).

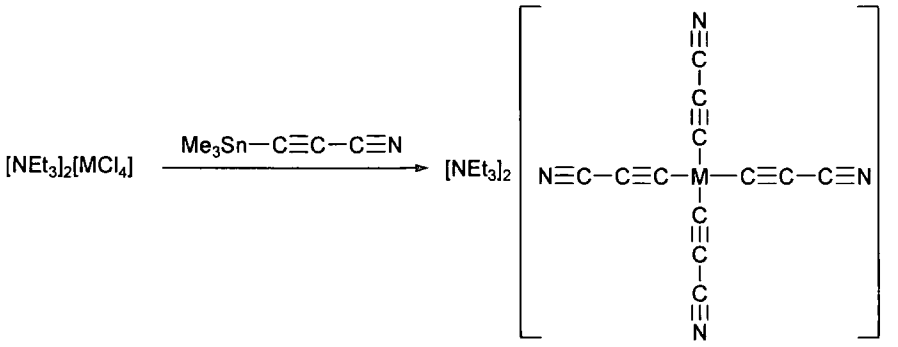

Scheme 6.4. Synthesis of $[NEt_4]_2[M(C{\equiv}CC{\equiv}N)_4]$ (M = Ni, Pd, and Pt)

During the course of this study we have developed a novel synthesis of metal cyanoacetylides. Reaction of the appropriate half-sandwich metal acetylide with butyl or methyl lithium at low temperatures followed by treatment with phenyl cyanate and subsequent work-up has been shown to produce the metal cyanoacetylides $Ru(C{\equiv}CC{\equiv}N)(PPh_3)_2Cp$ (**22**), $Ru(C{\equiv}CC{\equiv}N)(dppe)Cp^*$ (**23**) and $Fe(C{\equiv}CC{\equiv}N)(dppe)Cp$ (**24**) in good yield. These complexes are shown to be good "metallo-ligands", and have been used in the production of a range of bimetallic complexes featuring μ-$C{\equiv}CC{\equiv}N$ ligands.

Results

Monometallic Cyanoacetylides

The ruthenium acetylide species $Ru(C{\equiv}CH)L_2Cp'$ (Cp' = Cp, L = PPh_3; Cp' = Cp*, L_2 = dppe) were deprotonated at low temperature in THF solution by reaction with butyl lithium (BuLi), and treated with phenyl cyanate (PhOCN) (Scheme 6.5). Subsequent purification by column chromatography followed by recrystallisation resulted in the formation of yellow crystals of the ruthenium cyanoacetylide species $Ru(C{\equiv}CC{\equiv}N)(PPh_3)_2Cp$ (**22**) and $Ru(C{\equiv}CC{\equiv}N)(dppe)Cp^*$ (**23**) in good yield.

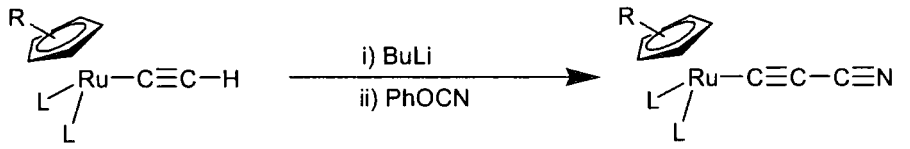

Scheme 6.5. Synthesis of Ruthenium Cyanoacetylides

(R = H, L = PPh_3 (**22**); R = Me, L_2 = dppe (**23**))

Both materials were readily characterised spectroscopically (Table 6.1). In the ^1H NMR spectrum the expected resonances from the Cp' ligands at 4.37 ppm (Cp, **22**) and 1.51 ppm (Cp*, **23**) and the C_2H_4 backbone of the dppe ligand in **23**, detected as two broad resonances at 2.14 ppm and 2.62 ppm, were evident. The ^{31}P NMR spectrum revealed the presence of the PPh_3 and dppe phosphorus ligands of **22** and **23** as singlet resonances at 49.77 and 80.22 ppm respectively. The Cp ligand of **22** was characterised in the $^{13}C\{^1H\}$ NMR spectrum by a single sharp resonance at 86.68 ppm whilst the Cp* ligand of **23** was evident as two singlet resonances occurring at 93.09

ppm (C_5Me_5) and 8.79 ppm ($C_5\mathit{Me}_5$). The carbon atoms of the cyanoacetylide ligand were also apparent, with signals from C_α, C≡N, and C_β occurring at 121.64, 107.75 and 83.08 ppm respectively (**22**) and 150.41, 107.35 and 77.05 ppm (**23**). Coupling of C_α to the phosphine ligands was observed for **23** (J_{CP} = 22.5 Hz) but could not be resolved for **22**. The cyanoacetylide ligand was also observed in the IR spectrum with ν(C≡C) and ν(C≡N) bands apparent at 2000 and 2180 (**22**) and 1994 and 2176 (**23**) cm^{-1}. Finally, positive-ion electrospray mass spectrometry (ES(+)-MS) of **22** displayed isotopic envelopes corresponding to $[M+Na]^+$ and $[M+H]^+$ at *m/z* = 764 and 742 respectively as well as the fragment ion $[Ru(PPh_3)_2Cp]^+$ at *m/z* = 691. Similarly, an isotopic envelope corresponding to [M+H]+ for **23** was observed at *m/z* = 686.

The analogous reaction of the iron acetylide Fe(C≡CSiMe$_3$)(dppe)Cp with methyl lithium (MeLi) and PhOCN at low temperature, followed by chromatography and subsequent crystallisation, led to the formation of the iron cyanoacetylide Fe(C≡CC≡N)(dppe)Cp (**24**) in moderate yield. The Cp ligand was evident in the ^{1}H NMR spectrum as a singlet resonance at 4.29 ppm and two broad resonances arising from the protons of the dppe backbone were observed at 2.32 and 2.60 ppm. The Cp and dppe ligands were also observed in the $^{13}C\{^1H\}$ NMR spectrum as a singlet at 80.42 ppm and a multiplet in the range 27.88-28.35 ppm respectively. Furthermore, three resonances arising from the cyanoacetylide ligand were observed, two as singlets at 106.13 ppm (CN) and 87.02 (C_β) and one as a triplet at 153.95 (J_{CP} = 37 Hz, C_α). The ^{31}P NMR spectrum confirmed the presence of the dppe ligand with a single sharp resonance at 104.91 ppm. The IR spectrum showed two absorption bands

at 2174 cm^{-1} (ν(C≡N)) and 1991 cm^{-1} (ν(C≡C)), while ES(+)-MS displayed an isotopic envelope at *m/z* = 570 corresponding to $[M+H]^+$.

Table 6.1. Selected spectroscopic data for **22-24**.

Compound	**22**	**23**	**24**
δ Cp (^{1}H NMR)	4.37	1.51	4.29
δ Cp (^{13}C{^{1}H} NMR)	83.08	93.09/8.79	80.42
δ phosphine (^{31}P NMR)	49.77	80.22	104.91
ν(C≡N)	2180	2176	2174
ν(C≡C)	2000	1994	1991

Single crystals suitable for X-ray diffraction studies were obtained for **23** and **24**. Crystallographic details for these complexes are summarised in Table 6.2 and selected bond lengths and angles are summarised in Table 6.3. Both structure determinations confirm the formation of the half-sandwich metal complexes with the expected connectivity in each case. The metal-ligand contacts of **24** are shorter than those for **23**, reflecting the effect of the smaller iron atom; consequently there is a smaller P(1)-M-P(2) angle for **23** (82.12(2)°) than **24** (86.27(2)°). The bond lengths and angles along the cyanoacetylide chain are essentially identical within the limits of precision of the measurements, and confirm the alternating short-long-short bond lengths consistent with the description of a cyanoacetylide moiety C≡CC≡N. The C(1)-C(2)-C(3) angle in **23** (172.2(2)°) shows a slightly greater deviation from linearity than **24** (176.19(14)°) but this minor deviation is probably a consequence of crystal packing effects rather than any underlying electronic factors.

Table 6.2. Crystallographic details of compounds **23** and **24**

Compound	**23**	**24**
Formula	$C_{39}H_{39}NP_2Ru$	$C_{34}H_{39}NP_2Fe.CH_2Cl_2$
M	684.72	653.45
***a* (Å)**	19.121(3)	9.718(2)
***b* (Å)**	17.516(5)	12.415(3)
***c* (Å)**	19.594(4)	13.013(3)
α (°)	90	87.444(4)
β (°)	90	88.471(4)
γ (°)	90	76.206(4)
V (Å^3)	6562(3)	1523.1(5)
D (Mg/m^3)	1.386	1.427
T (K)	120(2)	120(2)
Crystal system	Orthorhombic	Triclinic
Space Group	Pbca (No. 61)	$P\bar{1}$
Z	8	2
μ (mm^{-1})	0.604	1.427
Reflections collected	72508	18007
Independent reflections (R_{int})	7532 [R(int) = 0.0492]	9055 [R(int) = 0.0151]
Final R indices (all data)	$R_1 = 0.0266$, $wR_2 = 0.0616$	$R_1 = 0.0356$, $wR_2 = 0.0911$

Table 6.3. Selected bond lengths and angles for **23** and **24**.

Compound	**23**	**24**
M-P(1) (Å)	2.270(1)	2.174(1)
M-P(2) (Å)	2.264(1)	2.173(1)
M-C(1) (Å)	1.961(2)	1.852(1)
C(1)-C(2) (Å)	1.221(3)	1.228(2)
C(2)-C(3) (Å)	1.366(3)	1.367(2)
C(3)-N (Å)	1.153(3)	1.156(2)
P(1)-M-P(2) (°)	82.12(2)	86.27(2)
M-C(1)-C(2) (°)	175.13(16)	176.00(10)
C(1)-C(2)-C(3) (°)	172.2(2)	176.19(14)
C(2)-C(3)-N (°)	178.8(2)	178.97(15)

Reactivity of the cyanoacetylide ligand

The availability of the cyanoacetylide complexes **22-24** allowed, for the first time, an investigation of the organometallic and coordination chemistry of the unusual cyanocarbon fragment. In principle, the nitrogen lone pair and the π-systems of both the nitrile and alkyne moieties are available for further coordination to other metal systems and reaction with electrophiles. The reactivity profile of the ligand has been investigated and the results of the initial studies in this area form the subject of the report that follows.

Coordination compounds of Ru(C≡CC≡N)(PPh$_3$)$_2$Cp

Reaction of the ruthenium cyanoacetylide Ru(C≡CC≡N)(PPh$_3$)$_2$Cp (**22**) in refluxing methanol with MClL$_2$Cp (M = Ru, L = PPh$_3$, M = Fe, L$_2$ = dppe) in the presence of NH_4PF_6 led to the formation of the bimetallic complex salts [{Ru(PPh$_3$)$_2$Cp}$_2$(C≡CC≡N)](PF$_6$) (**25**) and [{Ru(PPh$_3$)$_2$Cp}(C≡CC≡N){Fe(dppe)Cp}](PF$_6$) (**26**) as bright yellow and brick red solids respectively in moderate yields (Scheme 6.6).

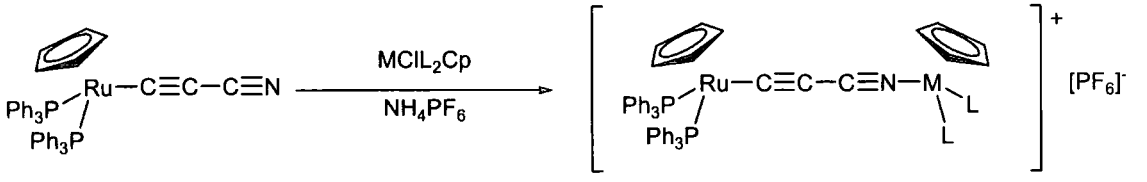

Scheme 6.6. Coordination Complexes of Ru(C≡C-C≡N)(PPh$_3$)$_2$Cp

(M = Ru, L = PPh$_3$ (**25**); M = Fe, L$_2$ = dppe (**26**))

The ^{1}H NMR spectrum of **25** revealed two sharp Cp resonances at 4.36 and 4.48 ppm, which were assigned to the ligands of the metal centres at the carbon and nitrogen ends of the C_3N bridge respectively by comparison with the ^{1}H NMR of **22** (Cp resonance at δ_H 4.37 ppm) and **17** (Cp resonance at δ_H 4.52 ppm). In the case of compound **26**, two overlapping resonances arising from the Cp moieties were observed at 4.24 and 4.20 ppm. In both cases the resonances arising from phosphine ligands at each metal centre could be clearly distinguished in the ^{31}P NMR spectrum. The PPh_3 resonances of compound **25** were observed at 48.92 and 42.16 ppm (corresponding to the carbon and nitrogen bonded metal fragments respectively by comparison with **22** and **17**) and the phosphine ligands of **26** were apparent at 98.02 ppm (dppe) and 48.76 ppm (PPh_3). Furthermore in both cases the $[PF_6]^-$ counter-ion was observed as a heptet at -143.05 ppm (**25**) and -143.06 ppm (**26**). The $^{13}C\{^{1}H\}$ NMR spectrum of **25** showed singlet resonances arising from the Cp moieties at 87.55 and 83.64 ppm as well as C_β and C≡N resonances at 83.49 and 117.07 ppm respectively. In the case of the $^{13}C\{^{1}H\}$ NMR spectrum of **26**, Cp resonances were observed at 79.16 and 87.22 ppm as well as resonances arising from C_α and C_β at 121.60 and 84.12 ppm respectively. The IR spectrum revealed ν(C≡N) and ν(C≡C) bands at 2197 and 1986 cm^{-1} (**25**) and 2194 and 1986 cm^{-1} (**26**). Comparison with the ν(C≡N) and ν(C≡C) bands of the monometallic metallo-ligand **22** (2180 and 2000 cm^{-1} respectively) show that in both cases there is an increase of about 15 cm^{-1} in the ν(C≡N) frequency upon coordination and a corresponding decrease of about 15 cm^{-1} in the ν(C≡C) band. Finally, ES(+)-MS displayed isotopic envelopes arising from the cations $[\{Ru(PPh_3)_2Cp\}_2(C{\equiv}CC{\equiv}N)]^+$ (**25**) and $[\{Ru(PPh_3)_2Cp\}(C{\equiv}CC{\equiv}N)\{Fe(dppe)Cp\}]^+$ (**26**) at *m/z* = 1432 and *m/z* = 1260

respectively. Isotopic envelopes corresponding to the metal fragments $[Ru(PPh_3)_2Cp]^+$ and $[Fe(dppe)Cp]^+$ were also observed at m/z = 691 and 519 in the mass spectra of **25** and **26** respectively. Selected spectroscopic data is summarised in Table 6.4.

Table 6.4. Selected spectroscopic data for compounds **25** and **26**.

Compound	25	26
δ Cp (^{1}H NMR)	4.36, 4.48	4.24, 4.20
δCp (^{13}C{^{1}H} NMR)	87.55, 83.64	87.22, 79.16
δ phosphine (^{31}P NMR)	48.92, 42.16	98.02, 48.76
ν(C≡N)	2197	2194
ν(C≡C)	1986	1986

Both bimetallic compounds were subjected to X-ray crystallographic studies. Their crystallographic details are summarised in Table 6.5 and selected bond lengths and angles are summarised in Table 6.6. In each case the molecular structure showed the expected connectivity with the C_3N bridge linking the two half-sandwich metal centres. In the case of **25**, the two metal centres adopted a *cis*-oid geometry (Figure 6.1).

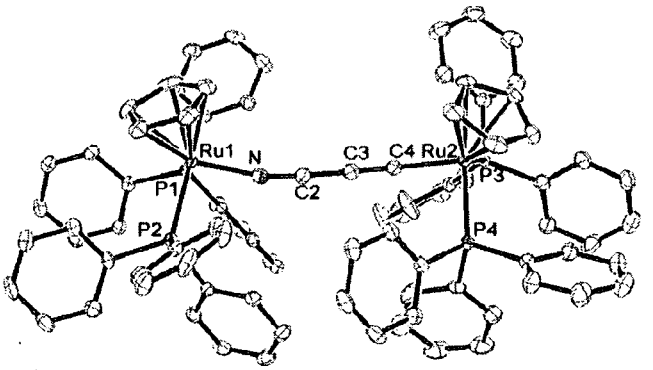

Figure 6.1. ORTEP plot of $[\{Ru(PPh_3)_2Cp\}_2(C{\equiv}CC{\equiv}N)]^+$ (**25**).

The bond lengths and thermal ellipsoids about the positions labeled N and C(4) were invariant with assignment and these positions were modeled as 50:50 C:N occupancy. The geometry about each ruthenium centre is essentially identical with Ru-P bond lengths of 3.326(1) and 3.325(1) Å (Ru(2)-P(1) and Ru(2)-P(2)) and 3.321(1) and 3.323(1) Å (Ru(1)-P(3) and Ru(1)-P(4)). The Ru(2)-C(4) and N-Ru(1) bond lengths are effectively identical (2.011(3) and 1.999(3) Å respectively) and the remaining bond lengths across the C_3N bridge show the expected triple-single-triple bonds pattern (C(4)-C(3) = 1.192(5) Å, C(3)-C(2) = 1.359(5) Å, C(2)-N = 1.198(5) Å). The bridge itself is essentially linear, however there is a marked degree of curvature at either end with Ru(2)-C(4)-C(3) and C(2)-N-Ru(1) angles of 169.8(3)° and 166.9(3)° respectively. This is, no doubt, a result of steric interactions between the bulky triphenylphosphine groups of the metal fragments.

There are marked differences between the molecular structures of **25** and **26**. The diffraction data showed a disorder at the Fe end of the C_3N chain which showed two possible conformations of **26**, a *cis*-oid and a *trans*-oid conformation (see Figure 6.2). The conformation modelled made no difference to the overall packing of the complex and the structure was successfully modelled as 50% of each conformation. As a result of this there are two distinct Ru-C(4)-C(3) angles corresponding to the two modes: 172.1(6)° (*trans*-oid) and 157.1(8)° (*cis*-oid). There is little variation in the rest of the bond lengths and angles between the two conformers with the exception of the C(4)-C(3) bond which is markedly shorter in the *trans*-oid conformation. The Fe-ligand contacts are noticeably shorter than the corresponding Ru(1)-ligand contacts of compound **25**, a result accounted for by the smaller iron atom.

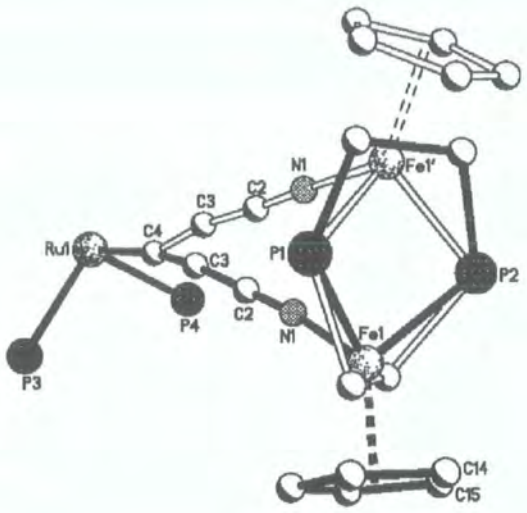

Figure 6.2. Disorder about iron centre from cis and trans forms of

$[\{Ru(PPh_3)_2Cp\}(C{\equiv}CC{\equiv}N)\{Fe(dppe)Cp\}][PF_6]$ (**26**)

Table 6.5. Crystallographic details of compounds **25** and **26**

Compound	25	26
Formula	$C_{85}H_{70}NP_5F_6Ru_2.3(CH_2Cl_2)$	$C_{75}H_{64}P_5F_6NFeRu.0.5(CH_2Cl_2)$
M	1831.19	1447.5
a (Å)	13.1761(5)	14.6968(4)
b (Å)	45.882(2)	23.7690(7)
c (Å)	14.4799(6)	19.6918(5)
α(°)	90	90
β(°)	112.92(1)	106.61(1)
γ(°)	90	90
V ($Å^3$)	8062.9(5)	6591.9(3)
D (Mg/m^3)	1.509	1.459
T (K)	120(2)	120(2)
Crystal system	Monoclinic	Monoclinic
Space Group	$P2_1/n$	$P2_1/c$
Z	4	4
μ(mm^{-1})	0.734	0.673
Reflections collected	61477	59855
Independent reflections (R_{int})	16576 [R(int) = 0.0379]	15905 [R(int) = 0.0446]
Final R indices (all data)	R1 = 0.0582, wR2 = 0.1029	R1 = 0.0900, wR2 = 0.1769

Table 6.6. Selected bond lengths and angles for compounds **25** and **26**.

Compound	25	26
M-P(3) (Å)	2.326(1)	2.309(1)
M-P(4) (Å)	2.325(1)	2.309(1)
M-C(4) (Å)	2.011(3)	1.971(5)
C(4)-C(3) (Å)	1.192(5)	1.226(9)/1.318(16) [a]
C(3)-C(2) (Å)	1.359(5)	1.374(10)/1.36(2) [a]
C(2)-N (Å)	1.198(5)	1.161(9)/1.16(2) [a]
N-M' (Å)	1.999(3)	1.904(6)/1.916(3) [a]
M'-P(1) (Å)	2.321(1)	2.131(2)
M'-P(2) (Å)	2.323(1)	2.147(2)
P(3)-M-P(4) (°)	100.73(3)	104.61(5)
M-C(4)-C(3) (°)	169.8(3)	172.1(6)/157.1(8) [a]
C(4)-C(3)-C(2) (°)	176.4(4)	173.0(8)/168.6(16) [a]
C(3)-C(2)-N (°)	176.0(4)	178.4(8)176.7(17) [a]
C(2)-N-M' (°)	166.9(3)	172.8(6)/175.9(13) [a]
P(1)-M'-P(2) (°)	99.20(3)	88.56(7)

[a] denotes *trans*-oid/*cis*-oid conformations

*Coordination compounds of Ru(C≡CC≡N)(dppe)Cp**

In a manner similar to that described above, reaction of Ru(C≡CC≡N)(dppe)Cp* with $MClL_2Cp'$ (M = Ru, Cp' = Cp, L = PPh_3, Cp' = Cp*, L_2 = dppe; M = Fe, Cp' = Cp, L_2 = dppe) resulted in the formation of

[{Ru(dppe)Cp*}(C≡CC≡N){$Ru(PPh_3)_2Cp$}](PF_6) (**27**) and

[{Ru(dppe)Cp*}$_2$(C≡CC≡N)](PF_6) (**28**) as yellow powders and

[{Ru(dppe)Cp*}(C≡CC≡N){Fe(dppe)Cp}](PF_6) (**29**) as a red solid in good yields (Scheme 6.7).

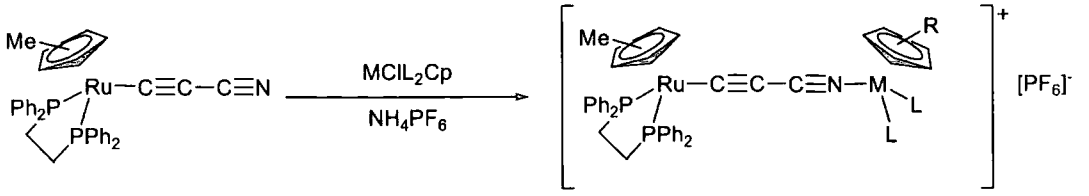

Scheme 6.7. Coordination Complexes of Ru(C≡CC≡N)(dppe)Cp* (M = Ru, R = H, L = PPh_3 (**27**); M = Ru, R = Me, L_2 = dppe (**28**); M = Fe, R =H, L_2 = dppe (**29**)).

The compounds were readily characterised by the usual spectroscopic techniques, and data are summarised in Table 6.7. Resonances arising from the Cp* moieties were observed in the ^{1}H NMR spectrum in the range 1.37-1.51 ppm with the Cp ligands of **27** and **29** observed at 4.25 ppm and 4.17 ppm respectively. The ^{31}P NMR spectrum showed resonances arising from the dppe moiety of the coordinated Ru(C≡CC≡N)(dppe)Cp* metallo-ligand in the narrow range 77.36-79.58 ppm (by comparison with the monometallic precursor **23**). The phosphine ligands attached to the N-bound metal centre were observed at 42.12 ppm (PPh_3, **27**) 75.64 ppm (dppe, **28**) and 98.59 (dppe, **29**). Furthermore, the $[PF_6]^-$ counter-ion was observed in each case as a heptet in the narrow range -143.17--143.21 ppm, which indicates little ion pairing in the $CDCl_3$ solvent. The $^{13}C\{^1H\}$ NMR spectra of **27** - **29** revealed resonances arising from the Cp* ligands at 95.10 and 10.03 ppm (**27**), 94.78 and 92.12 ppm (C_5Me_5, **28**) and 10.02 and 9.79 ppm ($C_5\mathit{Me}_5$, **28**), and 94.81 (C_5Me_5) and 10.05 ($C_5\mathit{Me}_5$) ppm (**29**). The Cp and dppe resonances for **27** were observed at 83.44 ppm and 29.80-29.43 ppm respectively. The dppe resonances of **28** were observed at 29.51-29.15 ppm and 28.64-28.28 ppm. The Cp and dppe resonances for **29** were observed at 78.78 ppm (Cp) and 29.31 and 27.66 ppm (dppe). Infra-red spectroscopy revealed the presence of ν(C≡N) and ν(C≡C) bands in the ranges 2190-2195 cm^{-1} (ν(C≡N)) and 1980-1987 cm^{-1} (ν(C≡C)). As with compounds **25** and **26**, there is an

increase in ν(C≡N) and a decrease in ν(C≡C) upon coordination of the metallo-ligand. In each case, ES(+)-MS revealed isotopic envelopes corresponding to the complex cations at *m/z* = 1376 (**27**), 1319 (**28**) and 1204 (**29**).

A sample of $W(CO)_6$ in THF was irradiated with a medium pressure Hg lamp for 90 minutes to generate $W(CO)_5(THF)$[5] and the resulting deep yellow solution treated with Ru(C≡CC≡N)(dppe)Cp*. Subsequent purification by preparative thin-layer chromatography followed by recrystallisation led to the isolation of [{Ru(dppe)Cp*}(C≡CC≡N){$W(CO)_5$}] (**30**) as bright, yellow crystals (Scheme 6.8).

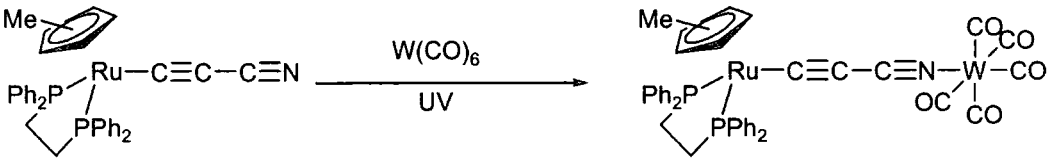

Scheme 6.8. Coordination of Ru(C≡CC≡N)(dppe)Cp* to $W(CO)_6$

For this complex, ^1H NMR spectroscopy showed a single sharp resonance arising from the Cp* ligand at 1.53 ppm as well as resonances from the ethyl protons of the dppe back-bone at 2.64 and 2.16 ppm. A single, sharp resonance was observed at 79.68 ppm in the ^{31}P NMR spectrum, corresponding to the dppe moiety. The $^{13}C\{^1H\}$ NMR spectrum revealed resonances arising from the carbonyl ligands at 200.67 and 197.21 ppm. The former signal was assigned to the carbonyl ligand *trans* to the cyanoacetylide moiety and the latter to the four *cis* carbonyls on the basis of relative intensities, assuming that the carbon nuclei of the carbonyl ligands relax at approximately the same rate. The Cp* moiety was observed as two singlet resonances at 95.06 ppm (C_5Me_5) and 10.12 ppm ($C_5\mathit{Me}_5$). Furthermore, resonances

corresponding to the carbon atoms of the C_2H_4 backbone of the dppe ligand were observed as a an unresolved multiplet in the range 29.78-29.40 ppm. Infra-red spectroscopy in DCM solution revealed ν(C≡N) and ν(C≡C) bands at 2192 cm^{-1} and 2071 cm^{-1} respectively whilst bands arising from the carbonyl ligands were observed at 1977, 1929 and 1882 cm^{-1}. Finally, ES(+)-MS displayed isotopic envelopes corresponding to $[M+H]^+$ and $[Ru(C_3N)(dppe)Cp^*+H]^+$ at *m/z* = 1010 and 686 respectively.

Finally, reaction of Ru(C≡CC≡N)(dppe)Cp* with one-half equivalent of $RuCl_2(dppe)_2$ in refluxing methanol in the presence of NH_4PF_6 resulted in the formation of $[\{Ru(C{\equiv}CC{\equiv}N)(dppe)Cp^*\}_2\{Ru(dppe)_2\}][PF_6]_2$ (**31**) as a bright yellow powder in good yield (Scheme 6.9).

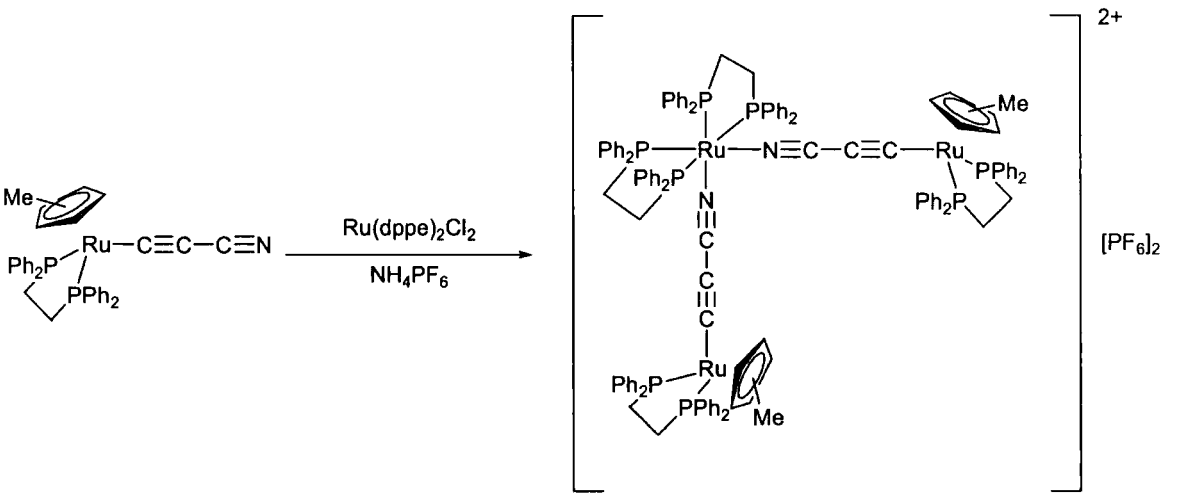

Scheme 6.9. Formation of trimetallic complex

$[\{Ru(C{\equiv}CC{\equiv}N)(dppe)Cp^*\}_2\{Ru(dppe)_2\}][PF_6]_2$ (**31**)

Characterisation by the usual spectroscopic techniques confirmed the trimetallic nature of the product (**31**) and single-crystal X-ray diffraction studies showed the

cyanoacetylide metallo-ligands to have adopted a *cis* geometry about the central ruthenium atom. Two Cp* resonances were observed in the ^{1}H NMR spectrum at 1.54 and 1.57 ppm and these were also visible in the $^{13}C\{^{1}H\}$ NMR spectrum at 97.10 and 95.93 ppm (C_5Me_5) and 10.18 and 10.01 ppm ($C_5\mathit{Me}_5$). In addition, three resonances in the ^{31}P NMR confirmed the presence of the dppe ligands. The $Ru(dppe)_2$ fragment gave rise to two signals in the ^{31}P NMR spectrum, a "roofed" doublet of doublets at 78.17 ppm ($J_{PP(trans)}$ = 316 Hz, $J_{PP(cis)}$ = 15 Hz) corresponding to the two *cis* phosphorous atoms, and a poorly resolved doublet of triplets at 46.46 corresponding to the two *trans* phosphorous atoms, and a sharp singlet at 32.48 ppm arising from the Ru(C≡C-C≡N)(dppe)Cp* moieties. Electrospray mass spectrometry (ES(+)-MS) displayed isotopic envelopes consistent with $[[\{Ru(C{\equiv}CC{\equiv}N)(dppe)Cp^*\}_2\{Ru(dppe)_2\}][PF_6]]^+$ and $[\{Ru(C{\equiv}CC{\equiv}N)(dppe)Cp^*\}_2\{Ru(dppe)_2\}]^{2+}$ at m/z = 2411 and 1135 respectively. Finally, ν(C≡N) and ν(C≡C) bands were observed in the IR spectrum at 2178 and 1966 cm^{-1} respectively. A shoulder to the ν(C≡C) band was also observed at 1994 cm^{-1}.

Table 6.7. Selected spectroscopic data for compounds **27-31**

Compound	**27**	**28**	**29**	**30**	**31**
δ Cp* (^{1}H NMR)	1.51	1.45, 1.37	1.38	1.53	1.57, 1.54
δ Cp* ($^{13}C\{^{1}H\}$ NMR)	95.10, 10.03	94.78, 92.12, 10.02, 9.79	94.81, 10.05	95.06, 10.12	97.10, 95.93, 10.18, 10.01
ν(C≡N) (cm^{-1})	2194	2195	2190	2192	2178
ν(C≡C) (cm^{-1})	1980	1987	1982	2071	1994, 1966
ν(CO) (cm^{-1})	n/a	n/a	n/a	1977, 1929, 1882	n/a

Of the bimetallic complexes, single crystals suitable for X-ray diffraction studies could be obtained for **27**, **28** and **30**. As described above for compound **25**,

compound **28** was modelled with a 50:50 C:N occupancy at the C(3) and N sites. Crystallographic details are summarised in Table 6.8 and selected bond lengths and angles for these complexes are presented Table 6.9, along with those for the metallo-ligand precursor **23** (which has been described in more detail above) for convenience. Each structure confirmed the expected connectivity and structure. In each case there is a lengthening of the Ru-P bond lengths at the carbon-end of the C_3N chain, with these lengths falling in the range 2.277(2)-2.292(1) Å compared to 2.270(1) and 2.264(1) Å for **23**. This is consistent with a withdrawal of electron density from this metal centre upon coordination, and consequently a reduced contribution to the Ru-P back-bonding interaction. Along with this, there is an decrease in the Ru-C(1) bond length upon coordination in the case of the unsymmetrical species **27** and **30**. This length was found to be 1.961(2) Å in **23** but drops upon coordination to 1.935(6) Å for **27** and 1.946(3) Å for **30**. In the case of the symmetrical compound **28**, the 50:50 occupancy of the C(3) and N sites mean that only the average of the two occupancies are seen, resulting in an apparent lengthening of the Ru-C(1) and C(3)-N bonds (1.996 and 1.184 (5) Å) and a contraction of the C(1)-C(2) bond (1.221(3) Å).

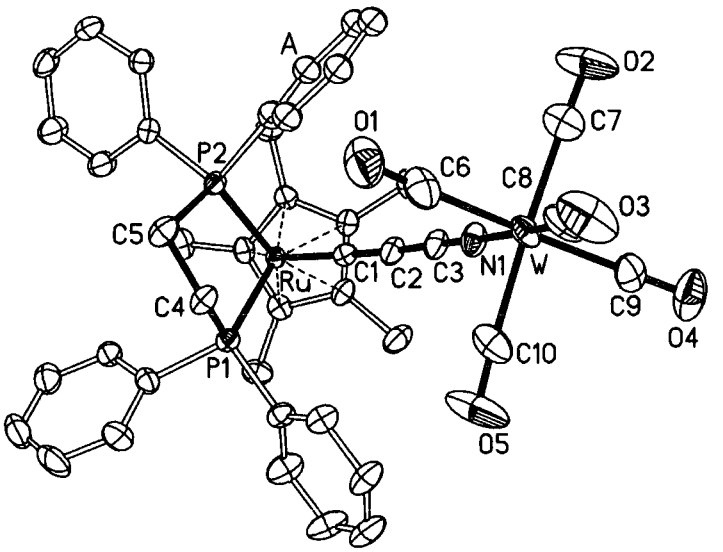

Figure 6.3. ORTEP plot of [{Ru(dppe)Cp*}(C≡CC≡N){W(CO)$_5$}] (**30**)

In addition to the features described above, the complex [{Ru(dppe)Cp*}(C≡CC≡N){W(CO)$_5$}] (**30**) (Figure 6.3) shows some variation in the CO parameters. The W-C bond lengths corresponding to those CO groups *cis* to the coordinated cyanoacetylide fall in the range 2.018(5)-2.049(3) Å whilst the W-C bond length for the *trans* carbonyl group is markedly shorter than this at 1.967(4) Å. The corresponding C-O bond length for this carbonyl group is 1.158(5) Å. Whilst this does fall in the range of bond lengths spanned by the *cis* carbonyl groups (1.127(4)-1.159(6) Å) it is worth noting that it falls at the extreme "long" end of that range.

The trimetallic compound [{Ru(C≡CC≡N)(dppe)Cp*}$_2${Ru(dppe)$_2$}][PF$_6$]$_2$ (**31**) also produced crystals suitable for x-ray diffraction studies (see Table 6.8 for crystallographic details). The molecular structure confirmed the expected half-sandwich geometry of the metallo-ligand and showed that the cyanoacetylide ligands had adopted a *cis* geometry about the octahedral ruthenium centre. There is slight distortion of the angles about the central atom from 90° but this is most likely due to steric crowding of the bulky phosphine ligands. The bond lengths and angles across the two cyanoacetylide ligands are effectively identical and match closely with those of the parent monometallic cyanoacetylide. The exceptions are the Ru-P and Ru-C(1) bond lengths of the metallo-ligand. The Ru-P bond lengths fall in the narrow range 2.2776(13)-2.2886(13) Å and, whilst being longer than those of the uncoordinated complex (2.173(1) and 2.174(1) Å). are markedly shorter than those of the Ru(dppe)$_2$ fragment (Ru(3)-P(X) = 2.3544(11)-2.3996(12) Å). Interestingly, the two Ru(3)-P bonds which are *trans* to the cyanoacetylide ligand are shorter than the two which are *trans* to each other (2.3544(11) and 2.3550(12) Å vs. 2.3822(12) and 2.3996(12) Å

respectively). The Ru-C(1) bonds of the coordinated cyanoacetylide, as with the coordinated complexes described above, are longer (1.942(4) and 1.948(4) Å) than that of the uncoordinated complex (1.852(1) Å).

Table 6.8. Crystallographic details of compounds **27**, **28**, **30** and **31**

Compound	**27**	**28**	**30**	**31**
Formula	$C_{80}H_{74}F_6NP_5Ru_2$	$C_{76}H_{78}F_6NP_5Ru_2.CHCl_3$	$C_{44}H_{39}NO_5P_2RuW$	$C_{130}H_{126}N_2P_{10}F_{12}Ru_3.7(MeOH)$
M	1520.39	1587.97	1008.62	2781.53
a (Å)	13.342(2)	13.9837(16)	22.727(2)	17.505(1)
b (Å)	43.508(8)	15.4545(18)	11.7465(11)	17.590(1)
c (Å)	14.392(3)	17.815(2)	30.664(3)	23.514(1)
α (°)	90	87.352(2)	90	104.21(1)
β (°)	104.273(3)	71.544(2)	90	99.48(1)
γ (°)	90	83.487(2)	90	95.29(1)
V (Å^3)	8096(3)	3628.2(7)	8185.9(14)	6856.3(6)
D (Mg/m^3)	1.247	1.453	1.637	1.347
T (K)	120(2)	120(2)	120(2)	200(2)
Crystal system	Monoclinic	Triclinic	Orthorhombic	Triclinic
Space Group	$P2_1/n$	$P\bar{1}$	Pbca	P-1 (2)
Z	4	2	8	2
μ(mm^{-1})	0.525	0.695	3.301	0.51
Reflections collected	42496	42065	70053	70291
Independent reflections (R_{int})	17386 [R(int) = 0.0420]	19680 [R(int) = 0.0544]	12480 [R(int) = 0.0625]	32578 [R(int) = 0.0390]
Final R indices (all data)	R_1 = 0.0990, wR_2 = 0.2791	R_1 = 0.0931, wR_2 = 0.1163	R_1 = 0.0712, wR_2 = 0.0851	R_1 = 0.054, wR_2 = 0.181

Table 6.9. Selected bond lengths and angles of **23**, **27**, **28**, and **30**

Compound	23	27	28	30
M-P(1) (Å)	2.270(1)	2.277(2)	2.289(1)	2.287(1)
M-P(2) (Å)	2.264(1)	2.285(2)	2.289(1)	2.292(1)
M-C(1) (Å)	1.961(2)	1.935(6)	1.996(3)	1.946(3)
C(1)-C(2) (Å)	1.221(3)	1.228(9)	1.187(5)	1.232(5)
C(2)-C(3) (Å)	1.366(3)	1.370(8)	1.355(5)	1.343(5)
C(3)-N (Å)	1.153(3)	1.163(7)	1.184(5)	1.162(5)
N-M' (Å)	n/a	2.030(5)	2.003(3)	2.169(3)
M'-P(3) (Å)	n/a	2.318(2)	2.288(1)	n/a
M'-P(4) (Å)	n/a	2.329(2)	2.302(1)	n/a
P(1)-M-P(2) (°)	82.12(2)	83.40(6)	83.46(4)	83.86(4)
M-C(1)-C(2) (°)	175.13(16)	177.4(6)	172.6(3)	178.0(4)
C(1)-C(2)-C(3) (°)	172.2(2)	175.4(6)	174.1(4)	168.3(4)
C(2)-C(3)-N (°)	178.8(2)	178.9(6)	178.4(4)	177.8(5)
C(3)-N-M' (°)	n/a	174.8(5)	168.7(3)	166.9(3)
P(3)-M'-P(4) (°)	n/a	100.63(5)	84.19(4)	n/a

In addition to the nitrile moiety, the π-system of the alkyne moiety of the cyanoacetylide ligand should be susceptible to attack by electrophiles. As has been stated previously (see cyanoacetylenes chapter), the organic species tetracyanoethylene (TCNE) will react readily with metal acetylide complexes to form both [2+2] cyclisation products as well as highly conjugated cyanocarbon species as a result of subsequent ring-opening, the reaction product being function of the metal substituent of the acetylide (Scheme 6.10).[6-15]

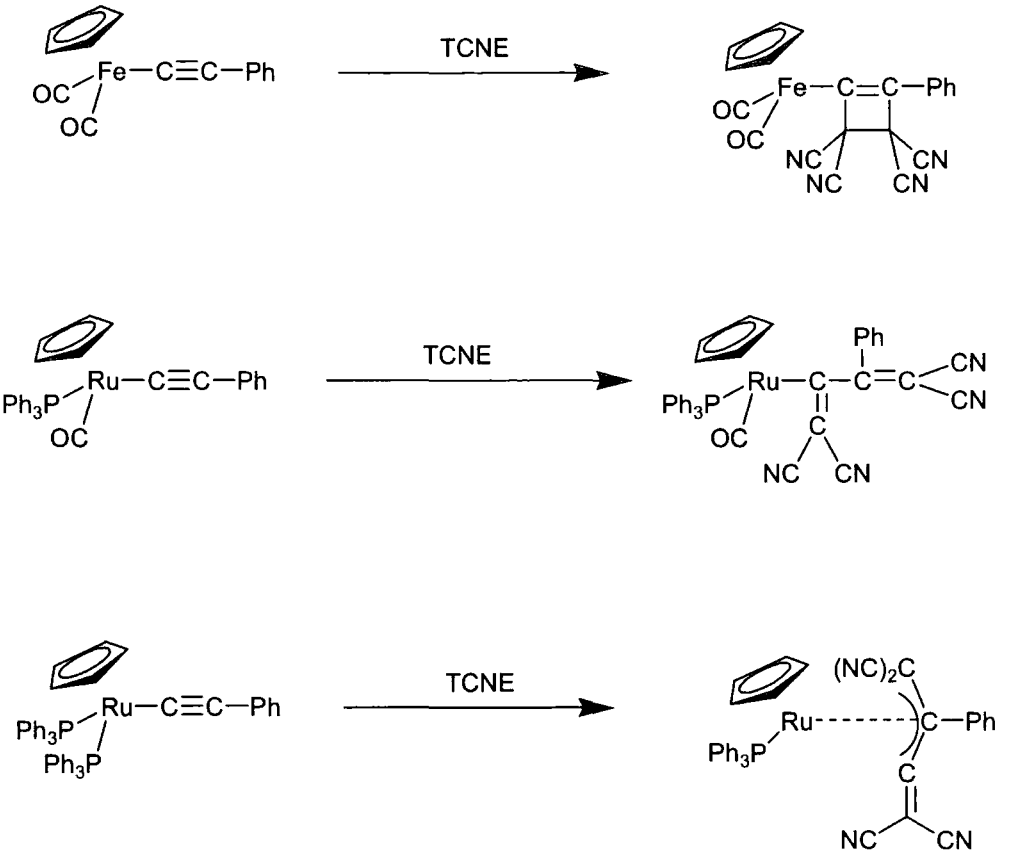

Scheme 6.10. Products of reaction of TCNE with metal centre determined by nature of metal centre.

To our knowledge, the only previous examples of coordination of the electron-poor TCNE species to a metal cyanoacetylide are its reactions with the iron complexes $Fe(C{\equiv}CC{\equiv}N)(CO)_2Cp$ and $Fe(C{\equiv}CC{\equiv}N)(CO)(PPh_3)Cp$ to give green [2+2] cyclisation products as shown below (Scheme 6.11).[2]

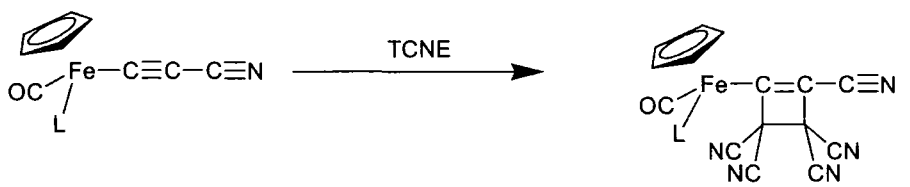

Scheme 6.11. Reaction of $Fe(C{\equiv}CC{\equiv}N)(CO)(L)Cp$ with TCNE (L = CO, PPh_3).

The ruthenium cyanoacetylide Ru(C≡CC≡N)(dppe)Cp* (23) reacted rapidly with TCNE in DCM solution to form a dark green solution. Subsequent recrystallisation resulted in the formation of dark blue crystals of the resultant adduct in good yield. ES(+)-MS confirmed the presence of a 1:1 adduct with an isotopic envelope corresponding to $[M+H]^+$ at m/z = 814. IR spectroscopy displayed absorption bands arising from the C≡N and C=C moieties at 2213 cm^{-1} and 1608 cm^{-1} respectively. ^1H NMR spectroscopy showed resonances arising from the ethyl protons of the dppe ligand as a multiplet in the range 2.83-5.58 ppm, and the Cp* moiety was observed as a singlet resonance at 1.47 ppm. ^{31}P NMR revealed two doublets at 76.90 and 56.91 ppm (J_{PP} = 15 Hz), comparable with those found for the analogous phenyl complex Ru[C{C(CN)$_2$}C{C(CN)$_2$}Ph](dppe)Cp* (48.47 and 77.30 ppm, J_{PP} = 13 Hz).[16]

Whilst spectroscopic data could not confirm the formation of either the ring-open or ring-closed adduct, single crystal X-ray diffraction studies revealed the adduct to be the ring-opened product, or the ruthenium pentacyanobutadienide Ru[C{C(CN)$_2$}C{C(CN)$_2$}CN](dppe)Cp* (**35**) as represented below (Scheme 6.12).

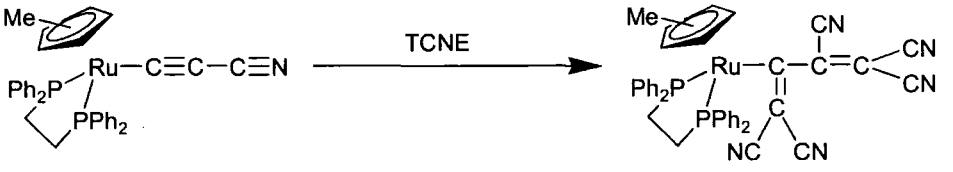

Scheme 6.12. Reaction product of Ru(C≡CC≡N)(dppe)Cp* with TCNE.

The molecular structure of **35** shows the expected half-sandwich geometry about the ruthenium centre although there is a marked increase in the lengths of the Ru-P bonds in **35** (2.362(1) and 2.333(1) Å) relative to the precursor **23** (2.270(1) and 2.264(1) Å) as well as the Ru-C(1) distance (2.060(2) Å in **35** vs. 1.961(2) Å in **23**). The C(1)-C(2) and C(2)-C(3) bonds are effectively identical (1.471(3) and 1.473(3) Å respectively), as are the formally "double" bonds at 1.368(3) and 1.354(3) Å. The remaining CN bond lengths fall in the narrow range 1.138(3)-1.143(3) Å and the =C-$C(CN)_2$ bond lengths fall in the range 1.430(3)-1.449(3) Å. This values are slightly smaller than might be expected and may indicate some degree of conjugation with the -C=C- moieties. The bonds about the C(1) and C(2) sites adopt a distorted trigonal planar geometry, which may be due to steric interactions between the cyanocarbon and phosphine ligands. The crystallographic details for compound **35** are shown in Table 6.10 below.

Table 6.10. Crystallographic details of compound **35**.

Compound	**35**
Formula	$C_{45}H_{39}N_5P_2Ru$
M	812.82
a (Å)	13.657(2)
b (Å)	12.626(2)
c (Å)	21.838(3)
α(°)	90
β(°)	93.32(1)
γ(°)	90
V ($Å^3$)	3759(1)
D (Mg/m^3)	1.436
T (K)	120(2)
Crystal system	Monoclinic
Space Group	$P2_1/c$ (14)
Z	4
μ(mm^{-1})	0.54
Reflections collected	28618
Independent reflections (R_{int})	11362 [R(int) = 0.0270]
Final R indices (all data)	R1 = 0.037, wR2 = 0.09

Coordination compounds of Fe(C≡CC≡N)(dppe)Cp

Reaction of the iron cyanoacetylide Fe(C≡CC≡N)(dppe)Cp in refluxing methanol with $MClL_2Cp$ (M = Ru, L = PPh_3, M = Fe, L_2 = dppe) in the presence of NH_4PF_6 led to the formation of [{Fe(dppe)Cp}(C≡CC≡N){Ru(PPh_3)$_2$Cp}](PF_6) (**32**), [{Fe(dppe)Cp}(C≡CC≡N){Ru(dppe)Cp*}](PF_6) (**33**) and [{Fe(dppe)Cp}$_2$(C≡CC≡N)](PF_6) (**34**) as red/brown solids in good yield (Scheme 6.13).

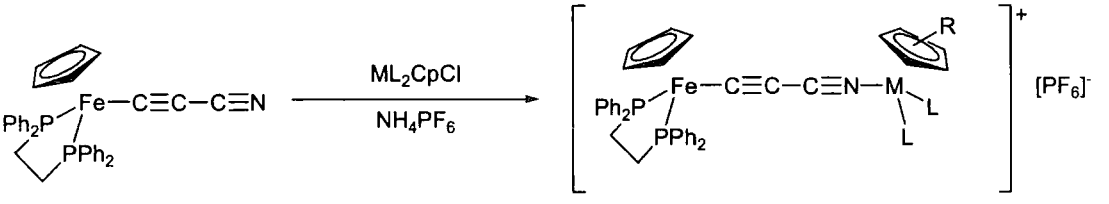

Scheme 6.13. Coordination Complexes of Fe(C≡CC≡N)(dppe)Cp (M = Ru, R = H, L = PPh_3 (**32**); M = Ru, R = Me, L_2 = dppe (**33**); M = Fe, R =H, L_2 = dppe (**34**)).

Whilst the acquisition of a ^{13}C NMR spectrum for compound **32** proved difficult with complications arising from paramagnetic impurities in the samples, no other problems were found in this regard. The ^1H NMR spectra revealed resonances arising from the Cp moieties at 4.35 and 4.21 ppm (**32**), 4.25 ppm (**33**), and 4.20 and 4.13 ppm (**34**) The Cp* moiety of **33** was observed as a singlet resonance at 1.31 ppm. The Cp' moieties of **33** and **34** were also observed in the $^{13}C\{^1H\}$ NMR spectra. The Cp and Cp* moieties of **33** were found at 81.46 ppm (Cp) and 91.87 (Cp*, C_5Me_5) and 9.45 (Cp*, C_5Me_5). In the case of **34** the two Cp moieties were observed at 81.30 and 78.80 ppm. Whilst the CN carbon of the cyanoacetylide bridge could be observed for

both complexes (occurring at 107.36 and 119.73 ppm for **33** and **34** respectively), the C_β was only observed in the spectrum of **34**, occurring at 89.06 ppm. The ^{31}P NMR spectra of **32** - **34** displayed the expected resonances arising from the phosphine ligands at 103.91 and 42.20 ppm (dppe and PPh_3 respectively, **32**), 103.42 and 75.52 ppm (dppe, **33**), and 123.66 and 76.90 ppm (dppe, **34**). In each case ES(+)-MS revealed isotopic envelopes consistent with the cations $[\{Fe(dppe)Cp\}(C{\equiv}CC{\equiv}N)\{Ru(PPh_3)_2Cp\}]^+$ (*m/z* = 1260), $[\{Fe(dppe)Cp\}(C{\equiv}CC{\equiv}N)\{Ru(dppe)Cp^*\}]^+$ (*m/z* = 1204) and $[\{Fe(dppe)Cp\}_2(C{\equiv}CC{\equiv}N)]^+$ (*m/z* = 1088). In the IR spectra ν(C≡N) and ν(C≡C) bands were observed for all three compounds with ν(C≡N) bands falling in the range 2192-2186 cm^{-1} and ν(C≡C) bands in the range 1976-1983 cm^{-1}. As with the coordination complexes described above, there is an increase of ν(C≡N) and a decrease of ν(C≡C) relative to Fe(C≡CC≡N)(dppe)Cp (**24**) upon coordination.

Discussion

Monometallic compounds

The monometallic cyanoacetylides in this study all show similar behaviour to each other and to those complexes described in the introduction. The ν(C≡C) stretches of Ru(C≡CC≡N)(PPh_3)$_2$Cp (**22**), Ru(C≡CC≡N)(dppe)Cp* (**23**) and Fe(C≡CC≡N)(dppe)Cp (**24**) all fall in the narrow range 1991-2000 cm^{-1}, a lower frequency than those already described. This suggests a greater reduction of electron density within with the π system of the cyanoacetylide moiety in **22-24** than in the examples described above. As the ruthenium and iron fragments used herein are more electron-rich than those in the previously described examples this is consistent with a π/π or π/π* interaction between the metal fragment and the cyanoacetylide ligand. Indeed, within the samples **22-24** there is some variation in ν(C≡C) that can be accounted for by the same explanation. The ν(C≡C) frequency for **23** (1994 cm^{-1}) is lowered relative to **22** (2000 cm^{-1}) due to the greater electron-donating ability of the Cp*/dppe ligands of **23**. This is seen to a greater extent in **24** which bears the even more electron rich $[Fe(dppe)Cp]^+$ end-cap (ν(C≡C) = 1991 cm^{-1}). Furthermore, the ν(C≡N) frequencies of the samples **22-24** also appear to be sensitive to the nature of the metal end-cap, being observed at 2180 cm^{-1} (**22**), 2176 cm^{-1} (**23**) and 2174 cm^{-1} (**24**). That this progression follows the same pattern as that observed for ν(C≡C) suggests that the π-system of the CN moiety is influenced to an extent by the nature of the metal centre in a similar manner to that of the C≡C fragment, albeit to a lesser extent.

As with the tetracyanoacetylide compounds of Miller described above, the ν(C≡N) frequencies of the compounds **22** and **24** are higher than those of their cyanide equivalents ($Ru(C{\equiv}N)(PPh_3)_2Cp$ = 2070 cm^{-1}, $Fe(C{\equiv}N)(dppe)Cp$ = 2060 cm^{-1}).[17] The cyanide moiety is a good π-acceptor and so electron density is drawn from the metal centre into the π* anti-bonding orbitals of the cyano ligand, resulting in a low ν(C≡N). In the case of the cyanoacetylide complexes **22** and **24** the higher ν(C≡N) value suggests a weaker interaction with the metal centre brought about by the C≡C spacer unit. It is, however, impossible to determine the nature of the metal/ligand interaction on the basis of the IR data alone.

The molecular structures of the compounds **23** and **24** show little variation. The bond lengths along the C_3N chain are identical in both cases but there are slight differences between these bond lengths and those of the organic cyanoacetylene $HC{\equiv}CC{\equiv}N$.[18] The C≡C bond length in cyanoacetylene is 1.18 Å which is slightly shorter than that observed in **23** and **24** (1.221(3) and 1.228(2) Å respectively), as is the C≡N bond length (1.14 Å vs. 1.153(3) Å (**23**) and 1.156(2) Å). There is also a slight shortening of the CC-CN bond in the metal cyanoacetylides (1.366(3) and 1.367(2) Å for **23** and **24** respectively) relative to cyanoacetylene (1.38 Å). Given that there is such a small change in bond lengths upon coordination of a metal fragment to the carbon end of the C_3N chain it is, perhaps, unsurprising that the effects of varying the *nature* of that metal fragment will have little effect on the molecular structure. These structural data are, therefore, an insufficiently sensitive probe of the bonding interactions across these mono-metallic cyanoacetylides, a conclusion which has been reached in many other studies of the interactions between metal centres and conjugated ligands as well as elsewhere within this work.

The metal cyanoacetylides may be thought of as metal acetylide complexes bearing strong electron-withdrawing substituents. There have been several computational studies of metal-acetylide interactions in order to determine the factors that influence the nature the metal/ligand bonding.[19-22] It was determined that, although the primary interaction between the metal and the alkyne system was a σ interaction between the σ* anti-bonding orbital of the alkyne fragment and the dz^2 orbital of the metal centre, the HOMO consisted of filled/filled interactions between the π orbitals of the acetylide fragment and the relevant d-orbitals of the metal centre. There is little evidence for π back-bonding between the metal centre and the acetylide ligand. Although there may be a small degree of involvement of the π* anti-bonding orbitals of the acetylide fragment in the HOMO of the complex, especially in those cases where there is a strongly electron-withdrawing substituent on the acetylide moiety, this contribution is extremely small, with the nature of the metal/acetylide interaction being dominated by the σ and filled/filled π interactions.[20-22]

This model accounts for the infra-red data found for compounds **22-24**. The dominant interaction between the cyanoacetylide ligand and the metal centre is a σ-interaction between the σ* orbitals of the CN moiety and the dz^2 orbitals of the metal centre. There is also, however, a filled/filled π interaction between the metal centre and the π-bonding orbitals of the cyanoacetylide ligand. This draws electron-density out of the π-bonding orbitals of the cyanoacetylide ligand and hence the ν(C≡C) and ν(C≡N) stretching frequencies are reduced. The contribution of the cyanoacetylide fragment to the HOMO is greater in the more electron-rich examples and so there is a greater reduction in stretching frequencies in those cases. That this effect is seen in the CN

portion of the cyanoacetylide moiety indicates that the HOMO is delocalised across the entirety of the M-C≡C-C≡N chain as suggested above.

The π-system of the cyanoacetylide moiety is available for reaction with electron-deficient species such as tetracyanoethylene (TCNE). Reaction of metal alkynes with TCNE can lead to a variety of products such as the ring-closed and ring open structures already described in the results section of this chapter.

The reaction of a metal acetylide with TCNE was first examined by Davidson and Solar who found that reaction of $Fe(C{\equiv}CPh)(CO)_2Cp$ with TCNE in DCM led to the ring-closed product shown below (Scheme 6.14).[6]

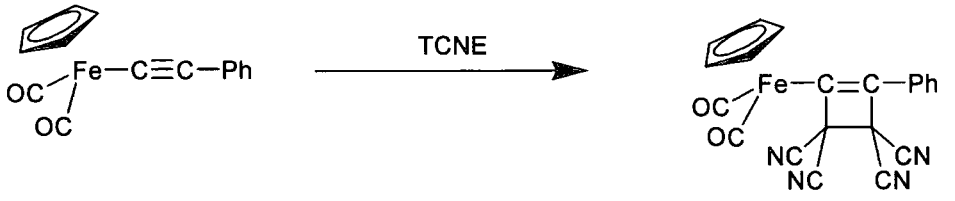

Scheme 6.14. Reaction of $Fe(C{\equiv}CPh)(CO)_2Cp$ with TCNE

Bruce and co-workers demonstrated that the tungsten complex $W(C{\equiv}CPh)(CO)_3Cp$ also gave the ring-closed product on reaction with TCNE but if it were left to stand in DCM solution for a period of 24 hours the product would then ring would open to give the butadienyl product.[7] Reaction of TCNE with the more electron-rich metal centres of the ruthenium complex $Ru(C{\equiv}CPh)(PPh_3)_2Cp$, however, resulted in the formation of the allylic product shown below (Scheme 6.15).[8]

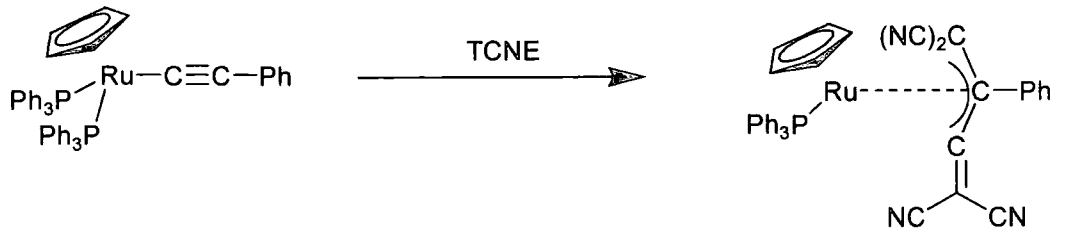

Scheme 6.15. Reaction of $Ru(C{\equiv}CPh)(PPh_3)_3Cp$ with TCNE

It was suggested that the reaction of $Ru(C{\equiv}CPh)(PPh_3)_2Cp$ with TCNE rapidly proceeded through the [2+2] cyclo-addition of TCNE to give the ring-closed product which rapidly opened and re-arranged to give the allyl compounds shown above. In contrast, reaction of the ruthenium-based compounds $Ru(C{\equiv}CPh)L_2Cp$ (L_2 = $(PPh_3)(CO)$, $(PPh_3)(P(OMe)_3)$, dppe) gave the ring-closed products which ring-opened more or less quickly to give the butadienyl products.[8]

In order to determine the effect of substitution at the coordinating organic fragment, Bruce and co-workers examined the reaction of $Ru(C{\equiv}CPh)L_2Cp$ (L_2 = $(PPh_3)(CO)$, $(PPh_3)_2$, dppe) with a series of substituted ethylene compounds of type $(NC)_2C{=}C(H)R$ (R = C_6H_4-4-NO_2, C_6H_4-4-NMe_2, C_6H_5). None of the metal acetylides were found to react with the $(NC)_2C{=}C(H)C_6H_4$-4-NMe_2 fragment and it was deemed to be too electron-rich to act as an alkyne-sequestering agent. The complex $Ru(C{\equiv}CPh)(PPh_3)_2Cp$ in reaction with the other substituted ethylene compounds always gave the allylic product and the Ru(C≡CPh)(dppe)Cp compound always gave the ring-closed material The $Ru(C{\equiv}CPh)(PPh_3)(CO)Cp$ complex gave the ring-closed product in reaction with $(NC)_2C{=}C(H)C_6H_5$ but reaction with the less-electron-rich $(NC)_2C{=}C(H)C_6H_4$-4-NO_2 compound resulted in the ring-closed complex which rapidly ring-opened. This suggested that the resultant product from

reaction of the metal phenylacetylide complexes was determined predominantly by the degree of electron-density at the metal centre. The more electron-poor metal complexes gave the ring-closed products but those with greater electron-density at the metal centre resulted in ring-opened systems. The allylic product was observed only in the reaction with the $Ru(C{\equiv}CPh)(PPh_3)_2Cp$ complex and not the $Ru(C{\equiv}CPh)(dppe)Cp$ material as the dppe ligand was insufficiently labile to allow for re-arrangement of the butadienyl ligand.[9] Similarly, reaction of the ruthenium phosphite complex $Ru(C{\equiv}CPh)(P(OPh)_3)_2Cp$ with TCNE resulted in the formation of the ring-opened material, the stronger Ru-P bonds to the phosphite ligands preventing the formation of the allylic material.[12]

As with the metal phenylacetylide complexes described above, the product of the reaction of metal-cyanoacetylide complexes seems to be determined by the degree of electron density at the metal centre, despite the substitution of the more electron-withdrawing CN moiety for the phenyl ring. Reaction of the iron complexes $Fe(C{\equiv}C\text{-}C{\equiv}N)(CO)_2Cp$ and $Fe(C{\equiv}C\text{-}C{\equiv}N)(CO)(PPh_3)Cp$ gave the green, ring closed [2+2] cyclisation products.[2] Reaction of the more electron-rich ruthenium cyanoacetylide $Ru(C{\equiv}CC{\equiv}N)(dppe)Cp^*$ (**23**) with TCNE, however, resulted in the formation of the ring-opened ruthenium pentacyanobutadienide complex $Ru[C\{C(CN)_2\}C\{C(CN)_2\}CN](dppe)Cp^*$ (**35**) (Scheme 6.16).

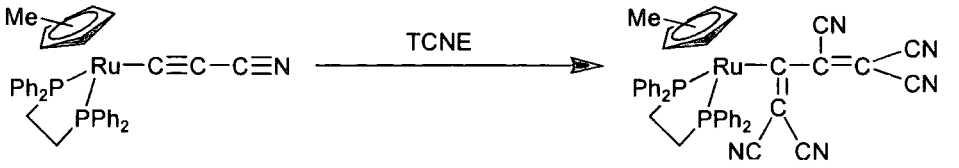

Scheme 6.16. Reaction product of Ru(C≡CC≡N)(dppe)Cp* with TCNE.

The spectral properties of **35** may be compared with that of the reaction product of Ru(C≡C-Ph)(dppe)Cp* with TCNE which also formed the ring-opened butadienyl derivative.[16] The ^{31}P NMR of the product displayed a pair of coupled doublet resonances (J_{PP} = 13 Hz) at 48.47 and 77.30 ppm which are comparable with those found for **35** (J_{PP} = 15.3 Hz, resonances at 56.91 and 76.90 ppm).

Bimetallic compounds

As has been stated in the results section of this chapter, the cyanoacetylide ligand should, in principle, be able to co-ordinate to another metal centre via the lone pair on the nitrogen atom and the π-system of the nitrile and alkyne moieties. However, the precise nature of the coordination interaction is uncertain. Nitriles have been shown to coordinate to a metal centre exclusively via the σ-set with little or no π back-bonding evident (see Nitriles chapter). The cyanide anion, however, will permit back-bonding from the metal d-orbitals into the π* anti-bonding orbitals of the C≡N moiety. It is also possible to draw comparisons between the cyanoacetylide anion $^-$[C≡C-C≡N] and the isoelectronic and isolobal diynyl anion $[C{\equiv}C\text{-}C{\equiv}C]^{2-}$. In this case the metal/ligand interaction is predominantly a σ-interaction between the σ* orbitals of the diyndiyl ligand and the dz^2 orbitals of the metal centre whilst the HOMO

consists of a filled/filled interaction between the π-bonding orbitals of the diyndiyl ligand and the d-orbitals of the metal.

Coordination of the cyanoacetylide "metallo-ligand" $Ru(C{\equiv}C\text{-}C{\equiv}N)(PPh_3)_2Cp$ to the metal fragments $[Ru(PPh_3)_2Cp]^+$ and $[Fe(dppe)Cp]^+$ resulted in the formation of the cyanoacetylide-bridged, bimetallic compounds $[\{Ru(PPh_3)_2Cp\}_2(\mu\text{-}C{\equiv}CC{\equiv}N)](PF_6)$ (**25**) and $[\{Ru(PPh_3)_2Cp\}(\mu\text{-}C{\equiv}CC{\equiv}N)\{Fe(dppe)Cp\}](PF_6)$ (**26**). Infra-red spectroscopy of the products showed that in each case there was a marked change in the stretching frequencies associated with the cyanoacetylide ligand upon coordination at the N-terminus. In the case of these compounds (and indeed all of the cyanoacetylide coordination compounds), two IR absorptions were observed. Without in-depth vibrational studies, however, it is impossible to determine whether these are two, independent vibrational modes corresponding to the C≡C and C≡N fragments or are, in fact, coupled vibrational modes of the combined cyanoacetylide moiety and both happen to be IR active. For the purposes of this study we have assumed that the higher frequency absorption corresponds to the CN moiety and the lower frequency absorption corresponds to the C≡C moiety.

In both cases coordination resulted in an increase in the ν(C≡N) stretching frequencies from 2180 cm^{-1} in the parent metallo-ligand **22** to values of 2197 cm^{-1} (**25**) and 2194 cm^{-1} (**26**). This increase would be consistent expectations as the lone pair of electrons on the N-atom of the bridging ligand is formally located at the σ* anti-bonding orbital of the CN. Hence coordination of the metallo-ligand removes electron density from this anti-bonding orbital, the bond is strengthened and ν(C≡N) is increased.

There is, however a change on the ν(C≡C) frequencies as well. Coordination of the metallo-ligand results in these stretching frequencies *decreasing* from 2000 cm^{-1} in the parent compound **22** to 1986 cm^{-1} in both **25** and **26**. This may be brought about by the loss of electron density from a bonding orbital or an increase of electron density to an anti-bonding orbital. This behaviour suggests that the bonding between the N-terminus of the cyanoacetylide ligand and a second metal centre may be similar to that for di-acetylide bridged complexes.

The same behaviour may be seen in the coordination products of the cyanoacetylide metallo-ligands Ru(C≡CC≡N)(dppe)Cp* (**23**) and Fe(C≡CC≡N)(dppe)Cp (**24**). There is an increase in ν(C≡N) and a concomitant decrease in ν(C≡C) upon coordination to the metal centres $[Ru(PPh_3)_2Cp]^+$, $[Ru(dppe)Cp^*)]^+$ and $[Fe(dppe)Cp]^+$. It is reasonable to suppose, therefore, that the same processes are occurring upon coordination in these species as for the coordination of **22**.

Several computational, electrochemical and spectro-electrochemical studies have shown that the interaction between the diyndiyl (C≡C-C≡C) bridge and the metal centre consists of a σ interaction between the metal d-orbitals and the σ* orbital of the diynyl anion as well as a filled/filled π-interaction between the metal and the diynyl π-system.[23-26] This results in a HOMO delocalized via the π-system over 6 atoms along the M-C_3X-M' chain (X = C, N). In forming such a system, there would be a loss of electron density from the π-bonding orbitals of the cyanoacetylide metallo-ligand, weakening the C≡C and C≡N bonds and so reducing their IR absorption frequencies relative to the monometallic precursors. In the case of the C≡N portion of the ligand, this effect is counterbalanced by a simultaneous loss of electron density

from the σ* anti-bonding orbital and the net effect is a strengthening of the C≡N bond and an increase in ν(C≡N).

The molecular structures of the bimetallic compounds give further evidence for the bonding description used above. The "symmetrical" bridged species $[\{Ru(PPh_3)_2Cp\}_2(\mu\text{-}C{\equiv}CC{\equiv}N)](PF_6)$ (**25**), i.e. that with identical metal end-caps at either end of the C_3N bridge is difficult to analyse. As a result of the 50:50 C:N modelling of the C(1) and N sites, the structure observed is a superposition of the two possible orientations of the C_3N bridge. However, there is still some useful information to be gained. As has been stated earlier (see Nitriles section), the M-P bond lengths of a system are a very useful probe of electron density at a metal centre. Humphrey has determined the structure of the metal phenyl acetylides $Ru(C{\equiv}C\text{-}C_6H_5)(PPh_3)_2Cp$ (Ru-P = 2.229(3) and 2.228(3) Å) and $Ru(C{\equiv}C\text{-}C_6H_4\text{-}4\text{-}NO_2)(PPh_3)_2Cp$ (Ru-P = 2.297(2) and 2.301(2) Å).[27] This demonstrates the sensitivity of the Ru-P bond lengths to the nature of the R-group in a $Ru(C{\equiv}C\text{-}R)(PPh_3)_2Cp$ system. A strongly electron-withdrawing group such as the nitro-phenyl group draws electron density from the ruthenium centre. This in turn reduces the degree of back-bonding between the metal and the phosphine ligand and so the Ru-P bond length is increased. In the case of compound **25**, the Ru-P bond lengths are 2.326(1) and 2.325(1) Å, indicating a large loss of electron density from the metal centre upon coordination of a metal fragment to the N-terminus.

Coordination of the N-terminus to the more electron-rich $[Fe(dppe)Cp]^+$ fragment results the unsymmetrical species $[\{Ru(PPh_3)_2Cp\}(\mu\text{-}C{\equiv}CC{\equiv}N)\{Fe(dppe)Cp\}](PF_6)$ (**26**). In this case the iron fragment is a stronger π-donor than the $[Ru(PPh_3)_2Cp]^+$

fragment and so has a greater contribution to the HOMO of the bimetallic complex. This is demonstrated by the shorter Ru-P bond lengths of **26** relative to **25** (2.309(1) Å vs. 2.326(1) and 2.325(1) Å). The cyanoacetylide "metallo-ligand" donates less electron density to the filled/filled π-bonding interaction in **26** and so a greater degree of electron density is available at the ruthenium centre for back-bonding to the phosphine ligands, hence the Ru-P distances are shorter. In addition, the Ru-C(1) and C(1)-C(2) bonds in **26** are respectively shortened (1.971(5) Å) and lengthened (1.318(16) Å) relative to those in the "symmetrical" compound **25** (2.011(3) Å and 1.192(5) Å respectively). This is, again, an effect of the increased contribution of the N-bound metal to the HOMO. This results in a HOMO with a greater degree of delocalisation across the 6-atom M-C3N-M system, increasing the bond order at the C-terminus and reducing the bond order of the C≡C bond and respectively contracting and lengthening the bonds.

Similar behaviour is seen in the compounds bearing the Ru(C≡C-C≡N)(dppe)Cp* metallo-ligand (**23**). In that case the Ru-P bond-lengths (2.270(1) and 2.264(1) Å) are lengthened slightly upon coordination at the N-terminus. In the case of the species [{Ru(dppe)Cp*}(μ-C≡CC≡N){Ru(PPh_3)$_2$Cp}] (**27**) and [{Ru(dppe)Cp*}(μ-C≡CC≡N){W(CO)$_5$}] (**30**) where the N-terminus is a more electron-deficient species than the C-terminus, this lengthening of the Ru-P bonds is matched by respective shortening and lengthening of the Ru-C and C≡C bonds relative to both the metallo-ligand and the symmetrical species. This, as with **25** and **26** above, shows that there is a greater degree of delocalisation across the M-C_3N-M' system in the unsymmetrical systems than the symmetrical ones *regardless of the orientation of the C_3N bridging ligand.* This is comparable to the heterometallic C_4-bridged materials, for which there

is a shortening of the M-C bonds and a lengthening of the C≡C bonds in the heterometallic examples, furthering the analogy between cyanoacetylide and diynyl bridging ligands.[25,28] This effect may be less apparent at the nitrogen end of the C_3N chain due to the varying σ-acceptor properties of the different N-termini masking the effect of the changes in the π-system.

The Trimetallic Complex [{Ru(C≡CC≡N)(dppe)Cp}$_2${Ru(dppe)$_2$}][PF$_6$]$_2$*

Both the IR data and the molecular structure of the trimetallic compound [{Ru(C≡CC≡N)(dppe)Cp*}$_2${Ru(dppe)$_2$}][PF$_6$]$_2$ (**31**) are very similar to that of the uncoordinated metallo-ligand. There is little change in the ν(C≡N) stretching frequency upon coordination and the bond-lengths and angles change little between the coordinated and uncoordinated species. The geometry about the central metal is of note, however, as it gives an idea of both the *trans effect* and the *trans influence* of the cyanoacetylide metallo-ligand, relative to the phosphine moieties.

The *trans* effect is a kinetic effect whereby a ligand coordinated to a metal centre (T) affects the lability of a ligand trans to it (X). If the ligand T is a strong, polarisable σ donor or π acceptor then it will draw electron density away from the metal centre and from the position *trans* to T. This results in a lowering of the activation energy of the substitution (in the case of a σ-donor *trans* effect) or a stabilization of the transition state (in the case of a π-acceptor *trans* effect).

The *trans influence* is a thermodynamic factor whereby a coordinated ligand (T) affects the properties of a coordinated species *trans* to itself (X) such as M-X bond lengths. This *trans* influence, which can be the result of a good, polarisable σ-donor or π-acceptor can be used to account for the variations in the phosphine bond-lengths about the central ruthenium atom. A good polarisable σ-donor or π-acceptor will draw electron density at the metal centre away from the ligand *trans* to itself, as with the *trans* effect.

The geometry about the central ruthenium atom is unusual when compared to the $Ru(dppe)_2(C{\equiv}C\text{-}R)_2$ complexes. These compounds tend to adopt a *trans*-orientation about the ruthenium centre in order to minimise steric crowding. In the case of **31**, however, a less sterically-favourable *cis*-geometry is observed. This is likely a case where the electronic effect of the *trans*-influence has a greater effect on the adopted conformation than the steric factors. The increased length of the cyanoacetylide bridging ligand relative to the acetylide means that the bulky ligands are held further away from the central $Ru(dppe)_2$ moiety and so the steric factors are reduced. This enables the ligands about the central ruthenium atom to act to reduce the unfavourable *trans*-phosphine interactions. The *cis*-conformation results in a system whereby two of the phosphine centres are *trans* to the cyanoacetylide moiety (which has a weaker trans-influence) and there is only one *trans*-phosphine interaction. The trans-conformation would result in two *trans*-phosphine interactions. Electronically, a system where the phosphine moieties are *trans* to a species with a weaker *trans*-influence is more stable than one where they are *trans* to themselves. Thus the cis geometry is the more electronically stable conformer. Whilst in the case of the acetylides the steric factors outweigh the electronic ones, the length of the

cyanoacetylide ligand reduce these factors and allow the electronic influences to come to the fore. The lengthening of the Ru-P bonds of the metallo-ligand, relative to the uncoordinated complex, indicates a loss of electron density from the metal centre. This is usually the case upon complexation of the metallo-ligand as described above. This, combined with the *trans* influence suggests that the cyanoacetylide metallo-ligand is a strong σ-donor.

Experimental

Monometallic Compounds

$Ru(C{\equiv}CC{\equiv}N)(PPh_3)_2Cp$ (22)

An 50ml, two-necked Schlenk flask was cooled under nitrogen, charged with $Ru(C{\equiv}CH)(PPh_3)_2Cp$ (390 mg, 0.55 mmol) in dry, distilled THF (30 ml) and cooled to -70°C (dry ice/acetone). To this yellow solution was added 0.4 ml of a 1.6M solution of BuLi in hexane. This was added at such a rate as to prevent the temperature from exceeding -60 °C. The solution was stirred for ten minutes at this temperature. It was then brought to -20 °C and cooled back down again. To the cooled solution was added PhOCN (0.4 ml, 3.5 mmol, 6.5 equivalents) and the solution was stirred for a further half hour before being allowed to come to room temperature. The solvent was then removed using a rotary evaporator to leave a dark-brown residue. This was then dissolved in the minimum amount of dichloromethane and micro-filtered into hexane. The resulting yellow/green solid was collected, dissolved in DCM, loaded onto a silica column and eluted with 30:70 acetone:hexane solution. A yellow band was collected and the solvent removed. Subsequent recrystallisation by slow diffusion of hexane into a solution in DCM resulted in the formation of yellow, block-like crystals of **22** (252 mg, 0.341mmol, 62 %). Found: C, 68.64; H, 4.63; N, 1.93. $C_{44}H_{35}P_2NRu.0.5CH_2Cl_2$ requires: C, 68.24; H, 4.63; N, 1.78. ^{1}H NMR ($CDCl_3$): δ 4.37 (s, 5H, Cp); 7.11-7.51 (m, 35H, Ph). $^{13}C\{H\}$ NMR ($CDCl_3$): δ 137.86-137.36 (m, C_{ipso}, PPh_3); 133.79 (t, J_{CC} = 5.09Hz, C_{ortho}, PPh_3); 129.33 (s, C_{para}, PPH_3); 127.87 (t, J_{CC} = 4.84Hz, C_{meta}, PPH_3); 121.64 (s, C_α); 107.75

(s, C≡N); 86.68 (s, Cp); 83.08 (s, C_β). $^{31}P\{H\}$ NMR ($CDCl_3$): δ 49.77 (s, PPh_3). ES(+)-MS (*m/z*) 764.1 $[M+Na]^+$; 742.1 $[M+H]^+$; 691 $[Ru(PPh_3)_2Cp]^+$. IR (CH_2Cl_2): ν(C≡N) 2180 cm^{-1}; ν(C≡C) 2000 cm^{-1}.

Ru(C≡CC≡N)(dppe)Cp* (23)

An analogous procedure using Ru(C≡CH)(dppe)(Cp*) (1.22g, 1.85 mmol), BuLi (1.4 ml of 1.6M solution), and PhOCN (0.26 ml, 2.22 mmol), followed by recrystallisation from slow evaporation of a DCM/MeOH solution afforded yellow crystals of **23** (890 mg, 1.3 mmol, 70%). Found: C, 67.97; H, 5.71; N, 2.03. $C_{39}H_{39}P_2NRu$ requires: C, 68.40; H, 5.74; N, 2.05. ^1H NMR ($CDCl_3$): δ 1.51 (m, 15H, Cp*); 2.14 (m, 2H, dppe); 2.62 (m, 2H, dppe); 7.61-7.16 (m, 20H, Ph). $^{13}C\{H\}$ NMR ($CDCl_3$): δ 150.41 (t, J_{CP} = 22.49Hz, C_α); 126.67-136.14 (m, Ph); 107.35 (s, CN), 93.09 (s, C_5Me_5); 77.05 (s, C_β); 28.06-28.43 (m, dppe); 8.79 (s, C_5Me_5). $^{31}P\{H\}$ NMR ($CDCl_3$): δ 80.22 (s, dppe). ES(+)-MS (*m/z*) 686.2 $[M+H]^+$. IR (CH_2Cl_2): ν(C≡N) 2176 cm^{-1}; ν(C≡C) 1994 cm^{-1}.

Fe(C≡CC≡N)(dppe)Cp (24)

A 50ml, 2-necked Schlenk flask was cooled under nitrogen and charged with Fe(C_2TMS)(dppe)Cp (567 mg, 0.92 mmol) in dry THF (20 ml). The red solution was cooled (dry ice/acetone) and MeLi (0.85 ml of 1.6M solution in Et_2O) was added at such a rate as to prevent the temperature exceeding –50 °C. After stirring for 40

minutes the solution was warmed to -20 °C before being cooled again. To the dark solution was added PhOCN (0.2 ml, 0.18 mmol) and the solution was then allowed to come slowly to room temperature before the solvent was removed. The dark red/brown residue was dissolved in DCM and precipitated into hexane. The resultant pale grey/brown solid was collected, dissolved in DCM and loaded onto a silica column and eluted with 30:70 acetone:hexane solution. A red/brown band was collected and the solvent removed. Subsequent recrystallisation by slow diffusion of Et_2O into a solution of the residue in DCM resulted in the formation of red crystals of **24** (212 mg, 0.37 mmol, 41 %). Found C, 70.55; H, 5.24; N, 3.11. $C_{34}H_{29}P_2NFe$ requires: C, 71.72; H, 5.13; N, 2.50. ^{1}H NMR ($CDCl_3$): δ 2.32 (m, 2H, dppe); 2.60 (m, 2H, dppe); 4.29 (s, 5H, Cp); 7.74-6.85 (m, 20H, Ph). $^{13}C\{H\}$ NMR ($CDCl_3$): δ 153.95 (t, J_{CP} = 37 Hz, C_α); 127.66-140.21.14 (m, Ph); 106.13 (s, CN), 87.02 (s, C_β); 80.42 (s, Cp), 27.88-28.35 (m, dppe). $^{31}P\{H\}$ NMR ($CDCl_3$): δ 104.91 (s, dppe). ES(+)-MS (*m/z*) 570.1 $[M+H]^+$. IR (CH_2Cl_2): ν(C≡N) 2174 cm^{-1}; ν(C≡C) 1991 cm^{-1}.

[{Ru(PPh$_3$)$_2$Cp}$_2$(C≡CC≡N)](PF$_6$) (25)

An oven-dried, two-necked Schlenk flask was cooled under nitrogen and charged with $RuCl(PPh_3)_2Cp$ (100 mg, 0.138 mmol), $Ru(C{\equiv}CC{\equiv}N)(PPh_3)_2Cp$ (102 mg, 0.138 mmol) and NH_4PF_6 (90 mg, 0.55 mmol). The mixture was suspended in methanol (20 ml) and heated to reflux. After 90 minutes at reflux a bright yellow suspension had formed. The reaction was then cooled and the precipitate was collected and washed with cold methanol to give **25** as a bright yellow (141 mg, 0.090 mmol, 65%). Crystals suitable for x-ray diffraction studies were obtained by slow diffusion of

MeOH into a DCM solution of **25**. Found: C, 63.93; H, 4.58; N, 1.08. $C_{85}H_{70}P_5F_6NRu_2.0.5CH_2Cl_2$ requires: C, 63.56; H, 4.40; N, 0.86. ^{1}H NMR ($CDCl_3$): δ 4.36 (s, 5H, Cp); 4.48 (s, 5H,Cp); 7.08-7.29 (m, 67H, Ph). ^{13}C{H} NMR ($CDCl_3$): δ 137.69-137.09 (m, C_{ipso}, PPh_3); 136.83-136.17 (m, C_{ipso}, PPh_3); 133.69 (t, J_{CC} = 5.03 Hz, C_{ortho}, PPh_3); 133.42 (t, J_{CC} = 5.03 Hz, C_{ortho}, PPh_3); 130.02 (s, C_{para}, PPH_3); 129.66 (s, C_{para}, PPH_3); 128.39 (t, J_{CC} = 4.78 Hz, C_{meta}, PPH_3); 127.96 (t, J_{CC} = 4.78Hz, C_{meta}, PPH_3); 117.07 (s, C≡N), 87.55 (s, Cp); 83.64 (s, Cp); 83.49 (s, C_β). ^{31}P{H} NMR ($CDCl_3$): 48.92 (s, PPh_3); 42.16 (s, PPh_3); -143.05 (ht, J_{PF} = 712 Hz, PF_6). ES(+)-MS (*m/z*) 1432 $[\{Ru(PPh_3)_2Cp\}_2(C{\equiv}CC{\equiv}N)]^+$; 691 $[Ru(PPh_3)_2Cp]^+$. IR (CH_2Cl_2): ν(C≡N) 2197 cm^{-1}, ν(C≡C) 1986 cm^{-1}.

[{Ru(PPh$_3$)$_2$Cp}(C≡CC≡N){Fe(dppe)Cp}](PF$_6$) (26)

An analogous procedure using FeCl(dppe)Cp (75 mg, 0.135 mmol), Ru(C≡CC≡N)$(PPh_3)_2$Cp (100 mg, 0.135 mmol) and NH_4PF_6 (88 mg, 0.54 mmol) resulted in the formation of **26** as a brick red solid (84 mg, 0.0598 mmol, 44%). Crystals suitable for x-ray diffraction studies were obtained by slow diffusion of MeOH into a DCM solution of **26**. Found: C, 62.27; H, 4.52; N, 1.10. $C_{75}H_{64}P_5F_6NRuFe.0.5CH_2Cl_2$ requires: C, 62.64; H, 4.52; N, 0.97. ^{1}H NMR ($CDCl_3$): δ 7.31-7.00 (m, 52H, Ph); 4.24, 4.20 (unresolved, 10H, Cp). ^{13}C{H} NMR ($CDCl_3$): δ 137.45-137.09 (m, C_{ipso}, PPh_3); 133.69 (t, J_{CC} = 5.28Hz, C_{ortho}, PPh_3); 133.12 (t, unresolved, C_{ortho}, dppe); 131.84 (t, unresolved, C_{ortho}, dppe); 130.80 (s, C_{para}, dppe); 130.60 (s, C_{para}, dppe); 129.67 (s, C_{para}, PPH_3); 129.12 (t, unresolved, C_{meta}, dppe); 128.96 (t, unresolved, C_{meta}, dppe); 127.92 (t, J_{CC} = 4.78Hz, C_{meta}, PPH_3); 121.60 (s,

C_α); 87.22 (s, Cp); 79.16 (s, Cp); 84.12 (s, C_β); 28.02 (t, J_{CP} = 21.62Hz, CH_2, dppe). $^{31}P\{H\}$ NMR ($CDCl_3$): 98.02 (s, dppe); 48.76 (s, PPh_3); -143.06 (ht, J_{PF} = 712 Hz, PF_6). ES(+)-MS (*m/z*) 1260 [{Ru(PPh_3)$_2$Cp}(C≡CC≡N){Fe(dppe)Cp}]$^+$; 519 [Fe(dppe)Cp]$^+$. IR (CH_2Cl_2): ν(C≡N) 2194 cm^{-1}, ν(C≡C) 1986 cm^{-1}.

[{Ru(dppe)Cp*}(C≡CC≡N){Ru(PPh_3)$_2$Cp}](PF_6) (27)

A two-necked, 50 ml Schlenk flask was cooled under nitrogen and charged with Ru(C≡CC≡N)(dppe)(Cp*) (100 mg, 0.146 mmol), RuCl(PPh_3)$_2$Cp (106 mg, 0.146 mmol) and NH_4PF_6 (95 mg, 0.583 mmol). The mixture was suspended in dry MeOH (10 ml) and heated to reflux. After one hour at reflux a clear yellow solution had formed. This was allowed to cool and the solvent was removed. The yellow residue was then dissolved in the minimum quantity of DCM, filtered and the solvent was removed to afford **27** as a yellow powder (209 mg, 0.138 mmol, 94%). Crystals suitable for X-ray diffraction studies were obtained by slow diffusion of hexane into a DCM solution of **27**. Found: C, 63.03; H, 4.91; N, 0.95. $C_{80}H_{74}P_5F_6NRu_2$ requires: C, 63.20; H, 4.91; N, 0.92. ^1H NMR ($CDCl_3$): δ 1.51 (s, 15H, Cp*); 2.54, 2.18 (2 x m. 4H, dppe); 4.25 (s, 5H, Cp); 7.02-7.50 (m, 50H, Ph). $^{13}C\{H\}$ NMR ($CDCl_3$): δ 136.69-127.93 (m, Ph); 95.10 (s, C_5Me_5), 83.44 (s, Cp); 29.80-29.43 (m, dppe); 10.03 (s, C_5Me_5). $^{31}P\{H\}$ NMR ($CDCl_3$): δ 79.34 (s, dppe); 42.12 (s, PPh_3); -143.20 (ht, J_{PF} = 713 Hz [PF_6]$^-$). ES(+)-MS (*m/z*) 1376 [{Ru(dppe)Cp*}(C≡CC≡N){Ru(PPh_3)$_2$Cp}]$^+$. IR (CH_2Cl_2): ν(C≡N) 2194 cm^{-1}, ν(C≡C) 1980 cm^{-1}.

[{Ru(dppe)Cp*}$_2$(C≡CC≡N)](PF$_6$) (28)

An analogous procedure using Ru(C≡CC≡N)(dppe)(Cp*) (100 mg, 0.146 mmol), RuCl(dppe)Cp* (98 mg, 0.146 mmol) and NH_4PF_6 (95 mg, 0.583 mmol) afforded **28** as a bright, canary yellow solid (157 mg, 0.107 mmol, 74%). Crystals suitable for X-ray diffraction studies were obtained by slow diffusion of MeOH into a $CHCl_3$ solution of **28**. Found: C, 60.51; H, 5.35; N, 1.00. $C_{75}H_{78}P_5F_6NRu_2.0.25CHCl_3$ requires: C, 60.80; H, 5.24; N, 0.93. ^{1}H NMR ($CDCl_3$): δ 1.45, 1.37 (2 x s, 30H, 2 x Cp*); 2.23, 2.17 (2 x br, 8H, 2 x dppe); 7.48-7.07 (m, 40H, Ph). ^{13}C{H} NMR ($CDCl_3$): δ 136.41-127.78 (m, Ph); 113.85 (s, CN); 94.78 (s, C_5Me_5), 92.12 (C_5Me_5), 78.84 (s, C_β); 29.51-29.15 (m, dppe); 28.64-28.28 (m, dppe); 10.02 (s, C_5Me_5); 9.79 (s, C_5Me_5). ^{31}P{H} NMR ($CDCl_3$): δ 79.58 (s, dppe); 75.64 (s, dppe); -143.21 (ht, *J*PF = 713 Hz, $[PF_6]^-$). ES(+)-MS (*m/z*) 1319 $[\{Ru(dppe)Cp^*\}_2(C{\equiv}CC{\equiv}N)]^+$; 635 $[Ru(dppe)Cp^*]^+$. IR (CH_2Cl_2): ν(C≡N) 2195 cm^{-1}, ν(C≡C) 1987 cm^{-1}.

[{Ru(dppe)Cp*}(C≡CC≡N){Fe(dppe)Cp}](PF$_6$) (29)

An analogous procedure using Ru(C≡CC≡N)(dppe)(Cp*) (100 mg, 0.146 mmol), FeCl(dppe)Cp (81 mg, 0.146 mmol) and NH_4PF_6 (95 mg, 0.583 mmol) afforded **29** as a red solid (184 mg, 0.138 mmol, 94%). ^{1}H NMR ($CDCl_3$): δ 1.38 (s, 15H, Cp*); 2.40, 1.99 (2 x br, 8H, dppe); 4.17 (s, 5H, Cp); 7.06-7.63 (m, 40H, Ph). ^{13}C{H} NMR ($CDCl_3$): δ 133.31-127.78 (m, Ph); 94.81 (s, C_5Me_5); 78.78 (s, Cp); 29.31 (m, dppe); 27.66 (m, dppe); 10.05 (s, C_5Me_5). ^{31}P{H} NMR ($CDCl_3$): δ 98.59 (s, dppe); 77.36 (s,

dppe); -143.17 (ht, J_{PF} = 713 Hz $[PF_6]^-$). ES(+)-MS (*m/z*) 1204 $[\{Ru(dppe)Cp^*\}(C{\equiv}CC{\equiv}N)\{Fe(dppe)Cp\}]^+$. IR ($CH_2Cl_2$): ν(C≡N) 2190 cm^{-1}, ν(C≡C) 1982 cm^{-1}.

[{Ru(dppe)Cp*}(C≡CC≡N){W(CO)$_5$}] (30)

An oven-dried Schlenk tube was cooled under nitrogen and charged with $W(CO)_6$ (51 mg, 0.146 mmol) in dry THF (30 ml). The solution was irradiated for 90 minutes with a medium pressure Hg lamp during which time it became a deep yellow colour. Ru(C≡CC≡N)(dppe)Cp* was added (100 mg, 0.146 mmol) and the solution was stirred for a further 10 minutes before the solvent was removed. The yellow residue was then eluted up a preparative TLC plate using 3:7 acetone:hexane. The upper yellow band was collected, dried and recrystallised from slow diffusion of methanol into a DCM solution to give bright yellow crystals. (52 mg, 0.052 mmol, 35%). ^1H NMR ($CDCl_3$): δ 1.53 (s, 15H, Cp*); 2.16 (m, 2H, dppe); 2.64 (m, 2H, dppe); 7.17-7.58 (m, 20H, Ph). ^{13}C NMR ($CDCl_3$): δ 200.67 (s, *trans*-CO); 197.21 (s, *cis*-CO), 165.32 (br, C_α); 136.84-128.14 (m, Ph); 112.08 (s, CN); 95.06 (s, C_5Me_5); 77.72 (s, C_β); 29.78-29.40 (m, dppe); 10.12 (s, C_5Me_5). ^{31}P NMR ($CDCl_3$): 79.68 (dppe). ES(+)-MS (*m/z*): 1010 $[M+H]^+$; 686 $[Ru(C_3N)(dppe)Cp^*+H]^+$. IR (CH_2Cl_2): ν (C≡N) 2192(m) cm^{-1}, ν(C≡C) 2071(m) cm^{-1}, ν(CO) 1977(m), 1929(s), 1882(m) cm^{-1}. IR (cyclohexane): ν(C≡N) 2197(w) cm^{-1}, ν(C≡C) 2069(w) cm^{-1}, ν(CO) 1990(w), 1932(s), 1904(m) cm^{-1}

[{Ru(C≡CC≡N)(dppe)Cp*}$_2${Ru(dppe)$_2$}][PF$_6$]$_2$ (31)

A two-necked, 50 ml Schlenk flask was cooled under nitrogen and charged with Ru(C≡CC≡N)(dppe)Cp* (104 mg, 0.152 mmol), $RuCl_2(dppe)_2$ (74 mg, 0.076 mmol) and NH_4PF_6 (99 mg, 0.607 mmol). The mixture was suspended in dry MeOH (15 ml) and heated to reflux. After two hours at reflux a pale yellow suspension had formed. The reaction was allowed to cool and the solvent was removed. The resulting yellow residue was dissolved in DCM and filtered. The solvent was then removed to afford **34** as a pale yellow powder (143 mg, 0.056 mmol, 74 %). Crystals suitable for X-ray diffraction studies were obtained by slow diffusion of methanol into a DCM solution. ^{1}H NMR ($CDCl_3$): δ 1.54 (s, 15H, Cp*); 1.57 (s, 15H, Cp*); 6.15-8.05 (m, 80H, Ph). ^{13}C NMR ($CDCl_3$): δ 134.11-127.23 (m, Ph); 97.10 (s, C_5Me_5); 95.93 (s, C_5Me_5); 30.28-29.14 (m, dppe); 10.18 (s, C_5Me_5); 10.01 (s, C_5Me_5). ^{31}P NMR ($CDCl_3$): 78.17 (dd, $J_{PP(trans)}$ = 316 Hz, $J_{PP(cis)}$ = 15 Hz, $Ru(dppe)_2$); 46.16 (dt, $Ru(dppe)_2$), 32.48 (s, dppe), -143.01 (ht, J_{PF} = 713 Hz, $[PF_6]^-$). ES(+)-MS (*m/z*): 2411 $[M+PF_6^-]^+$ 1135 $[M]^{2+}$; 686 $[Ru(C_3N)(dppe)Cp^*+H]^+$. IR (CH_2Cl_2): ν(C≡N) 2178 cm^{-1}, ν(C≡C) 1994(sh), 1966 cm^{-1}.

[{Fe(dppe)Cp}(C≡CC≡N){Ru(PPh$_3$)$_2$Cp}](PF$_6$) (32)

A two-necked, 50 ml Schlenk flask was cooled under nitrogen and charged with Fe(C≡CC≡N)(dppe)(Cp) (75 mg, 0.132 mmol), $RuCl(PPh_3)_2Cp$ (966 mg, 0.132 mmol) and NH_4PF_6 (86 mg, 0.528 mmol). The mixture was suspended in dry MeOH

(15 ml) and heated to reflux. After one hour at reflux a dark red/brown solution had formed. This was allowed to cool and the solvent was removed. The red/brown residue was then dissolved in the minimum quantity of DCM and precipitated into hexane. The precipitate was then collected and washed with cold hexane to afford **30** as a pale brown solid (105 mg, 0.075mol, 57%). ^{1}H NMR ($CDCl_3$): δ 1.62 (br, 8H, dppe); 4.35, 4.21 (2 x s, 10H, 2 x Cp); 6.97-7.64 (m, 40H, Ph). ^{31}P{H} NMR ($CDCl_3$): δ 103.91 (s, dppe); 42.20 (s, PPh_3); -143.11 (ht, J_{PF} = 711 Hz $[PF_6]^-$). ES(+)-MS (*m/z*) 1260 $[\{Fe(dppe)Cp\}(C{\equiv}CC{\equiv}N)\{Ru(PPh_3)_2Cp\}]^+$; 691 $[Ru(PPh_3)_2Cp]^+$. IR (CH_2Cl_2): ν(C≡N) 2192 cm^{-1}, ν(C≡C) 1977 cm^{-1}.

[{Fe(dppe)Cp}(C≡CC≡N){Ru(dppe)Cp*}](PF$_6$) (33)

An analogous procedure using Fe(C≡CC≡N)(dppe)(Cp) (75 mg, 0.132 mmol), RuCl(dppe)Cp* (88 mg, 0.132 mmol) and NH_4PF_6 (86 mg, 0.528 mmol) afforded **31** as a red/brown solid (98 mg, 0.073 mmol, 55%). Found C, 61.73; H, 5.04; N, 1.12. $C_{70}H_{68}P_5F_6NRuFe$ requires: C, 62.32; H, 5.08; N, 1.04. ^{1}H NMR ($CDCl_3$): δ 1.31 (s, 15H, Cp*); 2.25 (m, dppe); 2.07 (m, dppe); 4.25 (s, 5 H, Cp); 7.16-7.56 ppm (m, 40H, Ph). ^{13}C{H} NMR ($CDCl_3$): δ 138.08-128.18 (m, Ph); 107.36 (s, CN); 91.87 (s, C_5Me_5); 81.46 (s, Cp); 27.75 (m, unresolved, CH_2 dppe); 27.11 (m, unresolved, CH_2 dppe); 9.45 (s, C_5Me_5). ^{31}P{H} NMR ($CDCl_3$): δ 103.42 (s, dppe); 75.52 (s, dppe); -143.18 (ht, J_{PF} = 713 Hz $[PF_6]^-$). ES(+)-MS (*m/z*) 1204 $[\{Fe(dppe)Cp\}(C{\equiv}CC{\equiv}N)\{Ru(dppe)Cp^*\}]^+$; 635 $[Ru(dppe)Cp^*]^+$. IR (CH_2Cl_2): ν(C≡N) 2192 cm^{-1}, ν(C≡C) 1983 cm^{-1}.

[{Fe(dppe)Cp}$_2$(C≡CC≡N)](PF$_6$) (34)

An analogous procedure using Fe(C≡CC≡N)(dppe)(Cp) (75 mg, 0.132 mmol), FeCl(dppe)Cp (73 mg, 0.132 mmol) and NH_4PF_6 (86 mg, 0.528 mmol) afforded **32** as a red/brown solid (130 mg, 0.105 mmol, 78%). Found: C, 62.84; H, 4.70; N, 1.10. $C_{65}H_{58}P_5F_6NFe_2$ requires: C, 63.28; H, 4.74; N, 1.14. ^{1}H NMR ($CDCl_3$): δ 1.62 (br, 8H, dppe); 4.20, 4.13 (2 x s, 10H, 2 x Cp); 7.08-7.56 (m, 40H, Ph). ^{13}C{H} NMR ($CDCl_3$): δ 139.67-128.16 (m, Ph); 119.73 (s, CN); 89.06 (s, C_β); 81.30 (s, Cp); 78.80 (s, Cp); 28.45-28.28 (m, dppe); 27.45-27.29 (m, dppe). ^{31}P{H} NMR ($CDCl_3$): δ 103.42 (s, dppe); 75.52 (s, dppe); -143.18 (ht, J_{PF} = 713 Hz $[PF_6]^-$). ES(+)-MS (*m/z*) 1088 [{Fe(dppe)Cp}(C≡CC≡N){ Fe(dppe)Cp }]$^+$; 519 [Fe(dppe)Cp]$^+$. IR (CH_2Cl_2): ν(C≡N) 2186 cm^{-1}, ν(C≡C) 1976 cm^{-1}.

Ru(C≡CC≡N)(dppe)Cp* + TCNE (35)

A two-necked, 50 ml Schlenk flask was cooled under nitrogen and charged with dry DCM (10 ml). This was degassed and to it was added Ru(C≡CC≡N)(dppe)(Cp*) (100 mg, 0.146 mmol) resulting in a yellow solution. To this was added TCNE (19 mg, 0.146 mmol) upon which the solution rapidly became a dark green colour. The reaction was followed by solution IR and when the band corresponding to the C≡C stretch of the parent cyanoacetylide had disappeared the solvent was removed. The

resultant dark blue/green residue was crystallised by slow diffusion of methanol into a DCM solution to afford **35** as dark blue crystals (72 mg, 0.092 mmol, 63%). ^{1}H NMR (CD_2Cl_2): δ 1.22 (s, 15H, Cp*); 1.47 (s, 15H, Cp*); 2.83-5.58 (m, 4 H, dppe); 6.56-7.96 (m, 20H, Ph). ^{31}P NMR ($CDCl_3$): 123.66 (s, dppe); 76.90 (d, J_{PP} = 15.3 Hz, dppe); 56.91 (d, J_{PP} = 15.3 Hz, dppe). ES(+)-MS (*m/z*): 814 $[M+H]^+$. IR (CH_2Cl_2): ν(C≡N) 2213 cm^{-1}, ν(C=C) 1608 cm^{-1}.

References

1 W. H. Baddley, C. Panattoni, G. Bandoli, D. A. Clemente, U. Belluco, *J. Am. Chem. Soc.*, 1971, **93**, 5590.

2 R. Kergoat, M. M. Kubicki, L. C. Gomes de Lima, J. E. Guerchais, P. L'Haridon, *J. Organomet. Chem.*, 1989, **367**, 143.

3 R. Kergoat, L. C. Gomes de Lima, C. Jegat, N. Le Berre, M. M. Kubicki, J. E. Guerchais, P. L'Haridon, *J. Organomet. Chem.*, 1990, **389**, 71.

4 Y. Zhou, A. M. Arif, J. S. Miller, *Chem.Commun.*,1986, 1881.

5 N. Zhu, H. Vahrenkamp, *Chem. Ber./ Recueil*, 1997, **130**, 1241.

6 A. Davison,J. P. Solar, *J. Organomet. Chem.*, 1979, **166**, C13.

7 M. I. Bruce, T. W. Hambley, M. R. Snow, A. G. Swincer, *Organometallics*, 1985, **4**, 494.

8 M. I. Bruce, T. W. Hambley, M. R. Snow, A. G. Swincer, *Organometallics*, 1985, **4**, 501.

9 M. I. Bruce, P. A. Humphrey, M. R. Snow, E. R. T. Tiekink, *J. Organomet. Chem.*, 1986, **303**, 417.

10 M. I. Bruce, D. N. Duffy, M. J. Liddell, M. R. Snow, E. R. T. Tiekink, *J. Organomet. Chem.*, 1987, **335**, 365.

11 M. I. Bruce, M. J. Liddell, M. R. Snow, E. R. T. Tiekink, *Organometallics*, 1988, **7**, 343.

12 M. I. Bruce, M. P. Cifuentes, M. R. Snow, E. R. T. Tiekink, *J. Organomet. Chem.*, 1989, **359**, 379.

13 M. I. Bruce, T. W. Hambley, M. J. Liddell, M. R. Snow, A. G. Swincer, E. R. T. Tiekink, *Organometallics*, 1990, **9**, 96.

14 M. I. Bruce, P. J. Low, B. W. Skelton and A. H. White, *New J. Chem.*, 1998, 419.

15 M. I. Bruce, B. D. Kelly, B. W. Skelton and A. H. White, *J. Organomet. Chem.*, 2000, **604**, 150.

16 M. I. Bruce, B. W. Skelton, A. H. White, N. N. Zaitseva, *J. Organomet. Chem.*, 2002, **650**, 141.

17 G. J. Baird, S. G. Davies, *J. Organomet. Chem.*, 1984, **262**, 215.

18 F. V. Shalcross, G. B. Carpenter, *Acta. Crystallogr.*, 1958, **11**, 490.

19 D. L Lichtenberger, S. K. Renshaw, A. Wong, C. D. Tagge, *Organometallics*, 1993, **12**, 3522.

20 J. E. McGrady, T. Lovell, R. Stranger, M. G. Humphrey, *Organometallics*, 1997, **16**, 4004.

21 D. L. Lichtenberger, N. E. Gruhn, S. K. Renshaw, *J. Mol. Struct.*, 1997, **405**, 79.

22 O. F. Koentjoro, R. Rousseau, P. J. Low, *Organometallics*, 2001, **20**, 4502.

23 P. Belanzoni, N. Re, A. Sgamellotti, C. Floriani, *J. Chem. Soc., Dalton Trans.*, 1998, 1825

24 M. I. Bruce, P. J. Low, K. Kostuas, J-F. Halet, , S. P. Best, G. A. Heath, *J. Am. Chem. Soc.*, 2000, **122**, 1949.

25 F. Paul, W.E. Meyer, L. Toupet, H. Jiao, J. A. Gladysz, C. Lapinte, *J. Am. Chem. Soc.*, 2000, **122**, 9405.

26 M. I. Bruce, B. G. Ellis, P. J. Low, B. W. Skelton, A. H. White, *Organometallics*, 2003, **22**, 3184.

27 I. R. Whittall, M. G. Humphrey, D. C. R. Hockless, B. W. Skelton, A. H. White, *Organometallics*, 1995, **14**, 3970

28 M. I. Bruce, K. Costuas, T. Davin, B. G. Ellis, J-F. Halet, C. Lapinte, P. J. Low, M. E. Smith, B. W. Skelton, L. Toupet, A. H. White, *Article in Press.*

Compounds List - Cyanoacetylides

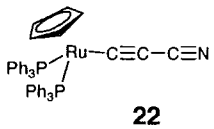

22

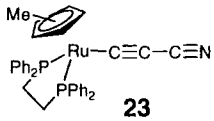

23

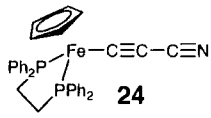

24

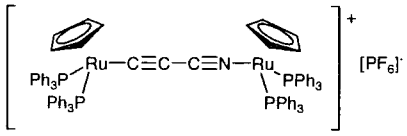

25

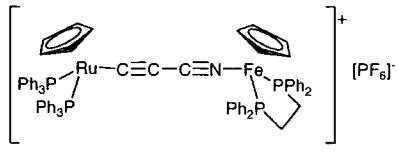

26

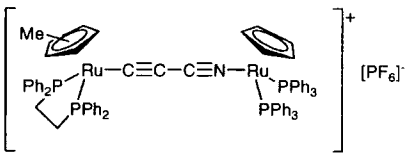

27

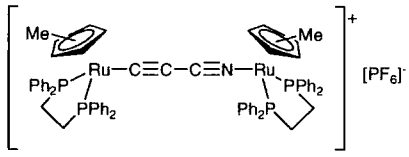

28

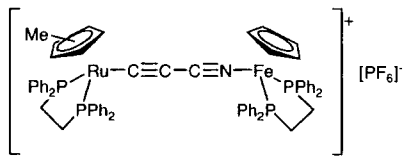

29

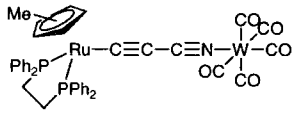

30

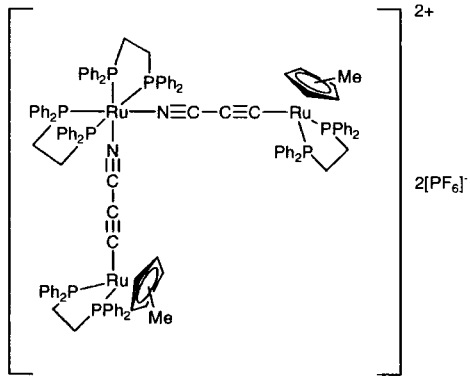

31

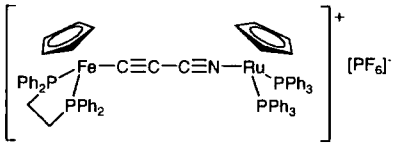

32

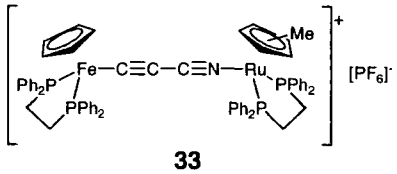

33

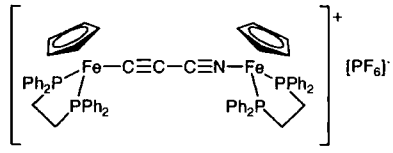

34

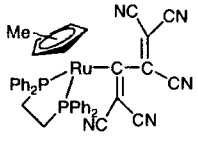

35

Introduction

Diyndiyl Systems Bearing Identical Termini

As has been indicated several times in this thesis, there is a great deal of interest in bimetallic complexes featuring conjugated bridging ligands. One of the simplest examples of a bridge between two metal centres is a chain of unsaturated carbon atoms to give compounds of type ML_x-$(C{\equiv}C)_n$-ML_x. The earliest examples of diyndiyl systems (n = 2) are the nickel complexes $[\{Ni(CN)(NH_3)_3\}_2(\mu\text{-}C{\equiv}CC{\equiv}C)]$ and $[\{Ni(PPh_3)Cp\}_2(\mu\text{-}C{\equiv}CC{\equiv}C)]$ and the iron complex $[\{Fe(CO)_2Cp\}_2(\mu\text{-}C{\equiv}CC{\equiv}C)]$.[1,2] However, the majority of work in this are has been in the last 15 years with several groups using specific metal centres, of which the most relevant to this thesis are the group 8 half-sandwich metal centres $[RuL_2Cp']^+$ and $[FeL_2Cp']^+$ (Cp' = Cp, L = phosphine ligand, Cp' = Cp*, L = chelating bisphosphine). The rhenium centre $[Re(NO)(PPh_3)Cp^*]$ is included here for comparative purposes.[3-8] These homometallic complexes and their observed oxidation potentials are summarised in Table 7.1 below.

Table 7.1. Homometallic bridged diyndiyl complexes

ML_x	Observed Oxidation Potentials vs. SCE (V)	Ref.
Fe(dppe)Cp* (**Fe.1**)	-0.69, +0.03, +0.95	3
Fe(dippe)Cp* (**Fe.2**)	-0.97, -0.18, +0.81	4
$Ru(PPh_3)_2Cp$ (**Ru.1**)	-0.23, +0.41, +1.03, +1.68[a]	9
$Ru(PPh_3)(PMe_3)Cp$ (**Ru.2**)	-0.26, +0.33, +0.97, +1.46[a]	9
Ru(dppe)Cp* (**Ru.3**)	-0.43, +0.23, +1.02, +1.5[a]	7
Ru(dppm)Cp* (**Ru.4**)	-0.48, +0.15, +1.04, +1.4[a]	7
Ru(dppf)Cp (**Ru.5**)	-0.22, +0.43, +0.74[b], +1.28[a]	10
$Re(NO)(PPh_3)Cp^*$ (**Re.1**)	+0.01, +0.54	8

[a]Irreversible oxidation, [b]Quasi-reversible oxidation

As has been stated previously, cyclic voltammetry is a convenient probe of the electrochemical behaviour of these diyndiyl-bridged systems and allows the determination of the potentials required to oxidise the compounds relative to a known reference potential. The di-iron complex $[\{Fe(dppe)Cp^*\}_2(\mu\text{-}C{\equiv}CC{\equiv}C)]$ (**Fe.1**) displays three reversible, one-electron oxidation processes at -0.69, +0.03 and +0.95 V vs. SCE.[3] Whilst the neutral, mono- and di-oxidised species **Fe.1**, $[\mathbf{Fe.1}]^+$, and $[\mathbf{Fe.1}]^{2+}$ could be isolated by chemical oxidations, attempts to isolate the tri-cation were unsuccessful. In order to reduce the oxidation potential of the third oxidation and hence stabilise the tri-cation, the more strongly electron-donating dippe ligand was substituted for the dppe ligand[4] (**Fe.2**). The oxidation potentials of the resulting complex were found to be -0.97, -0.18 and +0.81 V vs. SCE. These oxidations in **Fe.2** are not only moved to lower potential relative to **Fe.1** but there is also an increase in the separation of the potentials in the dippe system, an indication of greater

thermodynamic stability of the mono-oxidised material. In addition, changes in the structure of the complex were observed upon oxidation (see below). By comparison, the di-ruthenium complex [{Ru(PPh_3)$_2$Cp}$_2$(μ-C≡CC≡C)] (**Ru.1**) undergoes three, reversible, one-electron oxidations (at -0.23, +0.41 and +1.03 V vs. SCE) followed by a single, irreversible multi-electron redox process at +1.68 V.[9] The increased oxidation potentials of the ruthenium complex versus **Fe.1** and **Fe.2** are a result of the less electron-rich ruthenium centres. The tetra-cation generated at the electrode surface apparently undergoes a rapid chemical transformation into a new species which, at the applied potential, undergoes further oxidative processes. As with the iron complexes, substitution of more strongly electron-donating supporting ligands at the ruthenium centre leads to the reduction of the oxidation potentials. The complexes [{Ru(PPh_3)(PMe_3)Cp}$_2$(μ-C≡CC≡C)] (**Ru.2**) and [{Ru(dppe)Cp*}$_2$(μ-C≡CC≡C)] (**Ru.3**) undergo four oxidation processes at -0.26, +0.33, +0.97 and +1.46 V and -0.43, +0.23, +1.02, and +1.51.[7,9] The fourth oxidation is irreversible in both cases.

The large separation of the sequential oxidation events for the complexes discussed above leads to large values of K_c (K_c values for the complexes discussed here fall in the range $9.5 \times 10^{10} - 2.3 \times 10^{13}$). By comparison, the K_c values found for the Creutz-Taube ion are $10^{6.6}$ (aqueous solution) and $10^{7.3}$ (acetonitrile solution).[11,12] The K_c values for the homometallic, diyndiyl bridged species therefore demonstrate a high degree of thermodynamic stability with respect to disproportionation.

Spectro-electrochemical methods revealed that upon successive oxidations, the ν(C≡C) frequencies of the di-ruthenium complex [{Ru(PPh_3)$_2$Cp}$_2$(μ-C≡CC≡C)]

(**Ru.1**) move to progressively lower wavenumbers (Table 7.2).[9] The fact that stretching frequency of the mono-oxidised species (1855 cm^{-1}) is mid-way between that of the neutral (1971 cm^{-1}) and di-oxidised species (1767 cm-1) suggests that the unpaired electron is delocalised over the molecule on the time-scale of the IR measurements (~10^{-13} seconds). After the second oxidation, the stretching frequency has moved to a region more associated with a carbon-carbon double bond stretching frequency and suggests a more cumulenic nature to the material. In addition, an IVCT transition was observed in the NIR region of the electronic absorption spectrum (11, 400 cm^{-1}) of the mono-oxidised complex which disappeared on progression to the di-oxidised material.

Similar spectro-electrochemical behaviour was observed for the analogous complex [{Ru(dppe)Cp*}$_2$(μ-C≡CC≡C)] (**Ru.3**) with IR stretching frequencies observed at 1963 cm^{-1} (neutral), 1860 cm^{-1} (mono-oxidised), and 1770 cm^{-1} (di-oxidised.) (Table 7.2).[7] In addition, chemical oxidation of **Ru.3** with [$FeCp_2$][PF_6] allowed the isolation of the mono- and di-oxidised species and their crystallographic characterisation. In the neutral complex, the Ru-C bond lengths (2.001(3) and 2.003(3) Å), the central C-C bond of the bridging ligand (1.382(4) Å) and the C≡C bond lengths (1.223(4) and 1.218 (4) Å) are consistent with the alternating single/triple bond structure expected for the diyndiyl system. Oxidation results in a slight lengthening of the "triple" bonds (1.248(3) Å) and a contraction of the Ru-C and C-C bonds (1.931(2) and 1.338(3) Å respectively). Upon reaching the di-oxidised complex, all of the carbon-carbon bonds fall in the narrow range 1.269(7) – 1.294(7) Å and are very similar to those of the butatriene complex $H_2C=C=C=CH_2$ (1.283(5) –

1.318(5) Å).[13] Thus it is possible to suggest the valence bond structures shown below for these complexes (Scheme 7.1).

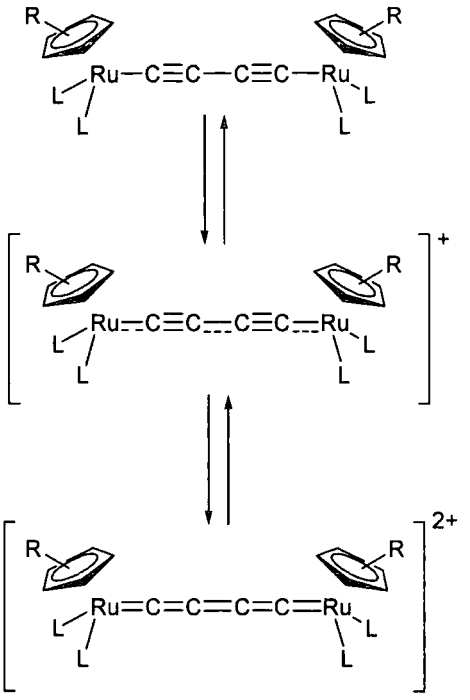

Scheme 7.1. Valence bond structures of di-ruthenium complexes

(R = H, L = PPh_3; R = Me, L_2 = dppe).

Table 7.2. IR data for $[\{ML_x\}C{\equiv}CC{\equiv}C\{ML_x\}]^{n+}$ (cm^{-1}).

ML_x	n = 0	n = 1	n = 2	Ref
$Ru(PPh_3)_2Cp$	1971	1855	1767	9
Ru(dppe)Cp*	1963	1860	1770	7
$Re(NO)(PPh_3)Cp^*$	1964	1872	[a]	8
Fe(dppe)Cp*	1955, 1880	1973, 1880	2160, 1050	3

[a]Not observed.

The rhenium complex [{Re(NO)(PPh_3)Cp}$_2$(μ-C≡CC≡C)] is of interest in these studies as it bears the NO ligand which acts as a "reporting group" at the Re centre. The di-rhenium complex undergoes two, reversible oxidation processes at +0.01 and +0.54 V vs. SCE.[8] As with the ruthenium complexes discussed above, oxidation of this complex results in a decrease in the ν(C≡C) stretching frequency (from 1963 cm^{-1} in the neutral complex to 1872 cm^{-1} in the mono-oxidised material) as well as a contraction of the "single" bonds (neutral: Re-C = 2.037(5) Å. C-C = 1.389 (5) Å; di-oxidised: Re-C = 1.909/1.916(7) Å. C-C = 1.305 (10) Å) and lengthening of the "triple" bonds (neutral: 1.202(7) Å; di-oxidised, 1.263/1.260(10) Å). However, the rhenium centre also bears the NO ligand for which there is an increase in the ν(NO) stretching frequency with each successive oxidation (n = 0, 1623; n = 1, 1665; n = 2, 1719 cm^{-1}). This is due to the removal of electron density from the rhenium centre reducing the degree of back-bonding from the Re d-orbitals into the π* anti-bonding orbitals of the NO moiety. Thus the NO fragment is a "reporting group" in that its physical properties are affected by the oxidation of the complex despite the fact that it is not directly involved in the oxidation. The NIR region of the electronic absorption spectrum showed an IVCT band at ~7600 cm^{-1} and the complex was assigned as a Class 3 system.

The di-iron complex [{Fe(dppe)Cp*}$_2$(μ-C≡CC≡C)] (**Fe.1**) shows somewhat different behaviour upon oxidation. Whilst there is a slight change in the bond lengths between the neutral and mono-oxidised species (with the "single" bonds contracting and the "triple" bonds lengthening), the IR absorptions move to *higher* frequency rather than to *lower* frequency as observed for the ruthenium and rhenium complexes.[3] This indicates that there is less of a contribution from the π-system of the bridging ligand

to the HOMO in the di-iron complex. The NIR region of the electronic absorption spectrum of $[\mathbf{Fe.1}]^+$ showed an IVCT band at ~7600 cm^{-1}, with band shape analysis giving a high coupling constant suggestive of a Class 3 system. Further oxidation to the di-oxidised species resulted in the disappearance of the IVCT band from the electronic absorption spectrum and a further increase in the IR stretching frequencies of the bridging moiety.

To gain an insight into the exact nature of metal/bridge interaction in the homometallic diyndiyl-bridged complexes, several theoretical studies have been carried out.[7,9,14,15] These Density Functional Theory (DFT) and Extended Hückel (EH) studies have shown that, in these compounds, the interaction between the two metal centres across the diyndiyl bridge results in an HOMO with some degree of delocalisation across the 6-atom M-C_4-M chain. Thus, any oxidation process, which involves loss of electrons from these orbitals, will not be exclusively metal-centred. Comparison of models with different supporting ligands suggests that molecules containing strong electron-donating ligands should be more readily oxidised.

Diyndiyl Systems Bearing Differing Termini

Whilst diyndiyl complexes bearing identical termini have been under study for some time, the detailed study of complexes bearing termini of differing electron density is a relatively recent development. Modifications to one iron end-cap in the $[\{Fe(dppe)Cp^*\}_2(\mu\text{-}C{\equiv}CC{\equiv}C)]$ (**Fe.1**) complex have been made to produce $[\{Fe(dppe)Cp^*\}(\mu\text{-}C{\equiv}CC{\equiv}C)\{Fe(CO)_2Cp^*]$ (**Fe.3**).[16] Complex **Fe.3** undergoes two

oxidation processes which, at -0.36 and +0.74 V, the latter being poorly chemically reversible, are markedly different from those of the monometallic model complexes $Fe(C{\equiv}CC{\equiv}CSiMe_3)(dppe)Cp^*$ (0.00 V) and $Fe(C{\equiv}CC{\equiv}CSiMe_3)(CO)_2Cp^*$ (+1.15 V, irreversible). The differences in electrochemical response of the bimetallic compound **Fe.3** and the model monometallic systems provide an indication of electronic communication between the two metal centres in **Fe.3**, with a marked increase in the thermodynamic stability of the mono-oxidised complex relative to $Fe(C{\equiv}CC{\equiv}CSiMe_3)(dppe)Cp^*$.

A more significant change to the bimetallic complex is made when one iron end-cap is replaced by the $[Re(NO)(PPh_3)Cp^*]$ centre to form $[\{Re(NO)(PPh_3)Cp^*\}(\mu\text{-}C{\equiv}CC{\equiv}C)\{Fe(dppe)Cp^*]$ (**ReFe.1**).[15] This mixed iron/rhenium complex undergoes three oxidation events at -0.50, +0.23, and +1.33 V vs. SCE, the latter of which appears just at the edge of the observable window provided by the DCM solvent. Comparison of these potentials with those of the **Fe.1** (-0.69, +0.03, and +0.95V) and **Re.1** (+0.01 and +0.54 V) analogues suggest that the first oxidation potential of the heterometallic complex is predominantly iron in character with the increase in potential from -0.69 V to -0.50 V brought about by the rhenium end-cap drawing electron density away from the iron centre. The same effect reduces the second oxidation potential of the heterometallic complex relative to that of the di-rhenium analogue. The electronic absorption spectrum of the mono-oxidised species $[\mathbf{ReFe.1}]^+$ revealed a broad, weak absorption band in the NIR region of the spectrum which was absent in both the neutral and di-oxidised species and was therefore assigned as an IVCT band. The coupling constant derived from this band was much lower than those found for the di-iron and di-rhenium analogues and the complex was

assigned as a Class 2 system. This indicates a diminished interaction between the metal centres in the heterometallic diyndiyl systems when compared with the homometallic analogues.

Only recently have the iron/ruthenium complexes [{Fe(dppe)Cp*}(μ-C≡CC≡C){Ru(dppe)Cp*] (**FeRu.1**) and [{Fe(dppe)Cp*}(μ-C≡CC≡C){Ru(PPh_3)$_2$Cp] (**FeRu.2**) been isolated.[17] The complex [{Fe(dppe)Cp*}(μ-C≡CC≡C){Ru(dppe)Cp*] is of particular interest as it differs from the homometallic materials [{Fe(dppe)Cp*}$_2$(μ-C≡CC≡C)] (**Fe.1**) and [{Ru(dppe)Cp*}$_2$(μ-C≡CC≡C)] (**Ru.3**) solely in the substitution of a single Ru atom for Fe (or vice versa). The electrochemical data for these materials are summarised in Table 7.3.

Table 7.3. Oxidation potentials of heterometallic diyndiyl complexes and their homometallic analogues.

Compound	E_1 (V)	E_2 (V)	E_3 (V)	E_4 (V)
[{Re(NO)(PPh_3)Cp*}(μ-C≡CC≡C){Fe(dppe)Cp*] (**ReFe.1**)	-0.50	+0.23	+1.33	
[{Fe(dppe)Cp*}(μ-C≡CC≡C){Ru(dppe)Cp*] (**FeRu.1**)	-0.59	+0.18	+0.99	
[{Fe(dppe)Cp*}(μ-C≡CC≡C){Ru(PPh_3)$_2$Cp] (**FeRu.2**)	-0.51	+0.30	1.00	
[{Fe(dppe)Cp*}$_2$(μ-C≡CC≡C)] (**Fe.1**)	-0.69	+0.03	+0.95	
[{Ru(dppe)Cp*}$_2$(μ-C≡CC≡C)] (**Ru.3**)	-0.43	+0.23	+1.02	+1.51[a]
[{Re(NO)(PPh_3)Cp*}$_2$(μ-C≡CC≡C)] (**Re.1**)	+0.01	+0.54		

[a]Irreversible

The first oxidation potentials of the heterometallic complexes **FeRu.1** (-0.59 V) and **FeRu.2** (-0.51 V) are markedly less favourable than that in the di-iron complex **Fe.1** (-0.69 V) which suggests that the substitution of a ruthenium centre for an iron centre results in a stabilisation of the HOMO, making the removal of an electron less thermodynamically favourable.

It was noted above that for homometallic diyndiyl-bridged species the HOMO was delocalised over the six atom M-C≡CC≡C-M chain in the di-ruthenium complexes **Ru.1-3** whilst in the di-iron complex **Fe.1** there was a greater degree of metal character in the HOMO. Recently, a Mulliken atomic orbital population analysis has been performed on these compounds as well as the heterometallic complexes **FeRu.1** and **FeRu.2**.[17] These calculations were used to determine the metal vs. diyndiyl weighting of the HOMO orbital. It was found that the metal/diyndiyl weightings for the homometallic complexes were 41 % metal and 46 % diyndiyl for the di-iron complex, and 26 % metal and 69 % diyndiyl for the di-ruthenium analogue. Substitution of one metal for another led to the heterometallic complex where the diyndiyl weighting is 57 % whilst the metal weighting is distributed unevenly between the iron and ruthenium centres (18 and 12 % respectively).

The IR stretching frequencies of the oxidised materials seem to confirm the distribution of the HOMO as described above. Oxidation of **Fe.Ru1** and **Fe.Ru2** leads to a change in the ν(C≡C) stretching frequencies to lower wavenumbers, consistent with the removal of a significant degree of electron density from the M-C≡CC≡C-M π^* anti-bonding orbital. Furthermore, whilst only a single ν(C≡C) band is observed in the neutral materials, this was found to split upon oxidation into two

bands. This spitting of the bands implies a reduction in the symmetry of the HOMO orbital, consistent with uneven removal of electron density from the metal centres.

Spectro-electrochemical studies of the heterometallic complex revealed intense absorptions in the NIR region of the spectrum for compounds **FeRu.1** and **FeRu.2** at 9,900 cm^{-1} and 10,300 cm^{-1} respectively assigned as IVCT bands. Also found were very weak bands of lower energy (~7,400 cm^{-1}). Analysis of the IVCT bands found coupling constants for the heterometallic complexes that were consistent with Class 2 complexes, albeit at the higher end of the range. These observations are consistent with those for the iron/rhenium complex [{Re(NO)(PPh_3)Cp*}(μ-C≡CC≡C){Fe(dppe)Cp*] and suggest that the degree of interaction between the metal centres in the heterometallic iron/ruthenium diyndiyl complex is less than that in the homometallic analogues.

It has been noted that the cyanoacetylide ligand $[C{\equiv}CC{\equiv}N]^-$ is both isolobal and isoelectronic with the diyndiyl dianion $[C{\equiv}CC{\equiv}C]^{2-}$. Coordination of the cyanoacetylide moiety to metal centres as a bridging ligand would then be expected to occur in a similar manner to the diyndiyl analogues, resulting in similar orbitals. However, the cyanoacetylide ligand is polarised, in contrast to the symmetrical C≡CC≡C bridge. To investigate the effect of this novel bridging moiety, electrochemical and spectro-electrochemical studies were performed on the monometallic and bimetallic cyanoacetylides discussed in the previous chapter.

Results and Discussion

Clues to the electronic structures of the monometallic cyanoacetylides and their coordination complexes are presented by their molecular structures and physical properties especially their vibrational spectra. In order to probe the underlying electronic structure of these materials, electrochemical and spectro-electrochemical studies were performed on the cyanoacetylide compounds described in Chapter 6.

Electrochemistry – Monometallic Compounds

Electrochemical studies utilising cyclic voltammetry (CV) were performed on each of the compounds **22-34**, using a platinum disc working electrode and platinum wire counter and pseudo-reference electrodes. Measurements were carried out in a 0.1M solution of $[N(C_4H_9)_4][BF_4]$ in DCM. Electrode potentials are reported against an internal ferrocene (Fc/Fc^+ = 0.46 V vs. SCE) or decamethylferrocene (Fc^*/Fc^{*+} = -0.02V vs. SCE) standard.[18]

The CVs of the monometallic compounds **22-24** each displayed a single oxidation event at a platinum electrode (Table 7.4). Whilst for the ruthenium complexes $Ru(C{\equiv}CC{\equiv}N)(PPh_3)_2Cp$ (**22**) and $Ru(C{\equiv}CC{\equiv}N)(dppe)Cp^*$ (**23**) this oxidation was poorly chemically reversible at room temperature, a consequence of the reactivity of the electro-generated product, a chemically and electrochemically reversible wave

was observed upon cooling the solution to –30 °C. In the case of the iron cyanoacetylide Fe(C≡CC≡N)(dppe)Cp (**24**) the oxidation was fully reversible at room temperature. For the mono-ruthenium complex Ru(C≡CC≡N)$(PPh_3)_2$Cp (**22**) the oxidation event occurred at +0.92 V. In the case of the compounds Ru(C≡CC≡N)(dppe)Cp* (**23**) and Fe(C≡CC≡N)(dppe)Cp (**24**) the oxidation events were observed at +0.69 and +0.53 V respectively. Not surprisingly, the ease of oxidation reflects the increased degree of electron-richness at the metal centres.

These potentials also reflect the influence of the electron-withdrawing CN moiety when compared to other substituted acetylides. The oxidation potentials of the phenylacetylide compounds Ru(C≡CC_6H_5)$(PPh_3)_2$Cp and Ru(C≡CC_6H_4-4-NO_2)$(PPh_3)_2$Cp, for example, are +0.58 and +0.76 V vs. SCE respectively.[19] The presence of the electron-withdrawing NO_2 group draws electron density away from the ruthenium centre an makes it harder to oxidise, thus increasing the oxidation potential. When the phenylacetylide moiety C_6H_4-R (R = H, NO_2) is replaced by the CN substituent the oxidation potential is increased by almost 300 mV to +0.92 V. The same behaviour is seen in complexes bearing the $[Fe(dppe)Cp]^+$ end-cap. For example, the oxidation potential of Fe(C≡C-C_6H_4-4-NO_2)$(PPh_3)_2$Cp is +0.21 V vs. SCE which rises to +0.53 V in **24**.

Furthermore, the diynyl complex Ru(C≡CC≡CH)$(PPh_3)_2$Cp undergoes an irreversible oxidation at +0.52 V.[20] Similarly, the diynyl complex Ru(C≡CC≡CH)(dppe)Cp* undergoes an irreversible oxidation at +0.44 V.[20] In each case the oxidation potential of the diynyl complex is lower than that of the analogous cyanoacetylide complex, implying that substitution at the extreme end of the 5-atom Ru-C≡C-C≡X chain has a

direct effect on the electron density at the metal centre. This is consistent with suggestions in the previous chapter that the HOMOs of the monometallic cyanoacetylide compounds are delocalised across the M-C_3N chain (see Chapter 6).

Electrochemistry – Group 8 Bimetallic Compounds

In the previous chapter it was suggested (on the basis of molecular structures and vibrational spectra) that the degree of delocalisation of the HOMO in the group 8 bimetallic compounds was dependant on the nature of the metal end-cap (see Cyanoacetylides synthesis chapter). It was postulated that the HOMO was similar to that of the diyndiyl-bridged species M-C≡CC≡C-M' as illustrated below (Figure 7.1).

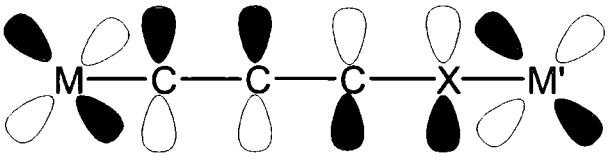

Figure 7.1. HOMO of bridged species (X = C, N)

It was suggested that there was a greater degree of delocalisation across the HOMO in the case where the two metal end-caps were not identical (an "unsymmetrical" species). In the case where the metal end-caps were identical (the "symmetrical" case) then the degree of orbital interaction across the 6-atom M-C≡CC≡N-M' chain would be reduced.

The cyclic voltammograms of the group 8 bimetallic species **25-29** and **32-34** each display two oxidation waves in their cyclic voltammograms (Table 7.4). Whilst there at first appears to be a correlation between the oxidation potentials of the homo-bimetallic complexes and their mono-metallic components (for example the two oxidation potentials for **25** [+0.91 and +1.43 V] are very similar to those of the $Ru(C{\equiv}CC{\equiv}N)(PPh_3)_2Cp$ metallo-ligand (**22**) [+0.92 V] and the cyanoacetylene complex $[Ru(NCC{\equiv}CC_6H_5)(PPh_3)_2Cp](PF_6)$ (**17**) [+1.47 V]) this is unlikely to actually be the case. The bimetallic complexes differ by one charge unit from the cyanoacetylide metallo-ligands and hence their electrochemical responses are not directly comparable to each other. The similarity in oxidation potentials between the homo-bimetallic complexes and their mono-metallic components is most likely a matter of coincidence.

Table 7.4. Oxidation potentials of bimetallic compounds and their monometallic models.

Compound	1st Oxidation Potential (V)	2nd Oxidation Potential (V)
[{Ru $(PPh_3)_2Cp$}$_2$(C≡CC≡N)](PF_6) (**25**)	+0.91	+1.43
[{Ru$(PPh_3)_2Cp$}(C≡C-C≡N){Fe(dppe)Cp}](PF_6) (**26**)	+0.62	+1.22
[{Ru(dppe)Cp*}(C≡CC≡N){Ru$(PPh_3)_2Cp$}](PF_6) (**27**)	+0.79	+1.37
[{Ru(dppe)Cp*}$_2$(C≡CC≡N)](PF_6) (**28**)	+0.71	+1.17
[{Ru(dppe)Cp*}(C≡CC≡N){Fe(dppe)Cp}](PF_6) (**29**)	+0.58	+1.03
[{Fe(dppe)Cp}(C≡CC≡N){Ru$(PPh_3)_2Cp$}](PF_6) (**32**)	+0.66	+1.34
[{Fe(dppe)Cp}(C≡CC≡N){Ru(dppe)Cp*}](PF_6) (**33**)	+0.63	+1.22
[{Fe(dppe)Cp}$_2$(C≡CC≡N)](PF_6) (**34**)	+0.55	+0.96
[Ru(NCC_6H_5)(dppe)Cp*](PF_6) (**2**)	+1.10	n/a
[Ru$(NCC{\equiv}CC_6H_5)(PPh_3)_2Cp](PF_6)$ (**17**)	+1.47	n/a
[Fe(NCC_6H_5)(dppe)Cp](PF_6) (**3**)	+0.83	n/a
Ru(C≡CC≡N)$(PPh_3)_2Cp$ (**22**)	+0.92	n/a
Ru(C≡CC≡N)(dppe)Cp* (**23**)	+0.69	n/a
Fe(C≡CC≡N)(dppe)Cp (**24**)	+0.53	n/a

The oxidation potentials of the bridging isomeric pairs **26/32** and **29/33**, however, display some interesting behaviour. Firstly, the first oxidation potentials of the heterometallic complexes are lower than those of *any* of the appropriate monometallic components. Indeed, the first oxidation potentials of **26** and **29** are almost identical and the range spanned by the first oxidation potentials across the four complexes (+0.58 V- +0.66 V) is appreciably smaller than the range spanned by the second oxidation potentials (+1.03 V – +1.34 V). Secondly, the oxidation potentials of the Fe-C bound bridging isomers are higher than those of their N-Fe bound analogues. Furthermore, the oxidation potentials of the complexes bearing the $[Ru(dppe)Cp^*]^+$

end-cap are lower than those with the $[Ru(PPh_3)_2Cp]^+$ end-cap, no doubt a consequence of the greater electron-donating strength of the Cp*/dppe ligands over their PPh_3/Cp analogues. These trends show that the substitution of the metal centre at either end of the C_3N chain to form a heterometallic complex results in a substantial change in the degree of delocalisation across the bridge. In addition, the near-identical values of the first oxidation potentials of the bridging isomers suggest that the redox-active orbital is relatively insensitive to the orientation of the cyanoacetylide bridge. In order to better understand the nature of the metal-metal interactions in the group 8 bimetallic compounds it is necessary to investigate the changes in the vibrational and electronic spectra that occur upon the oxidation of these species (see spectro-electrochemical discussions below).

Electrochemistry – Trimetallic Compound

The trimetallic complex $[\{Ru(C{\equiv}CC{\equiv}N)(dppe)Cp^*\}_2\{Ru(dppe)_2\}][PF_6]_2$ (**31**) displayed a single, reversible oxidation event at +0.96 V. This suggests that both the ruthenium centres of the metallo-ligands are being oxidised simultaneously and that there is little or no communication between them. This in turn indicates that the communication between remote metal centres is via the π-system. In this *cis*-complex the π-system of the two metallo-ligands do not interact with each other and hence there is no communication between the two.

Infra-Red Spectro-electrochemistry – Monometallic Compounds

As has been stated previously (see cyanoacetylides synthesis chapter) the two absorptions observed in the IR spectrum may be either independent vibrational modes corresponding to the C≡C and C≡N fragments or coupled vibrational modes of the combined cyanoacetylide moiety. For the purposes of the description that follows we have assumed that the higher frequency absorption corresponds to the CN moiety and the lower frequency absorption corresponds to the C≡C moiety. The data obtained is summarised in Table 7.6 below.

Table 7.6. IR data for neutral and oxidised samples of **22-24**

Compound	**Observed IR absorptions (neutral) (cm^{-1})**	**Observed IR absorptions νCN/νCC (oxidised) (cm^{-1})**
Ru(C≡CC≡N)(PPh_3)$_2$Cp (**22**)	2180/2011/1997	2214/2180/2048/2010/1995/1975
Ru(C≡CC≡N)(dppe)Cp* (**23**)	2176/2010/1994	2188/2162/2070/1963
Fe(C≡CC≡N)(dppe)Cp (**24**)	2174/1991	2201/not observed

In an effort to gather more information about the nature of the oxidation products, infra-red spectro-electrochemical studies were performed on a series of these compounds. Whilst the mono-ruthenium complexes **22** and **23** displayed reversible oxidations in the cyclic voltammogram at –30 °C the redox processes were insufficiently chemically stable on the time-scale required for bulk electrolysis in the cell at this temperature. Hence the spectro-electrochemcial measurements were performed at –90 °C in butyronitrile solution using $TBAPF_6$ electrolyte. At this low temperature there are slight changes in the IR spectra of the neutral complexes. In

each case, the ν(C≡N) frequency is unchanged but two absorptions are apparent in the ν(C≡C) region at 2011 and 1997 cm^{-1} (**22**) and 2010 and 1994 cm^{-1} (**23**). This may be due to some degree of vibronic coupling between the CC and CN moieties which is not observed at room temperature but becomes apparent at low temperatures. Oxidation of these materials leads to the formation of a new series of bands, with two absorptions being observed in the 2160-2220 cm^{-1} region in either case as well as a series of absorptions in the 2070-1960 cm-1 region. Whilst the patterns are not identical in both cases they are similar (Figures 7.2 and 7.3).

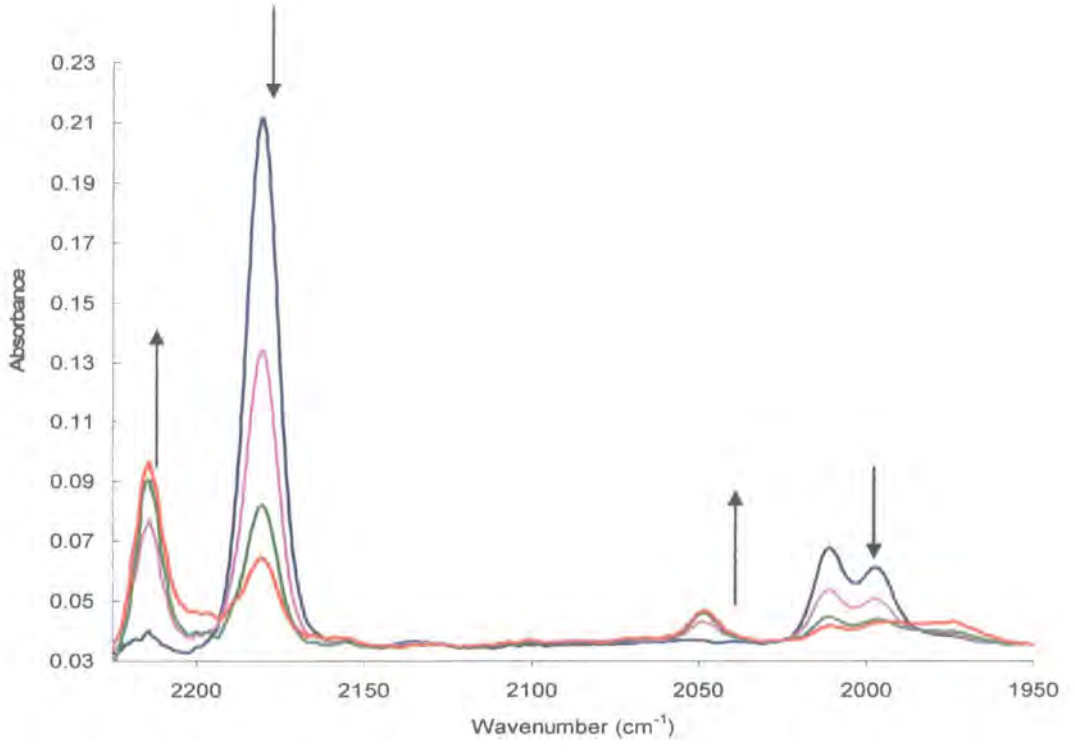

Figure 7.2. Oxidation of $Ru(C{\equiv}CC{\equiv}N)(PPh_3)_2Cp$ (**22**)

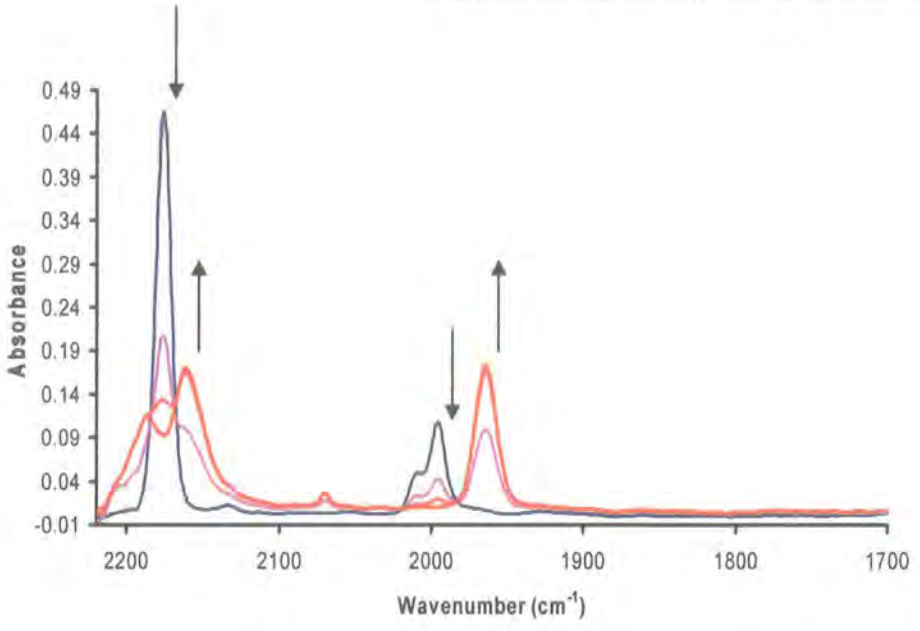

Figure 7.3. Oxidation of Ru(C≡CC≡N)(dppe)Cp* (**23**)

Given that the only variations between the complexes **22** and **23** are the nature of the supporting ligands then it is likely that the bonding interactions between the metal centres and the cyanoacetylide ligand are similar in each case. This, not surprisingly, results in similar IR stretching frequencies being observed in both the neutral and oxidised forms. In both the neutral and oxidised cases, the observed IR frequencies are moved to lower energy in the case of **23** which bears the more strongly electron-donating metal centre.

In the case of the iron cyanoacetylide Fe(C≡CC≡N)(dppe)Cp (**24**), oxidation led to an increase of the ν(C≡N) stretching frequency from 2174 cm^{-1} to 2201 cm^{-1}. The ν(C≡C) band at 1991 cm^{-1} from the parent complex was not observed in the oxidised material but no corresponding absorption band was seen. Back reduction led to the recovery of the original spectrum. The fact that there is only a small shift in the ν(C≡N) frequency upon oxidation ($\Delta\nu C{\equiv}N$ = -26 cm^{-1}) indicates that the oxidation in

this complex is predominantly metal centred and has little effect on the cyanoacetylide moiety. This in turn suggests a poorer interaction between the orbitals of the metal and the cyanoacetylide ligand in the iron complex than the ruthenium examples.

Infra-Red Spectro-electrochemistry – Bimetallic Compounds

In addition to the monometallic compounds discussed above, infra-red spectro-electrochemical studies were also performed on the bimetallic complexes **25-29** and **32-34**. These spectro-electrochemical studies were performed at –30 °C in DCM solution as, again, a lower temperature was required in order to improve the chemical stability of the oxidation products. However, even at this temperature, only the first oxidation product was found to be reversible and so only that product is discussed herein. In each case, the absorption bands arising from the C≡N and C≡C moieties were moved to lower wavenumbers upon oxidation. Furthermore, the relative intensities of these two absorption bands changed from being of nearly equal intensity to result in the band of higher wavenumber becoming the more intense (Figure 7.4).

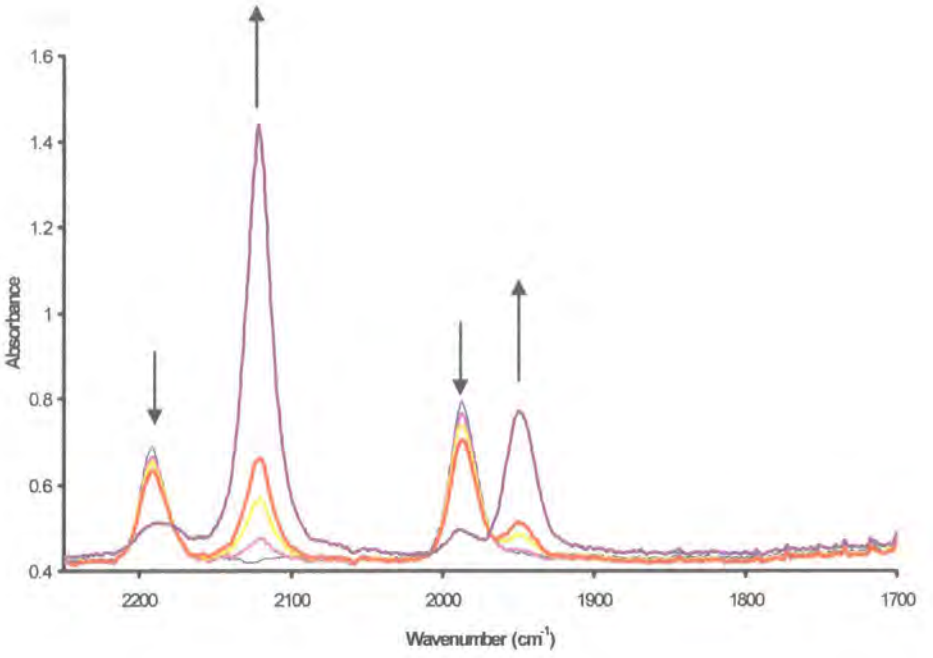

Figure 7.4. Oxidation of $[\{Ru(PPh_3)_2Cp\}(\mu\text{-}C{\equiv}CC{\equiv}N)\{Fe(dppe)Cp\}][PF_6]$

Although the ν(C≡N) and ν(C≡C) bands are very similar for all of the parent species **22-24**, with the variation in ν(C≡N) and ν(C≡C) modes falling within a range of about 10 cm^{-1}, it is interesting to note that there is a greater degree of variation within the bimetallic oxidation products (see Table 7.7 below).

Table 7.7. IR data for neutral and oxidised samples of **25-29** and **32-34**

Compound	νCN/νCC (neutral) (cm^{-1})	νCN/νCC (oxidised) (cm^{-1})	ΔνCN/ΔνCC
[{Ru $(PPh_3)_2Cp$}$_2$(C≡CC≡N)][PF_6) (**25**)	2197/1986	2062/1868	-135/-118
[{Ru$(PPh_3)_2Cp$}(C≡CC≡N){Fe(dppe)Cp}][PF_6) (**26**)	2189/1984	2121/1946	-68/-38
[{Ru(dppe)Cp*}(C≡CC≡N){Ru$(PPh_3)_2Cp$}][PF_6) (**27**)	2196/1982	2072/1868	-124/-114
[{Ru(dppe)Cp*}$_2$(C≡CC≡N)][PF_6) (**28**)	2196/1987	2056/1856/1573	-140/-131
[{Ru(dppe)Cp*}(C≡CC≡N){Fe(dppe)Cp}][PF_6) (**29**)	2194/1985	2116/1942	-78/-43
[{Fe(dppe)Cp}(C≡CC≡N){Ru$(PPh_3)_2Cp$}][PF_6) (**32**)	2191/1976	2136/1932	-55/-44
[{Fe(dppe)Cp}(C≡CC≡N){Ru(dppe)Cp*}][PF_6) (**33**)	2195/1985	2084/1884	-111/-101
[{Fe(dppe)Cp}$_2$(C≡CC≡N)][PF_6) (**34**)	2190/1984	2188/2065/1862	-125/-122

The first point of note is that in no cases do the changes in ν(C≡CC≡N) frequencies for any of the bimetallic compounds match with those of the cyanoacetylide metallo-ligands. The largest shifts in stretching frequencies upon oxidation appear to occur in the homometallic complexes. In these case the Δν(C≡N)/ Δν(C≡C) are of the order of -120 - -140 cm^{-1}. In the heterometallic complexes, however, these shifts tend to fall in the range -40 - -80 cm^{-1}. This would seem to indicate a greater degree of ligand involvement in the HOMO of the homometallic complexes.

The IR spectra of the bridging isomers **26/32** and **29/33** are distinct. The shifts in stretching frequency are lower for the isomers bearing the $[Ru(PPh_3)_2Cp]^+$ end-cap than those with the $[Ru(dppe)Cp^*]^+$ end-cap, irrespective of the orientation of the bridging ligand. This may suggest that the difference in electron-richness between the two metal centres in the isomers **26/32** increases the metal-metal interaction and leads

to a greater degree of delocalisation across the six-atom M-C≡C-C≡N-M' chain than in the case of the **29/33** pair, and thus the electronic structure is sensitive to the orientation of the bridging ligand. Indeed, if a reduced shift in stretching frequency is taken as an indicator of a greater degree of delocalisation then the $[Ru(PPh_3)_2Cp]^+$ complexes are more delocalised with an N-bound ruthenium centre whilst the $[Ru(dppe)Cp^*]^+$ complexes favour the $[Fe(dppe)Cp]^+$ centre at the N-terminus. It is, however, impossible to determine on the basis of the IR and electrochemical data alone the degree of orbital delocalisation in these systems. Mössbauer spectroscopy could be used to determine to what extent, if at all, the oxidation process is localised at the iron centre in the mixed-metal complexes, although attempts to obtain solid samples of the oxidised forms have, as yet, been unsuccessful. However, UV-vis-NIR spectra of the oxidised complexes should show absorptions arising from both intervalence charge transfer as well as d-d transitions within an oxidised metal centre. In addition to those changes described above, the spectra of the oxidation products of the homometallic complexes $[\{Ru(dppe)Cp^*\}_2(C{\equiv}CC{\equiv}N)](PF_6)$ (**28**) and $[\{Fe(dppe)Cp\}_2(C{\equiv}CC{\equiv}N)](PF_6)$ (**34**) each revealed a new absorption band at 1573 and 2188 cm-1 respectively. The assignment of these bands is not clear at present.

UV-vis-NIR spectro-electrochemistry

The samples **22-29** and **32-34** were subjected to UV-vis-NIR spectro-electrochemical studies. These were performed at room temperature in DCM solution utilising $TBABF_4$ as an electrolyte and with a 0.1 mM sample concentration. All of the samples showed changes in the 30,000-15,000 cm^{-1} region of the spectrum upon

oxidation with two absorption bands forming at about 25,000 cm^{-1} and about 18,000 cm^{-1} (Figure 7.5). Upon back-reduction of the sample the original spectra were recovered, demonstrating the chemical reversibility of the redox cycle.

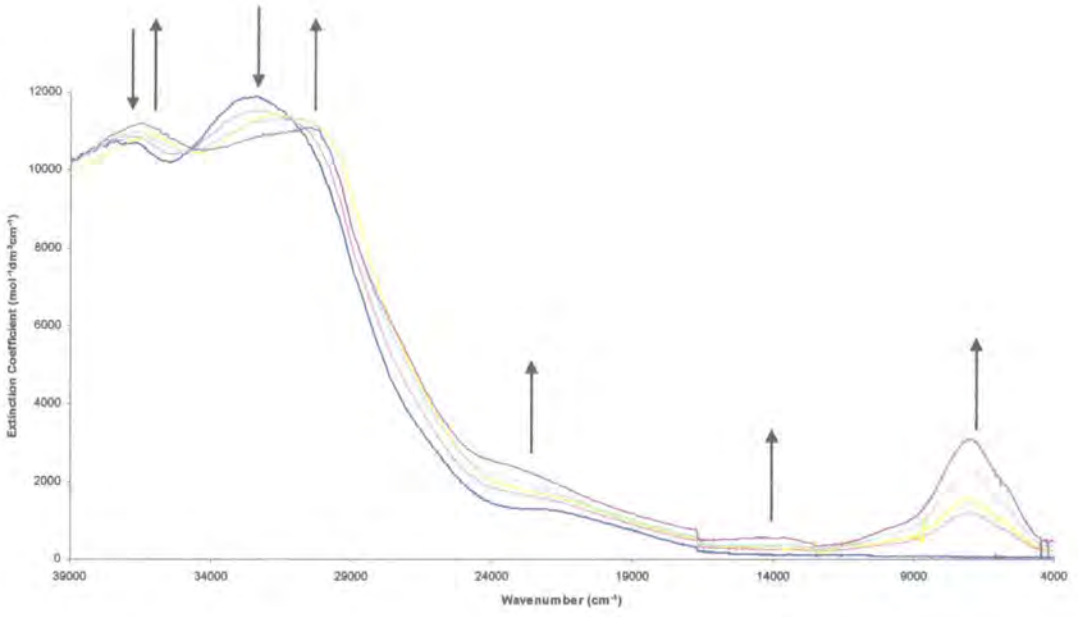

Figure 7.5. Oxidation of $[\{Fe(dppe)Cp\}_2(\mu\text{-}C{\equiv}C\text{-}C{\equiv}N)][PF_6]$

There were, however, major differences in the near infra-red (NIR) region of the electronic absorption spectrum between the monometallic samples (**22-24**) and the bimetallic samples. In the case of the monometallic materials no absorption bands were observed in this region upon oxidation. The bimetallic samples, however, showed an intense absorption envelope in the 11,000-6,000 cm^{-1} region of the spectrum. Close inspection showed this envelope to consist of three overlapping absorption bands, and this band envelope was deconvoluted. The data resulting from the Gaussian-shaped bands is summarised in Table 7.8 and an example is shown in Figure 7.6.

Table 7.8. NIR absorption data for compounds $[\mathbf{25}]^+$-$[\mathbf{29}]^+$ and $[\mathbf{32}]^+$-$[\mathbf{34}]^+$

Compound	$\bar{\nu}_{max}$ (cm^{-1}) (ε ($mol^{-1}dm^3cm^{-1}$))
$[\{Ru(PPh_3)_2Cp\}_2(C{\equiv}CC{\equiv}N)]^{2+}$ $[\mathbf{25}]^+$	5,680 (88); 7,400 (3,600); 10,110 (810)
$[\{Ru(PPh_3)_2Cp\}(C{\equiv}CC{\equiv}N)\{Fe(dppe)Cp\}]^{2+}$ $[\mathbf{26}]^+$	5,980 (190); 9,300 (4,800); 11,070 (1,664)
$[\{Ru(dppe)Cp^*\}(C{\equiv}CC{\equiv}N)\{Ru(PPh_3)_2Cp\}]^{2+}$ $[\mathbf{27}]^+$	6,300 (1,800); 7,900 (3,500); 8,740 (3,020)
$[\{Ru(dppe)Cp^*\}_2(C{\equiv}CC{\equiv}N)]^{2+}$ $[\mathbf{28}]^+$	6,600 (2,600); 8,700 (1,400); 10,320 (840)
$[\{Ru(dppe)Cp^*\}(C{\equiv}CC{\equiv}N)\{Fe(dppe)Cp\}]^{2+}$ $[\mathbf{29}]^+$	6,355 (500), 8,400 (1,300); 10,720 (1,130)
$[\{Fe(dppe)Cp\}(C{\equiv}CC{\equiv}N)\{Ru(PPh_3)_2Cp\}]^{2+}$ $[\mathbf{32}]^+$	5260 (140); 9,200 (2000); 11,190 (840)
$[\{Fe(dppe)Cp\}(C{\equiv}CC{\equiv}N)\{Ru(dppe)Cp^*\}]^{2+}$ $[\mathbf{33}]^+$	4,800 (260); 7,600 (900); 10, 350 (460)
$[\{Fe(dppe)Cp\}_2(C{\equiv}CC{\equiv}N)]^{2+}$ $[\mathbf{34}]^+$	5,400 (630), 7,000 (2,900); 9,400 (330)

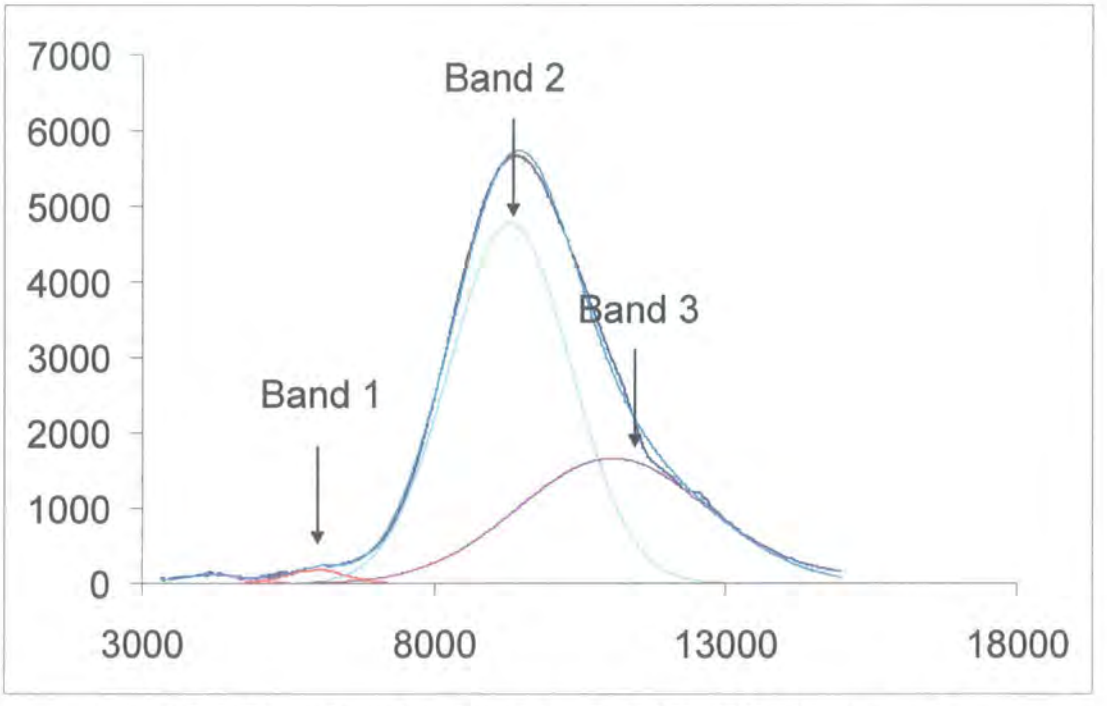

Figure 7.6. Three Gaussian-shaped bands of $[\{Ru(PPh_3)_2Cp\}(\mu\text{-}C{\equiv}C\text{-}C{\equiv}N)\{Fe(dppe)Cp\}][PF_6]$

The origin of these three bands in bimetallic mixed-valence complexes have been discussed in some detail by Meyer, with the conceptual treatment beginning from the premise that the oxidation processes may be regarded as being purely metal centred.[21] Meyer suggested that each of the three bands arises from inter-valence charge transfer (IVCT) from one M^{II} (d^6) metal to the other M^{III} (d^5) centre. As two of these transitions are formally symmetry forbidden, Meyer suggests that the low symmetry of these complexes, along with spin-orbit coupling and extensive overlap between the metal orbitals and those of the bridging ligand allows mixing of the d_{xy}, d_{xz} and d_{yz} orbitals of the donor M^{II} centre with the hole at the M^{III} centre. Thus there are three possible IVCT transitions and hence three bands observed in the NIR region of the electronic absorption spectrum (see Figure 7.7). The lowest energy transition is designated IVCT(1) and the two higher energy transitions as IVCT(2) and IVCT (3).

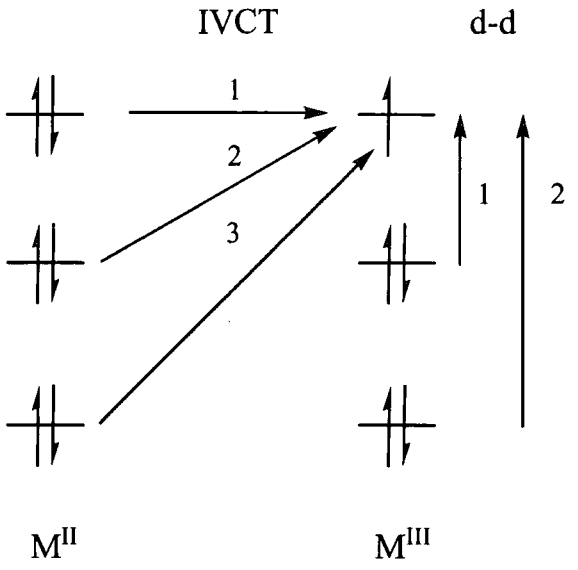

Figure 7.7. IVCT and d-d transitions for bimetallic mixed-valence complexes

In the case of the Ru/Fe based systems under study here there is unlikely to be a significant degree of spin-orbit coupling. Instead, the low symmetry of the metal

centres and extensive orbital-mixing allows the mixing of some M^{II} character into the M^{III} centre, resulting in the allowance of two d-d transitions at the M^{III} centre which are normally LaPorte forbidden (see Figure 7.7). The energy of these d-d transitions is approximated by the difference in energy between the IVCT transitions. Thus the lowest energy d-d transition (d-d(1)) is given by the difference in energies IVCT(2)-IVCT(1) and the higher energy transition (d-d(2)) is given by IVCT(3)-IVCT(1).[21]

These compounds as described by Meyer sit on the borderline between Class 2 (valence trapped) and Class 3 mixed-valence compounds. However, the appearance of 'pseudo-d-d' transitions suggests some degree of charge localisation at a metal centre and hence a Class 2 coupling model will be used in the discussion of the NIR data presented in this chapter. The NIR data, along with coupling constants and theoretical band-width at half height (based on a Hush-type analysis of the band shapes) for the bimetallic complexes is presented in Table 7.9. For a description of the derivation of these parameters, see Chapter 4.

Table 7.9. Near-IR data and coupling constant for homometallic compounds.

Compound	Band	$\bar{\nu}_{max}$ (cm^{-1})	$\Delta\bar{\nu}_{1/2\ (calc)}$ (cm^{-1})	$\Delta\bar{\nu}_{1/2\ (found)}$ (cm^{-1})	ε ($mol^{-1}dm^3cm^{-1}$)	r (Å)	V_{ab}	Calculated d-d energies (cm-1)
$[25]^+$	IVCT(1)	5678	3620	1698	88	7.64	78	
$[25]^+$	IVCT(2)	7395	4130	2586	3590	7.64	703	d-d(1) = 1717
$[25]^+$	IVCT(3)	10107	4830	3040	810	7.64	423	d-d (2) = 4429
$[26]^+$	IVCT(1)	5982	3715	1184	190	7.62	99	
$[26]^+$	IVCT(2)	9310	4635	2458	4780	7.62	890	d-d(1) = 3328
$[26]^+$	IVCT(3)	11070	5055	3810	1665	7.62	713	d-d (2) = 5088
$[27]^+$	IVCT(1)	6147	3770	1072	872	7.71	202	
$[27]^+$	IVCT(2)	7994	4300	1710	3196	7.71	556	d-d(1) = 1847
$[27]^+$	IVCT(3)	8331	4385	3998	3005	7.71	841	d-d (2) = 2184
$[28]^+$	IVCT(1)	6609	3905	3630	2602	7.68	667	
$[28]^+$	IVCT(2)	8711	4485	1808	1433	7.68	401	d-d(1) = 2102

Table 7.9 (continued).

Compound	Band	$\bar{\nu}_{max}$ (cm^{-1})	$\Delta\bar{\nu}_{1/2\ (calc)}$ (cm^{-1})	$\Delta\bar{\nu}_{1/2\ (found)}$ (cm^{-1})	ε ($mol^{-1}dm^3cm^{-1}$)	r (Å)	V_{ab}	Calculated d-d energies (cm-1)
[**28**]$^+$	IVCT(3)	10322	4885	2746	820	7.68	407	d-d (2) = 3713
[**29**]$^+$	IVCT(1)	6355	3830	2532	498	7.63	241	
[**29**]$^+$	IVCT(2)	8449	4420	2042	1285	7.63	400	d-d(1) = 2090
[**29**]$^+$	IVCT(3)	10720	4975	5180	1127	7.63	670	d-d (2) = 4365
[**32**]$^+$	IVCT(1)	5258	3485	1532	135	7.62	89	
[**32**]$^+$	IVCT(2)	9170	4600	2646	1989	7.62	590	d-d(1) = 3912
[**32**]$^+$	IVCT(3)	11185	5085	4546	841	7.62	555	d-d (2) = 5927
[**33**]$^+$	IVCT(1)	4778	3320	1524	263	7.63	118	
[**33**]$^+$	IVCT(2)	7586	4185	2280	901	7.63	335	d-d(1) = 2810
[**33**]$^+$	IVCT(3)	10345	4890	6654	457	7.63	477	d-d (2) = 5564
[**34**]$^+$	IVCT(1)	5387	3530	1136	627	7.49	170	
[**34**]$^+$	IVCT(2)	6998	4020	2356	2853	7.49	593	d-d(1) = 1611
[**34**]$^+$	IVCT(3)	9398	4660	1674	326	7.49	196	d-d (2) = 4011

An important point needs to be raised at this juncture. The coupling constants calculated for these compounds are derived from the formula:

$$V_{ab} = \frac{0.0205\sqrt{\nu_{max}\Delta\nu_{1/2}\varepsilon}}{r}$$

The value r in this formula is the charge transfer distance and for the purposes of this discussion that is assumed to be the point-to-point distance between the metal centres. However, the IR data for these oxidised complexes has shown that there is some degree of ligand character in the redox active orbital and hence the real charge transfer distance will be less than that used. This means that the coupling constants derived above are an approximation and at best correspond to a lower limit.

Perhaps of more interest in these compounds are the calculated d-d transitions energies. Whilst any absorption bands arising from the d-d transitions are, in most cases, hidden under other absorptions such as those arising from IVCT transitions, the calculated energies of the d-d transitions for $[[Ru(dppe)Cp^*\}(\mu\text{-}C{\equiv}CC{\equiv}N)[Ru(PPh_3)_2Cp]^{2+}$ ($[\mathbf{27}]^+$) are 1847 and 2184 cm^{-1} and as such should be visible in the IR spectrum of the oxidised product. Close inspection of the IR spectrum reveals shoulders to the ν(C≡N) and ν(C≡C) bands at 2111 and 1826 cm^{-1} which may correspond to these pseudo d-d transitions (see Figure 7.8 below).

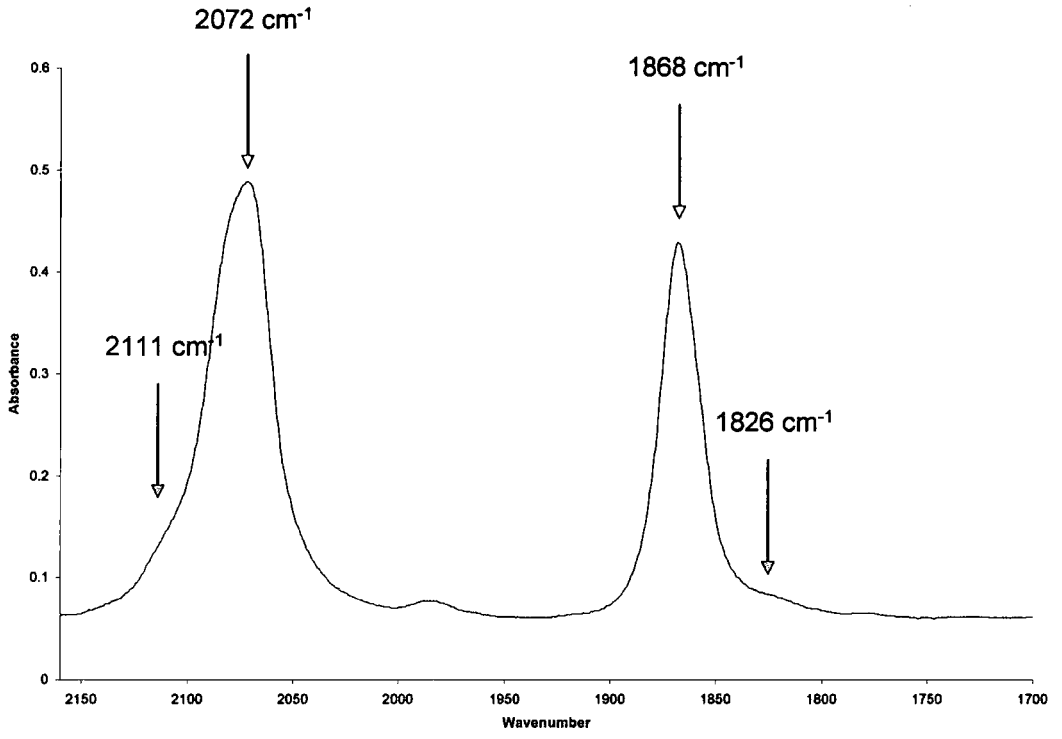

Figure 7.8. IR spectrum of $[[Ru(dppe)Cp^*\}(\mu\text{-}C{\equiv}CC{\equiv}N)[Ru(PPh_3)_2Cp]^{2+}$ ($[\mathbf{27}]^+$) showing d-d transitions.

As stated above, the coupling constants for these complexes represent a lower limit to the value as the charge transfer distance is likely to be much less than the point-to-point distance between metal centres, especially as the electrochemical and IR data suggest a greater degree of orbital mixing in these complexes as compared to the homometallic examples. However, there is a trend towards higher coupling constants and lower IVCT energies in the heterometallic complexes which seems to concur with the idea of stronger coupling between metal centres in these cases. Interestingly the NIR data seems to indicate that the metal-metal interaction in these bridging isomers is stronger in the cases where the iron centre is at the carbon end of the C_3N chain regardless of the supporting

ligands at the ruthenium centre. This is in contrast to the IR data for which it was suggested that the reverse was true for the $[Ru(dppe)Cp^*]^+$ complexes.

Furthermore, there is a trend towards a greater metal-metal interaction in those materials where the difference in electron density between metal end-caps is greatest, i.e. $[\{Ru(PPh_3)_2Cp\}(\mu\text{-}C{\equiv}CC{\equiv}N)\{Fe(dppe)Cp\}]^{2+}$ and $[\{Fe(dppe)Cp\}(\mu\text{-}C{\equiv}CC{\equiv}N)\{Ru(PPh_3)_2Cp\}]^{2+}$. This observation matches well with the electrochemical and spectro-electrochemical observations in this chapter as well as conclusion drawn from the physical properties and molecular structures of these compounds in the previous chapter.

In summary, the work presented herein shows that the cyanoacetylide ligand represents a novel bridging ligand to allow metal-metal interactions between two metal centres. The studies suggest that the strength of this interaction is dependent on the nature of the metal end-caps and will be stronger where there is a difference in electron-density between the metal centres. However, whilst suggestions have been made as to the nature of these metal-metal interactions, these are by no means definitive. The demonstrated stability of the mono-oxidised species means that the oxidation products should be isolable and thus allow for crystallographic characterisation. These studies, along with Mössbauer and Stark spectroscopy techniques should be of help in determining the oxidations states of the metals under study. Further to these studies, computational modelling of these systems is under way at the present time and the results of these studies, along with rationalisation, should further our understanding of these systems.

References

1 R. Nast, F. Urban, Z. *Anorg. Allg. Chem.*, 1957, **289**, 244.

2 J. Kim, H. Masai, K. Sonogashira, N. Hagihara, *Inorg. Nucl. Chem. Lett.*, 1970, **6**, 181.

3 N. Le Narvor, L. Toupet, C. Lapinte, *J. Am. Chem. Soc.*, 1995, **117**, 7129.

4 M. Guillemot, L. Toupet, C. Lapinte, *Organometallics*, 1998, **17**, 1928.

5 M. I. Bruce, P. Hinterding, B. W. Skelton, E. R. T. Tiekink, A. H. White, *J. Orgaomet. Chem.*, 1993, **450**, 209.

6 M. I Bruce, L. I. Denisovich, P. J. Low, S. M. Peregudova, A. N. Ustynyuk, *Mendeleev Commun.*, 1996, 200.

7 M. I. Bruce, B. G. Ellis, P. J. Low, B. W. Skelton, A. H. White, *Organometallics*, 2003, **22**, 3184.

8 M. Brady, W. Weng, Y. Zhou, J. W. Seyler, A. J. Amoroso, A. M. Arif, M. Bohme, G. Frenking, J. A. Gladysz, *J. Am. Chem. Soc.*, 1997, **119**, 775.

9 M. I. Bruce, P. J. Low, K. Costuas, J-F. Halet, S. P. Best, G. A. Heath, *J. Am. Chem. Soc.*, 2000, **122**, 1949.

10 L.-B. Gao, L.-Y. Zhang, L.-X. Shi, Z.-N. Chen, *Organometallics*, 2005, **24**, 1678.

11 C. Creutz, Prog. *Inorg. Chem.*, 1983, **30**, 1.

12 C. Creutz, M. H. Chou, *Inorg. Chem.*, 1992, **31**, 3170.

13 H. Irngartinger, W. Grotzmann, *Angew. Chem. Int. Ed. Engl.*, 1986, **25**, 340.

14 P. Belanzoni, N. Re, A. Sgamellotti, C. Floriani, *J. Chem. Soc. Dalton Trans.*, 1998, 1825.

15 F. Paul, W.E. Meyer, L. Toupet, H. Jiao, J. A. Gladysz, C. Lapinte, *J. Am. Chem. Soc.*, 2000, **122**, 9405.

16 F. Coat, M.-A. Guillevic, L. Toupet, F. Paul, C. Lapinte, *Organometallics*, 1997, **15**, 5988.

17 M. I. Bruce, K. Costuas, T. Davin, B. G. Ellis, J.-F. Halet, C. Lapinte, P. J. Low, M. E. Smith, B. W. Skelton, L. Toupet, A. H. White, *Organometallics*, 2005, in press.

18 N.G. Connelly and W.E. Geiger, *Chem. Rev.*, 1996, **96**, 877.

19 I.R. Whittall, M.G. Humphrey, D.C.R. Hockless, B.W. Skelton, A.H. White, *Organometallics*, 1995, **14**, 3970.

20 M.I. Bruce, B.G. Ellis, M. Gaudio, C. Lapinte, G. Melino, F. Paul, B.W. Skelton, M. E. Smith, L. Toupet, A. H. White, *Dalton Trans.*, 2004, 1601

21 K. D. Demadis, C. M. Hartshom, T. J. Meyer, *Chem. Rev.*, 2001, **101**, 2655.